

Design and Synthesis of Histone Deacetylase Inhibitors with Antiplasmodial and Anticancer Activities

Inaugural dissertation

for the attainment of the title of doctor
in the Faculty of Mathematics and Natural Sciences
at the Heinrich Heine University Düsseldorf

presented by

Leandro Antonio Alves Avelar
from Passos

Düsseldorf, April 2018

from the institute for Pharmaceutical and Medicinal Chemistry
at the Heinrich Heine University Düsseldorf

Published by permission of the
Faculty of Mathematics and Natural Sciences at
Heinrich Heine University Düsseldorf

Supervisor: Prof. Dr. Thomas Kurz

Date of the oral examination: 13.06.2018

Declaration of Academic Integrity

I declare under oath that I have concluded my dissertation independently and without any undue assistance by third parties under consideration of the ‘Principles for the Safeguarding of Good Scientific Practice at Heinrich Heine University Düsseldorf’.

This dissertation has not been submitted in its present or a similar form in any other institution. I have not made any successful or unsuccessful attempt to obtain a doctorate before.

Düsseldorf, 20/04/2018

Leandro Antonio Alves Avelar

Acknowledgements

I would like to thank Prof. Dr. Thomas Kurz for the supervision during my PhD and the chance to be part of his working group, also for the shared scientific knowledge and experience, which resulted in my personal and scientific development.

I would like to thank Prof. Dr. Mathias U. Kassack and his working group, specially to Dr. Alexandra Hamacher and MSc. Christian Schrenk for the successful work achieved in the anticancer studies. I would also like to thank Prof. Dr. Mathias U. Kassack for the correction of my thesis.

I would like to thank Prof. Dr. Holger Gohlke and his working for the support during my work and for being my mentor.

I would like to thank Dr. Jana Held from the University of Tübingen and Prof. Dr. Katharine Andrews from the Griffith University for collaboration with antimalarial assays.

I would like to thank Dr. Marc Remke for performing the enzymatic assays with the molecules synthesized during this work.

I would like to thank Prof. Dr. Finn Hansen from the University of Leipzig for the scientific discussions and shared knowledge.

I would like to thank all past and present members of my working group for the support and friendly atmosphere.

I would also like to thank my family and friends for the unconditional support.

I would like to thank the Coordenação de Aperfeiçoamento de Pessoal de Nível Superior for the financial founding through the process number 99999.012014/2013-0.

Table of Contents

Abbreviations.....	iv
1. Introduction.....	1
1.1. Histone Deacetylases	1
1.1.1. HDAC in Epigenetics.....	1
1.1.2. Classification of HDACs	3
1.1.3. Mechanism of catalysis of HDAC class I, II and IV	4
1.1.4. Histone deacetylase binding site and HDACi pharmacophore	6
1.1.5. Zinc Binding Groups in HDACi.....	7
1.1.6. Histone deacetylases class I.....	9
1.1.7. Histone deacetylases class II	12
1.1.7.1. Histone deacetylases class IIa	12
1.1.7.2. Histone deacetylases class IIb	14
1.1.8. Histone deacetylases class IV.....	17
1.1.9. Applications of Histone Deacetylase Inhibitors in Therapy	18
2. Objectives.....	23
3. Histone Deacetylase inhibitors with antimalarial activity	23
3.1. Project background.....	23
3.2. Histone deacetylase in <i>Plasmodium falciparum</i>	28
3.3. Project overview	30
3.4. Publication	32
4. Histone Deacetylase inhibitors with Antineoplastic activity.....	55
4.1. Anticancer effects of HDACi.....	55
4.2. Rational design of novel HDACi.....	59
4.3. Synthesis of the second set of designed HDACi.....	63
4.4. Biological evaluation of the second set of designed inhibitors	65
4.5. Design of the third set of inhibitors	67
4.6. Synthesis of the third set of inhibitors.....	68
4.7. Biological evaluation of the third set of inhibitors	70
4.8. Evaluation of 6r, 8a and 8c in Glioblastomas	75
4.9. Enzymatic assays	78
4.10. Molecular docking	81
4.11. Evaluation of chemosensitizing effects of selected HDACi.....	86
4.12. Conclusion	91
4.13. Experimental Part	93
4.13.1. General procedures for the synthesis of the designed compounds.....	93
4.13.2. Computational details.....	116

5. Summary	117
6. Zusammenfassung	119
7. References	121

List of Publications

Publication included in the thesis

Alves Avelar, L. A. (70%), Held, J., Engel, J. A., Sureechatchaiyan, P., Hansen, F. K., Hamacher, A., Kassack, M. U., Mordmüller, B., Andrews, K. T. and Kurz, T. Design and Synthesis of Novel Anti-Plasmodial Histone Deacetylase Inhibitors Containing an Alkoxyamide Connecting Unit. *Arch. Pharm.* **2017**, 350: n/a, 1600347.

Other Publications

D. Diedrich, A. Hamacher, C. G. W. Gertzen, **L. A. Alves Avelar**, G. J. Reiss, T. Kurz, H. Gohlke, M. U. Kassack and F. K. Hansen. Rational design and diversity-oriented synthesis of peptoid-based selective HDAC6 inhibitors. *Chem Commun.* **2016**, 15, 3219-22.

Abbreviations

A

4-AQ	4-Aminoquinoline
8-AQ	8-Aminoquinoline
AAA	Aryl-amino alcohol
Ac	Acetyl
ACT	Artemisinin-based combination therapy
ACUC	Acetoin utilization C protein
AD4.2	Autodock 4.2
ADT	Autodock Tools
Ala	Alanine
AMC	7-Amino-4-methylcoumarin
APHA	Acetylpolyamine amidohydrolases
Asp	Aspartate
ATP4	Adenylpyrophosphatase 4

B

BCS	Biopharmaceutical classification system
BET	Bromodomain and extraterminal domain
Boc	<i>tert</i> -Butyloxycarbonyl group
Bps	Base pairs of nucleic acids

C

CARL	Cyclic amine resistance locus protein
Cbz	Carboxybenzyl
CD	Catalytic domain
CDDp	Cisplatin
CHOP	Cyclophosphamide, doxorubicin, vincristine, and prednisone
CI	Combination index
CoREST	Co-repressor for element-1-silencing transcription factor
CQ	Chloroquine
CTCL	Cutaneous T-cell lymphoma
CU	Connecting unit
Cys	Cystein

D

DAD	Deacetylase activation domain
-----	-------------------------------

DCM	Dichloromethane
DHFR	Dihydrofolate reductase
DHODH	Dihydroorotate dehydrogenase
DMAP	4-Dimethylaminopyridine
DMNT	DNA methyltransferase
DMSO	Dimethyl sulfoxide
DNA	Deoxyribonucleic acid
DNTTIP1	Deoxynucleotidyltransferase terminal-interacting protein 1

E

EDCI	1-Ethyl-3-(3-dimethylaminopropyl)-carbodiimide hydrochloride
ELISA	Enzyme-linked immunosorbent assay
EMA	European Medicines Agency
ESI	Electrospray ionization

F

FDA	Food and Drug Administration
-----	------------------------------

G

GAPDH	Glyceraldehyde-3-phosphate dehydrogenase
GBM	Glioblastoma
Glu	Glutamate

H

HAT	Histone acetyltransferase
HCC	Hepatocellular carcinoma
HDA	Yeast histone deacetylase A
HDAC	Histone deacetylase
HDACi	Histone deacetylase inhibitor
HDB	Yeast histone deacetylase B
His	Histidine
HIV-1	Human immunodeficiency virus type 1
HDLP	Histone deacetylase like protein
HPLC	High-performance liquid chromatography
HRMS	High resolution mass spectrometry
HRP2	Histidine-rich protein 2
Hsp90	heat shock protein 90
hTERT	Human telomerase reverse transcriptase

I

IBCF Isobutyl chloroformate

L

LCoR Ligand-dependent corepressor

Leu Leucine

LSG Late stage gametocytes

Lys Lysine

M

MAL Boc-Lys(ϵ -Ac)-AMC

MBG Metal binding group

MEF2 myocyte enhancer factor 2 binding domain

Met Methionine

MiDAC Mitotic deacetylase complex

MM Multiple myeloma

MMV Medicines for Malaria Venture

mp Melting point

MTA1 Metastasis-associated protein 1

MTT 3-(4,5-Dimethylthiazole-2-yl)-2,5-diphenyltetrazoliumbromide

N

NAD⁺ Nicotinamide adenine dinucleotide

N-CoR Nuclear receptor co-repressor

NMM *N*-Methylmorpholine

NMR Nuclear magnetic resonance

NuRD Nucleosome remodeling and deacetylation

O

OSCC Oral squamous cell carcinomas

P

PDAC Polyamine deacetylase

PDB Protein Data Base

Phe Phenylalanine

PI4K Phosphatidylinositol-4-kinase

PPI Protein-protein interaction

Pro Proline

PTCL Peripheral T-cell lymphoma

PTM	Post transcription modification	
		R
RBC	Red blood cell	
RMSD	Root-mean-square deviation	
		S
SAHA	Suberoylanilide hydroxamic acid	
Ser	Serine	
SF	Shift factor	
SI	Selectivity index	
Sir2	Sirtuin 2	
SMRT	Silencing mediator for retinoid and thyroid receptors	
		T
TFA	Trifluoroacetic acid	
TFMO	Trifluoromethyloxadiazole	
Thr	Threonine	
TLC	Thin layer chromatography	
TMZ	Temozolomide	
Trp	Tryptophan	
TSA	Trichostatin A	
Tyr	Tyrosine	
		U
UV	Ultraviolet	
		W
WHO	World Health Organization	
		Z
ZBG	Zinc binding group	
ZMAL	Cbz-Lys(ϵ -Ac)-AMC	
ZnF-UBP	Zinc-finger ubiquitin-specific protease	

1. Introduction

1.1. Histone Deacetylases

1.1.1. HDAC in Epigenetics

The enzymatic acetylation/deacetylation of the histones could be observed first in the 1960s. During this time the importance of chromatin in gene regulation started to be uncovered and particularly, the close relationship between the turnover of histone acetylation and information transfer in the DNA.¹ Nowadays it has been demonstrated that the reversible acetylation, a post-transcription modification (PTM) of histones, along with DNA methylation and phosphorylation are the most important regulators of gene transcription and DNA accessibility. Therefore it is a crucial mechanism in the epigenetic regulation of gene transcription.²

Epigenetics is defined as heritable modifications in gene expression without alterations in the DNA sequence. These alterations can occur in the structure of histones or in the DNA directly. Epigenetic modifications can be divided into three classes: writers add the modification, readers recognize the modification and initiate its effect and “erasers” remove the alteration done by writers.^{2,3}

The acetylation of histones is performed by the Histone Acetyl Transferases (HATs). These writers acetylate ϵ – amino groups of lysine in specific regions which are present in four types of histones, H2A, H2B, H3, and H4. The acetylation results in a loss of the positive charge in the side chain and consequently a loss of ionic interactions with the negatively charged phosphate group in the nucleotides of the DNA. This causes the chromatin to open and makes it easier accessible for transcription. Furthermore, acetylation can disturb the protein-protein interaction (PPI) between the different histones that compose the nucleosome (octamer formed by two copies of histones surrounded by 150-200 bps) and thereby alter the structure of the heterochromatin (Figure 1).²

The readers of histone acetylation are short sequences of amino acids (around 120 residues) known as Bromodomains. They are present in a relatively wide range of enzymes including HATs and can appear more than once in the same macromolecule. All members of the Bromodomain class interact with the acetylated amino groups via an asparagine, but the differences in the region surrounding the asparagine allow the domains to build specific interactions with acetylated lysine residues in different environments. This circumstance can explain the specificity of bromodomains for different interaction partners.⁴

Histone deacetylases (HDACs), the focused biological target of this work, act as the erasers of histone acetylation. Therefore, they reverse the opening of the chromatin, transferring it to a condensed state decreasing the DNA accessibility (Figure 1).

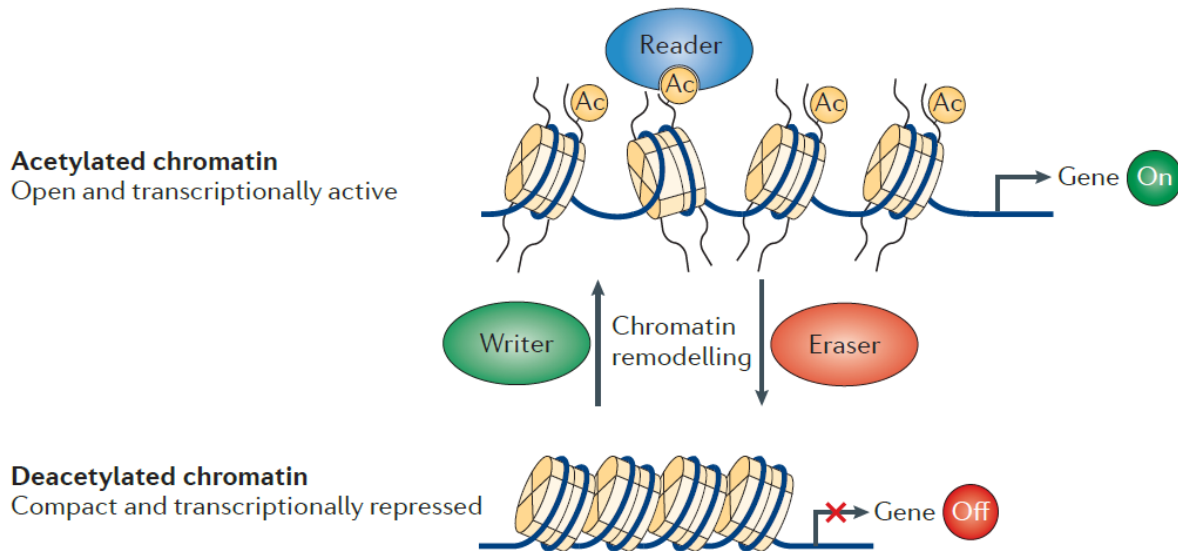


Figure 1: Histone acetylation and its influence in gene transcription. In this process writers are HATs, readers the Bromodomains and Erasers HDACs.¹

Although a connection between the inhibition of HDACs and unspecific, uncontrolled increase of gene transcription could be drawn, it has been observed that instead, an orchestrated activation/inactivation of specific sets of genes is triggered. HDAC inhibition leads to a consequent decrease of HATs, the respective writers, which balances the aberrant acetylation. The complex regulation of histone deacetylation shows that inhibition of this target is not necessarily lethal, making it a valuable biological target.⁵ In addition to the complexity of the biological roles of HDACs, their varied tissue-distribution and the deacetylation of non-histone substrates pose a possible explanation of their importance in a wide range of diseases such as: cancer, cardiovascular diseases, metabolic disorders, neurological disorders, inflammatory diseases and autoimmune disorders.^{6,7}

HDACs and DNA methyltransferases (DNMT) are so far, the only epigenetic targets with inhibitors used in therapy. However, their potential as therapeutic targets is still far from being fully explored.⁷

1.1.2. Classification of HDACs

The histone deacetylase superfamily includes eukaryotic histone deacetylases (HDAC), acetoin utilization proteins (ACUC), that are expressed in eubacteria and acetylpolyamine amidohydrolases (APHA) from archaeal bacteria, eubacteria, and some eukaryotic organisms.⁸ Humans express eighteen different isoforms of HDACs. The human enzymes are divided on the basis of their homology to yeast proteins in four classes, the zinc-dependent classes I, II and IV and the NAD⁺ dependent class III. Class I consists of the isoforms HDAC1, 2, 3 and 8, which present similarity to yeast HDA (inhibited by Trichostatin A). Class II with homology to HDB (not inhibited by inhibited by Trichostatin A), further subdivided in class IIa consisting of HDAC4, 5, 7 and 9 and class IIb with HDAC6 and 10.⁹ Class III is related to the yeast protein Sir2 also known as sirtuins. The members of this class are NAD⁺ dependent deacetylases and are not related in structure or mechanism of catalysis to the other classes and will not be discussed in this work.¹⁰ Class IV has only one member, HDAC11, which has no similarity to HDA or HDB.⁹ The numbering of the isoforms represents the chronological order in which they were discovered.

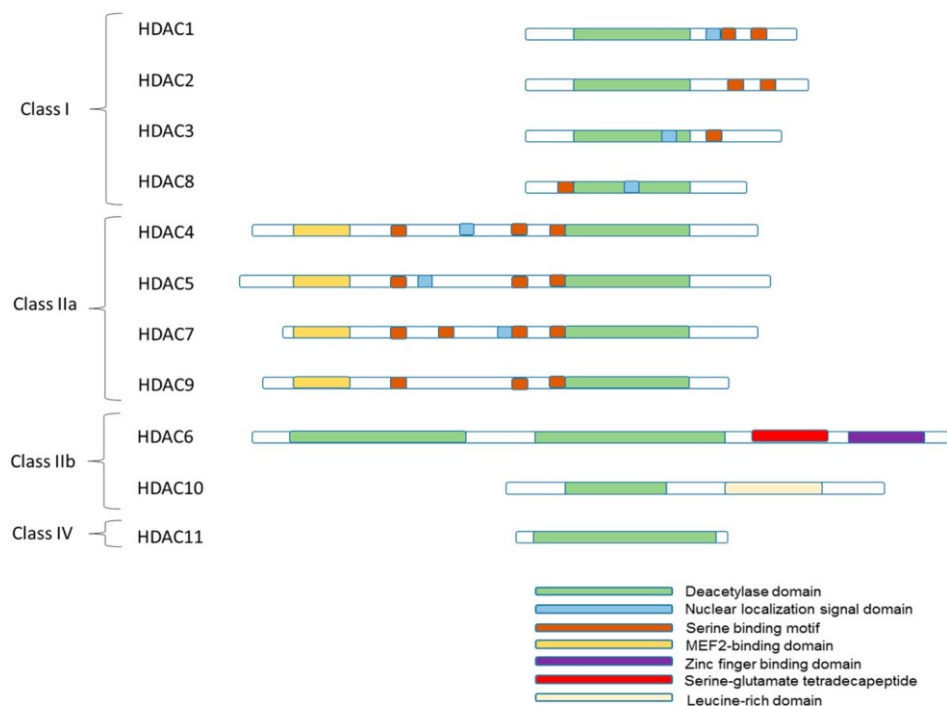


Figure 2: Classification HDAC classes I, II and IV.¹¹

The classification of HDACs by sequence similarity is restrictive. Despite the highly conserved structure of the binding site observed among the isoforms, the substrate specificity (HDAC1,

2, 3 and 6 have significant deacetylase activity when compared to class II and HDAC8, while HDAC10 and HDAC11 no significant activity)¹² and sensibility towards distinct classes of inhibitors are different. As a consequence of the high homology of the structure of the catalytic site, the mechanism of catalysis is conserved in classes I, II and IV. The arrangement of the binding site, however, enable HDACs to interact with a wide range of substrates.¹²

1.1.3. Mechanism of catalysis of HDAC class I, II and IV

As the first crystal structures of the bacteria *Aquifex. eolicus* HDAC, a human homolog histone deacetylase-like protein (HDLP), was available, the first mechanism of catalysis was proposed.¹³

The classical mechanism was initially proposed for HDLP and later confirmed for HDAC8.¹⁴ Due to the similarity of the binding site of HDAC to zinc proteases and serino-proteases, the authors based on the mechanism of these enzymes to propose the steps. Starting in a similar manner to zinc proteases, the *N*-acetyl amide carbonyl of the acetylated substrate interacts with the metal in the catalytic site, causing the polarization of the carbon thus increasing its electrophilicity. Additionally, the coordination places the activated carbon next to a water molecule which is also coordinated to the zinc.

The nucleophilic attack from the zinc-coordinated water molecule to the carbonyl is facilitated due to the increase of nucleophilicity by the interaction with the histidine-aspartate His142-Asp176 (HDAC8 numbering) dyad in a similar way to serine proteases. After the nucleophilic attack, the formed tetrahedral intermediate is stabilized by both the Tyr306 and coordination with the catalytic zinc. Lastly, the bond breakage is aided by a second dyad His143-Asp183 which also protonates the generated amine.^{13,14}

So far, the different models of the mechanism of catalysis proposed for HDAC8 (this isoform is especially accessible to *in vitro* characterization thus an efficient target for the study of all HDAC metal-dependent catalysis) diverge mainly in the role of two His-Asp dyads in the base/acid catalysis¹⁵⁻¹⁷. More recently Gantt et al., supported by enzymatic studies and crystal structures of enzymes containing mutations in the dyads, revised the mechanism (Figure 3).¹⁷ In the revised mechanism His143-Asp183 acts as a basic and acidic catalyst, while the role of His142-Asp176 remains partly undefined. Employing the results of this work, the authors hypothesize that the second dyad has an electrostatic catalytic effect, aiding the stabilization of the negative charge of the tetrahedral intermediate and the charge of His143-Asp183.

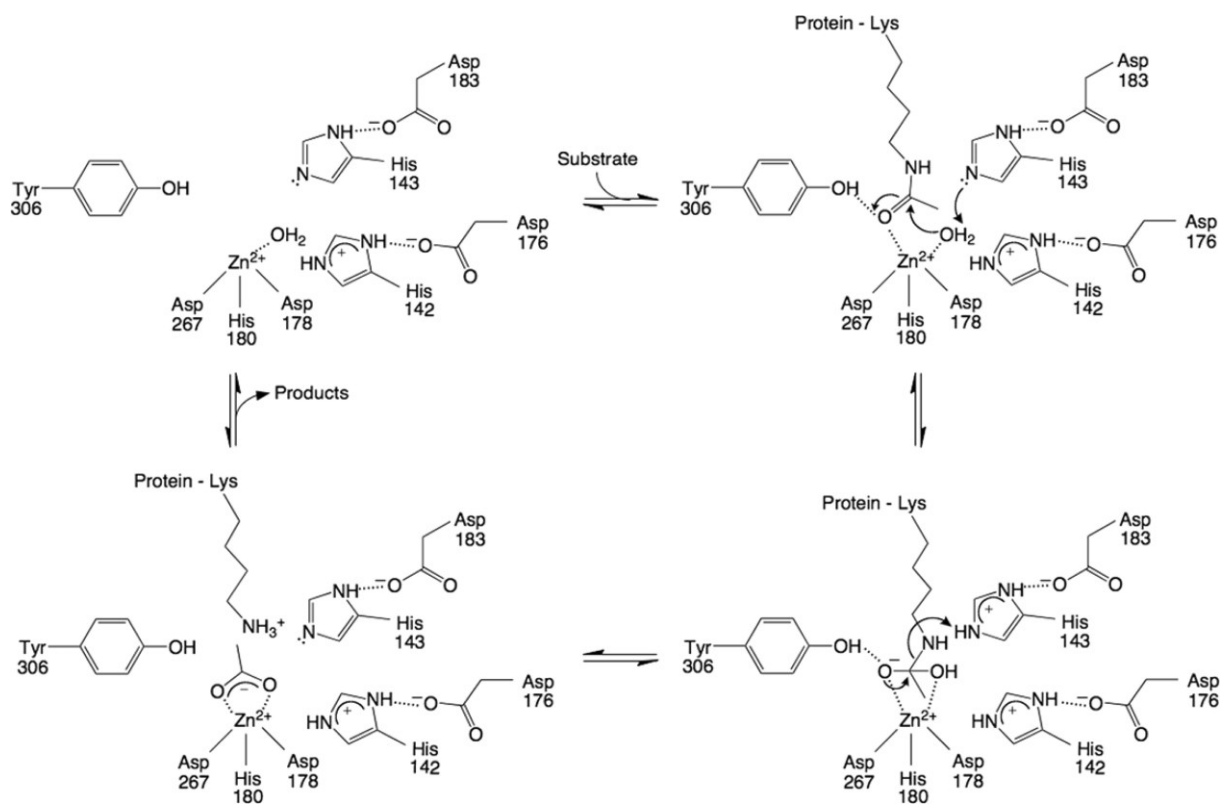


Figure 3: Mechanism of catalysis of HDAC8 proposed by Gantt et al.¹⁷

A crucial point of the mechanism is the influence of the metal cofactor. The designation of HDACs as zinc-dependent enzymes arose from the observation of increased HDAC8 activity with increased Zn^{2+} concentration. However, due to HDAC8 homology to the di-manganese enzyme Arginase, it was considered that HDACs could contain two catalytic metals and different metals than zinc could be used by the enzymes.¹⁸ The first hypothesis was no longer considered as Gantt et al. demonstrated that HDAC8 is only active with one metal ion in the catalytic site although still no specificity to the zinc. In contrast, the enzyme showed increased activity (and affinity of its inhibitor) in the presence of Fe^{2+} and Co^{2+} , which can be explained by the ability of these metals to expand their coordination sphere in contrast to zinc, leading to a more stable coordination of the inhibitors and intermediates formed during the catalysis.¹⁸ In physiological conditions, however, HDACs would unlikely contain Co^{2+} due to the rarity and specificity of cobalt in cellular environments. Furthermore, Fe^{2+} is also unlikely to act as co-factor although iron is indeed more trivial in cellular conditions because of the approximately 106 fold lower affinity of the enzymes to iron when compared to Zn^{2+} .¹⁹ Given these points the initial assumption that HDACs are zinc-dependent enzyme is still in accordance with the experimental data.

1.1.4. Histone deacetylase binding site and HDACi pharmacophore

The analysis of HDLP crystal structures revealed important features common to all HDACs. HLPD was co-crystallized with two inhibitors, the natural product Trichostatin A (TSA) and the synthetic drug Vorinostat (SAHA). TSA is capable of inhibiting all known isoforms and is therefore classified as pan-inhibitor. The crystal structures provided enough details for the conception of a first general pharmacophore model of HDAC inhibitors (HDACi).¹³

The first model divides the molecule into three groups, the zinc-binding group (ZBG), a linker and a cap-group. (i) The ZBG is responsible for the interaction with the zinc at the bottom of the binding site and other catalytic residues (the Tyr and the two His from the Asp-His dyads colored in green in Figure 4). (ii) ZBGs are connected to the rest of the pharmacophore by a linker, which plays a role in the interaction with the tubular hydrophobic tunnel formed by two Phe residues (Figure 4 in dark grey). The tunnel connects the zinc ion to the surface of the protein, which is normally occupied by the aliphatic chain of the lysine residues in the substrate. At the end of the linker the third part of the pharmacophore is placed, the surface recognition motif commonly known as cap-group.

Due to the presence of a highly conserved aspartate at the entrance of the binding site, where the recognition and anchoring of the substrate occur²⁰, the initial pharmacophore model was further expanded (Figure 4 in blue).²¹ The Connecting Unit (CU) is localized between the cap-group and the linker and interacts with the aspartate at the rim of the binding site.²¹

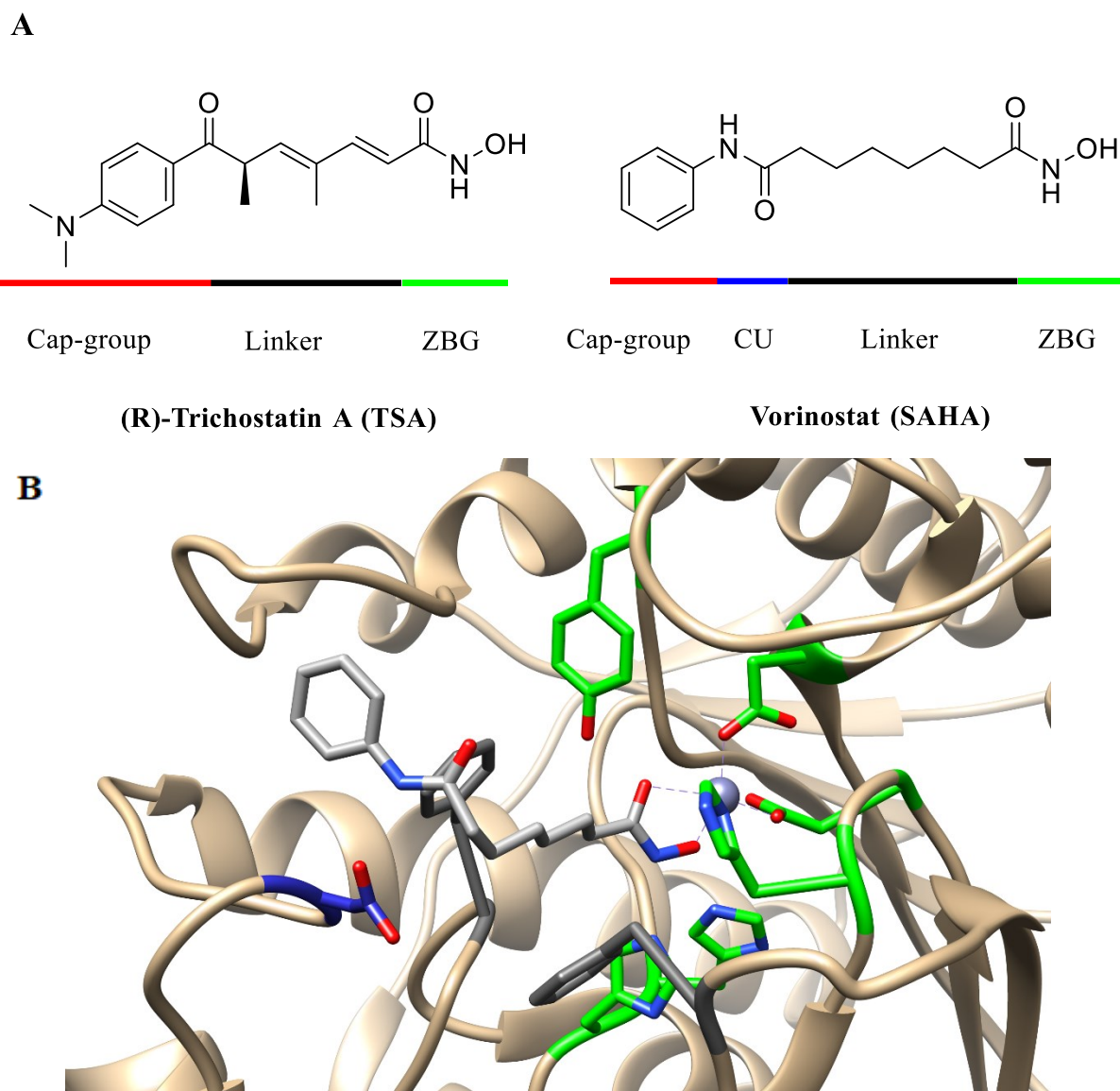


Figure 5: (A) Initial HDACi pharmacophore model¹³ represented by TSA and the expanded model²¹ represented by SAHA. (B) Schematic demonstration of the pharmacophore interaction with the binding site using the crystal structure of HDAC2 co-crystalized with SAHA (PDB ID 4LXZ).

Apart from the inclusion of the CU, no significant alteration of the HDACi general pharmacophore took place. The diverse set of chemical entities used as HDACi fits well this pharmacophore model. The inhibitors are classically classified according to their ZBG.²²

1.1.5. Zinc Binding Groups in HDACi

There are four major classes of HDACi zinc binding groups: hydroxamates, thiols, carboxylic acids and *ortho*-amino anilides. With the exception of the *ortho*-amino anilides, ZBGs do not show preference towards any HDAC isoform class. ZBGs have been associated with

problematic pharmacokinetic and this resulted in the searching for new alternatives (Figure 6).^{22,23}

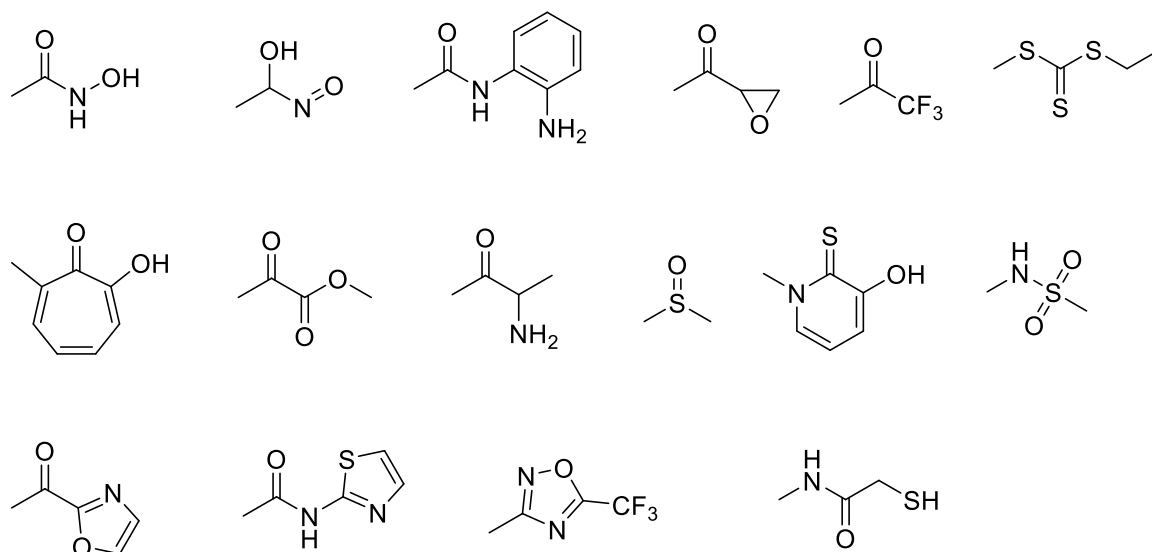


Figure 6: Selection of ZBGs groups present in known HDACi.²²

The understanding of the interaction between zinc and ZBGs is not only essential for the design of new structures but also to understand the binding mode of the known ones.

The zinc ion is among the most important metallic ions in enzymes, Zn^{2+} possess an electronic configuration of $[Ar] 3d^{10}$ and the ion lacks redox activity, differentiating it from the other lighter transition ions. In addition to that, zinc is a borderline Lewis acid, which allows it to coordinate with soft (Cys and His) and hard bases (Asp and Glu). Therefore the metal coordinates in different manners presenting different geometries, that are defined by the role of the metal in the protein.^{24,25}

In HDACs, the coordination of the zinc ion changes according to the occupation of the binding site (Figure 3). Without substrate, the metal is tetraordinated binding to two residues of aspartate, histidine (Asp_2His) and a water molecule assuming a tetrahedral geometry. The zinc becomes pentacoordinated by interacting with the substrate and after hydrolysis; the zinc ion interacts with the formed acetate in a bidentate manner remaining pentacoordinated (Figure 3). The pentacoordinate zinc geometry is always trigonal bipyramidal.²⁵ In a similar fashion ZBGs, regardless chemical structure, interact with the Zn^{2+} either in a monodentate way as the substrate or in a bidentate way as for the acetate.^{22,26}

The influence of the ZBGs mode of inhibition (mono or bidentate) in the enzymatic activity is still unclear. However it has been demonstrated by Suzuki et al. that replacement of the

hydroxamate, a known bidentate inhibitor, present in the structure of Vorinostat (Figure 5) by a thiol, a monodentate inhibitor, did not result in the loss of activity.²⁷

Modification of the ZBGs and/or other parts of the pharmacophore can be used to increase the selectivity of an inhibitor towards classes and even specific isoforms. HDACs show specific affinities to different substrates, despite their highly conserved binding site, implying that their differences can be explored.²⁸

1.1.6. Histone deacetylases class I

Class I consists of four isoforms HDAC1, 2, 3 and HDAC8. This class is ubiquitously expressed in human tissues and apart from HDAC8, all members play essential roles as catalytic cores in chromatin remodeling multienzymes complexes.²⁹ The complexes recruit and direct the activity of HDAC1, 2 and 3 in the chromatin, HDAC1 and HDAC2 are part of the co-repressors Sin3, NuRD (nucleosome remodeling and deacetylation) and CoREST (co-repressor for element-1-silencing transcription factor). Although part of the same complexes, they are not necessarily together as catalytic core.³⁰⁻³²

HDAC3 is exclusively found in the complexes SMRT (silencing mediator for retinoid and thyroid receptors), N-CoR (nuclear receptor corepressor) and MiDAC (DNTTIP1-containing complex), which can interact with the HDAC1/2 complexes as well as with other isoforms of class II.^{30,33}

Proteins with very different structure and function form the corepressor complexes. To function, the complexes depend on intricate interactions between the proteins that build them. The myriad of ways how the HDACi influence the complexes, could be an explanation why HDACi have diverse effects in these complexes.³⁴ The use of molecules to modify the function of these complexes represents a new aspect to be explored.^{35,36} For example, inositol regulates the interaction between HDAC1-3 and their recruiting/activating factors (MTA1-HDAC1/2 and DAD-HDAC3). Consequently the region where inositol binds could be used as a target from the design of inhibitors.^{20,37}

HDAC1 and HDAC2 are sister enzymes sharing more than 80% of amino acid identity and showing also similar kinetic profiles against acetylated substrates.²⁸ Both enzymes appear to be essential for cell survival, the knockout of both isoform separately was incompatible with embryonic development in mice.

Still unclear is the difference between the two isoforms. One aspect explored by Zhou et al.³⁸ is the nature of the cation found close to the catalytic zinc, HDAC1 crystal structures show

always K^+ and HDAC2 Ca^{2+} . The presence of the calcium cation suggests a higher polarization of the zinc ion in HDAC2, leading to a higher catalytical capacity. It was observed in vivo that the isoforms display a certain degree of compensatory ability, however, they also show unequal importance in different physiological process.³⁹

HDAC3 is also structurally related to HDAC1 and 2 (more than 50% sequence identity)³⁷, showing comparable kinetic profile with acetylated substrates²⁸ and being essential for embryological development (mice).⁴⁰

HDAC8, although classified as class I, is structurally different from the other members of class I. The catalytic activity and substrate specificity do not relate with HDAC1-3¹⁴ and the histone deacetylase capacity of this enzyme is still not fully comprehended.^{28,41} HDAC8 is primarily located in the nucleus, but can also be present in the cytoplasm.⁴¹ However, this isoform shares a common structural feature specific from this class, a sub-pocket located lateral to the catalytic zinc ion.⁴²

The unique class I sub-pocket functions as an acetate release channel (Figure 7). This region differs in size and constitution in each isoform and also being referred to as foot pocket due to its shape.⁴³ As demonstrated in Figure 7, after lysine deacetylation, the formed acetate is guided through a channel to the exterior of the enzyme, simultaneously being replaced by a water molecule. The access to the channel is regulated by an amino acid residue acting as a gatekeeper. HDAC1-3 have Leu139, 144 and 133 respectively, while in HDAC8 Trp141 occupies this position.^{44,45}

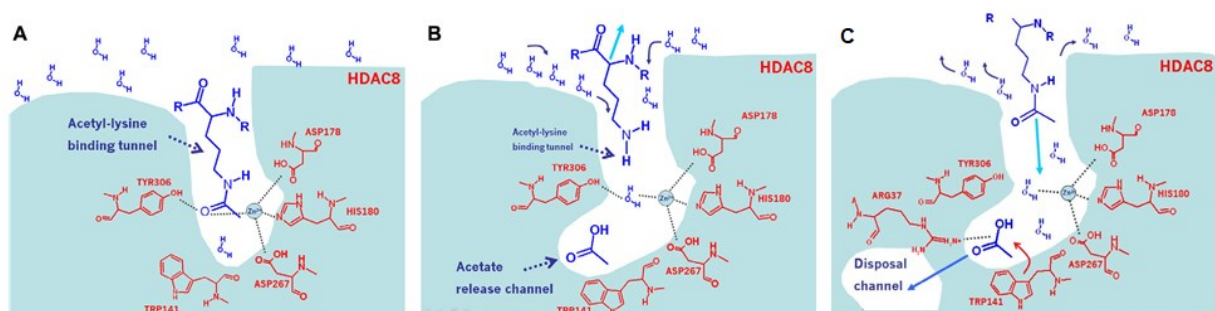


Figure 7: Steps of acetate release in HDAC8 (A) Substrate catalysis (B) Interaction of the acetate with the pocket (C) Release of the acetate.⁴⁶

The foot-pocket of HDAC1 and HDAC2 are identical, HDAC3 shares the same residue as gatekeeper, but due to the replacement of the Ser113/Ser118 in HDAC1/2 for the Tyr107, this region is smaller.⁴⁴ The foot pocket in HDAC8 has no similarity with the other class I isoforms and this difference, especially the replacement of a methionine gatekeeper present in HDAC1,

2 and 3 by the Trp141 was successfully exploited for the design of a HDAC8-selective compound, bearing an alfa-amino-ketone as ZBG (Figure 8).⁴⁶

HDAC1-3 are selectively inhibited by compounds containing *ortho*-amino anilides represented in Figure 8 by Chidamide, the first approved (China) member of this class.

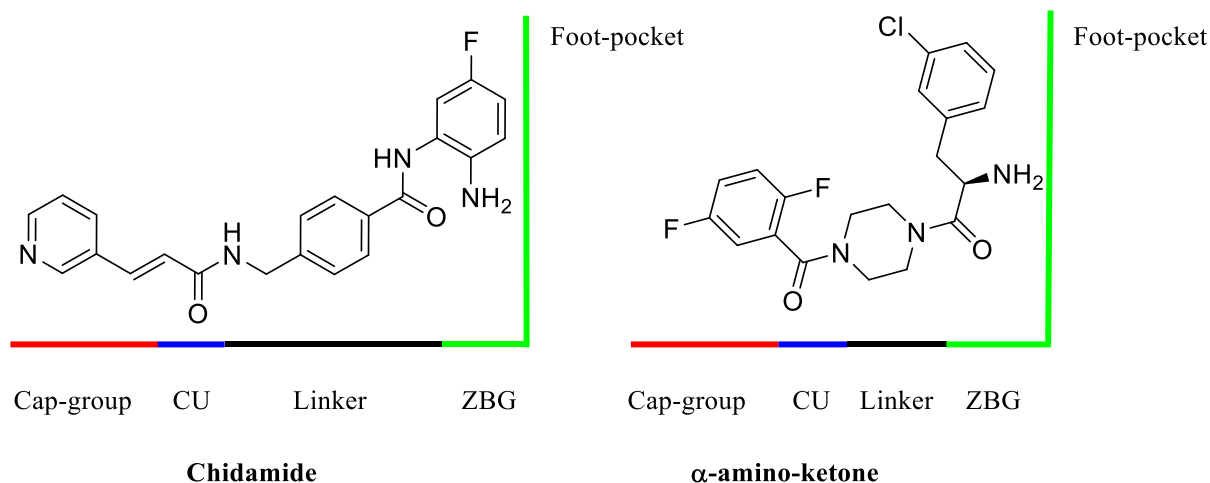


Figure 8: Pharmacophore of class I selective inhibitors.

Ortho-amino anilides interact with the zinc ion by the carbonyl of the amide and the nitrogen of the aniline. Assuming the right conformation for the zinc binding requires relatively a large area due to the size of the phenyl ring of the anilide. The size and complexity have been appointed as possible causes of a fast-on/fast-off kinetic behavior. In contrast to hydroxamates, *ortho*-amino anilides are slow tight-binding inhibitors, consequently causing prolongation of the histone acetylation in cells.⁴⁷ This behavior appears not to be detrimental since the class is well tolerated in rats, dogs, and humans.⁴⁸

Activity and selectivity of *ortho*-amino anilides are highly dependent on the structure of the ZBG core. Modification of the free amino position in the benzene ring causes total loss of activity.⁴⁹ Besides, the replacement of the amino by a hydroxyl group slightly increases the enzymatic potency, but decrease its activity in cellular assays.⁴⁹⁻⁵² Attempts to replace the phenyl ring for pyrimidine⁵³ and naphthalene^{53,54} were detrimental, what could be explained by the polarity of the pocket and also by its shape. However, naphthalene analogs were able to selectively inhibit the complex HDAC3-NCOR1.⁵⁴ The enzymatic evaluation of *N*-(Aminopyridine) *ortho*-amino anilides revealed that the presence of a nitrogen atom in different positions of the pyridine is tolerable.⁵⁵

In regards to selectivity of the *ortho*-amino anilides towards different class I isoforms, not only the core is relevant, but especially the modification of the different aromatic ring positions

(Figure 9).⁵⁶ Substitutions in the *ortho* position of the free amino group leads to steric clashes with the protein structure, which is incompatible to the shape of the binding site⁴⁹, while in meta position only specific modifications, namely the change of the hydrogen for a fluorine atom, are accepted.

Ortho-amino anilides containing fluorine at the meta-position to the free amino can be selective towards HDAC3. Not all *Ortho*-amino anilides with fluorine atoms in this position are more active towards HDAC3. This effect has been attributed to a particular increase of surface in the region where the fluorine interacts, only found in HDAC3 because the change occurs to accommodate the Tyr107 replaced in HDAC1 and 2 by serine residues.⁵⁶

The para position is more flexible to modifications and has been successfully explored in HDAC1 and 2 inhibitors containing aromatic systems capable to occupy its larger foot pocket.^{50,51,57-62}

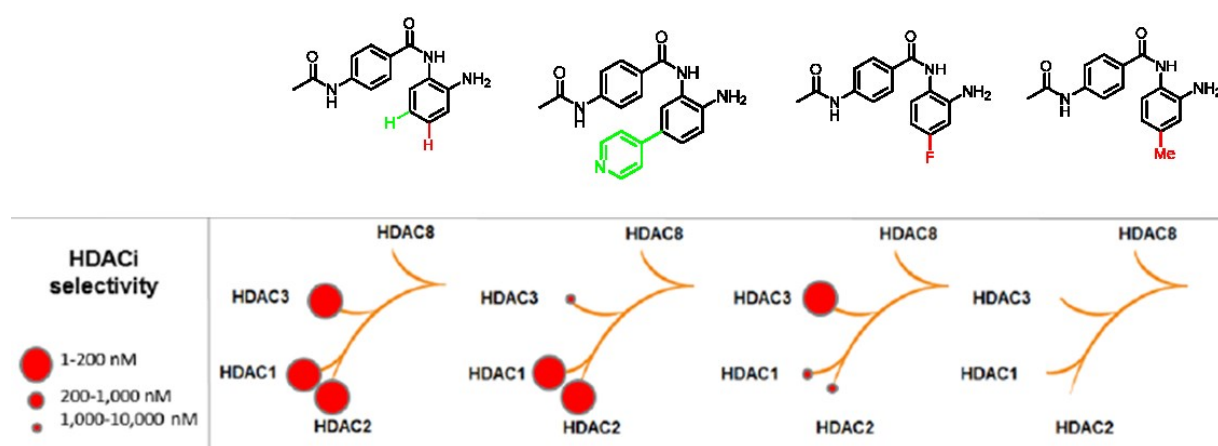


Figure 9: *Ortho*-amino anilides selectivity among class I isoforms.⁵⁶

Another important structural feature present exclusively in HDAC8 is a second sub-pocket in the tunnel region known as side pocket, where Phe152 rotates away from Met274 opening a space that can be occupied by bulkier linkers or substituents in the linker from HDACi.⁶³

1.1.7. Histone deacetylases class II

1.1.7.1. Histone deacetylases class IIa

Class IIa consists of HDAC4, 5, 7 and 9 and their expression occurs in various tissues being closely related to cell differentiation. Their cellular localization is important for this class since they can shuttle between cytoplasm and nucleus, which is essential for the control of the class

activity.⁶⁴ The members of this class are parts of multi-enzymatic corepressor complexes like HDAC1-3, an example of that is the existence of the myocyte enhancer factor 2 binding domain (MEF2) in all isoforms of this class. The presence of class IIa in complexes is not restricted to MEF, they are also parts of complexes such as N-COR and SMRT, which contain HDAC-class I isoforms.^{64,65}

The role of HDACs class IIa isoforms appears to not be related to their deacetylase activity, what can be surely attributed to their poor catalytic capacity. The low catalytic activity is a consequence of the switch of the classic catalytic tyrosine to a histidine residue.⁶⁶ This histidine shows two types of conformations in the crystal structures, it can face the inside of the binding site like the tyrosine found in the other isoforms (flipped-in) or oriented towards the outside of the binding site (flipped-out).⁶⁷

In the flipped-out position, the area between the histidine and the zinc ion forms a sub-pocket, known as lower-pocket. This structural feature of the class IIa has been successfully approached using two different chemical entities: tetra-substituted cyclopropane hydroxamates and trifluoromethyloxadiazolyl (TFMO) derivatives (Figure 10).⁶⁸⁻⁷⁰

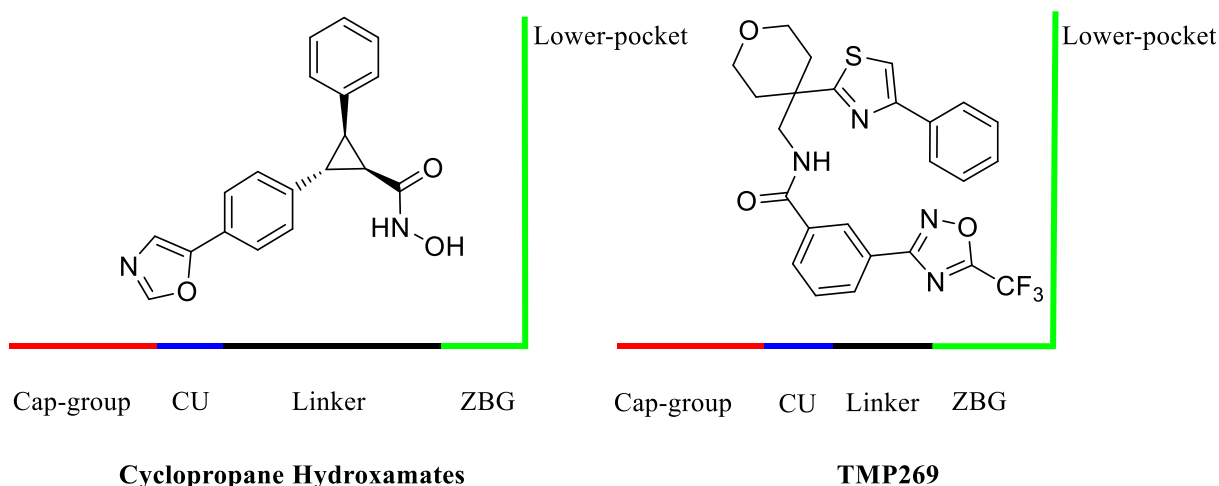


Figure 10: Pharmacophore of class IIa selective inhibitors.

The cyclopropane hydroxamates require a well-defined stereochemistry of its substituents in order to direct the phenyl ring to the lower-pocket. The necessary stereochemical requirements of this class represent a synthetic challenge, restricting the variation in their structures. However, despite the low synthetic tractability, these inhibitors are promising, since, in addition to high potency against class IIa enzymes, the cyclopropane ring improves the pharmacokinetic properties of the hydroxamic acid.^{68,69}

TFMO analogs were described as nonchelating inhibitors based on the distances of the ZBG to the zinc ion observed in their crystal structures.⁷⁰ It was also observed in the crystal structures that the inhibitors assume a U-shaped conformation. In this conformation, the phenyl ring opposite to the ZBG occupies the lower-pocket in a similar manner to cyclopropane hydroxamates.^{68,69}

1.1.7.2. Histone deacetylases class IIb

Class IIb consists of HDAC6 and HDAC10, two isoforms with different biological function. The structure of HDAC6 is more complex compared to the other isoforms, which differentiate the protein from all the other orthologues, also explaining the variety of processes the isoform is involved. Moreover, due to the presence of an ubiquitin-binding zinc finger domain (ZnF-UBP), HDAC6 can interact with ubiquitinated misfolded proteins acting in the ubiquitin-proteasomes system.^{71,72}

HDAC6 is a major α -tubulin and cortactin deacetylase. These substrates are crucial in the cytoskeletal dynamics thus affecting the cellular shape, division, transport, and migration.^{73,74} Additionally, HDAC6 can deacetylate the heat shock protein 90 (Hsp90), which depends on its modification to be able to interact with the respective client protein, being also associated with the removal of misfolded proteins.^{75,76}

HDAC6 is mainly found in the cytoplasm, anchored by a serine-glutamate rich region. However, the enzyme is also found in the nucleus normally associated with ligand-dependent corepressor (LCoR).⁷⁶

To fulfill its intricate physiological role, HDAC6 has a specialized catalytic machinery consisting of two catalytic domains, being the only HDAC possessing two fully functional catalytic domains (CD). CDI (residues 87-404) and CDII (residues from 482-800). The two domains interact with each other through a large domain-domain interface, being physically connected by a loop, this loop is also responsible for the interaction with motor proteins.⁷⁷

Although both domains are necessary for the enzyme activity, CDI contributes to the overall activity less than CDII and isolated CDI shows no catalytic activity. CDI is, however, active when bound to an inactivated CDII and in a similar manner CDII is slightly less active in the absence of CDI, suggesting that the catalytic domains stabilize the general structure of the protein.^{77,78}

The structure of CDII catalytic site shares more similarity to the other HDAC isoforms than CDI. In the catalytic site of CDI, one of the two phenylalanine residues that form the

hydrophobic tunnel is replaced by the Trp261 (HDAC6 numbering). The catalytic site of CDI is also tighter compared to CDII catalytic site due to Lys330, which is encountered directly over the catalytic site. In CDII instead of Lys330 the Leu712 occupies this region.

The Lys330 acts as a gatekeeper and explains the selectivity of this catalytic domain towards C-terminal acetyl-lysine substrates, where it can interact with the free carboxyl group. Given that, the commonly used fluorogenic substrates used in HDAC6 assays do not interact with CDI.^{77,78}

Mutations in the structure of the Helix H25 and the loop H20-H21 of the second catalytic domain CDII lead to a loss of tubulin-deacetylase activity, however not affecting the deacetylase of small peptides. The crystal structure indeed revealed a large basin formed between the helix and the loop, which should serve as recognition platform for large peptides (Figure 11).⁷⁸

Despite the differences, both catalytic domains share a common characteristic. Instead of an aspartate residue anchoring the peptide bond in the substrates, CDI and CDII have a serine residue (Ser150 in CDI and Ser531 in CDII). In the crystal structures of HDAC6, this residue was shown to have the ability to build a direct/indirect hydrogen bond with the connecting unit of inhibitors.⁷⁷⁻⁷⁹ Another common structural feature present in both CDs is the shape of the binding site since HDAC6 binding site entrance is wider and shallower compared to the other orthologues (Figure 11).^{78,79}

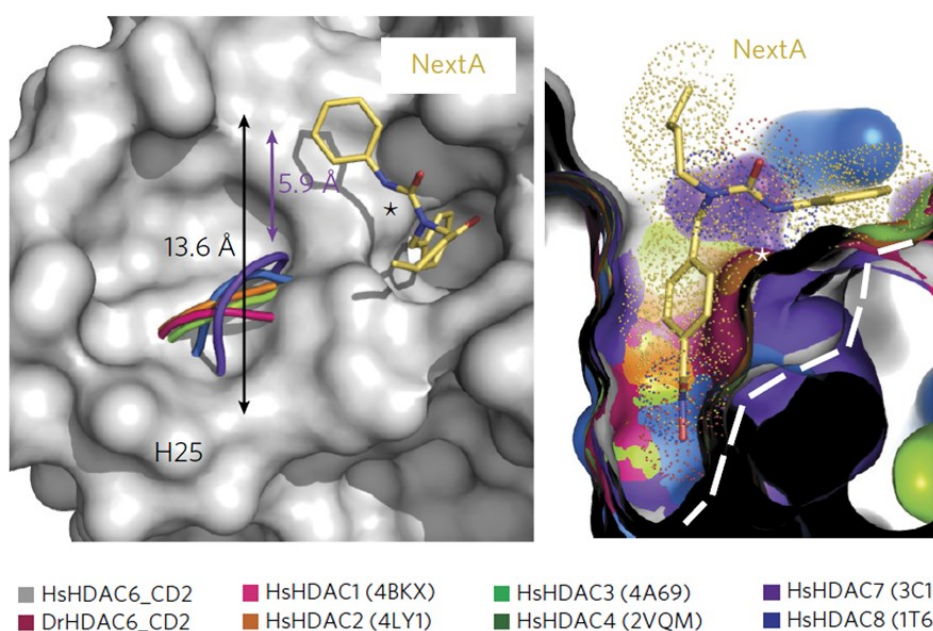


Figure 11: Crystal structure HDAC6 CD2 showing the large basin (left) and the shallow binding site (right).

The crystal structures of HDAC6 containing classical pan-HDACi such as TSA, Belinostat and, Panobinostat demonstrated the tendency of these molecules to interact with a specific region in HDAC6-CDII ranging from Asp460 to Pro484. Furthermore, the hydroxamates were coordinated in a bidentate fashion, while the HDAC6-selective inhibitors, with the exception of Ricolinostat, were found to not disrupt the water present in the binding site, therefore showing a monodentate interaction with the metal.⁷⁷⁻⁷⁹ As mentioned previously, the connection between mono and bidentate coordination and inhibitory activity is inconsistent. To support this affirmation, it was found in the TSA ultra-high resolution crystal structure that the hydroxamate binds in both bidentate/monodentate ways on the ratio 70:30⁷⁹, which is also observed in other metalloproteins.⁸⁰

Isoform selectivity towards HDAC6 is better explained by the shape and interaction with its surface rather than the zinc binding. The shallow binding site can accommodate inhibitors containing short-bulky inhibitors as Nexturastat A, which can roughly present Y-shaped conformation. Additionally, the unique recognition surface present in this isoform favors the interaction with large cap-group as observed in Ricolinostat (Figure 12).

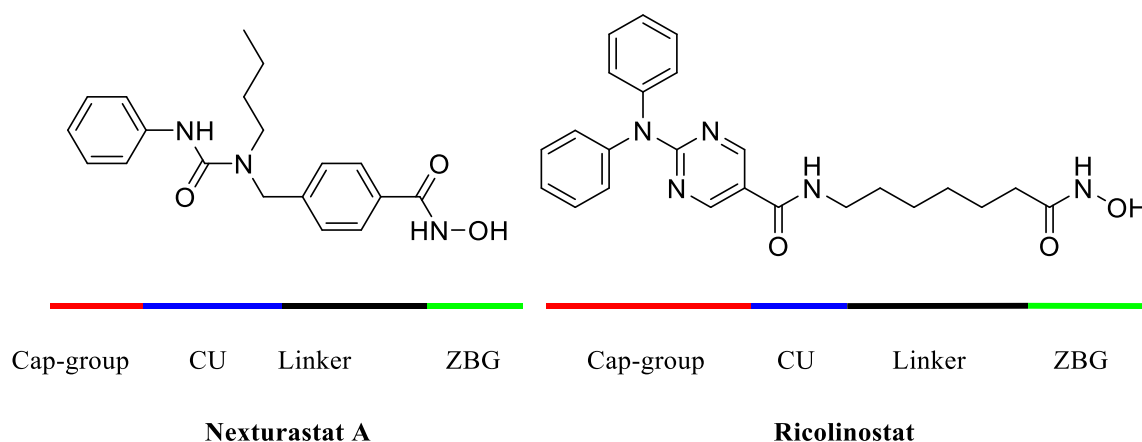


Figure 12: HDAC6 selective inhibitor pharmacophore

HDAC10 is as HDAC6 mainly found in the cytoplasm. The enzyme contains also two spaced catalytic domains, but only one of them is active. The functional catalytic site, however, has poor deacetylase activity towards different acetylated substrates⁸¹. Not much is known about this isoform, but recently the role of HDAC10 as polyamine deacetylase (PDAC) was uncovered.⁸²

Polyamines are vital to all living organisms and its metabolism is highly compartmentalized. The acetylated forms of the polyamines, for example, are only found in the cytoplasm. Structurally, the active catalytic domain could be compared to HDAC6-CDI, since it also

contains an amino acid responsible for the substrate selectivity, but in this case Glu274 (HDAC10 numbering), which is also found directly over the catalytic site, acting as a gatekeeper. Opposite to Lys330 (HDAC6 numbering), the gatekeeper favors interaction with the cationic polyamines instead of C-terminal acetyl-lysine. The Glu274 is also responsible for the specificity towards the different acetylated polyamine. Interestingly, the absence of this specific glutamate enables the enzyme to catalyze deacetylation of acetylated lysine substrates.⁸²

For HDAC10 still, no isoform-specific inhibitor has been identified, what does not necessary discards it as a biological target. On the contrary, the role played in chemo-resistant cancer cell lines and the structural uniqueness make this isoform an interesting good target to be explored.^{83,84}

1.1.8. Histone deacetylases class IV

Class IV contains only HDAC11, the most recently discovered and smallest of all HDAC isoforms. HDAC11 expression is limited to brain, heart, skeletal muscle, and kidney and its cellular localization is still not fully defined, however, it was shown to be associated with HDAC6 in both cytoplasm and nucleus.^{85,86}

HDAC11 shows very low deacetylase activity towards acetylated lysine substrates, and to substrates with different kinds of acetylation.²⁸ It has been just recently observed, that the enzyme has a high catalytic activity towards substrates that release after deacetylase carboxylic acids with long alkylic chains instead of the acetyl group, therefore acting as a fatty-acid deacetylase. HDAC11 amino acid sequence shares the highest similarity with HDAC8, the only other isoform known to have the same affinity to the mentioned substrates. These findings raised the hypothesis that HDAC11 preference for these substrates could be explained by the presence of two internal side-pockets, but lack of crystal structures and studies with mutant enzymes impair the confirmation of this theory.⁸⁷

HDAC11 is the least studied human isoform; consequently, the requirements for molecular selectivity are not clear. Elevenostat was recently reported as the first selective inhibitor, although the structure of this hydroxamate is yet not available, what limits further discussions.⁸⁶

1.1.9. Applications of Histone Deacetylase Inhibitors in Therapy

Understanding and improvement of chemical entities as lead structures for the development of potential drug candidates can be exponentially increased by the analysis of the properties of the drugs being used in clinics.

Histone deacetylase inhibitors have been introduced successfully in cancer therapy in 2006. Vorinostat (Zolinza®), which was approved by the American agency Food and Drug Administration (FDA), is the first HDACi to reach the market. Vorinostat was approved for its use in the treatment of cutaneous T-cell lymphoma (CTCL), a rare heterogeneous group of lymphomas, being considered an orphan drug. In the clinical trials, Vorinostat was well tolerated and the most common adverse effects were diarrhea, fatigue, nausea, thrombocytopenia, and anorexia.⁸⁸

Three years later Romidepsin (Istodax®), a depsipeptide administrated as a prodrug, received the approval for the same indication (CTCL). In the clinical trial, the most common adverse effects were, similar to Vorinostat, diarrhea, fatigue, nausea, thrombocytopenia and anorexia. The indication of Romidepsin was extended in 2011 to be used in the treatment of peripheral T-cell lymphoma (PTCL) in patients with insufficient response to at least one prior systemic treatment.⁸⁹

PTCL is a group of twenty-three aggressive lymphomas. These heterogeneous diseases are considered to be rare; however, they have an aggressive clinical course normally associated with poor prognosis. The first line therapy consists of the combination of cyclophosphamide, doxorubicin, vincristine, and prednisone (CHOP). Therapeutic responses to CHOP are restricted and associated with cancer remission, justifying the urgency of innovation in therapy.⁹⁰

Considering the difficulties in the therapy of PTCL, in 2014 Belinostat (Beleodaq®) received an accelerated approval by the FDA. Belinostat like Vorinostat and Romidepsin showed nausea, fatigue, thrombocytopenia, and anemia as most common adverse effects.⁹¹

The latest HDACi approved for PTCL is Chidamide (Epidaza®), the first *ortho*-amino anilide to reach the market, being so far only approved in China. The new class showed better pharmacokinetic properties and was more tolerated than the previous HDACi, however, the most common adverse effects were similar to the other HDACi consisting of nausea, fatigue, and anemia.⁹²

Panobinostat (Farydak®), approved few months before Chidamide, is the only HDACi approved by the European Medicines Agency (EMA). Different from drugs mentioned before,

Panobinostat was approved for the therapy of Multiple myeloma (MM) in patients who received at least two prior treatment regimens with insufficient tumor response. The approval of Panobinostat like the other HDACi was part of an accelerated approval program, due to the difficulties of the treatment of MM.

Multiple myeloma differs from CTCL and PTCL, is a very common disease responsible for approximately 1% of all cancers. MM is however similar to the mentioned lymphomas in terms of challenging therapy. First line treatment for this cancer is still not well-defined, despite the availability of many novel drugs with different and complementary mechanisms of action. Examples of novel drugs are antibodies (Daratumumab, Elotuzumab), proteasome inhibitors (Carfilzomib, Ixazomib) and with the approval of Panobinostat, histone deacetylases inhibitors.⁹³

Panobinostat most common adverse effects also included diarrhea, fatigue, and thrombocytopenia. Special attention should be given to the fact that Panobinostat is used in combination with Bortezomib, a proteasome inhibitor, and dexamethasone.^{94,95}

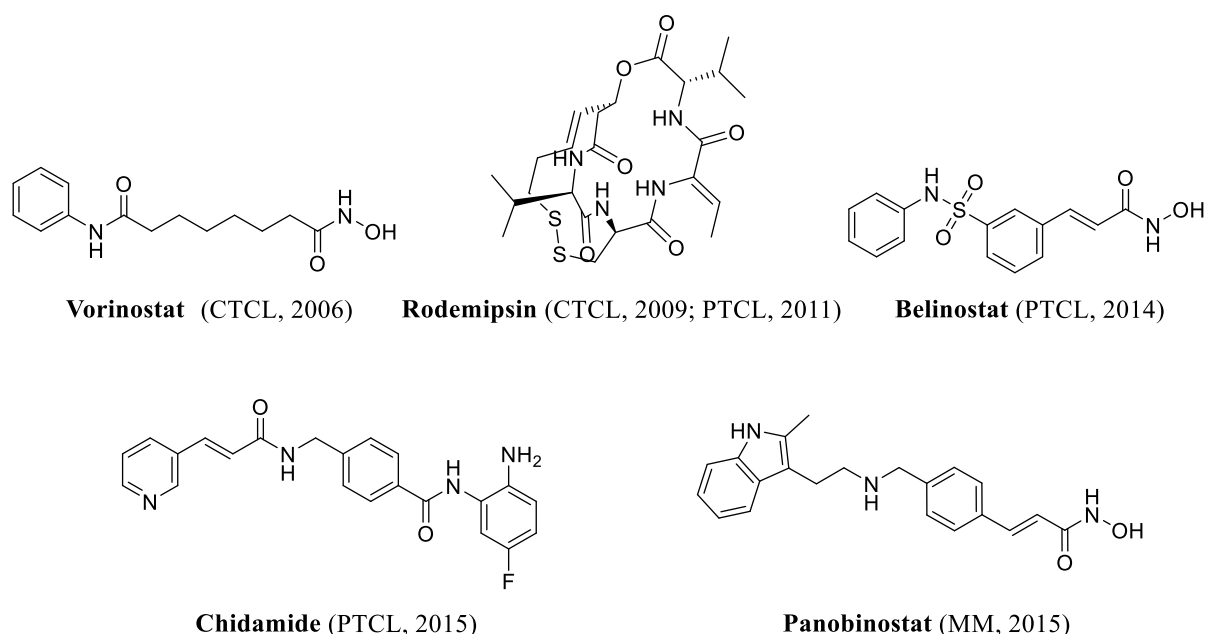


Figure 13: Structures, application and commercial names of approved HDACi.

As exemplified by Panobinostat and Bortezomib, the combination of HDACi with other anticancer drugs, radiotherapy, and immunotherapy have resulted not only in high rates of success in the treatment of specific tumors but also in a powerful alternative to overcome cancer resistance. Epigenetic drugs can lead to specific gene regulation and more generalized effects, which can be beneficial against tumors. Since their growth and development is highly

dependent on chromatin modulation, it is not surprising that synergistic and additive effects can be achieved. Despite the success of HDACi combinations, the underlying mechanisms of potentiating effects are still to be understood and explored.⁹⁶⁻⁹⁸

Following the advances of combination therapy, the advent of HDAC dual inhibitors became another profiting use of HDACi. The inclusion of epigenetic drugs in the multi-target strategy is promising. Several types of combinations of epigenetic drugs with other classes such as: inosine monophosphate dehydrogenase, statin inhibitors, nitric oxide (NO) donors, thalidomide and tubulin-targeting drugs have been performed.^{22,99}

Naturally also the association with DNA-modifying agents (cisplatin, nitrogen mustards, DNA topoisomerases), drugs that interact with hormone-receptors (retinoid X, androgen/estrogen receptors) and other epigenetic modulators (BET, HAT, DNMTs) have been explored.^{22,97,99} However, the most successful association is HDACi and tyrosine kinase inhibitors as exemplified by the compounds CUDC-101 and CUDC-907, which are currently in clinical trials.

Both inhibitors contain an HDACi moiety and a tyrosine kinase inhibitor nucleus, both connected by the solvent-exposed/protein-surface interaction part of each inhibitor (Figure 14).

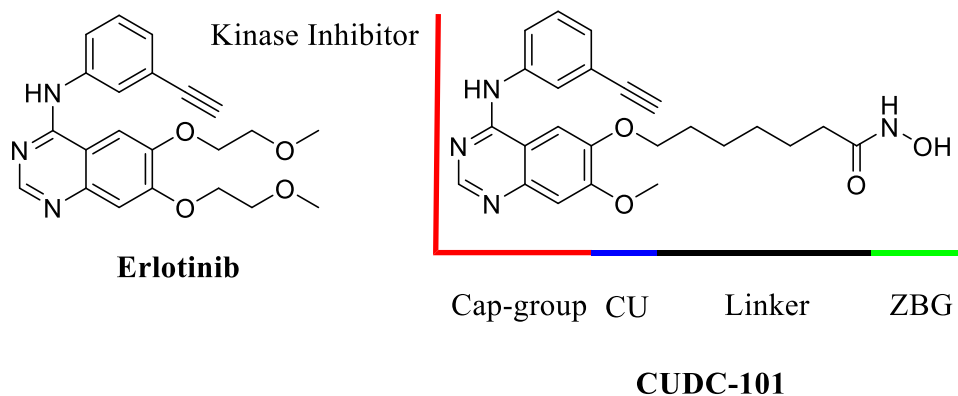


Figure 14: CUCD-100 a dual HDAC/Kinase inhibitor adapted to the classical HDACi pharmacophore.⁹⁹

Most of the epigenetic dual inhibitors have HDAC as target⁹⁹, reinforcing the importance to this class as direct and indirect (non-histone related actions) epigenetic modulator.

Despite the focus of the application of HDACi as anticancer agents, the complexity of the isoforms and the physiological actions, their application in infirmities related to genetic alterations is also consistent (Figure 15).

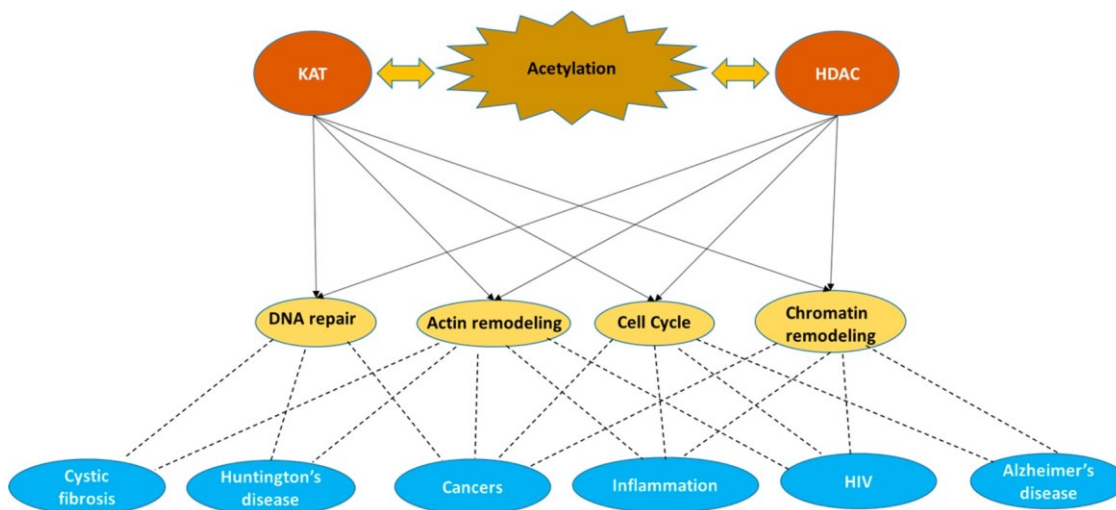


Figure 15: Schematic representation of process related to acetylation regulation and their influence in different human diseases.¹¹

The regulation of protein acetylation affects not only genetic and physiological diseases but also infectious diseases. The process is related to both host response to a pathogen and disrupting the pathogen homeostasis.⁹⁸

Coordination and balance between innate and adaptive immune response depend on a fine regulation of gene expression, both responses require adaptability to respond to different photogenic organisms making chromatin configuration crucial for immune response. Furthermore, the replication of retrovirus as, for example, HIV-1 is directly related to the host transcription factors, which is especially relevant in the elimination of the latent forms of the virus. In this context, HDACi are part of the ‘Shock and Kill’ strategy, in which the inhibitors activate the expression of the viral protein consequently facilitating the identification of the affected cells by the host immune system. The success of this approach is currently being evaluated in clinical trials involving different types of HDACi against HIV-1.^{100,101}

HDACi can also be used to directly disrupt pathogen homeostasis, which is suitable for higher organisms like parasitic Protozoa, notably *Leishmania*, *Plasmodium*, *Schistosoma*, and *Trypanosoma*. This particular set of parasites is responsible for a great burden to human health, being promising targets for the study of HDACi as a novel therapeutic option.¹⁰²

The use of HDACi in these pathologies is supported by the fact that parasites express their own specific HDACs with different rates of structural identities to the human proteins and HDACs of other parasites.¹⁰³ Allied to structural difference of parasite orthologues and the drug resistance commonly observed particularly in the genus *Plasmodium*.¹⁰²

The diverse myriad of possible applications implies that safety and bioavailability are undoubtedly aspects to be accounted for. As mentioned, the most common adverse effects

related to the human use of the different classes of HDACi have constitutional, gastrointestinal or hematological character, more specifically fatigue, diarrhea, and thrombocytopenia. The fact that different members of the class share the same toxicities suggests a drug target- and not drug structure- or chemical related toxicity.^{88,89,91,92,94,95,104}

Besides the classical adverse effects, heart-related problems have also been related to HDACi, particularly with Panobinostat, and Romidepsin, in a smaller extent to *ortho*-amino anilide containing HDACi.¹⁰⁴ Indeed some HDACi can interact with the human ether-a-go-go-related gene (hERG) what is known to potentialize the chances of cardiac problems, but also this undesired interaction is structure-related and can be avoided by molecular modification.^{59,105}

Another relevant issue with HDACi consists in its mutagenic potential, the exact cause of this is yet unknown. Among the commercial HDACi, only three hydroxamates have demonstrated *in vitro* mutagenic potential. Therefore, the hypothesis that the hydroxamates could undergo a Lossen rearrangement resulting in the formation of a reactive isocyanate was raised. The mutagenicity of hydroxamates are however not embedded in all HDACi-containing hydroxamates and still, no direct relationship between the structures of the inhibitors and mutagenicity has been defined.^{106,107}

The possible hydroxamate-related mutagenicity is an example of the critics regarding the utilization of metal binding groups in medicinal chemistry. One-third of our proteins are metalloproteins basically present in all biological processes, concurrently showing its importance and the necessary carefulness with off-target effects.¹⁰⁸

Vorinostat along with other drugs containing MBG was demonstrated to in fact not interact *in vitro* with other metalloproteins than their specific target. The drugs were not able to act as siderophore and therefore unable to remove iron from transferrin. Additionally, no significant change of the activity of this set of drugs in the presence of an excess of other competing metalloproteins could be found. The results show that enzymatic inhibitors containing MBGs are not more promiscuous than other inhibitor classes.¹⁰⁸

The selectivity of metalloprotein inhibitors can be explained by the crucial role of the pharmacophores and also the structural and electronic properties of the MBG, supported by the fact that the selectivity in these assays was observed only in molecules possessing less developed pharmacophores.¹⁰⁸

As mentioned above not only adverse effects are challenging in the application of HDACi in therapy, but also the pharmacokinetic properties of HDACi are another concern.

Commercial HDACi present a heterogeneous behavior regarding pharmacokinetics. Romidepsin, although used as a prodrug, has poor bioavailability, being classified as class IV

drug according to the Biopharmaceutical Classification System (BCS), since it is also extensively metabolized by human liver microsomes. Vorinostat shows likewise poor solubility and moderate permeability. The metabolism is focused mainly in the hydroxamic region as observed in Belinostat, which predominantly consists of glucuronidation or hydrolysis of the hydroxamic acid. Panobinostat, on the other hand, is highly soluble and permeable being a class I drug in the BCS, however, it shows low bioavailability due to the high rate of metabolism.¹⁰⁴

The great part of the bioavailability problems with the hydroxamates is caused by the hydrolysis to its respective carboxylic acid, although it can be avoided by changing the electronic environment adjacent to the hydroxamate.¹⁰⁹

The approval of HDACi mainly occurred in accelerated programs, consequently, pharmacokinetic proprieties and adverse effects are still problematic. However, the current clinical experience indicates that adverse effects are rarely life-threatening and generally well manageable. Also, the pharmacokinetic characteristics of this class can be optimized through molecular modifications, making the design of HDACi a complex, but a promising task.

2. Objectives

The aims of this work were to design and synthesize novel molecules as HDACi and explore their biological activity: (i) to evaluate their antimalarial activity against the protozoa *Plasmodium falciparum* in sensitive (3D7) and multi-resistant (Dd2) cell strains (ii) to evaluate their anticancer potential of the synthesized compounds by cell viability assays in three types of cancer, oral squamous carcinoma, ovarian carcinoma and glioblastoma.

3. Histone Deacetylase inhibitors with antimalarial activity

3.1. Project background

The human infection by the protozoa from the genus *Plasmodium*, commonly known as Malaria, remains a threat to human health substantially for children. Five species of the parasite can infect humans, *P. falciparum*, *P. malariae*, *P. ovale*, *P. vivax* and rarely *P. knowlesi*. *P. falciparum* and *vivax* are the most menacing ones, since *P. falciparum* is the major cause of malaria on the African continent and *P. vivax* in the rest of the world.¹¹⁰

The life cycle of the genus *Plasmodium* alternates between vertebrate and invertebrate hosts (Figure 16). In the vertebrate host, the cycle begins when sporozoites reach human blood by a bite of the *Anopheles* mosquito (Figure 16A). After the parasite reaches the bloodstream, they infect hepatocytes and start the asexual replication (Figure 16B).¹¹¹

The asexual replication results in the formation of schizonts but can also lead in some cases to the generation of latent forms known as hypnozoites. When the schizont lysis occurs, merozoites are released in the bloodstream infecting red blood cells (RBC). Inside the RBC, merozoites change to the ring stage (Figure 16C) and can transform into an asexual form called trophozoite or a sexual form called gametocytes (Figure 16D).¹¹¹

In the invertebrate host, the cycle continues when the *Anopheles* mosquito ingests contaminated blood containing gametocytes and the male and female gametocytes fuse inside the insect gut resulting in a zygote. The zygote invades the mosquito cells becoming an oocyst, which after lysis liberates sporozoites, the form responsible for infecting the vertebrate host, closing the cycle (Figure 16E).¹¹¹

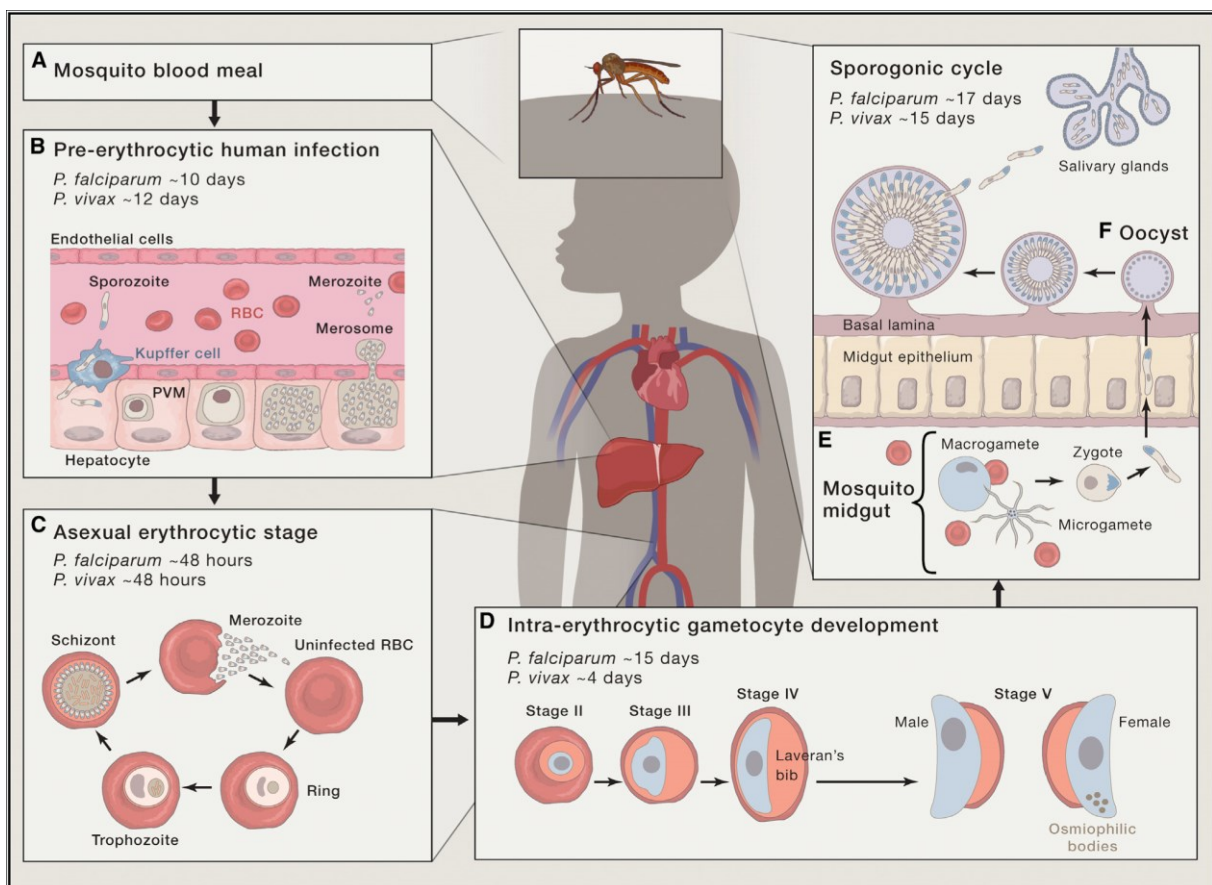


Figure 16: The life cycle of the *Plasmodium sp*¹¹¹

Malaria can manifest in an uncomplicated or severe form. Symptoms of the uncomplicated form are fever, malaise, headache and lethargy; however, it has a good prognosis. In the severe form, the central nervous system is compromised, severe anemia and pulmonary edema can be observed, being the main cause of death associated to Malaria.¹¹¹

Despite considerable research efforts, still no vaccine reached the market and treatment of malaria is restricted to antimalarial drugs. The standard therapy includes different classes of drugs: analogues of the alkaloid Quinine; analogues of the sesquiterpene Artemisinin; naphthoquinones and antimetabolites targeting the folic acid metabolism (Figure 17). The use of Quinine or Artemisinin as monotherapy is limited because of the recurrent resistance. The World Health Organization (WHO) recommends the treatment of Malaria using the Artemisinin-based combination therapy (ACT). However, resistance to the combination therapy has already been observed, showing the importance of the development of new therapeutic classes.¹¹⁰⁻¹¹²

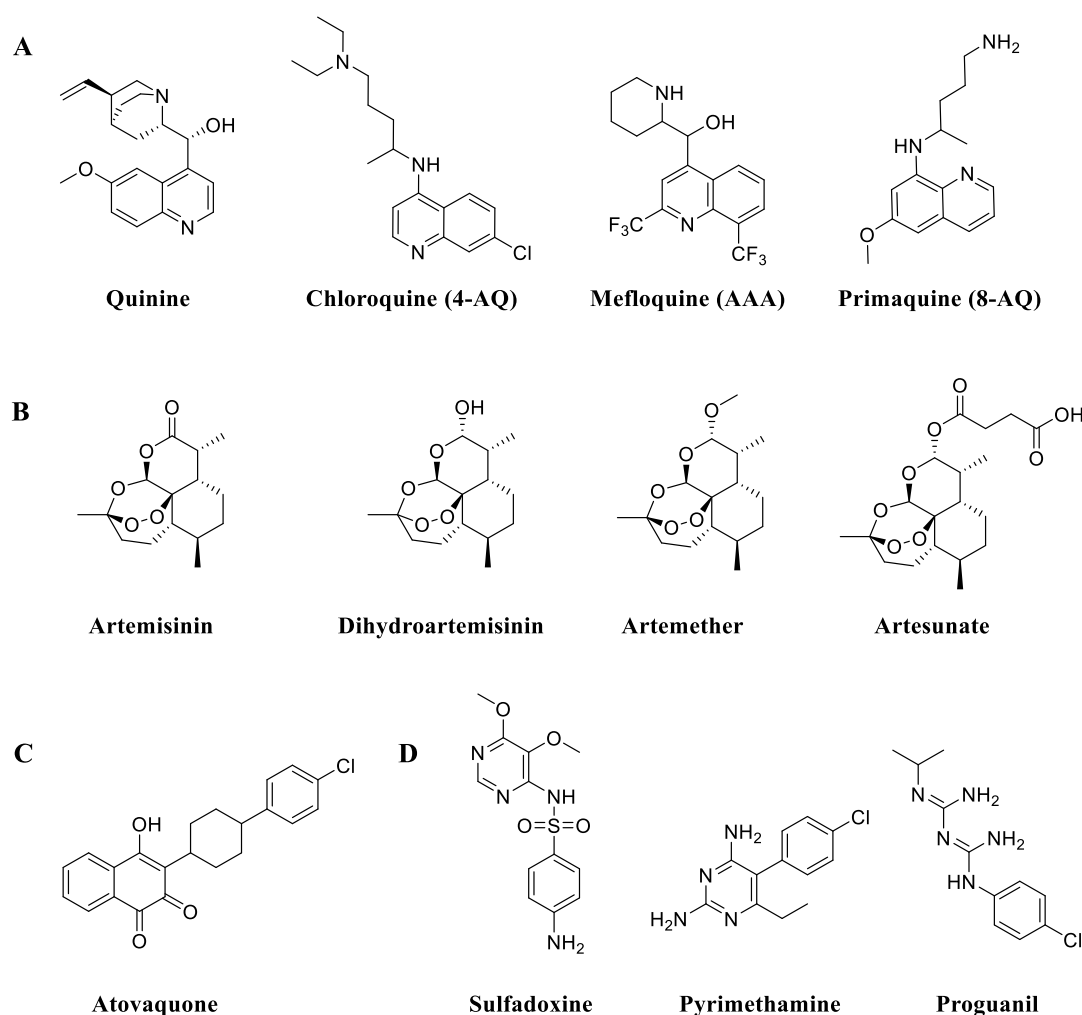


Figure 17: Classes of antimalarial drugs A) Quinine derivatives: aryl-amino alcohol (AAA), 4-aminoquinoline (4-AQ) and 4-aminoquinoline (8-AQ) B) Artemisinin-based drugs C) Naphthoquinones D) Folate antimetabolites.¹¹¹

In the classical therapy, only asexual stages are affected, resulting in the exclusive treatment of the symptoms related to the high parasitemia. But also, elimination of sexual stage is vital, since it interrupts the transmission of the diseases. Additionally, without elimination of the latent forms relapse of the disease can occur.^{110,112}

New classes of antimalarial drugs should ideally affect multiple stages of the parasite at low concentrations and have novel mechanism of actions, which are unable to select resistance. Another important characteristic for potential new chemical entities are long plasma half-life, therefore being possibly used as a preventive measure. Figure 18 shows the global portfolio of new antimalarial medicines organized by Medicines for Malaria Venture (MMV), containing the most promising drug-candidates to be included in malaria therapy.^{113,114}

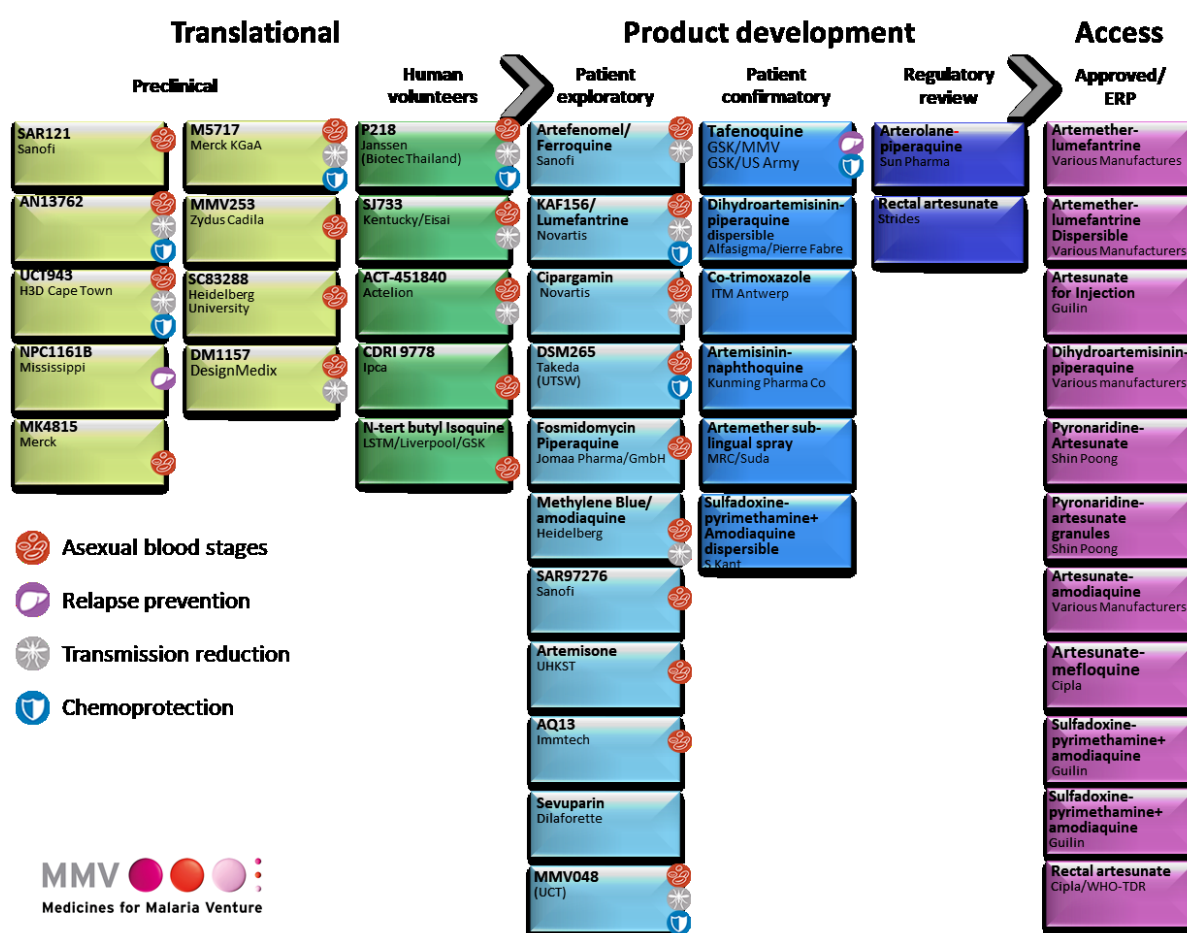


Figure 18: Global Portfolio of Antimalarial Medicines.¹¹³

In this pipeline, only ACTs and members of the classical antimalarials classes are in the more advanced stages. Molecules with novel mechanisms of action have reached so far patient exploratory phases. The antimalarial drug candidates with novel mechanism of action include two adenylypyrophosphatase-4 inhibitors (ATP4) SJ733 and Cipargamin; KAF156, which

interferes with cyclic amine resistance locus protein (CARL) and four enzymatic inhibitors P218, MMV048, DSM265 and Fosmidomycin (Figure 19).

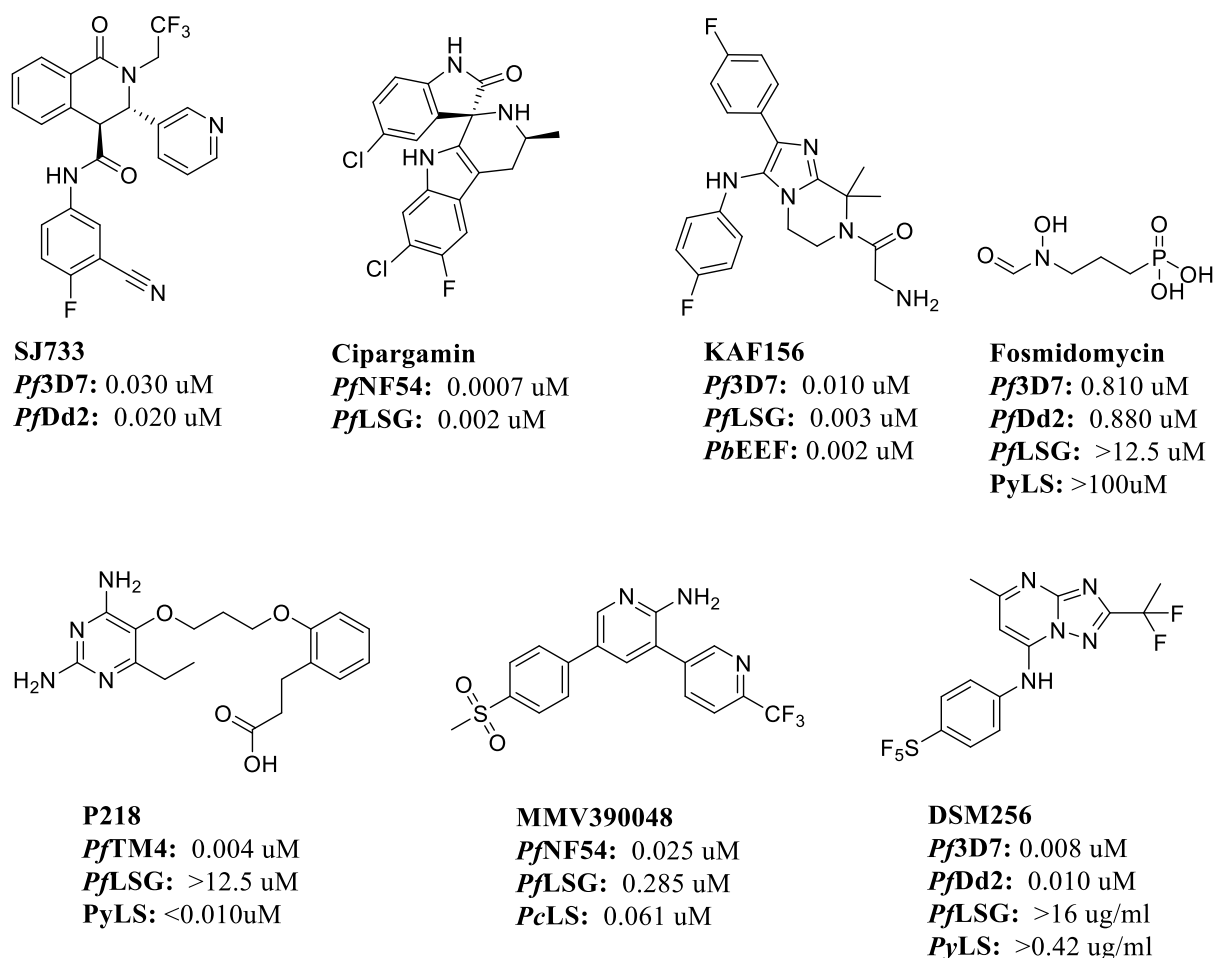


Figure 19: Malaria drug candidates with new mechanism of action to reach clinical trials and their *in vitro* potency against asexual blood stages (*Pf3D7* and *PfNF54* and *PfTM4* sensitive to chloroquine and the multiresistant strain *PfDd2*)^{112,115–118}, late stage gametocytes (*PfLSG*)^{119–123} and liver stages of *P. yoelii* (*PyLS*), *PfNF54* (*PfNF54*-LS), *P. cynomolgi* (*PcLS*) and *P. berghei* exo-erythrocytic forms (*PbEEF*).^{121–124}

PfATP4 transporters are important in the osmotic regulation in several stages of the parasite, being also associated to mechanism of resistance against different antimalarial classes. This biological target is also found in humans, but no significant toxicity was observed in their clinical trials.¹²⁵ In addition to *PfATP4* inhibitors SJ733 and Cipargamin, the drug candidate KAF156 introduced a new class of antimalarials. This molecule interacts with the cyclic amine resistance locus protein, which is exclusively found in the parasite. The physiological role of this protein is still unclear, but studies of homologs suggested its possible role in protein folding.¹²⁶

The four enzymatic inhibitors to reach clinical studies against malaria, either hit a target exclusively present in the parasite or preferentially inhibit the parasitic isoenzyme.¹²⁷ Fosmidomycin inhibits the enzyme 1-deoxy-D-xylulose-5-phosphate found in apicoplasts of the parasite. The enzyme catalyzes the second step of the non-mevalonate pathway of the isoprenoid biosynthesis, which is not present in humans.¹²⁸ The compounds P218 and DSM265 inhibit dihydrofolate reductase (DHFR) and dihydroorotate dehydrogenase (DHODH) respectively. DHODH is part of the de novo synthesis of pyrimidines, while DHFR in the de novo synthesis of purines both essential to the parasite, but not to humans.¹¹¹ MMV048 inhibits phosphatidylinositol-4-kinase (PI4K), which is strongly related to resistance mechanisms to multiple antimalarials drugs, while in humans their inhibition is well tolerated.¹²⁷ The success of the enzymatic inhibitors in reaching clinical phases as antimalarial agents reinforce the potential of HDACi as antimalarial agents.

3.2. Histone deacetylase in *Plasmodium falciparum*

Plasmodium falciparum expresses five HDAC isoforms, two are sirtuin-like proteins and three are zinc-dependent enzymes, namely PfHDAC1, 2 and 3. PfHDAC1 is a nuclear enzyme and is present in asexual intraerythrocytic parasites, gametocytes, and sporozoites. The structure of PfHDAC1 is related to human class I enzymes and is the main responsible for deacetylation of histone and non-histone substrates.¹⁰² This isoform shares more than 50% amino acid identity to human HDAC1, 2 and 3, being highly conserved among the other species from the genus Plasmodium, with more than 90% of amino acid identity to *P. vivax* and *knowlesi*.¹²⁹ The isoforms PfHDAC2 and 3 have yet not being isolated, however, the genes encoding their amino acid sequence have been identified. According to the genetic information, their amino acid sequence differs from all other isoforms from human and protozoans. Even the catalytic site in these isoforms has a low amino acid sequence identity to other HDACs (16% to the HDAC8 catalytic site), what is unusual in this class of enzymes. PfHDAC2 and 3 due to the atypical primary structure could not be included in any of the existing HDAC classes and it is also uncertain if the other parasites of the *Plasmodium* species express these enzymes.^{102,130,131} Different HDACi have been evaluated as antimalarials. Among them, the approved drugs Romidespin, Belinostat, Panobinostat and Vorinostat are known to affect more than one class of human HDACs, were able to inhibit *in vitro* the growth of both sensitive and resistant asexual

blood stage of the parasite at nanomolar concentrations (Figure 20), demonstrating the potential of this class against malaria.^{129,132}

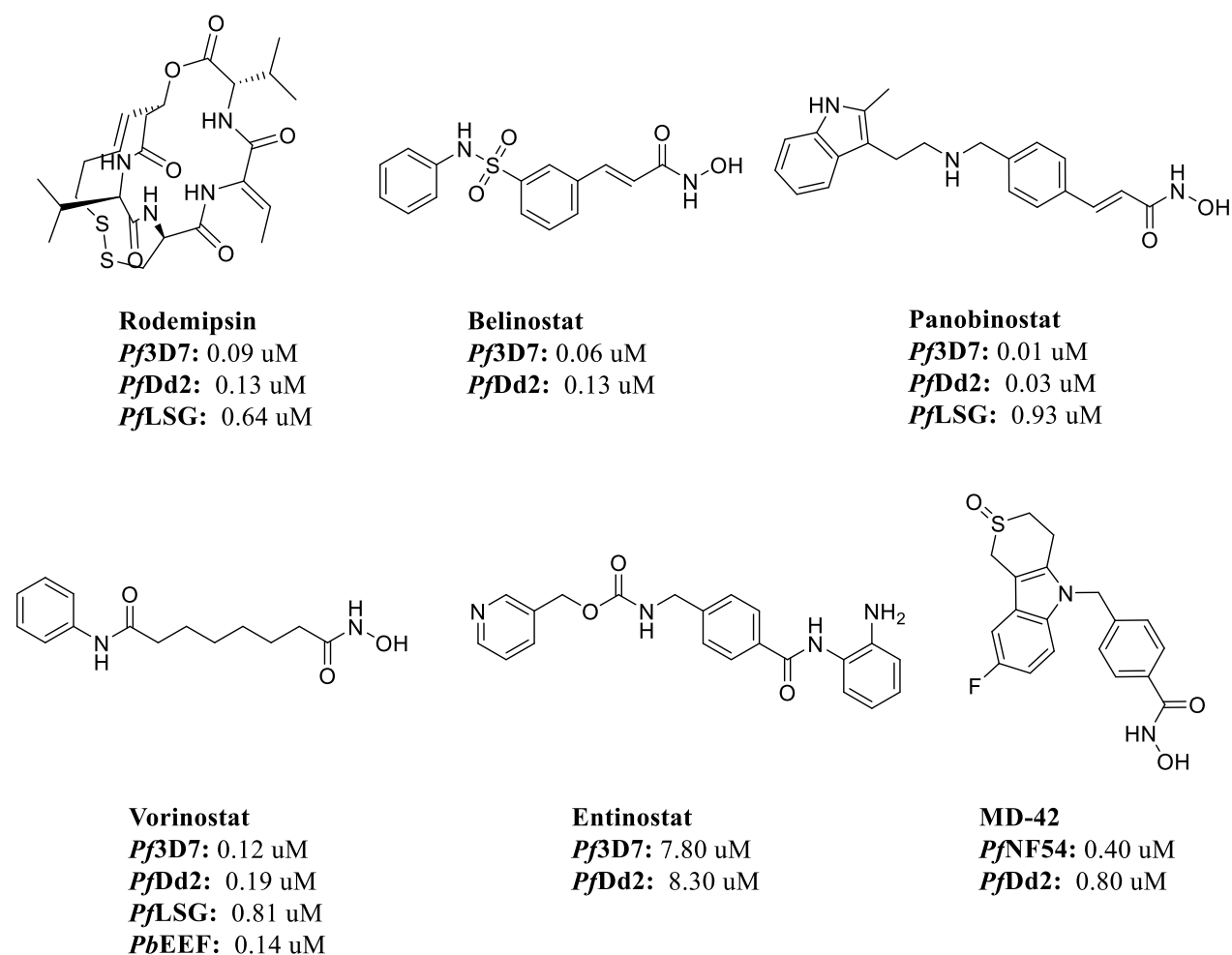


Figure 20: HDACi and their *in vitro* activity against chloroquine sensitive (*Pf3D7* and *NF54*) and multi-resistant (*Dd2*) asexual stages of *P. falciparum*.^{130,132,133}, late stage gametocytes (*PfLSG*)^{132,134,135} and *P. berghei* exo-erythrocytic forms (*PbEEF*).^{132,134}

The effects of isoform-selective HDACi in malaria parasites is still not clear. The selective inhibitor of human HDAC6 MD-42, despite the lack of an orthologue of this isoform in *P. falciparum*, was able to stop the growth of asexual blood stages of the parasite in similar concentrations to the commercial HDACi (Figure 20).¹³³ However, the *ortho*-amino anilide Entinostat, a class I selective inhibitor, was considerably less potent against the same strains.¹³⁰ These findings demonstrated the importance of the evaluation of new HDACi against the malaria parasites.

In order to further explore the potential of HDACi as antimalarial agents, focusing on the structure of the structure of *Pf*HDAC1 a homology model was used to aid the design novel selective hydroxamates as antimalarial agents.

3.3. Project overview

Histone deacetylase inhibitors have shown promising results against different stages of the malaria parasite. The hydroxamate **1** (Figure 21), identified in the working group of Prof. Thomas Kurz at the University of Düsseldorf, was shown to be active at nanomolar concentration against *Pf*3D7 cells, a chloroquine sensitive asexual strain of *P. falciparum*. Compound **1** was also selective towards the parasite cells, showing low toxicity when assayed against the mammalian cells HepG2. In addition to that, the compound was also active against the exo-erythrocytic stage of *P. berghei* (Figure 21).¹³⁴ Based on the activity of this compound against all tested parasite stages, it was chosen as the lead structure in this work for further molecular modifications.

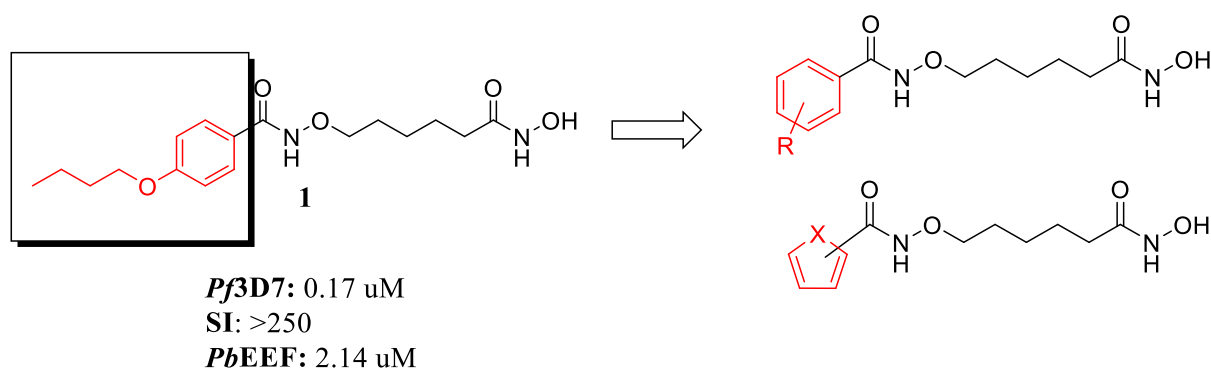


Figure 21: Lead structure of the HDACi designed against Malaria and proposed modifications.

To increase selectivity and potency towards the parasite, the modifications were proposed focusing on the structure of *Pf*HDAC1, the only commercially available isoform.

No crystal structure of *Pf*HDAC1 has been published so far; therefore, to explore its structural features, several homology models of *Pf*HDAC1 were created in this work, using all available human HDAC1, 2 and 3 crystal structures. After that, the models were classified by their structural quality using the programs PROCHECK, PROSA, and ANOLEA.

The homology model with the highest scores in the tested tool was calculated using the crystal structure of human HDAC2 PDB ID 5IWG and used for the comparison of *Pf*HDAC1 and HDAC1, 2 and 3. The structural analysis revealed dissimilarity in a loop at the rim of

*Pf*HDAC1, where the cap-group of HDACi usually binds. Human enzymes HDAC1, 2 and 3 have shorter loops in this region. The elongation of the loop occurs due to the presence of Ala95 and Thr95. To explore this difference, the inclusion of different cap-groups containing hydrogen-bond acceptors in the structure of the compound **1** was proposed.

Based on the difference between parasitic and human HDAC class I isoforms, twelve new inhibitors were synthesized in five-steps and assayed against the *P. falciparum* strains 3D7 and Dd2. The assays were performed in collaboration with the working group of Priv. Doc. Dr. Benjamin Mordmüller and Dr. Jana Held at the University of Tübingen. To assess the selectivity of the inhibitor towards the parasite, the compounds were also tested against the human cells HepG2 in cooperation with the working of Prof. Matthias U. Kassack at the Heinrich Heine Universität of Düsseldorf.

Among all assayed compounds, the compound **6h** containing benzothiophene as cap-group showed the highest activity against both parasite strains, but it was not well tolerated as the lead structure by the mammalian cells HepG2. The presence of methyl terephthalate as cap-group (**6i**) showed, on the other hand, an increase of the selectivity and moderate results against both asexual strains (Figure 22).

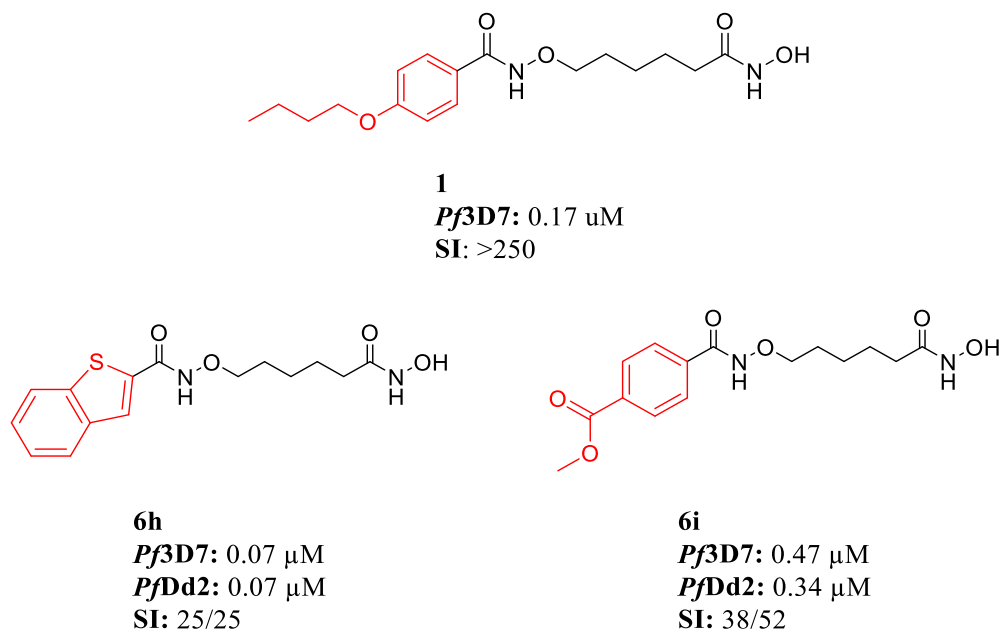


Figure 22: *In vitro* antiplasmodial activity of the lead structure **1** and the most promising synthesized HDACi.

Due to the lack of activity and purity of the recombinant *Pf*HDAC1, the mechanism of action of the compounds were confirmed by hyperacetylation assays performed in cooperation with

Prof. Dr. Katherine Andrews in the Eskitis Institute for Drug Discovery located in Brisbane. The hyperacetylation of H4, a substrate of PfHDAC1 from *P. falciparum* was observed in the presence of five structurally different inhibitors confirming their action as HDACi.

The compound **6h** was 2-fold more active than the lead structure and although its selectivity was lower than the lead structure, the benzothiophene cap-group of **6h** can be further modified by adding e.g. alkyl and alkoxy groups previously demonstrated favorable to the selectivity of HDACi towards *P. falciparum*.¹³⁴ Similarly, the replacement of the methyl group in **6i** by longer alkoxy groups could lead to an increase in the potency and selectivity.

In summary the compounds represent good starting points for the proposal of novel modifications, which could lead to HDACi with a higher selectivity and activity against *P. falciparum*.

3.4. Publication

Design and Synthesis of Novel Anti-Plasmodial Histone Deacetylase Inhibitors Containing an Alkoxyamide Connecting Unit.

*Leandro A. Alves Avelar, * Jana Held, # Jessica A. Engel, § Parichat Sureechatchaiyan, * Finn K. Hansen, * & Alexandra Hamacher, * Matthias U. Kassack, * Benjamin Mordmüller, # Katherine T. Andrews, § Thomas Kurz **

*Institut für Pharmazeutische und Medizinische Chemie, Heinrich-Heine-Universität Düsseldorf, Universitätsstr. 1, 40225 Düsseldorf, Germany.

#Institut für Tropenmedizin, Eberhard Karls Universität Tübingen, Wilhelmstr. 27, 72074 Tübingen Germany.

§Eskitis Institute for Drug Discovery, Don Young Road, Building N.75, Griffith University, Nathan, Queensland, Australia 4111.

&Pharmaceutical/Medicinal Chemistry, Institut für Pharmazie, Leipzig University, Brüderstr. 34, 04103 Leipzig, Germany.

Correspondence: Prof. Dr. Thomas Kurz, Institut für Pharmazeutische und Medizinische Chemie, Heinrich-Heine-Universität Düsseldorf, Universitätsstr. 1, 40225 Düsseldorf, Germany.

E-mail: thomas.kurz@uni-duesseldorf.de.

Tel.: +49 211 81-14984

Fax: +49 211 81-13847

KEYWORDS: Antiplasmodial activity, inhibitors, synthesis.

Summary

Despite recent declines in mortality, malaria remains an important global health problem. New therapies are needed, including new drugs with novel modes of action compared to existing agents. Among new potential therapeutic targets for malaria, inhibition of parasitic histone deacetylases (HDACs) is a promising approach. Homology modeling of *Pf*HDAC1, a known target of some anti-plasmodial HDAC inhibitors, revealed a unique threonine residue at the rim of the active site in close proximity to the location of the cap-group of vorinostat-type HDAC inhibitors. Aiming to obtain HDAC inhibitors with potent and preferential anti-plasmodial activity, we synthesized a mini-library of alkoxyamide-based HDAC inhibitors containing hydrogen bond acceptors in the cap-group. Using a five-step synthetic route, twelve new inhibitors were synthesized and assayed against *P. falciparum* asexual blood stage parasites (lines 3D7 and Dd2) and human cells (HepG2). The most active compound **6h** (*Pf*3D7 IC₅₀: 0.07 μM; *Pf*Dd2 IC₅₀: 0.07 μM) was 25-fold more toxic against the parasite versus human HepG2 cells. Selected compounds were shown to cause hyperacetylation of *P. falciparum* histone H4 indicating inhibition of one or more *Pf*HDACs.

Introduction

Parasites of the genus *Plasmodium* are responsible for considerable morbidity and mortality in tropical regions. According to the latest World Health Organization (WHO) World Malaria Report, malaria was responsible for 214 million cases and 438,000 deaths in 2015, remaining a major cause of death in children in tropical areas [1]. Regardless of high investments in different therapeutic strategies, including the RTS, S vaccine [2], movement towards elimination of malaria will continue to rely on a multi-pronged approach that includes development of new drugs for prevention and treatment of this disease [3]. Although the optimization of classical antimalarial classes still plays an important role (e.g. new combinations/formulations), the successful exploration of new therapeutic targets is a high priority and has led to recent

successes including current clinical development of inhibitors of *Pf*ATP4, *Pf*PI4K and *Pf*DHODH [4-8].

The *Plasmodium* life cycle is complex, involving a wide range of developmental stages that span the mosquito vector and mammalian host. This is associated with a coordinated cascade of gene transcription [9] that is disrupted by treatment with inhibitors targeting histone deacetylase (HDAC) and histone acetyltransferase (HAT) enzymes [10-13]. Targeting *Plasmodium* HDACs is recognized as a promising new antimalarial drug development strategy [4]. HDACs are divided into three zinc-dependent classes (I, II and IV) and one NAD-dependent class (III), also known as sirtuins [14]. The genome of *P. falciparum*, the most prevalent and lethal causative agent of malaria, has three annotated zinc-dependent HDAC isoforms, but recombinant protein (of low purity) is only available for *Pf*HDAC1 [15-19]. Amino acid sequence analysis of the three isoforms expressed by *P. falciparum*, shows that *Pf*HDAC1 has characteristics of class I HDACs, while *Pf*HDAC2 and *Pf*HDAC3 cannot unambiguously be assigned to any of the previously mentioned classes [20, 21].

The structures of HDAC inhibitors (HDACi) are commonly divided according to their binding mode in the HDAC active site and contain a zinc binding group (ZBG), a connecting unit (CU), a linker and cap-group (Figure 1). Vorinostat (SAHA), WR-301801 and SB939 are examples of HDACi with promising antiplasmodial activity (Figure 1). [20]. Our group showed in previous work that inhibitor **1**, containing a hydroxamic acid as ZBG, an alkoxyamide moiety as connecting unit linker region and a 4-butoxyphenyl cap-group was able to cause hyperacetylation of histones *in situ* in *P. falciparum* asexual blood stages and to kill multiple life cycles stages of *Plasmodium* parasites (*P. falciparum* 3D7 asexual blood stages, exo-erythrocytic stage of *P. berghei* and *P. falciparum* NF54 late stage gametocytes) [22].

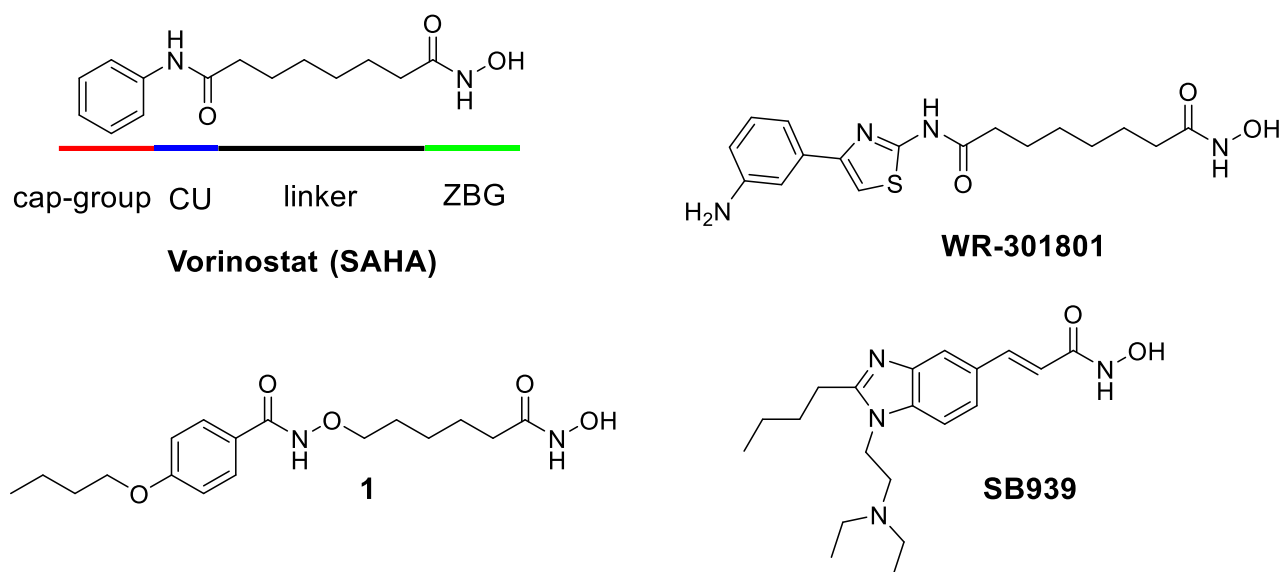


Figure 1: Structure and pharmacophore model of HDAC inhibitors with anti-plasmodial activity.

In this work we rationally designed and synthesized a series of analogues of **1** containing hydrogen bond acceptors in the cap-group. All compounds were tested for activity against drug sensitive and multi-drug resistant asexual blood stage parasites as well as for cytotoxicity against human HepG2 cells. The most promising compounds were further tested for hyperacetylation of *P. falciparum* histone H4 as a marker of HDAC inhibition.

Results

To date no crystal structure of *Pf*HDAC1 has been obtained, but diverse approaches used to create homology models can be found in the literature [15-19]. In this work we employed the software Modeller [23] to create a homology model of *Pf*HDAC1 using a human HDAC2 crystal structure (PDB ID 5IWG) [24] as template. Our homology model showed that the binding sites of *Pf*HDAC1 and human HDACs are highly conserved. However, in agreement with literature data, the homology model showed some subtle differences when comparing *Pf*HDAC1 to closely related human isoforms: one loop at the rim of *Pf*HDAC1 binding site differs from the human HDAC1, 2 and 3, as it is two amino acids longer in *Pf*HDAC1 (Ala95 and Thr95) (Figure 2A) [15-18]. In this region an aspartate residue can be found, which is present in all class I and II human isoforms as well in *Pf*HDAC1 (Asp97) [25]. This conserved amino acid is believed to interact via hydrogen bonding with the nitrogen of the peptide bond in substrates or of the connecting unit in the inhibitors which are critical for the interaction with

the enzyme [17, 25]. In particular Thr95 can be considered as a noteworthy difference when comparing *Pf*HDAC1 with human HDAC1, 2 and 3. Interestingly, Thr95 is located in the loop region where the cap-groups of Vorinostat-type HDAC inhibitors usually bind. Since only *Pf*HDAC1 possesses a hydrogen bond donating side chain in this loop region, we hypothesized that analogues of **1** containing alternative hydrogen bond acceptors might be a suitable scaffold to discover HDAC inhibitors with improved antiparasmodial activity and increased selectivity for the parasite.

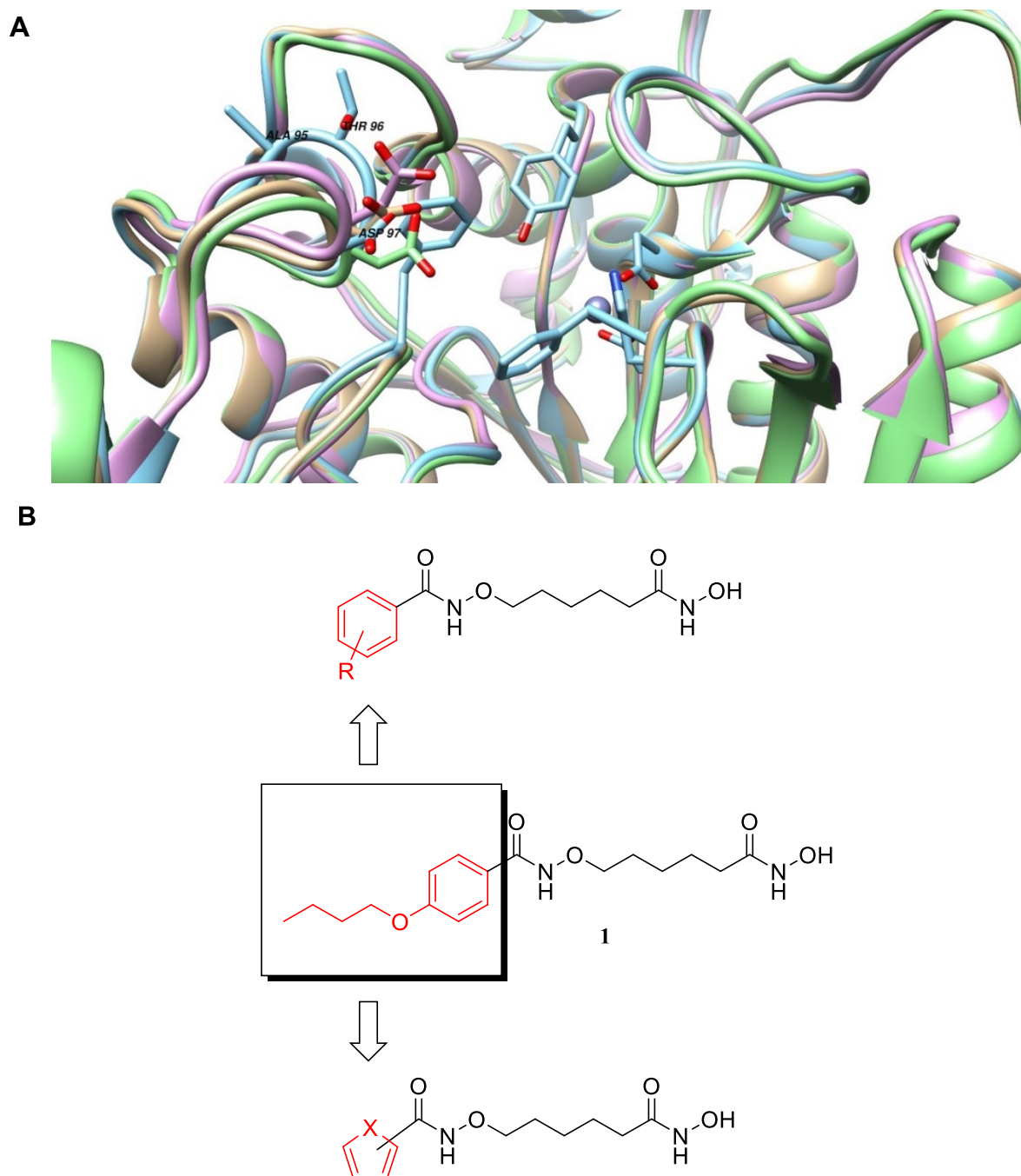
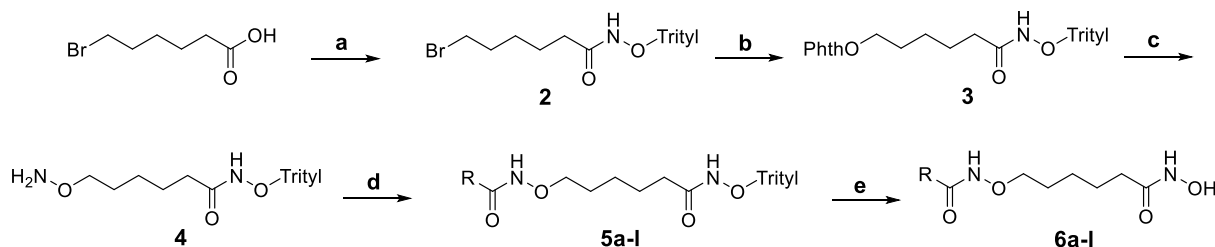


Figure 2: A) Superposition of *Pf*HDAC1 model (light blue) and HDAC1, 2 and 3 (PDB ID 5ICN, 5IWG and 4A69 in pink, light brown and green respectively). B) Proposed changes in the cap-group region.

We therefore designed two series of analogues of **1** featuring hydrogen bond acceptors in the cap-group while retaining the alkoxyamide connecting unit linker region and the hydroxamic acid as ZBG (Figure 2B). In the first series, 5-membered heterocycles were employed as cap-groups (**6a-f**). Since our previously reported structure-activity relationships on alkoxyamide-based HDAC inhibitors [22] indicated that bulky cap-groups can lead to increased anti-plasmodial activity, we also designed fused 5-membered heterocycles such as benzofuran and benzothiophene (**6g, h**). In the second series we replaced the 4-butoxyphenyl cap-group by methyl esters (**6i, j**) and 4-*N, N*-dimethylaminophenyl-based caps (**6k, l**).

The synthesis of the compounds was performed in five steps as demonstrated in Scheme 1 [26]. The alkoxyamide scaffold containing the *O*-trityl protected hydroxamic acid (**4**) was prepared by coupling 6-bromohexanoic acid with the *O*-trityl protected hydroxylamine (**2**) followed by the *O*-alkylation of *N*-hydroxyphthalimide (**3**). The key building block **4** was prepared by deprotection of the phthaloyl group with hydrazine hydrate. Subsequently, **4** was coupled with the respective carboxylic acid of the desired cap-group using EDCI/DMAP as coupling system. Finally, the free hydroxamic acids **6a-l** were obtained by deprotection of the trityl group. Employing the shown synthetic strategy, twelve new HDAC inhibitors were obtained.

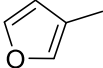
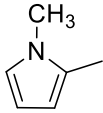
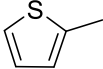
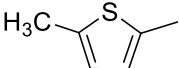
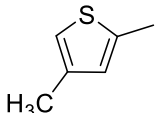
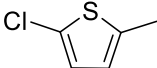
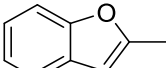


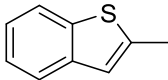
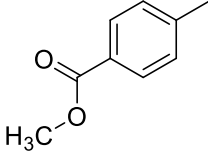
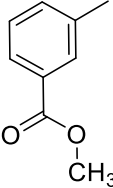
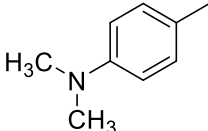
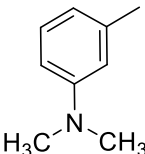
Scheme 1: Reagents and conditions for the synthesis of the hydroxamic acids: **a**) isobutyl chloroformate, NMM, trityl-O-NH₂, DCM **b**) PhthOH, Et₃N, acetonitrile **c**) NH₂NH₂·H₂O, MeOH **d**) EDCI, DMAP, RCOOH, DCM **e**) TFA, Et₃SiH, DCM.

Due to recently reported significant limitations of enzymatic assays with *Pf*HDAC1 in regards to purity of the commercially available enzyme and catalytic activity of the enzyme in the absence of endogenous cofactors [27], we pursued a phenotypic approach in this project [28, 29]. Consequently, compounds **6a-l** were assayed against the chloroquine sensitive *P. falciparum* 3D7 line and the multi-drug resistant *P. falciparum* Dd2 line by measuring growth inhibition based on histidine rich protein 2 assay (HRP2). [30] Compounds **6a-l** showed IC₅₀ values varying from low micromolar to low nanomolar concentrations for both *P. falciparum* strains (0.07–2.38 μM, Table 1). In order to determine the *in vitro* cytotoxicity

towards mammalian cells all inhibitors were tested in cell viability MTT-based assay against the HepG2 cell line [26, 31]. The tested compounds displayed IC₅₀ values at micromolar concentrations (1.12–17.60 μM) and are characterized by low to moderate parasite selectivity (SI 4–52) (Table 1). Additionally, selected inhibitors caused hyperacetylation of *P. falciparum* histone H4 in a hyperacetylation (Figure 3).

Table 1: Anti-plasmodial activity and cytotoxicity of HDAC inhibitors containing an alkoxyamide connecting unit.

Compound	R	<i>P. falciparum</i> IC ₅₀ (μM) ^d		HepG2 ^{b,d}	SI ^c
		3D7 ^a	Dd2 ^a	IC ₅₀ (μM)	3D7/Dd2
6a		0.95	0.78	12.60	13/16
6b		1.32	1.89	9.40	7/5
6c		0.76	2.38	15.40	20/6
6d		0.63	0.56	5.20	8/9
6e		0.20	0.13	2.50	13/18
6f		0.82	0.78	12.10	14/15
6g		0.16	0.08	1.97	12/26

6h		0.07	0.07	1.67	25/24
6i		0.47	0.34	17.60	38/52
6j		0.62	0.51	4.21	7/8
6k		0.12	0.17	1.32	10/8
6l		0.31	0.16	1.12	4/7
	SAHA	ND	ND	1.58	ND
	Chloroquine	0.02x10 ⁻¹	0.28	4.27	2135/15

^{a)} Values are the mean of at least two independent experiments conducted in duplicate, each using 12-point serial dilutions ^{b)} Values are the mean of three independent experiments conducted in triplicate. ^{c)} Selectivity Index (SI) shown for HepG2 IC₅₀/Plasmodium IC₅₀ for line 3D7 and Dd2. Values > 1 indicate greater parasite selectivity. ^{d)} The pIC₅₀ and the standard deviation of all values are provided in the Supplementary Information.

Discussion

Compounds containing the hydrogen bond acceptor as part of a five-membered heterocyclic ring (**6a-f**) inhibited the growth of *P. falciparum* infected erythrocytes with IC₅₀ values ranging from 0.13 to 2.38 μM. However, **6a-f** did not show a high selectivity towards human cells

(Table 1; $SI \leq 20$). The addition of substituents to the thiophene ring (**6d-f**) led to a slight increase in potency compared to the unsubstituted thiophene derivative (**6c**), but without a significant change in the selectivity. Compounds containing the bicyclic cap-group (**6g** and **6h**) had increased activity against *P. falciparum* (**6g** *Pf*3D7 IC_{50} : 0.16 μ M; *Pf*Dd2 IC_{50} : 0.08 μ M and **6h** *Pf*3D7 IC_{50} : 0.07 μ M; *Pf*Dd2 IC_{50} : 0.07 μ M) when compared to five-membered heterocyclic ring (**6c** *Pf*3D7 IC_{50} : 0.76 μ M; *Pf*Dd2 IC_{50} : 2.38 μ M), but the selectivity increased only in a modest degree (**6c** $SI_{3D7/Dd2}$: 20/6 and **6h** $SI_{3D7/Dd2}$: 25/24). The presence of a bicyclic ring in the cap-region (e.g. **6g** and **6h**) resulted in an improved inhibition to low nanomolar IC_{50} s, especially towards the multi-drug resistant *P. falciparum* Dd2 line. Compound **6h** (*Pf*3D7 IC_{50} : 0.07 μ M; *Pf*Dd2 IC_{50} : 0.07 μ M) showed the highest activity against asexual blood stage parasites and was ~25-fold more toxic to the parasites than to HepG2 cells. Among the inhibitors with substituted phenyl rings in the cap-region (**6i-l**), special attention was drawn to compound **6i** (*Pf*3D7 IC_{50} : 0.47 μ M; *Pf*Dd2 IC_{50} : 0.34 μ M). Although it did not present the lowest IC_{50} of this series, it showed low cytotoxicity to HepG2 cells (IC_{50} : 17.60 μ M; SI_{38} and SI_{52} for *P. falciparum* 3D7 and Dd2, respectively). This suggests that among the substitutions in the cap-region, the presence of esters in the para position can lead to an increased selectivity towards the parasite over human cells.

The mode of action of five of the most potent antiplasmodial compounds (**6c**, **6e**, **6g**, **6h**, **6i**) was evaluated by assessing *in situ* changes to the acetylation of *P. falciparum* histone H4, as demonstrated in Figure 3. All five compounds caused hyperacetylation of histone H4 relative to the vehicle control (Figure 3; **C-3h**). As expected, the antimalarial control compound chloroquine did not cause a hyperacetylation effect (Figure 3; **CQ**). Although the hyperacetylation data do not provide direct evidence of *Pf*HDAC1 inhibition, they confirm an effect (either direct or indirect) on *Pf*HDAC activity in a cellular environment. Once pure *Pf*HDAC1 and other recombinant *Pf*HDAC proteins become available, it will be important to profile these compounds for enzyme specificity.

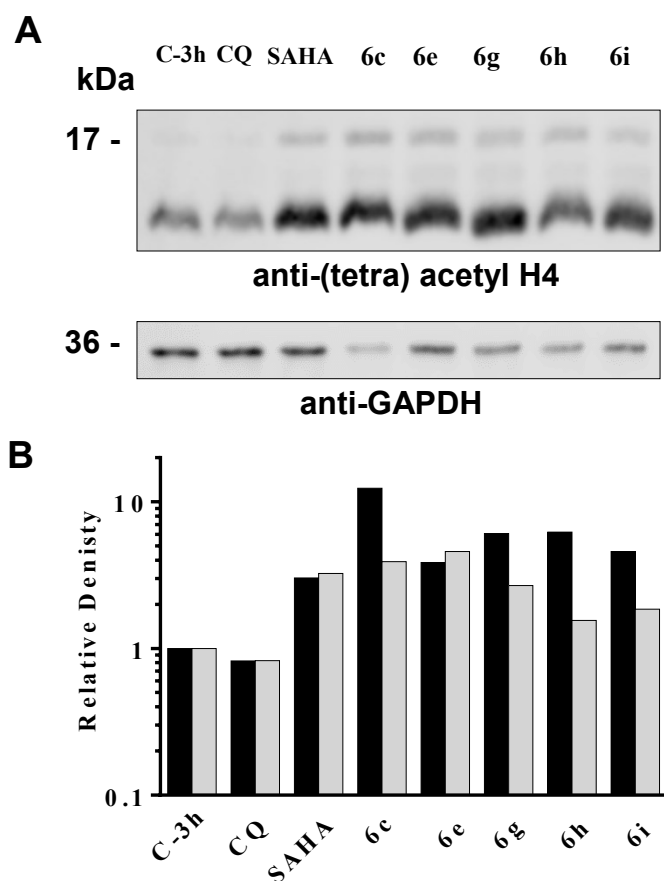


Figure 3: Hyperacetylation of *P. falciparum* histone H4 by HDAC inhibitors (A) Western blot analysis of *P. falciparum* 3D7 protein lysates following 3 h exposure to 5x IC₅₀ of test compounds or the HDAC inhibitor control SAHA (Figure 1). Negative controls were parasitized erythrocytes treated in the same way with 5x IC₅₀ of the antimalarial drug chloroquine (CQ) or compound vehicle only (0.1% DMSO; C-3h). Western blot was carried out with anti-(tetra)-acetyl-histone H4 antibody and IRDye 680RD goat anti-rabbit secondary antibody and, following imaging, sample loading was controlled by probing the same membrane with anti-*Pf*GAPDH antibody and IRDye 800CW donkey anti-rabbit secondary antibody. Membranes were imaged using an Odyssey FC (Li-Cor Biosciences). Sizes in kDa are indicated. (B) Relative density of protein bands detected in Western blot by anti-(tetra) acetyl-histone H4 antibody, normalized to the density of bands in lanes of the corresponding anti-*Pf*GAPDH loading controls and shown as fold change relative to the C-3h DMSO control (set to 1.0). Relative density data are shown for two independent experiments (B); black and grey bars represent independent experiments) with a representative Western blot shown in (A).

In conclusion, in this work we have rationally designed and synthesized a series of twelve new alkoxyamide-based HDAC inhibitors. All compounds inhibited the growth of drug sensitive and resistant *P. falciparum* lines. The benzothioephene derivative **6h** showed the best activity against asexual blood stages with nanomolar IC₅₀ values, albeit only with moderate parasite

selectivity (selectivity index range: 24–25). Notably, compound **6i** (*Pf*Dd2 IC₅₀: 0.34 μM; HepG2 IC₅₀: 17.6 μM) was > 50-fold cytotoxic against the multi-drug resistant *P. falciparum* Dd2 line compared to human HepG2 cells. Selected compounds were shown to cause hyperacetylation of *P. falciparum* histone H4 confirming a likely mode of action in the inhibition of *Pf*HDAC activity. Taken together, compounds **6h** and **6i** represent valuable starting points for further optimization, such as the introduction of substituents in the bicyclic ring, variation of the benzoic esters as well as the replacement of the hydroxamate group by alternating ZBGs.

Experimental

Chemistry

Chemicals and solvents were purchased from commercial suppliers (Sigma-Aldrich, Acros Organics, TCI, Fluorochem, ABCR and Alfa Aesar) and used without further purification. The reactions were monitored by thin layer chromatography (TLC) using Merck precoated silica gel plates (with fluorescence indicator UV254), being visualized by irradiation with ultraviolet light (254 nm) or staining in potassium permanganate solution. Column chromatography was performed using Macherey-Nagel Silica 60 (0.040-0.063 mm) and Flash chromatography using prepacked silica cartridge with the solvent mixtures of hexane/ethyl acetate or dichloromethane/methanol according to the reaction. Melting points (mp) analyses were performed using a Mettler FP 5 melting-point apparatus. Proton (¹H) and carbon (¹³C) NMR spectra were recorded on a Bruker Avance 300, 500 or 600 MHz using DMSO- d₆ as solvent. Chemical shifts are given in parts per million (ppm), relative to residual solvent peak for ¹H and ¹³C. High resolution mass spectra (HRMS) analysis was performed on a UHR-TOF maxi4G, Bruker Daltonics, Bremen by electrospray ionization (ESI). Analytical HPLC analysis were carried out on a Varian Prostar system equipped with a Prostar 410 (autosampler), 210 (pumps) and 330 (UV-detector) using a Phenomenex Luna 5u C18 (2) 1.8 μm particle (250 mm × 4.6 mm) column, supported by Phenomenex Security Guard Cartridge Kit C18 (4.0 mm × 3.0 mm). UV absorption was detected at 254 nm with a linear gradient of 10% B to 100% B in 20 min using HPLC-grade water +0.1% TFA (solvent A) and HPLC-grade acetonitrile +0.1% TFA (solvent B) for elution at a flow rate of 1 mL/min.

Preparation of 6-bromo-*N*-(triphenylmethoxy)-hexanamide (**2**)

6-Bromo hexanoic acid (1.1 eq) was dissolved in 120 mL tetrahydrofuran, followed by the addition of *N*-methylmorpholine (1.1 eq). The solution was then cooled to -10°C and isobutyl chloroformate (1.1 eq) was added. After stirring for 5 min, *O*-(triphenylmethyl)hydroxylamine (1.0 eq) was added and the reaction mixture was stirred overnight. The precipitate formed was filtered and the solvent evaporated under reduced pressure. The obtained product was dissolved in ethyl acetate and extracted with saturated solution of NaHCO₃ and brine. The combined organic layers were dried over Na₂SO₄ and evaporated under reduced pressure. The crude product was purified by flash chromatography using a mixture of hexane/ethyl acetate (0-100% of ethyl acetate).

White powder, yield 82%, mp: 122-123°C, ¹HNMR (600 MHz, DMSO-*d*₆): 1.06-1.11 (m, 2H), 1.19-1.24 (m, 2H), 1.62-1.67 (m, 2H), 1.78 (t, 2H, J = 7.1 Hz), 3.40 (t, 2H, J = 6.8 Hz), 7.29-7.33 (m, 15H), 10.18 (s, 1H). ¹³CNMR (151 MHz, DMSO-*d*₆): 24.33, 27.35, 32.27, 32.37, 35.34, 92.21, 127.87, 127.98, 129.42, 142.92, 170.59. HRMS-ESI [M+H]: m/z calcd. for C₂₅H₂₇BrNO₂: 452.1220, found: 452.1220.

Preparation of 6-[(1,3-dioxo-2,3-dihydro-1*H*-isoindol-2-yl)oxy]-*N*-(triphenylmethoxy)hexanamide (**3**)

N-Hydroxyphthalimide (1.0 eq) was suspended in 100 mL acetonitrile, triethylamine (2.0 eq) was added, resulting in a red solution. To this solution, **2** (1.2 eq) was added and the reaction was refluxed overnight. After cooling down to room temperature, the solvent was evaporated and ethyl acetate was added, followed by washing with saturated solution of NaHCO₃. The organic phase was separated and dried under Na₂SO₄, the solvent was evaporated and the crude product purified by flash chromatography using mixture of hexane/ethyl acetate (0-100% of ethyl acetate) as eluent.

White solid, 61% yield, mp: 143°C, ¹HNMR (600 MHz, DMSO-*d*₆): 1.13-1.16 (m, 2H), 1.25-1.29 (m, 2H), 1.52-1.62 (m, 2H), 1.81 (t, 2H, J = 6.8 Hz), 4.03 (t, 2H, J = 6.6 Hz), 7.34 (m, 15H), 7.86 (s, 4H), 10.21 (s, 1H). ¹³CNMR (151 MHz, DMSO-*d*₆): 24.29, 27.22, 31.69, 77.39, 91.61, 123.10, 127.30, 127.41, 128.50, 128.86, 134.64, 142.37, 163.17, 170.07.

Preparation of 6 (aminooxy)-*N*-(triphenylmethoxy)hexanamide (**4**)

Compound **3** (1.0 eq) was suspended in 50 mL of methanol and hydrazine monohydrate (10.0 eq) was added. The reaction was left under stirring for 2 h at room temperature, and then the solvent was evaporated; the crude product was dissolved in 100 mL of dichloromethane and

extracted with saturated solution of NaHCO₃. The organic phase was collected and dried under Na₂SO₄. The solvent was removed under reduced pressure and the crude product was purified by flash chromatography using mixtures of hexane/ethyl acetate (0-100% of ethyl acetate) as eluent.

White solid, 80.3% yield, mp: 126°C, ¹HNMR (600 MHz, DMSO-d₆): 0.94-0.96 (m, 2H), 1.13-1.18 (m, 2H), 1.32-1.35 (m, 2H), 1.74-1.76 (m, 2H), 3.40 (t, 2H, J = 6.6 Hz) 5.83 (s, 2H), 7.32 (m, 15H), 10.17 (s, 1H). ¹³CNMR (151 MHz, DMSO-d₆): 24.57, 24.87, 27.55, 31.85, 74.57, 91.60, 127.30, 127.40, 128.85, 142.36, 170.15.

General procedure for preparation of **5a-l**

To a stirring dichloromethane solution of the desired carboxylic acid (**5a-l**, 1.1 eq), 1-ethyl-3-(3-dimethylaminopropyl) carbodiimide (EDC) (1.1 eq) was added. The reaction was left under stirring at room temperature for 5 min, **4** (1.0 eq) and 4-(dimethylamino)-pyridine (DMAP) (0.2 eq) were added, after that the reaction was left under stirring overnight. The reaction was diluted with 50 mL of dichloromethane and extracted with 1 x 50 mL saturated solution of NaHCO₃, the organic phase was collected and dried under Na₂SO₄. After the evaporation of the solvent under reduced pressure the crude product was purified by flash chromatography using mixtures of hexane/ethyl acetate (0-100% of ethyl acetate) as eluent.

6-[(Furan-3-ylformamido)oxy]-*N*-(triphenylmethoxy)hexanamide **5a**

White solid, yield 56.0%, mp: 169°-170°C, ¹HNMR (600 MHz, DMSO-d₆): 1.06-1.09 (m, 2H), 1.22-1.25 (m, 2H), 1.44-1.46 (m, 2H), 1.79 (t, 2H, J = 7.3 Hz), 3.74 (t, 2H, J = 6.5 Hz), 6.77 (d, 1H, J = 1.8 Hz), 7.28-7.35 (m, 15H), 7.74 (t, 1H, J = 1.8 Hz), 8.15 (s, 1H), 10.20 (s, 1H), 11.34 (s, 1H). ¹³CNMR (151 MHz, DMSO-d₆): 25.00, 25.18, 27.79, 32.34, 75.77, 92.19, 109.01, 120.35, 127.87, 127.97, 129.43, 142.93, 144.65, 145.58, 170.68. HRMS-ESI [M+H]: m/z calcd. for C₃₀H₃₁N₂O₅: 499.2227, found: 499.2225.

6-[[1-(1-Methyl-1*H*-pyrrol-2-yl)formamido]oxy]-*N*-(triphenylmethoxy)hexanamide **5b**

Yellow solid, yield 53.0%, mp: 74-76°C, ¹HNMR (600 MHz, DMSO-d₆): 1.06-1.10 (m, 2H), 1.20-1.23 (m, 2H), 1.41-1.45 (m, 2H), 1.78 (t, 2H, J = 7.0 Hz), 3.72 (t, 2H, J = 6.5 Hz), 3.80 (s, 3H), 5.99 (dd, 1H, J = 2.6 Hz 3.9 Hz), 6.65 (dd, 1H, J = 1.7 Hz 3.9 Hz), 6.93 (t, 1H, J = 2.0 Hz), 7.29-7.33 (m, 15H), 10.19 (s, 1H), 11.06 (s, 1H). ¹³CNMR (151 MHz, DMSO-d₆): 25.04, 25.24, 27.84, 32.37, 36.38, 75.68, 92.20, 107.22, 112.24, 123.11, 127.87, 127.98, 128.65,

129.43, 142.92, 160.57, 170.71. HRMS-ESI [M+H]: m/z calcd. for C₃₁H₃₄N₃O₄: 512.2544, found: 512.2537.

6-[(Thiophen-2-ylformamido)oxy]-*N*-(triphenylmethoxy)hexanamide **5c**

White solid, yield 77.0%, mp: 176°C, ¹HNMR (600 MHz, DMSO-*d*₆): 1.06-1.10 (m, 2H), 1.22-1.24 (m, 2H), 1.44-1.47 (m, 2H), 1.79 (t, 2H, J = 7.0 Hz), 3.77 (t, 2H, J = 6.5 Hz), 7.14-7.15 (m, 15H), 7.28 (dd, 1H), 7.64 (s, 1H, J = 3.7 Hz 5.0 Hz), 7.79 (d, 1H, J = 5.0 Hz), 10.19 (s, 1H), 11.76 (s, 1H). ¹³CNMR (151 MHz, DMSO-*d*₆): 25.00, 25.18, 27.79, 32.35, 75.91, 92.20, 127.88, 127.99, 128.38, 129.44, 131.49, 142.94, 170.69. HRMS-ESI [M+H]: m/z calcd. for C₃₀H₃₁N₂O₄S: 515.1999, found: 515.1995

6{[(5-Methylthiophen-2yl)formamido]oxy}-*N*-(triphenylmethoxy)hexanamide **5d**

White solid, yield 64.4%, mp: 93-95°C, ¹HNMR (600 MHz, DMSO-*d*₆): 1.05-1.11 (m, 2H), 1.21-1.24 (m, 2H), 1.43-1.48 (m, 2H), 1.79 (t, 2H, J = 7.2 Hz), 2.47 (s, 3H), 3.75 (t, 2H, J = 7.2 Hz), 6.84 (d, 1H, J = 2.8 Hz), 7.29-7.35 (m, 15H), 7.46 (s, 1H), 10.20 (s, 1H), 11.49 (s, 1H). ¹³CNMR (151 MHz, DMSO-*d*₆): 15.62, 25.00, 25.18, 27.79, 32.85, 75.86, 92.12, 126.85, 127.87, 127.97, 142.93, 170.67. HRMS-ESI [M+H]: m/z calcd. for C₃₁H₃₃N₂O₄S: 529.2156, found: 529.2150.

6{[(4-Methylthiophen-2yl)formamido]oxy}-*N*-(triphenylmethoxy)hexanamide **5e**

White solid, yield 68.5%, mp: 102°C, ¹HNMR (500 MHz, DMSO-*d*₆): 1.05-1.11 (m, 2H), 1.22-1.25 (m, 2H), 1.43-1.49 (m, 1H), 1.79 (m, 2H), 2.22 (s, 3H), 3.75 (t, 2H, J = 6.6 Hz), 7.29-7.34 (m, 15H), 7.39 (s, 1H), 7.46 (s, 1H), 10.16 (s, 1H), 11.49 (s, 1H). ¹³CNMR (125 MHz, DMSO-*d*₆): 15.64, 24.87, 25.12, 27.67, 32.28, 75.79, 92.18, 126.73, 127.78, 127.87, 129.34, 130.70, 138.12, 136.38, 138.12, 142.86, 160.05, 170.63. HRMS-ESI [M+H]: m/z calcd. for C₃₁H₃₃N₂O₄S: 529.2156, found: 529.2150.

6{[(5-Chlorothiophen-2yl)formamido]oxy}-*N*-(triphenylmethoxy)hexanamide **5f**

White solid, yield 63.0%, mp: 134°C, ¹HNMR (500 MHz, DMSO-*d*₆): 1.06-1.09 (m, 2H), 1.22-1.24 (m, 2H), 1.46 (m, 2H), 1.79-1.81 (t, 2H, J = 6.5 Hz), 3.76 (t, 2H, J = 6.7 Hz), 7.20 (d, 1H, J = 4.0 Hz), 7.29-7.34 (m, 15H), 7.51 (s, 1H), 10.19 (s, 1H), 11.76 (s, 1H). ¹³CNMR (125 MHz, DMSO-*d*₆): 25.58, 25.61, 28.14, 32.75, 75.99, 92.02, 128.25, 128.54, 129.83, 169.64. HRMS-ESI [M+H]: m/z calcd. for C₃₀H₂₉ClN₂O₄S: 549.1609, found: 549.1609.

6-[(1-Benzofuran-2-ylformamido)oxy]-*N*-(triphenylmethoxy)hexanamide **5g**

White Solid, yield 78.4%, mp: 97°C, ¹HNMR (600 MHz, DMSO-d₆): 1.08-1.11 (m, 2H), 1.22-1.27 (m, 2H), 1.46-1.49 (m, 2H), 1.80 (t, J = 6.8 Hz, 2H), 3.81 (t, J = 6.7 Hz, 2H), 7.29-7.36 (m, 15H), 7.46-7.49 (m, 1H), 7.54 (s, 1H), 7.65 (d, J = 8.4 Hz, 1H), 7.77 (d, J = 7.8 Hz, 1H), 10.21 (s, 1H), 11.97 (s, 1H). ¹³CNMR (151 MHz, DMSO-d₆): 25.01, 25.15, 27.78, 32.35, 75.91, 92.20, 110.40, 112.26, 123.21, 124.25, 127.26, 127.43, 127.86, 127.97, 129.43, 142.94, 147.65, 154.71, 170.68. HRMS-ESI [M+H]: m/z calcd for C₃₄H₃₃N₂O₅: 549.2384, found: 549.2380.

6-[(1-Benzothiophen-2-ylformamido)oxy]-*N*-(triphenylmethoxy)hexanamide **5h**

White Solid, yield 78.0%, mp: 112°C, ¹HNMR (500 MHz, DMSO-d₆): 1.09-1.13 (m, 2H), 1.24-1.28 (m, 2H), 1.48-1.51 (m, 2H), 1.81-1.83 (m, 2H), 3.82 (t, 2H, J = 6.6 Hz), 7.30-7.36 (m, 15H), 7.46-7.48 (m, 2H), 7.95-8.04 (m, 3H), 10.17 (s, 1H), 11.37 (s, 1H). ¹³CNMR (125 MHz, DMSO-d₆): 24.89, 25.14, 32.29, 75.88, 92.17, 123.11, 125.56, 126.68, 125.75, 127.85, 127.85, 129.34, 136.95, 139.25, 142.85, 160.15, 170.60. HRMS-ESI [M+H]: m/z calcd. for C₃₄H₃₃N₂O₄S: 565.2156, found: 565.2155.

Methyl 4-[(5-[(triphenylmethoxy)carbamoyl]pentyl)oxy]carbamoyl]benzoate **5i**

White Solid, yield 67.2%, mp: 174°C, ¹HNMR (500 MHz, DMSO-d₆): 1.09-1.12 (m, 2H), 1.22-1.27 (m, 2H), 1.45-1.50 (m, 2H), 1.80 (t, 2H, J = 7.4 Hz), 3.80 (t, 2H, J = 6.6 Hz), 3.89 (s, 3H), 7.30-7.84 (m, 15H), 7.87 (d, 2H, J = 8.3 Hz), 8.03 (d, 2H, J = 8.3 Hz), 10.17 (s, 1H), 11.77 (s, 1H). ¹³CNMR (125 MHz, DMSO-d₆): 24.88, 25.14, 27.72, 32.29, 52.71, 75.55, 92.17, 127.76, 127.86, 129.34, 137.01, 142.86, 163.64, 166.00, 170.62. HRMS-ESI [M+H]: m/z calcd. for C₃₄H₃₅N₂O₆: 567.2490, found: 567.2486.

Methyl 3-[(5-[(triphenylmethoxy)carbamoyl]pentyl)oxy]carbamoyl]benzoate **5j**

White Solid, yield 51.4%, mp: 85°C, ¹HNMR (500 MHz, DMSO-d₆): 1.07-1.10 (m, 2H), 1.21-1.24 (m, 2H), 1.45-1.48 (m, 2H), 1.79 (m, 2H), 3.78 (t, 2H, J = 6.6 Hz), 3.88 (s, 3H), 7.29-7.33 (m, 15H), 7.62 (t, 1H, J = 7.8 Hz), 7.99 (d, 1H, J = 7.8 Hz), 8.10 (d, 1H, J = 7.7 Hz), 8.32 (s, 1H), 10.18 (s, 1H), 11.82 (s, 1H). ¹³CNMR (125 MHz, DMSO-d₆): 24.83, 25.11, 27.66, 52.73, 75.57, 127.29, 127.87, 129.28, 129.51, 130.29, 132.03, 132.35, 142.78, 166.09. HRMS-ESI [M+H]: m/z calcd. for C₃₄H₃₅N₂O₆: 567.2490, found: 567.2481.

6-([4-(Dimethylamino)phenyl]formamido)oxy)-*N*-(triphenylmethoxy)hexanamide **5k**

White solid, yield 56.0%, mp: 194°-196°C, ¹HNMR (600 MHz, DMSO-*d*₆): 1.06-1.11 (m, 2H), 1.21-1.26 (m, 2H), 1.43-1.47 (m, 2H), 1.79 (t, 2H, *J* = 6.8 Hz), 2.69 (s, 6H), 3.74 (t, 2H, *J* = 6.7 Hz), 6.69 (d, 2H, *J* = 8.9 Hz), 7.29-7.34 (m, 15H), 7.61 (d, 2H, *J* = 8.9 Hz), 10.20 (s, 1H), 11.21 (s, 1H). ¹³CNMR (151 MHz, DMSO-*d*₆): 25.04, 25.26, 27.88, 32.38, 75.42, 92.19, 111.31, 119.20, 128.87, 127.97, 128.82, 129.43, 142.94, 152.76, 165.10, 170.59. HRMS-ESI [M+H]: *m/z* calcd. for C₃₄H₃₈N₃O₄: 552.2857, found: 552.2855.

6-([3-(Dimethylamino)phenyl]formamido)oxy)-*N*-(triphenylmethoxy)hexanamide **5l**

White solid, yield 43.7%, mp: 143°-145°C, ¹HNMR (500 MHz, DMSO-*d*₆): 1.09-1.12 (m, 2H), 1.23-1.26 (m, 2H), 1.80 (t, 2H, *J* = 7.3 Hz), 2.83 (s, 6H), 3.77 (t, 2H, *J* = 6.6 Hz), 6.86 (dd, 1H, *J* = 2.3 Hz 8.2 Hz), 7.01 (d, 1H, *J* = 7.6 Hz), 7.06 (br, 1H), 7.24 (t, 1H, *J* = 7.8 Hz) (m, 15H), 7.30-7.35 (m, 15H), 10.17 (s, 1H), 11.45 (s, 1H). ¹³CNMR (125MHz, DMSO-*d*₆): 24.90, 25.19, 27.76, 32.30, 75.38, 92.17, 111.00, 114.98, 115.52, 127.76, 127.85, 129.24, 129.34, 133.54, 142.85, 150.65, 165.21, 170.61. HRMS-ESI [M+H]: *m/z* calcd. for C₃₄H₃₈N₃O₄: 552.2857, found: 552.2861.

General procedure for preparation of **6a-n**

The protected hydroxamates **5a-n** were dissolved in 30 mL of dichloromethane (1.0 eq) and to this stirring solution triethylsilane (20.0 eq) was added, followed by the addition of trifluoroacetic acid (20.0 eq). After 30 min under stirring the solvent was removed under reduced pressure and the crude product was purified by flash chromatography using mixtures of dichloromethane/ methanol as eluent (0-15% of methanol).

6-[(Furan-3-yl-formamido)oxy]-*N*-hydroxyhexanamide **6a**

White solid, yield 66.4%, mp: 135°C, HPLC: *t_r* = 7.45 min, purity 97.9%, ¹HNMR (500MHz, DMSO-*d*₆): 1.33-1.38 (m, 2H), 1.50-1.60 (m, 4H), 1.95 (t, 2H, *J* = 6.5Hz), 3.82 (t, 2H, *J* = 7.3 Hz), 6.77 (s, 1H), 7.73 (t, 1H, *J* = 1.8 Hz), 8.15 (s, 1H), 8.66 (s, 1H), 10.34 (s, 1H), 11.34 (s, 1H). ¹³CNMR (125 MHz, DMSO-*d*₆): 25.24, 25.43, 27.77, 32.56, 75.76, 108.99, 120.26, 140.30, 144.44, 145.41, 169.41. HRMS-ESI [M+H]: *m/z* calcd. for C₁₁H₁₇N₂O₅: 257.1132, found: 257.1133.

N-Hydroxy-6-[[*(1-methyl-1H-pyrrol-2-yl)formamido*]oxy]hexanamide **6b**

Yellow oil, Yield 79.0%, HPLC: t_r = 9.53 min, purity 98.9%, ^1H NMR (500 MHz, DMSO-d_6): 1.34-1.39 (m, 2H), 1.51-1.61 (m, 4H), 1.96 (t, 2H, J = 7,5 Hz), 3.81-3.84 (s+t, 5H), 6.00 (dd, 1H, J = 2.5 Hz 3.9 Hz), 6.66 (dd, 1H, J = 1.7 Hz 4.0 Hz), 6.93 (t, J = 2.0 Hz, 1H), 8.63 (s, 1H), 10.33 (s, 1H), 11.05 (s, 1H). ^{13}C NMR (125 MHz, DMSO-d_6): 25.29, 25.50, 27.85, 32.58, 36.21, 75.63, 107.09, 112.65, 123.21, 128.49, 160.54, 169.43. HRMS-ESI [$\text{M}+\text{H}$]: m/z calcd. for $\text{C}_{12}\text{H}_{20}\text{N}_3\text{O}_4$: 270.1448, found: 270.1450.

N-Hydroxy-6-[[*(thiophen-2-yl)formamido*]oxy]hexanamide **6c**

Yellow oil, yield 81.0%, HPLC: t_r = 8.87 min, purity 95.8%, ^1H NMR (600 MHz, DMSO-d_6): 1.32-1.39 (m, 2H), 1.50-1.60 (m, 4H), 1.94 (t, 2H, J = 7.5 Hz), 3.85 (t, 2H, J = 6.5 Hz), 7.14 (dd, 1H, J = 3.70 Hz 5.0 Hz), 7.64 (s, 1H), 7.80 (d, J = 4.0 Hz, 1H), 8.66 (s, 1H), 10.35 (s, 1H), 11.78 (s, 1H). ^{13}C NMR (151 MHz, DMSO-d_6): 25.36, 25.52, 27.88, 32.65, 75.93, 128.37, 128.67, 131.58, 169.49. HRMS-ESI [$\text{M}+\text{H}$]: m/z calcd. for $\text{C}_{11}\text{H}_{17}\text{N}_2\text{O}_4\text{S}$: 273.0904, found: 273.0904.

N-Hydroxy-6-[[*(5-methylthiophen-2-yl)formamido*]oxy]hexanamide **6d**

White solid, yield 91.9%, mp: 150°C, HPLC: t_r = 10.84 min, purity 98.9%, ^1H NMR (500 MHz, DMSO-d_6): 1.32-1.37 (m, 2H), 1.50-1.61 (m, 4H), 1.95 (t, 2H, J = 7.4 Hz), 3.83 (t, 2H, J = 6.5 Hz), 6.84 (d, 1H, J = 2.8 Hz), 7.45 (s, 1H), 8.68 (s, 1H), 10.36 (s, 1H), 11.53 (s, 1H). ^{13}C NMR (125 MHz, DMSO-d_6): 15.61, 25.37, 25.52, 27.88, 32.65, 75.91, 99.98, 126.86, 169.47. HRMS-ESI [$\text{M}+\text{H}$]: m/z calcd. for $\text{C}_{15}\text{H}_{24}\text{N}_3\text{O}_4$: 310.1761, found: 310.1763.

N-Hydroxy-6-[[*(4-methylthiophen-2-yl)formamido*]oxy]hexanamide **6e**

White solid, yield 92.3%, mp: 120-121°C, HPLC: t_r = 10.95 min, purity 97.9%, ^1H NMR (500 MHz, DMSO-d_6): 1.31-1.39 (m, 2H), 1.48-1.68 (m, 4H), 1.94 (t, 2H, J = 7.3 Hz), 2.21 (s, 3H), 3.84 (t, 2H, J = 6.0 Hz), 7.39 (s, 1H), 7.46 (s, 1H), 8.57 (s, 1H), 10.35 (s, 1H), 11.55 (s, 1H). ^{13}C NMR (125 MHz, DMSO-d_6): 15.63, 25.25, 25.43, 27.77, 32.57, 75.82, 126.69, 130.60, 136.35, 138.10, 160.00, 169.40. HRMS-ESI [$\text{M}+\text{H}$]: m/z calcd. for $\text{C}_{15}\text{H}_{24}\text{N}_3\text{O}_4$: 310.1761, found: 310.1763.

6-[[*(5-Chlorothiophen-2-yl)formamido*]oxy]-*N*-hydroxyhexanamide **6f**

Orange solid, yield 76.5%, mp: 121-123°C, HPLC: t_r = 12.00 min, purity 99.2%, ^1H NMR (600 MHz, DMSO-d_6): 1.34-1.36 (m, 2H), 1.50-1.55 (m, 2H), 1.57-1.60 (m, 2H), 1.95 (t, 2H, J = 7.4

Hz), 3.85 (t, 2H, J = 6.5 Hz), 7.19 (d, 1H, J = 4.0 Hz), 7.51 (s, 1H), 10.34 (s, 1H), 11.78 (s, 1H). ¹³CNMR (125 MHz, DMSO-d₆): 25.22, 25.39, 27.75, 32.55, 75.99, 128.27, 169.37. HRMS-ESI [M+H]: m/z calcd. for C₁₁H₁₆ClN₂O₄S: 307.0518, found: 307.0514.

6-[(1-Benzofuran-2-ylformamido)oxy]-*N*-hydroxyhexanamide **6g**

White solid, yield 89.6%, mp: 109-111°C, HPLC: t_r = 12.07 min, purity 97.5%, ¹HNMR (500 MHz, DMSO-d₆): 1.33-1.41 (m, 2H), 1.49-1.66 (m, 4H), 1.95 (t, 2H, J = 7.2 Hz), 3.87 (t, 2H, J = 6.5 Hz), 7.32-7.37 (m, 1H), 7.45-7.50 (m, 1H), 7.54 (d, 1H, J = 1.0 Hz), 7.64-7.67 (m, 1H), 8.68 (s, 1H), 10.36 (s, 1H), 11.99 (s, 1H). ¹³CNMR (125 MHz, DMSO-d₆): 25.25, 25.41, 27.77, 32.58, 75.92, 110.30, 112.13, 123.09, 124.12, 127.18, 127.30, 147.59, 154.65, 156.61, 169.43. HRMS-ESI [M+H]: m/z calcd. for C₁₅H₁₉N₂O₅: 307.1288, found: 307.1287.

6-[(1-Benzothiophen-2-ylformamido)oxy]-*N*-hydroxyhexanamide **6h**

White solid, yield 95.4%, mp: 175-176°C, HPLC: t_r = 13.12 min, purity 98.2%, ¹HNMR (600 MHz, DMSO-d₆): 1.35-1.40 (m, 2H), 1.53-1.58 (m, 2H), 1.60-1.65 (m, 2H), 1.97 (t, 2H, J = 7.4 Hz), 3.91 (t, 2H, J = 6.5 Hz), 7.44-7.49 (m, 2H), 7.95-7.98 (m, 2H), 8.03 (d, 1H, J = 7.8 Hz), 8.69 (s, 1H), 10.38 (s, 1H), 11.95 (s, 1H). ¹³CNMR (151 MHz, DMSO-d₆): 25.37, 25.32, 27.52, 32.67, 75.97, 123.25, 125.49, 125.71, 126.83, 137.13, 139.38, 140.45, 160.12, 169.50. HRMS-ESI [M+H]: m/z calcd. for C₁₅H₁₉N₂O₄S: 323.1060, found: 323.1059.

Methyl 4-([5-(hydroxycarbamoyl)pentyl]oxy)carbamoylbenzoate **6i**

White solid, yield 87.0%, mp: 159°-160°C, HPLC: t_r = 10.55 min, purity 97.3%, ¹HNMR (600 MHz, DMSO-d₆): 1.35-1.38 (m, 2H), 1.53-1.62 (m, 4H), 1.97 (t, 2H, J = 7.3 Hz), 3.87-3.90 (m, 5H), 7.87 (d, 2H, J = 8.2 Hz), 8.03 (d, 2H, J = 8.2 Hz), 8.69 (s, 1H), 10.38 (s, 1H), 11.84 (s, 1H). ¹³CNMR (151 MHz, DMSO-d₆): 25.37, 25.53, 27.91, 32.66, 52.86, 76.66, 127.97, 129.69, 166.09, 169.50. HRMS-ESI [M+H]: m/z calcd. for C₁₅H₂₁N₂O₆: 325.1394, found: 325.1394.

Methyl 3-([5-(hydroxycarbamoyl)pentyl]oxy)carbamoylbenzoate **6j**

White solid, yield 63.6%, mp: 102°C, HPLC: t_r = 10.69 min, purity 97.1%, ¹HNMR (500 MHz, DMSO-d₆): 1.33-1.41 (m, 2H), 1.49-1.63 (m, 4H), 1.94 (t, 2H, J = 7.2 Hz), 3.86-3.91 (m, 5H), 7.61 (t, 1H, J = 7.8 Hz), 8.00 (d, 1H, J = 7.9 Hz), 8.10 (d, 1H, J = 7.8 Hz), 8.33-8.359 (m, 1H), 8.67 (s, 1H), 10.36 (s, 1H), 11.85 (s, 1H). ¹³CNMR (125 MHz, DMSO-d₆): 25.26, 25.46, 27.82, 32.59, 75.62, 128.12, 129.47, 130.31, 132.08, 132.32, 133.37, 163.58, 166.05, 169.42. HRMS-ESI [M+H]: m/z calcd. for C₁₅H₂₁N₂O₆: 325.1394, found: 325.1394.

6-({[4-(Dimethylamino)phenyl]formamido}oxy)-*N*-hydroxyhexanamide **6k**

White solid, Yield 83%, mp: 140°-142°C, HPLC: t_r = 8.08 min, purity 97.4%, ^1H NMR (500 MHz, DMSO- d_6): 1.34-1.39 (m, 2H), 1.51-1.62 (m, 4H), 1.96 (t, 2H, J = 7.35 Hz), 2.96 (s, 6H), 3.82 (t, 2H, J = 6.5 Hz), 6.99 (d, 2H, J = 8.9 Hz), 7.61 (d, 2H, J = 8.9 Hz), 8.64 (s, 1H), 10.34 (s, 1H), 11.21 (s, 1H). ^{13}C NMR (125 MHz, DMSO- d_6): 25.30, 25.52, 27.88, 32.60, 75.41, 111.23, 119.22, 128.72, 140.29, 152.70, 165.09, 169.43. HRMS-ESI [$\text{M}+\text{H}$]: m/z calcd. for $\text{C}_{15}\text{H}_{24}\text{N}_3\text{O}_4$: 310.1761, found: 310.1758.

6-({[3-(Dimethylamino)phenyl]formamido}oxy)-*N*-hydroxyhexanamide **6l**

White solid, yield 72.8%, mp: 117°C, HPLC: t_r = 3.64 min, purity 95.3% ^1H NMR (500 MHz, DMSO- d_6): 1.35-1.38 (m, 2H), 1.53-1.61 (m, 4H), 1.96 (t, 2H, J = 7.4 Hz), 2.93 (s, 6H), 3.85 (t, 2H, J = 6.7 Hz), 6.87 (d, 1H, J = 6.7 Hz), 7.01 (d, 1H, J = 7.4 Hz), 7.06 (s, 1H), 7.23 (t, 1H, J = 7.9 Hz), 8.60 (br, 1H), 10.33 (s, 1H), 11.47 (s, 1H). ^{13}C NMR (125 MHz, DMSO- d_6): 25.27, 25.49, 27.85, 32.59, 70.18, 75.43, 111.03, 115.01, 115.55, 129.25, 133.52, 140.29, 150.63, 165.21, 169.40. HRMS-ESI [$\text{M}+\text{H}$]: m/z calcd. for $\text{C}_{15}\text{H}_{24}\text{N}_3\text{O}_4$: 310.1761, found: 310.1763.

Homology modelling

The *Pf*HDAC1 amino acid sequence (Uniprot; accession number Q7K6A1) formed by 449aa, was used to search for crystal structures of homologues in the Protein Data Bank (PDB) using the alignment tool BLAST [32]. Human HDAC1, 2 and 3 were shown to have the highest identity with the targeted sequence (57-62%). In the alignment a long C-terminal (His375-Tyr449) was observed which extends beyond the catalytic domain. This region was not covered by the template, therefore was not used in the model [12]. Using Modeller v9.16 [23] and all available crystal structures of HDAC1, 2 and 3 (PDB access code HDAC1: 4KBX, 5ICN HDAC2: 3MAX, 4LXZ, 4LY1, 5IWG, 5IX0 and HDAC3: 4A69) as templates, 15 models were created for each template. The models with the lowest DOPE score [23] were chosen to be further evaluated. The best models were checked regarding their quality of the structure by PROCHECK [33], PROSA [34] and ANOLEA [35]. The best overall scores were obtained with the model using 5IWG crystal structure as template.

P. falciparum hyperacetylation assay

Trophozoite-stage *P. falciparum* 3D7 parasitized erythrocytes (~4% parasitemia, 5% hematocrit) were incubated with 5x IC₅₀ test compounds or controls for 3 h, as previously described [29]. The HDAC inhibitor SAHA (5x IC₅₀; 0.6 μM) [15] was included as a positive control and negative controls were vehicle only (0.1% DMSO) and the antimalarial drug chloroquine (5x IC₅₀; 0.1 μM) [15]. Western blot was carried out using Odyssey blocking buffer (Li-Cor Biosciences) according to the manufacturer's instructions. Anti-(tetra)acetyl histone H4 (1:2,000 dilution; Merck Millipore) was used with IRDye 680RD goat anti-rabbit secondary antibody (1:15,000 dilution; Li-Cor Biosciences). Following imaging using an Odyssey FC (Li-Cor Biosciences), the same membrane was probed with anti-*Pf*GAPDH (1:5,000 dilution; a kind gift from Dr Matt Dixon, University of Melbourne, Australia) and IRDye 800CW donkey anti-rabbit secondary antibody (1:15,000 dilution; Li-Cor Biosciences) as a loading control. Densitometry analysis was carried out using Image Studio Lite Version 3.1 software. Signals detected by anti-(tetra)acetyl histone H4 were normalized to their respective anti-*Pf*GAPDH loading control on the same membrane, and results expressed as the fold change in relative density compared to the DMSO vehicle control (set to 1.0). Two independent experiments were performed.

Evaluation of in vitro activity against asexual blood stages

Two *P. falciparum* laboratory lines, 3D7 (chloroquine sensitive) and Dd2 (chloroquine resistant), were kept in continuous culture as described previously [36]. Briefly, infected erythrocytes were maintained in complete culture medium (RPMI 1640, 25 mM HEPES, 2 mM L-glutamine, 50 μg/ml gentamicin, 0.14 mM hypoxanthine and 0.5% w/v AlbuMAX) at 37°C, 5% CO₂, 90% N₂ and 5% oxygen at 2.5% hematocrit with daily change of medium. Synchronization was performed twice weekly by sorbitol or MACS purification [35]. Growth inhibition assays were carried out using the histidine-rich-protein 2 (HRP2) enzyme linked immunoassay (ELISA) assay method, as described previously [37]. Briefly, 96 well flat-bottomed tissue culture plates were pre-coated with a 3-fold serial dilution of test-compounds before addition of synchronous *P. falciparum* ring-stage infected erythrocytes (1.5% hematocrit; 0.05% parasitemia). Plates were incubated for three days and subsequently frozen before ELISA for HRP2 was performed. Compounds were tested in duplicate in at least two independent experiments. The 50% inhibitory concentration (IC₅₀) was calculated by

analyzing the nonlinear regression of log concentration–response curves using the drc-package v0.9.0 of R v3.2.5 [38].

Evaluation of cytotoxicity against human HepG2 cells

Human hepatocellular carcinoma cells (HepG2; a kind gift of Gerhard Fritz, Heinrich Heine University, Düsseldorf, Germany) were cultured in DMEM supplemented with 10% fetal calf serum, 120 IU/mL penicillin, and 120 µg/mL streptomycin (all PAN Biotech, Germany) at 37°C in a humidified atmosphere containing 5% CO₂. Effect of test compounds on cytotoxicity was evaluated by an improved MTT assay as previously described [26, 31]. In brief, HepG2 were seeded in 96 well plates (Corning, Germany). After 24 h, cells were exposed to increasing concentrations of test compounds. Incubation was terminated after 72 h and cell survival was determined by addition of MTT solution (5 mg/mL in phosphate buffered saline, Serva, Germany). The formazan precipitate was dissolved in DMSO (VWR, Germany). Absorbance was measured at 544 nm and 690 nm in a FLUOstar microplate-reader (BMG LabTech, Germany). Concentration-effect curves were constructed using Prism 4.0 (GraphPad, San Diego, CA) by fitting the pooled data of at least three experiments performed in triplicates to the four-parameter logistic equation.

Acknowledgements

This work was supported by CAPES (Coordenação de Aperfeiçoamento de Pessoal de Nível Superior) (grant 12014-13-3 to LAA). We also acknowledge the support of the Australian NHMRC (APP1093378 and APP1074016 to KTA), the A-PARADDISE program funded under the European Union's Seventh Framework Programme (grant agreement no. 602080 to KTA) and Griffith University (GUIPRS and GUPRS scholarships to JAE). We thank the Australian Red Cross Blood Service for the provision of human blood and sera.

The authors have declared no conflict of interest.

References

- [1] Malaria Report, *WHO* **2015**.
- [2] S. C. T. P Rts., *Lancet* **2015**, 386, 31-45.

- [3] Malaria vaccine: WHO position paper, *WHO* **2016**
- [4] T. N. Wells, R.H. Van Huijsduijnen, W. C. Van Voorhis, *Nat. Rev. Drug Discov.* **2016** 14, 424-442.
- [5] A. Kunfermann, C. Lienau, B. Illarionov, J. Held, T. Gräwert, C.T. Behrendt, P. Werner, S. Hähn, W. Eisenreich, U. Riederer, B. Mordmüller, *J. Med. Chem.* **2013**, 56, 8151-8162.
- [6] S. Konzuch, T. Umeda, J. Held, S. Hähn, K. Brücher, C. Lienau, C. T. Behrendt, T. Gräwert, A. Bacher, B. Illarionov, M. Fischer, *J. Med. Chem.* **2014**, 57, 8827-8838.
- [7] K. Trenholme, L. Marek, S. Duffy, G. Pradel, G. Fisher, F. K. Hansen, T. S. Skinner-Adams, A. Butterworth, C. J. Ngwa, J. Moecking, C. D. Goodman, G. I. McFadden, S. D. Sumanadasa, D. P. Fairlie, V. M. Avery, T. Kurz, K. T. Andrews, *Antimicrob. Agents Chemother.* **2014**, 58, 3666-3678.
- [8] F. K. Hansen, T. S. Skinner-Adams, S. Duffy, L. Marek, S. D. Sumanadasa, K. Kuna, J. Held, V. M. Avery, K. T. Andrews, T. Kurz, *ChemMedChem* **2014**, 9, 665-670.
- [9] F. Ay, E. M. Bunnik, N. Varoquaux, J. P. Vert, W. S: Noble, K. G. Le Roch, *BioEssays* **2015**, 37, 182-194.
- [10] L. Cui, J. Miao, T Furuya, Q. Fan, X. Li, P. K. Rathod, L. Cui, *Eukaryotic Cell* **2008**, 7, 1200-1210.
- [11] L. Cui, J. Miao, L. Cui, *Antimicrob. Agents Chemother.* **2007**, 51, 488-494.
- [12] B. K. Chaal, A. P. Gupta, B. D. Wastuwidyaningtyas, Y. H. Luah, Z. Bozdech, *PLoS Pathog.* **2010**, 6, e1000737.
- [13] K. T. Andrews, A. P. Gupta, T. N. , D. P. Fairlie, G. N. Gobert, Z. Bozdech, *PloS One* **2012**, 7, e31847.
- [14] A. J. de Ruijter, A. H Van Gennip, H. N. Caron, S. Kemp, A. B. Van Kuilenburg, *Biochem. J.* **2003**, 370, 737-749.
- [15] K. T. Andrews, T. N. Tran, A. J. Lucke, P. Kahnberg, G. T. Le, G. M. Boyle, D. P. Fairlie, *Antimicrob. Agents Chemother.* **2008**, 52, 1454-1461.
- [16] P. Mukherjee, A. Pradhan, F. Shah, B. L. Tekwani, M. A. Avery, *Bioorg. Med. Chem.* **2008**, 16, 5254-5265.
- [17] N. C. Wheatley, K. T. Andrews, T. N Tran, .A. J. Lucke, R. C. Reid, D. P. Fairlie, *Bioorg. Med. Chem. Lett.* **2010**, 20, 7080-7084.
- [18] S. D. Sumanadasa, C. D. Goodman, A. J., Lucke, T Skinner-Adams, I Sahama, A., Haque, K. T. Andrews, *Antimicrob. Agents Chemother.* **2012**, 56, 3849-3856.
- [19] J. Melesina, D. Robaa, R. J. Pierce, C. Romier, W. Sippl, *J. Mol. Graphics Modell.* **2015**, 62, 342-361.

- [20] K. T. Andrews, T. N. Tran, D. P. Fairlie, *Curr. Pharm. Des.* **2012**, 18, 3467-3479.
- [21] Q. Wang, B. A. Rosa, B. Nare, K. Powell, S. Valente, D. Rotili, M Mai, G. R. Marshall, M. Mitreva, *PLoS Neglected Trop. Dis.* **2015**, 9, e0004026.
- [22] F. K. Hansen, S. D. Sumanadasa, K. Stenzel, S. Duffy, S. Meister, L Marek, M. U. Kassack, *Eur. J. Med. Chem.* **2014**, 82, 204-213.
- [23] B. Webb, A. Sali, *Methods Mol. Biol.* **2014**, 1137, 1-15.
- [24] F. F. Wagner, M. Weïwer, S. Steinbacher, A. Schomburg, P. Reinemer, J.P. Gale, A. J. Campbell, S. L. Fisher, W. N. Zhao, S. A. Reis, K. M. Hennig, M. Thomas, P. Müller, M. R. Jefson, D. M. Fass, S. J. Haggarty, Y. L. Zhang, H. B. Holson, *Bioorg. Med. Chem.* **2016**, 24, 4008-4015.
- [25] P. J. Watson, C. J. Millard, A. M. Riley, N. S. Robertson, L. C. Wright, H. Y. Godage, S. M. Cowley, A. G. Jamieson, B. V. Potter, J. W. Schwabe, *Nat. Commun.* **2016**, 7, 11262.
- [26] L. Marek, A. Hamacher, F. K. Hansen, K. Kuna, H. Gohlke, M. U. Kassack, T. Kurz, *J. Med. Chem.* **2013**, 56, 427-436.
- [27] J. M. Ontoria, G. Paonessa, S. Ponzi, F. Ferrigno, E. Nizi, I. Biancofiore, S. Malancona, R. Graziani, D. Roberts, P. Willis, A. Bresciani, N. Gennari, O. Cecchetti, E. Monteagudo, M. V. Orsale, M. Veneziano, A. Di Marco, A. Cellucci, R. Laufer, S. Altamura, V. Summa, S. Harper, *ACS Med. Chem. Lett.* **2016**, 7, 454-459.
- [28] G. S. Dow, Y. Chen, K. T. Andrews, D. Caridha, L. Gerena, M. Gettayacamin, J. Johnson, Q. Li, V. Melendez, N. 3rd Obaldia, T. N. Tran, A. P. Kozikowski, *Antimicrob. Agents Chemother.* **2008**, 52, 3467-3477.
- [29] J. A. Engel, A. J. Jones, V. M. Avery, S. D. Sumanadasa, S. S. Ng, D. P. Fairlie, K. T. Andrews, *Int. J. Parasitol. Drugs Drug Resist.* **2015**, 5, 117-126.
- [30] H. Noedl, J. Bronnert, K. Yingyuen, B. Attlmayr, H. Kollaritsch, M. Fukuda, *Antimicrob. Agents Chemother.* **2005**, 49, 3575-3577
- [31] L. H. Engelke, A. Hamacher A, P. Proksch, M. U. Kassack, *J. Cancer.* **2016**, 7, 353-63
- [32] S. F. Altschul, W. Gish, W. Miller, E. W. Myers, D. J. Lipman, *J. Mol. Biol.* **1990**, 215, 403-410.
- [33] R. A. Laskowski, M. W. MacArthur, D. S. Moss, J. M. Thornton, *J. App. Cryst.* **1993**, 26, 283-291.
- [34] M. Wiederstein, M. J. Sippl, *Nucleic Acids Res.* **2007**, 35, 407-410.
- [35] F. Melo, D. Devos, E. Depiereux, E. Feytmans, *Proc. Int. Conf. Intell. Syst. Mol. Biol.* **1997**, 5, 187-190.
- [36] W. Trager, J. B. Jensen, *Science* **1976**, 193, 673-675.

[37] C. Lambros, J. P. Vanderberg, *J. Parasitol.* **1979**, 65, 418-420.

[38] R: A Language and Environment for Statistical Computing, *R Core Team* **2009**.

4. Histone Deacetylase inhibitors with Antineoplastic activity

4.1. Anticancer effects of HDACi

Alterations in cell proliferation, differentiation and death mechanisms can lead to uncontrolled growth of cells, also known as neoplasm. The cells resulting from this unregulated growth can either proliferate in an unstructured way or organize themselves in masses of tissues, which are commonly referred to as tumors. Neoplasms with slow growth rate delimited size and unable to invade adjacent tissues are classified as benign, while their counterpart is classified as malignant neoplasms or cancers.^{136,137}

Cancer is a broad set of more than 100 different pathologies characterized by uncontrolled growth of abnormal cells that can invade nearby tissues. The ability of malignant cells to sustain their growth and to invade other tissues can be rationalized by a set of capabilities defined as hallmarks of cancer, which consists in: maintenance of growth activation and evasion of suppression; invasion and metastasis, replicative immortalization; angiogenesis induction and death resistance.^{136,137}

The death of abnormal cells like cancer predominantly occurs by apoptosis, a programmed and regulated cell-death process also important for physiological processes such as embryogenesis and immune response. Neoplastic cells can alter apoptotic pathways through several different mechanisms, being able to evade this programmed death and proliferate.¹³⁸

The origin of this set of heterogeneous diseases is associated with clonal expansion of mutant premalignant stem and progenitor cells. Epigenetic modulators are essential for differentiation and adaptation in normal cells, consequently influencing both initiation and maintenance of cancers and as consequence mutated epigenetic modulators are observed in several cancer types.¹³⁹

Overexpression of HDACs is not found in all neoplasms and had not been directly correlated with a specific type of cancer. However, high levels of HDAC expression are associated with poor prognosis. Additional to overexpression, mutations of HDACs can be found in different kinds of cancer, but not being connected to a specific type. The presence of those mutations in HDACs occurs in pathologies, in which the carcinogenesis is associated with high exposure to carcinogens, suggesting genetic alterations found in HDACs have no specific cause.¹³⁹⁻¹⁴¹

Cancer responses to the presence of HDACi are changes in histone and non-histone acetylation (Figure 23) and the most common outcome is cell death, mediated by intrinsic and extrinsic pathways. In this case, cell death can also be attributed to the generation of reactive oxygen species (ROS) and/or accumulation of DNA damage.¹⁴²

HDACi were furthermore shown to induce cycle cell arrest at G1/S and G2/M cell cycle checkpoints, by the alteration of transcriptional changes and due to DNA damage, respectively. The induction of cycle cell arrest by these inhibitors is usually connected to apoptosis, senescence, and differentiation.¹⁴²

The mechanisms involved in senescence and cell-differentiation caused by HDACi are still unclear, but senescence has been related to the activity of the isoforms HDAC1 and HDAC2.¹⁴² As mentioned previously (section 1.1.9) innate and adaptive immune responses can be affected by HDACs. HDACi can enhance cancer immunogenicity by activating the production of antigens and antigen-processing machinery. They interfere with natural killer cells (NK) activation, although it is undefined whether it increases or decreases the NK anticancer activity.^{101,142}

Induction of autophagy can be promoted by HDACi, however, the relevance of this process in the antineoplastic activity is uncertain. The autophagic process has been related to the selection of tumor resistance, making it difficult to define the role of autophagy in the treatment of tumors.^{142,143}

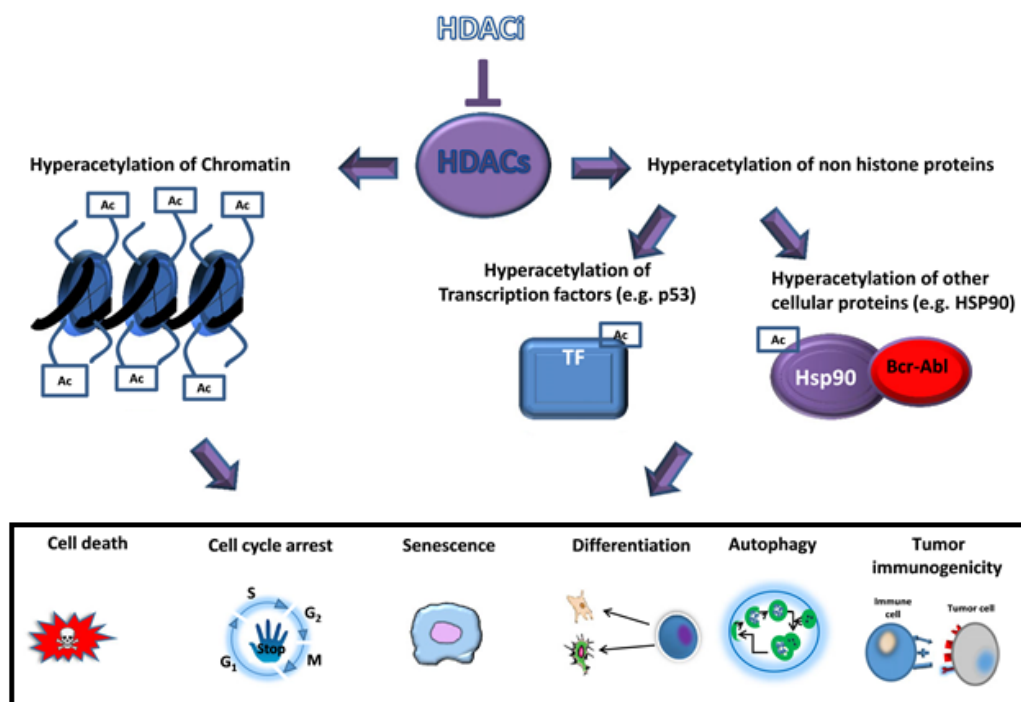


Figure 23: Biological responses of neoplastic cells to HDACis.¹⁴²

In this work, the synthesized HDACi were tested for their antiproliferative activity against two different carcinoma cell lines, oral squamous Cal27 and ovarian A2780. Carcinomas are the most common type of cancer, affecting the skin and the tissue on the surface of various organs. Oral squamous cell carcinomas (OSCC) are the most frequent malignancy in the oral cavity. This type of cancer is invasive and the first line of treatment is surgery and depending on the stage radiochemotherapy. Due to the high level of metastasis in OSCC, surgical procedures have limited efficacy and, in most cases, leads to debilitating anatomic alterations in the involved areas. Chemotherapy in OSCC is used only in combination with radiotherapy and comprises antimetabolites (Methotrexate and 5-Fluorouracil), platinum compounds (Cisplatin and Carboplatin) and taxanes (Docetaxel) (Figure 24).¹⁴⁴

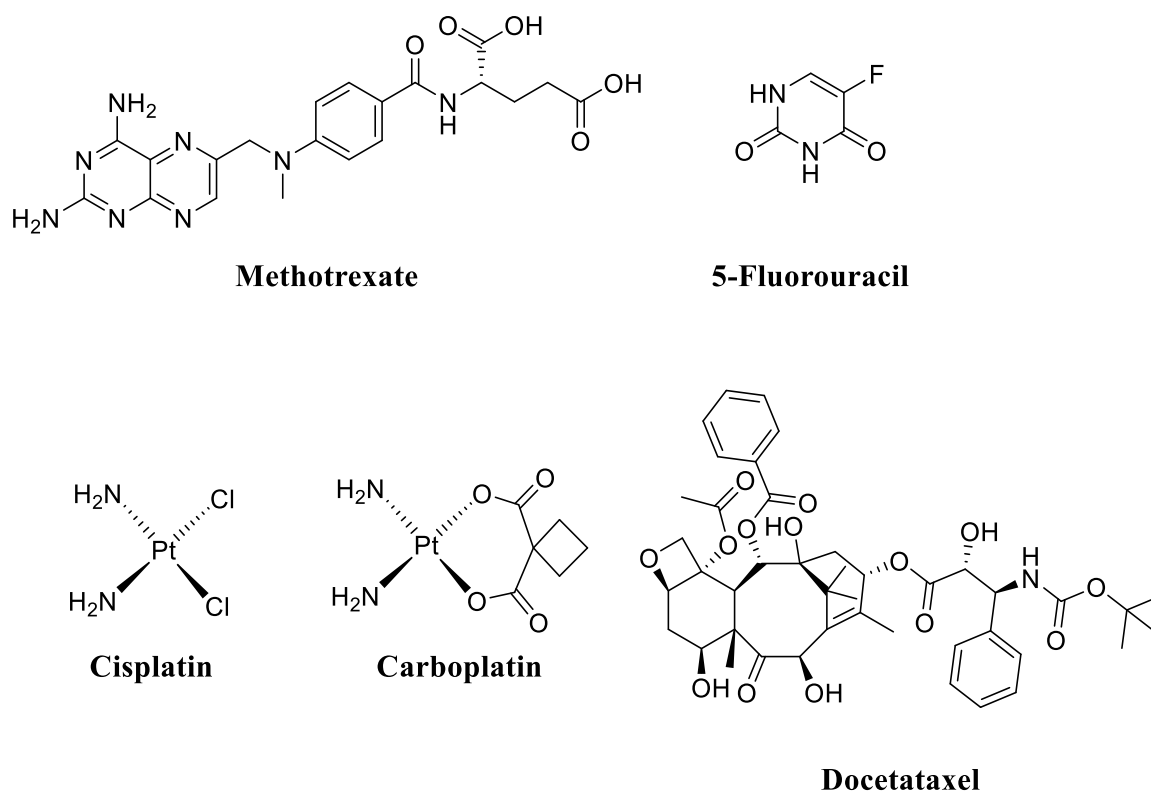


Figure 24: Drugs involved in the chemotherapy of OSCC.¹⁴⁴

HDACs roles in OSCC are not completely elucidated. However, the inhibition of HDAC1/2 was found to be an important mediator for *in vitro* apoptosis. These isoforms are related to an increase of the tumor aggressiveness, promoting migration and invasion processes. Moreover, an increase of HDAC2 expression is connected to a higher number of undifferentiated cells and therefore poor prognosis.¹⁴⁵ HDAC6 expression levels are, in addition, modified in different

tumor stages of this cancer and this activity of the isoform has been related to OSCC aggressiveness.

The roles of HDAC in OSCC cellular processes suggests a positive effect of the use of HDACi as a therapeutic class and although Valproic acid and Romidepsin were not successful in clinical studies, Vorinostat are currently being evaluated in phase II trials for recurrent oral cavity carcinomas, reinforcing the potential of HDACi in the treatment of oral carcinomas.^{145,146}

The second type of cancer studied in this work was ovarian cancer, the leading cause of death related to gynecological malignancies. The treatment of this malignancy involves surgery, radio, and chemotherapy. The standard chemotherapy approach for ovarian carcinoma is the combination of taxanes (Docetaxel and Paclitaxel) and platinum-based compounds (Cisplatin and Carboplatin) (Figure 25).¹⁴⁷⁻¹⁴⁹

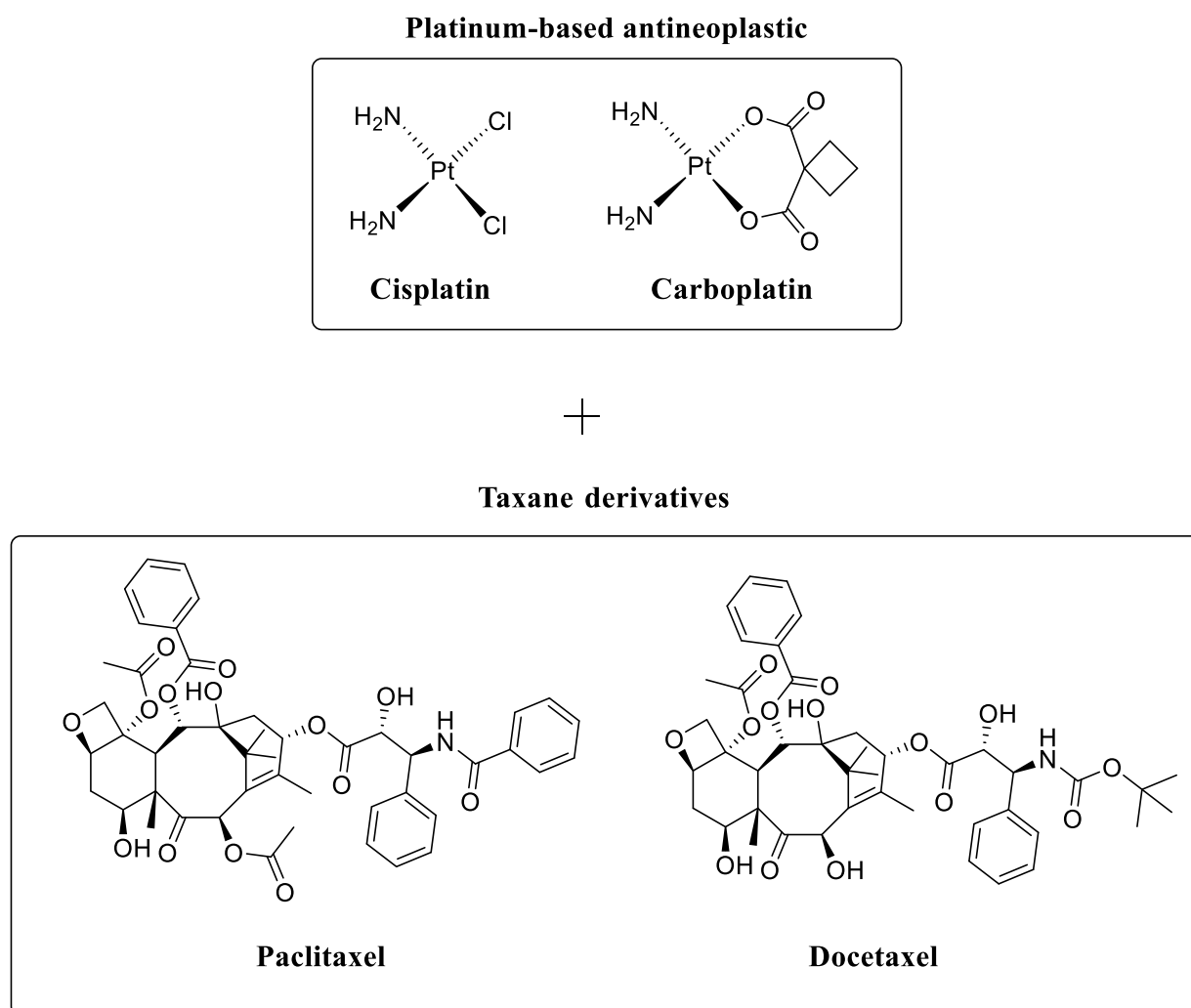


Figure 25: Standard chemotherapy of ovarian cancer.^{147,148}

Regarding HDACs in this disease, class I HDACs have a considerable impact on carcinogenesis. Their expression levels were shown to increase stepwise from benign, over borderline to malignant tumors. Class II enzymes are rarely overexpressed in this kind of cancer, however, HDAC4 inhibition was found to promote expression of cell cycle regulators, serving as a potential biologic target.^{149,150}

Clinical evaluation of the HDACi Vorinostat and Belinostat against different ovarian cancers as single agents and in combination with carboplatin showed lack of effectiveness in the treatment of this type of cancer.¹⁵¹ However, a different combination therapy using Quisinostat, a class I and II HDACi, Carboplatin and Paclitaxel demonstrated more promising results, being currently evaluated in phase II clinical trials against.¹⁵²

The combination of platinum-based chemotherapeutic agents (Figure 25) and HDACi have been demonstrated to be clinically effective against platin-resistant ovarian cancer cells lines, what consist in an important attribute for ovarian neoplasms. Ovarian malignancies despite being characterized by a good response to initial therapy have a high rate of recurrence. Also, the recurrent form of this cancer is often resistant to multiple chemotherapeutic agents, justifying the use of HDACi in its therapy due to their known chemosensitizer effect.^{152,153}

4.2. Rational design of novel HDACi

In the previously described project in this work, the first set of twelve HDACi containing an alkoxyamide connecting unit were synthesized and evaluated against *P. falciparum* (**6a-l**). The compounds showed promising results against both chloroquine-sensitive (3D7) and multi-resistant (Dd2) cell lines of the parasite (Figure 22). However, four out of the twelve analogs (**6g**, **6h**, **6k**, and **6l**) were able to decrease the cell viability of the human liver cells HepG2 in concentrations comparable to Vorinostat.¹⁵⁴

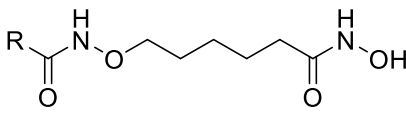
The HepG2 cells are commonly used to evaluate selectivity of antiparasitic agents to mammalian cells. Additionally, this liver cell line is often used to cultivate the hepatic intracellular form of the *Plasmodium* parasite. Therefore, molecules must not disrupt the homeostasis of these cell lines to be used in the assays involving the liver form of the parasite. However, these cells are immortalized liver cells, they are in fact derived from liver cancer, specifically from Hepatocellular carcinoma (HCC).¹⁵⁵

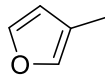
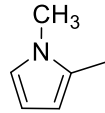
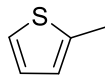
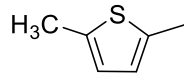
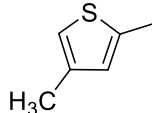
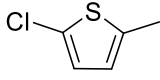
HCC is the most common type of primary liver cancer, making HepG2 also a classical model for the evaluation of new antiproliferative agents against this liver carcinoma.¹⁵⁵ The use of

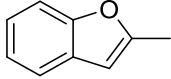
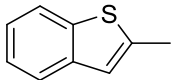
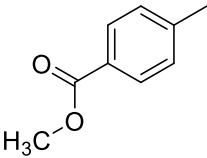
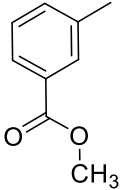
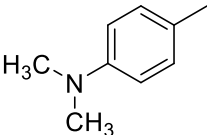
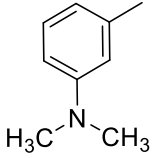
HDACi for the treatment of HCC indeed showed promising results against this neoplasm, since Vorinostat and Belinostat are currently in clinical trials for the treatment of HCC.¹⁵⁶

In the HepG2 assays performed in the previous project four compounds (**6g**, **6h**, **6k**, and **6l**) and showed similar activity to Vorinostat.¹⁵⁴ Based on these results the compounds were tested against two carcinomas cell lines, the ovarian carcinoma (A2780) and oral squamous cell carcinoma (Cal27). The half maximal inhibitory concentration (IC₅₀) of the hydroxamates **6a-l** was determined in whole cell HDAC-assays and in MTT-assays against A2780 and Cal27 by Dr. Alexandra Hamacher in the laboratory of Prof. Matthias U. Kassack at the Heinrich Heine Universität of Düsseldorf (Table 1).

Table 1: Antiproliferative activity of the previous synthesized compounds (**6a-l**) in MTT and HDAC whole cell assays performed against A2780 and Cal27 cell strains.



Compound	R	A2780 (μM) ^a		Cal27 (μM) ^a	
		HDAC	MTT	HDAC	MTT
6a		7.03	46.7	7.38	6.94
6b		5.01	4.00	5.14	5.62
6c		9.42	8.40	8.32	10.70
6d		3.29	10.70	4.30	2.06
6e		1.69	5.81	2.40	1.25
6f		6.46	7.84	6.91	7.28

6g		1.71	5.56	1.99	0.78
6h		1.58	4.88	2.25	0.50
6i		13.4	40.0	28.6	11.7
6j		2.22	24.2	2.10	1.35
6k		0.81	5.38	0.98	0.78
6l		1.18	5.16	1.13	0.50
Vorinostat		1.68	2.42	0.88	1.98
Cisplatin		ND	1.88	ND	2.27

^{a)} Values are the mean of three independent experiments conducted in triplicate. ND = not determined. The standard deviations are <10% of the mean.

The selection of A2780 and Cal27 as targets was due to the relevance of HDACs in their physiology and the established potency of hydroxamates containing alkoxyamides and alkoxyureas as CU against these strains. In this work, the alkoxyamide analogs were focused because of their higher potency compared to the respective alkoxyurea derivatives.^{157,158}

The 3-(4,5-dimethylthiazole-2-yl)-2,5-diphenyltetrazoliumbromide (MTT) assay is a colorimetric assay used to access cell viability. The MTT tetrazolium ring is reduced in living cells by mitochondrial dehydrogenases to formazan, resulting in a hypsochromic shift from yellow (MTT) to blue-magenta (Formazan) (Figure 26A).¹⁵⁹

The HDAC whole cell assay involves two enzymatic reactions (Figure 26). First, the cells are incubated with an acetylated substrate, in this case, the Boc-Lys(ϵ -Ac)-AMC (MAL), leading to the formation of Boc-Lys(ϵ -NH₂)-AMC. The second step consists in the formation of the fluorophore 7-Amino-4-Methylcoumarin (AMC) by the cleavage of the amide bond of Boc-Lys(ϵ -NH₂)-AMC by the addition of trypsin. Trypsin catalytic site is negatively charged and can selectively recognize and cleave the non-acetylated substrate (Figure 26B).^{157,160}

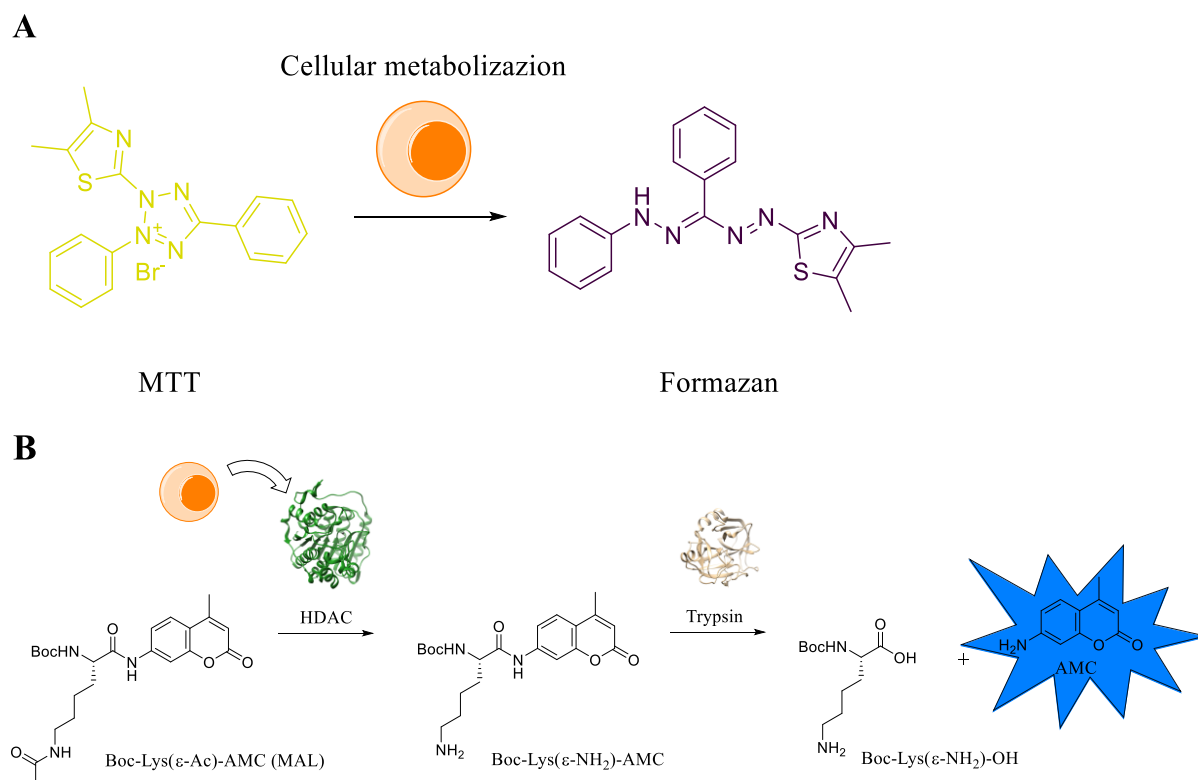


Figure 26: A) Conversion of MTT into Formazan. B) Representation of the whole cell HDAC assay.

In the assays conducted with the first set of HDACi synthesized in this work (Table 1), it was observed that more than half of the hydroxamates were more active than the controls Cisplatin and Vorinostat. The less potent analogs in the assays were the compounds containing 5-membered heterocycles **6a-c**, the chlorinated thiophene derivative **6d**, and compound **6i**. These compounds were less potent against the ovarian carcinoma compared with the oral squamous cell carcinoma cell line. In the MTT assay only IC₅₀ values lower than the controls were observed (Table 1). However, in the HDAC cell assay against these cells, the compounds **6e**, **6g**, **6h** and the dimethyl amino derivatives **6k** and **6l** showed comparable to higher activity (**6k**) than Vorinostat.

Altogether the compounds containing bicyclic rings and dimethyl amino benzoates as cap-groups were identified as the most promising structures. Based on these results, the second set of modifications were proposed (Figure 27). Further modifications of the dimethyl amino benzoates were not considered, the modifications were focused on the evaluation of novel heterocyclic cap-groups.

Despite the low activity of the compounds containing 5-membered heterocycles as cap-group in all performed assays, their structural variation was limited to heterocycles containing hydrogen acceptors. To study the effect of different 5-membered heterocycles, the introduction of pyrrole, pyrazole, imidazole, isoxazole, and thiazole as cap-groups was selected as the modification to further evaluate the effect of number and position of the heteroatoms in the activity of the compounds (Figure 27). Also, due to the high activity observed in compounds bearing a bicyclic ring, modification of the rings by the inclusion of indole, indazole, benzimidazole and benzimidazole as cap-groups was suggested (Figure 27).

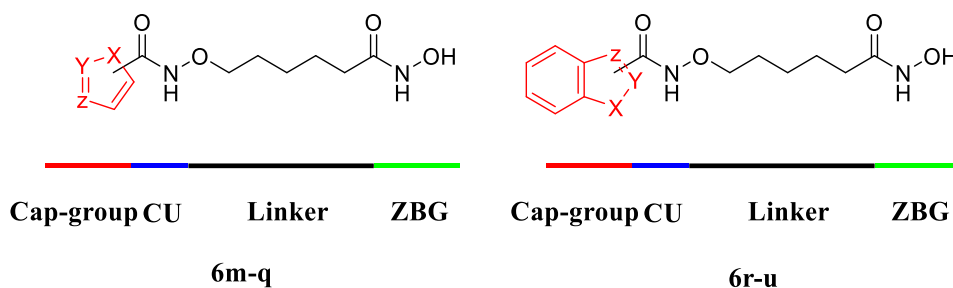
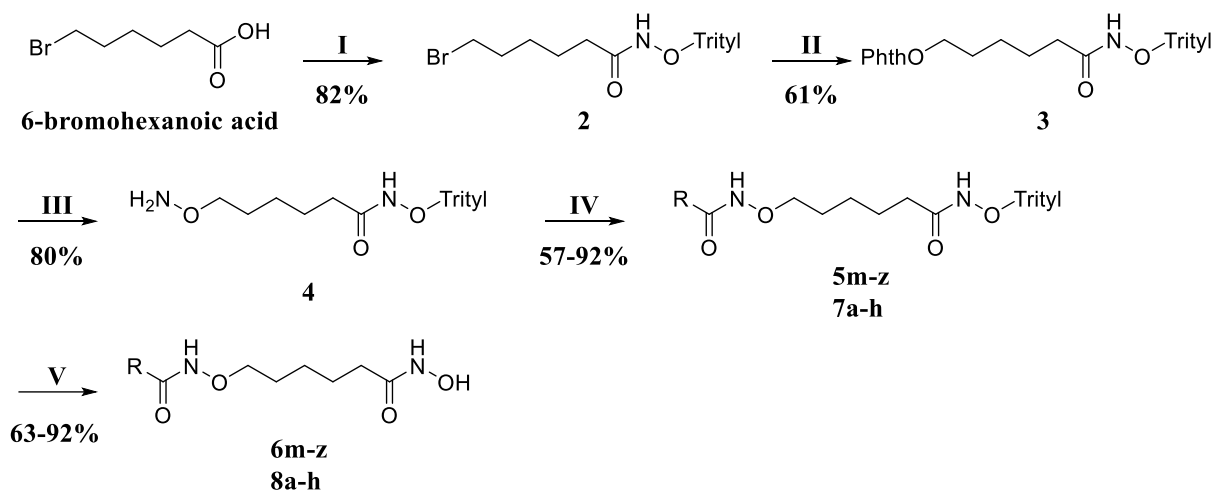


Figure 27: Representation of the first set of modifications proposed for HDACi in the classical pharmacophore model of HDACi

4.3. Synthesis of the second set of designed HDACi

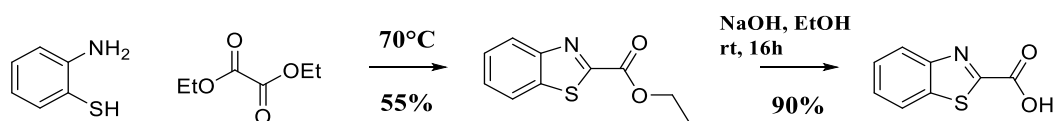
The proposed compounds were successfully synthesized by the previously described route (Scheme 1).¹⁵⁴ The key intermediary **4** was coupled with the respective carboxylic acid containing the desirable heterocycle as cap-group, followed by the deprotection of the trityl protected hydroxamate under acidic conditions and presence of triethylsilane as carbocation scavenger (Scheme 1).



Scheme 1: Reagents and conditions: I) IBCF, NMM, trityl-O-NH₂, DCM II) PhthOH, Et₃N, acetonitrile III) NH₂NH₂.H₂O, MeOH IV) EDCI, DMAP, RCOOH, DCM V) TFA, Et₃SiH, DCM.

All compounds were obtained in two steps starting from the key intermediary 4 in yields of 40-90%. In the alkoxyamide formation step, no relationship between the structure of the carboxylic acids and reaction yield could be identified. The carboxylic acids containing nucleophilic groups in the heterocycle were used without the protection of the potential nucleophile; the success of the use of unprotected heterocycles can be explained by the high nucleophilicity of the free alkoxy-amino group in the intermediary 4, compared to the weak nucleophiles present in the structure of the studied heterocycles.

Apart from the benzothiazole-2-carboxylic acid, all other carboxylic acids were purchased. The benzothiazole-2-carboxylic acid was synthesized in two steps, starting from the condensation of 2-amino thiophenol and diethyl oxalate, followed by the basic hydrolysis of the formed ethyl ester (Scheme 2). The synthesis of benzothiazole-2-carboxylic acid by the direct condensation of the 2-amino thiophenol and oxalic acid using described procedures was achieved.¹⁶¹

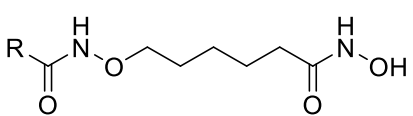


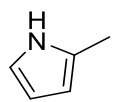
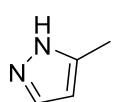
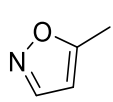
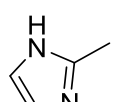
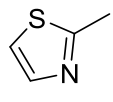
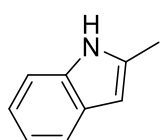
Scheme 2: Two step synthesis of benzothiazole-2-carboxylic acid.¹⁶¹

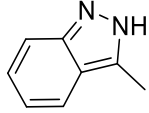
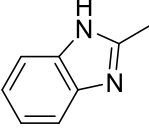
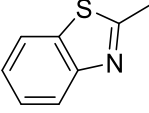
4.4. Biological evaluation of the second set of designed inhibitors

The nine hydroxamic acids **6m-u** were synthesized and their antiproliferative activity determined by the MTT and HDAC-cell assays against the cell lines A2780 and Cal27 (Table 2).

Table 2: Antiproliferative activity of the second set of designed inhibitors (**6m-u**) in MTT and HDAC whole cell assays performed against A2780 and Cal27 cell strains.



Compound	R	A2780 (μM) ^a		Cal27 (μM) ^a	
		HDAC	MTT	HDAC	MTT
6m		6.93	6.30	5.72	5.79
6n		8.09	72.2	5.41	21.3
6o		27.8	35.3	40.7	63.9
6p		16.8	86.8	11.2	90.7
6q		15.6	>100	1.70	48.4
6r		0.67	4.05	0.47	0.21

6s		0.71	7.60	0.43	1.80
6t		9.08	>100	4.17	58.2
6u		2.70	21.80	3.16	6.33
Vorinostat		1.68	2.42	0.88	1.98
Cisplatin		ND	1.88	ND	2.27

^{a)} Values are the mean of three independent experiments conducted in triplicate. ND = not determined. The standard deviations are <10% of the mean.

In all performed assays, the compounds of the second set containing 5-membered heterocycles (**6m-q**) were less active against both cells-lines compared to the controls (Table 2), reinforcing the importance of the ring size for the potency in the cell assays observed the results of the first inhibitors (Table 1). Moreover, it was also observed for both cell-lines that heterocycles containing more than one heteroatom (**6n-q**) were less active especially in the MTT-assays.

The hydroxamic analogs with isoxazole and imidazole rings (**6o** and **6p**) had the lowest *in vitro* activity among all the assayed compounds. Interestingly, the thiazole analog **6q** was particularly active in the HDAC assay in Cal27 despite the low activity in the MTT-assays cell-line.

The presence of bicyclic-containing cap-groups (**6r-u**) lead to an increase of the activity in all MTT-cytotoxicity and HDAC inhibition assays (Table 2), a trend that could already be observed in the first set of inhibitors (**6c** and **6h**) (Table 1). The bulkiness and lipophilicity of the fused phenyl ring were specifically beneficial for the activity of the inhibitors in the HDAC assays. An exception was only found for the benzothiazolic analog **6u**, where a 2-fold decrease in potency compared to Vorinostat, was detected in the Cal27 HDAC whole cell assay.

An explanation for the increase of the potency of the bicyclic compounds could be higher cell permeability. Also, the enlarged surface of the bicyclic cap-groups could favor a stronger interaction with the hydrophobic substrate recognition regions of different HDAC isoforms.

Despite the increased activity of the compounds compared to the controls, Cisplatin and Vorinostat, no compound was able to surpass the controls in the A2780 MTT-assay.

Compounds **6r** and **6s** presented the best results of all previously tested compounds, with the indole moiety **6r** showing 2-fold lower activity than the controls in the A2780 MTT assays.

4.5. Design of the third set of inhibitors

Based on the high potency in the MTT and HDAC-assays, the hydroxamate **6r** was chosen to serve as the lead structure for the third set of inhibitors (Figure 27).

Indoles are known as privileged structures in medicinal chemistry¹⁶², which can have positive effects on the pharmacokinetic properties of compounds containing this ring. Panobinostat, the only “globally” approved HDAC inhibitor indeed contains a 2-methyl-indole ring as cap-group.¹⁶³

In Panobinostat, the indole is attached to the CU at the position 3; while in compound **6r** is attached at position 2. The influence of the ring position connected to the rest of the molecule in the biological activities differs according to the HDACi scaffold. In case of Panobinostat, the determination of the optimal position occurred in late stages of drug development by studies conducted with the precursor LAK974.¹⁶⁴ The indole positions 2 and 3 were evaluated in analogues of this lead structure and, despite the fact that no considerable difference was observed in the HDAC assays, the analogue containing the 3-substituted indole was the most active against tumor cells.¹⁶⁵

Different from Panobinostat, in compounds containing indoles as cap-groups and amides as CU, the variation of the seven positions of the ring demonstrated that the with 2-substituted indole as cap-group was the most active molecule.¹⁶⁶ However, in this case only the most potent HDACi was further evaluated against tumor cells, leaving the influence of the variation of the ring position on the activity in the antitumor assays unclear.¹⁶⁶ For this reason, the first proposed modification was the alteration of position connecting the ring to the alkoxyamide unit.

The analysis of the activity of the previous set of molecules revealed that an increase of the cap-group surface caused the increase in potency of the inhibitors. To further explore this finding, the expansion of the indole to a quinoline ring was suggested. Also, the importance of the heteroatom in the cap region was investigated by introducing isoquinoline, naphthalene and quinazoline rings.

In addition to modifications in the cap-region, shortening of the linker and replacement of the ZBGs was considered. The optimal size of the linker in HDACi containing amide as CU is five

to six carbons¹⁶⁶, while in compounds containing alkoxyureas the optimal size is restricted to six carbons.¹⁵⁷ In alkoxyamides this has not yet been verified.

Among the four major classes of ZBGs found in HDACi, *ortho*-amino anilides and carboxylic acid were chosen as modifications. The *ortho*-amino anilides have the advantage of selectively inhibiting class I and carboxylic acids are weak inhibitors but can, therefore, show whether the cellular activity is affected by other parts of the molecule. Thiols require conversion to the respective pro-drug to be tested in cellular environments and are not active towards any specific class or isoform. Therefore, it was not considered in the design of the molecules. Figure 28 represents a summary of the proposed modifications of the third set of HDACi.

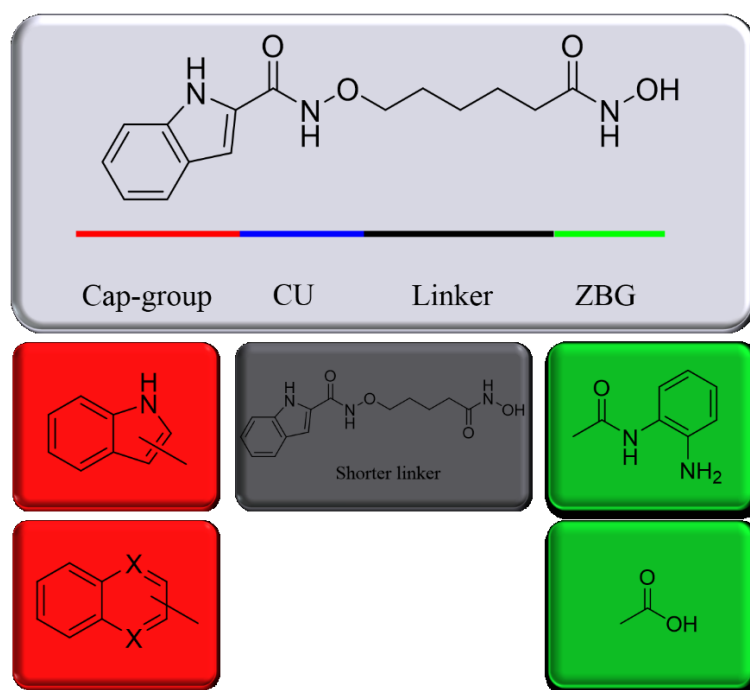
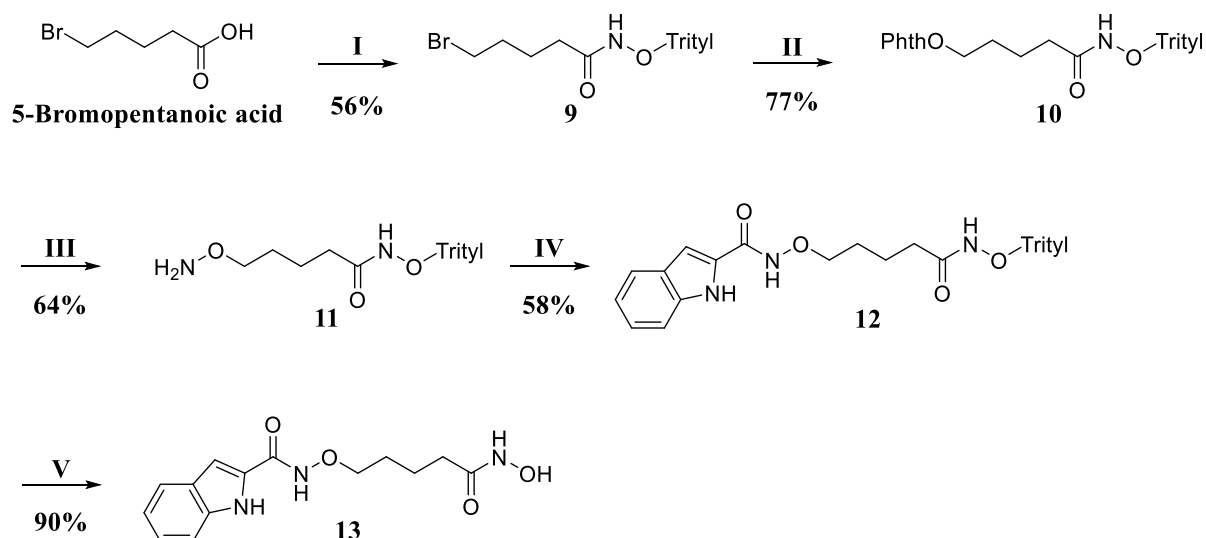


Figure 28: Proposed modifications performed on the lead structure **6r**

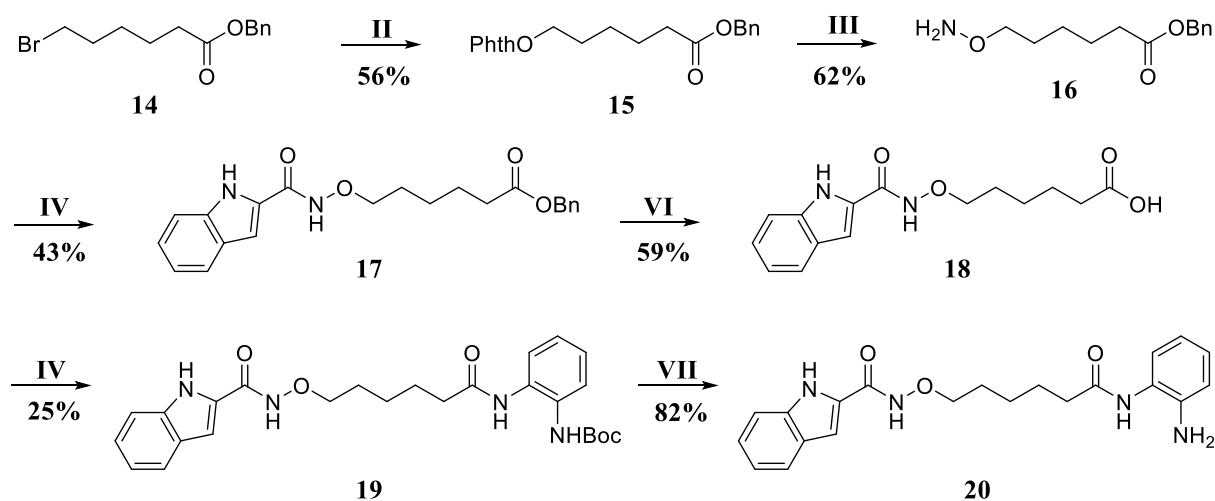
4.6. Synthesis of the third set of inhibitors

The designed compounds containing modifications in the cap-region were obtained according to the synthetic strategy illustrated by Scheme 1. The robustness of this synthetic route was observed since that in parallel to the other molecules synthesized with this method, all compounds were obtained in two steps starting from the intermediary **4** in more than 40% of yield (Scheme 1). The route was also successfully employed to obtain derivative containing a shorter linker of four methylene units **13** (Scheme 3).



Scheme 3: Reagents and conditions: I) IBCF, NMM, trityl-O-NH₂, DCM II) PhthOH, Et₃N, acetonitrile III) NH₂NH₂·H₂O, MeOH IV) EDCI, DMAP, 2-indole carboxylic acid, DCM V) TFA, Et₃SiH, DCM.

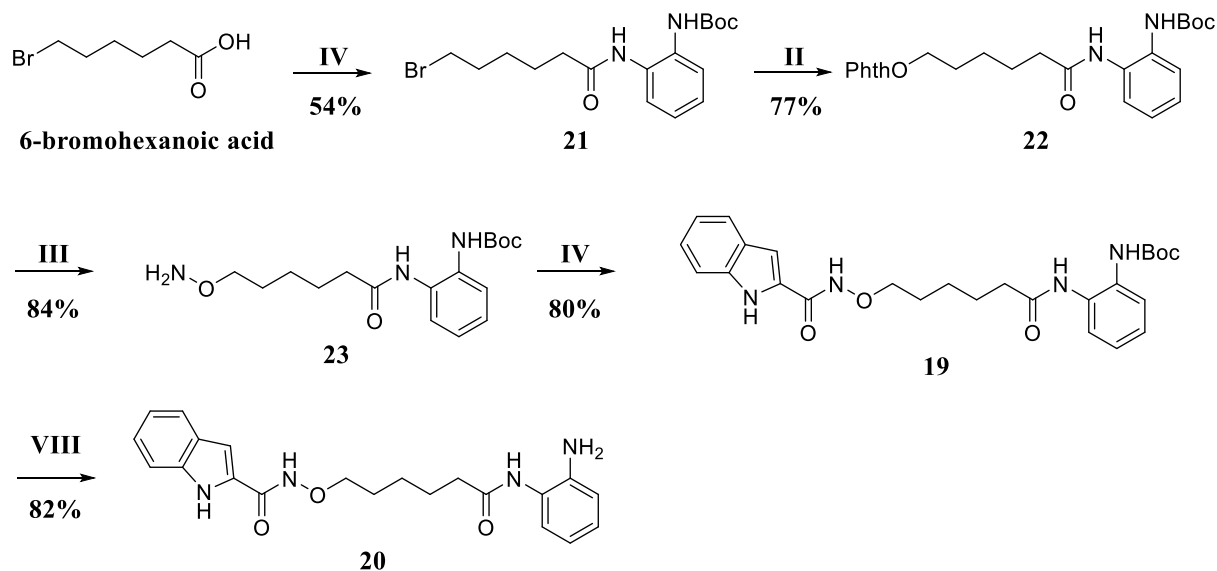
In the synthesis of the *ortho*-amino anilide analog **20** (Scheme 4), the introduction of the protected ZBG was done in later stages of the route similarly to the strategy used by Marek et al.¹⁵⁷ The modification of the synthetic route was that the desired carboxylic acid **18** could be used as starting material for the synthesis of the protected *ortho*-amino anilide **19**.



Scheme 4: Reagents and conditions: II) PhthOH, Et₃N, acetonitrile III) NH₂NH₂·H₂O, MeOH IV) EDCI, DMAP, 2-Indole carboxylic acid, DCM VI) H₂ (atm), Pd/C, EtOH IV) EDCI, DMAP, *N*-Boc-1,2-phenylenediamine, DCM VII) DCM/TFA 15%, NaHCO₃

In the synthesis of **20**, the reaction between **18** and *N*-Boc-1,2-phenylenediamine showed the lowest yield, what could be associated to the low nucleophilicity *N*-Boc-1,2-phenylenediamine and/or ineffectiveness of the coupling agent.

To test the previously established synthetic strategy¹⁵⁴ for *ortho*-amino anilides as HDACi-containing alkoxyamides, **20** was resynthesized according to the synthetic route presented in the Scheme 5.



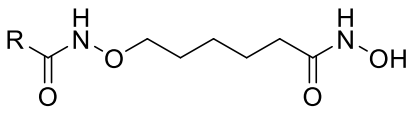
Scheme 5: Reagents and conditions: IV) EDCI, DMAP, *N*-Boc-1,2-phenylenediamine DCM II) PhthOH, Et₃N, acetonitrile III) NH₂NH₂·H₂O, MeOH d) VIII) DCM/TFA 15%, NaHCO₃.

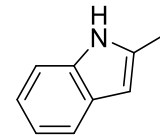
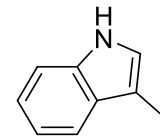
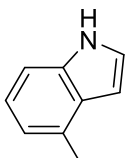
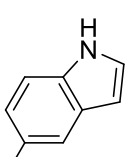
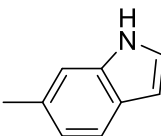
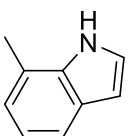
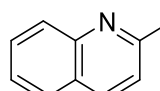
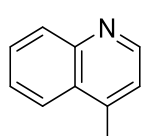
The synthetic approach used to resynthesize the compound **20** (Scheme 5) consisted in one step less than the initial strategy. The step with the lowest yield in route showed in Scheme 5 was the synthesis of **21** obtained in 54% yield, which is two times higher than the lowest yield obtained in the previous synthetic route (Scheme 4). Additionally, the key intermediary **23** obtained in the third step of the second synthetic strategy can be further used as building block for the synthesis of different alkoxy *ortho*-amino anilides with different cap-groups.

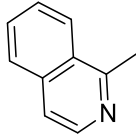
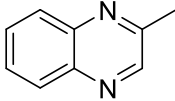
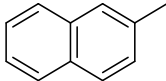
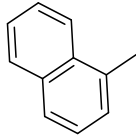
4.7. Biological evaluation of the third set of inhibitors

The synthesized molecules containing variations in the position of the indole ring attached to the CU **6v-z**, along with the extended aromatic heterocycles **8a-f** were tested in similar assays systems as the HDACi of the previous two sets of designed molecules. The result of the HDAC whole cell and MTT-assay are shown in Table 3.

Table 3: Antiproliferative activity of the third set of designed inhibitors (**6v-z** and **8a-f**) in MTT and HDAC whole cell assays performed against A2780 and Cal27 cell strains.



Compound	R	A2780 (μM) ^a		Cal27 (μM) ^a	
		HDAC	MTT	HDAC	MTT
6r		0.67	4.05	0.47	0.21
6v		1.36	7.80	0.81	1.70
6w		0.74	5.30	0.48	1.20
6x		0.85	7.50	0.45	1.30
6y		0.60	11.3	0.40	4.30
6z		0.64	1.00	0.46	1.00
8a		0.48	0.80	0.34	0.70
8b		7.62	70.00	5.97	11.90

8c		0.25	19.90	0.22	1.90
8d		0.19	7.70	2.13	4.40
8e		0.35	1.00	0.28	0.20
8f		2.39	7.60	1.89	4.20
Vorinostat		1.68	2.42	0.88	1.98
Cisplatin		ND	1.88	ND	2.27

^{a)} Values are the mean of three independent experiments conducted in triplicate. ND = not determined. The standard deviations are <10% of the mean.

Heterogeneous results were observed for the variation on the position of the indole ring. Interestingly, compound **6v** bearing the 2-substituted indole was the least active of the seven compounds with different ring positions (Table 3). Additionally, despite the comparable activity of compounds **6w-6z** to the lead structure in the HDAC-assays, all compounds were 5-fold less active in the Cal27 MTT-assays. The importance of the indole substitution was also identified in the cell viability assays performed with A2780 cells. In these assays, the 7-carboxy indole derivative **6z** was more active than the lead structure and both controls.

The analysis of the results of compounds **8a-f** confirmed that bicyclic cap-groups can be beneficial for the inhibitor potency since the use of the quinoline ring in **8a** and naphthalene in **8e** lead to an overall increase in potency compared to the lead structure. The rise in potency was especially dependent on the ring position as observed in **8b** and **8f**, which were less active against both cells lines than **6r** against both cells lines.

The isoquinoline and quinazolidine analogs **8c** and **8d** were particularly active in the HDAC cell assays against A2780 (0.25 μ M and 0.19 μ M, respectively), with **8c** also being able to inhibit Cal27 HDAC activity in nanomolar concentrations (0.22 μ M). In Cal27, the difference

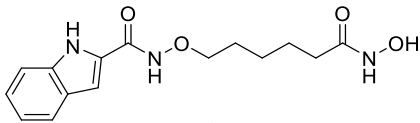
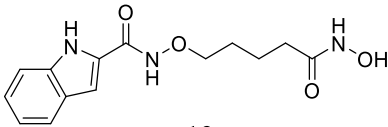
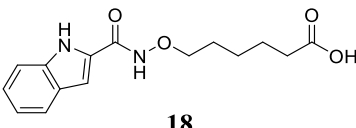
in the potency between HDAC and MTT assays of the compounds was similar to the other alkoxyamide derivatives and Vorinostat. However, in A2780 this difference was significantly higher.

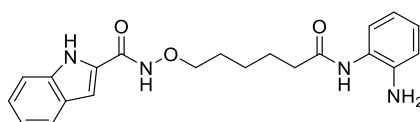
The understanding of this uncommon behavior requires further studies, but it could suggest that the set of HDAC/HDAC-containing complexes affected by these compounds does not trigger cell death or the specific targets of these compounds do not impair MTT metabolization. Another rationale assumption is cellular resistance towards the specific cellular response to these inhibitors.

The opposite behavior was observed for the dimethyl amino compounds **6k** and **6l** and in the bicyclic compounds **6g-h**, **6r**, and **8e** in the Cal27-assays. The six compounds showed higher potency in the MTT assay compared to HDAC assays, which cannot be explained without a deeper analysis of the compounds cellular targets. However, due to fact that the HDAC whole cell assay shows specifically alteration of lysine deacetylation, it would be possible that a decrease of the cell viability involves mechanisms related to isoforms with no significant lysine deacetylase activity or to off-targets.

The proposed analogs of **6r** containing alterations in the linker and ZBG **13**, **18** and **20** were also tested in HDAC and MTT assays against A2780 and Cal27 cells. The results obtained for these compounds are organized in Table 4.

Table 4: Antiproliferative activity of **13**, **18** and **20** in MTT and HDAC whole cell assays performed against A2780 and Cal27 cell strains.

Compound	A2780 (μM) ^a		Cal27 (μM) ^a	
	HDAC	MTT	HDAC	MTT
 6r	0.67	4.05	0.47	0.21
 13	3.41	9.72	1.69	4.56
 18	>100	>100	>100	>100

	3.35	2.31	1.25	5.54
20				
Vorinostat	1.68	2.42	0.88	1.98
Cisplatin	ND	1.88	ND	2.27

^{a)} Values are the mean of three independent experiments conducted in triplicate. ND = not determined. The standard deviations are <10% of the mean.

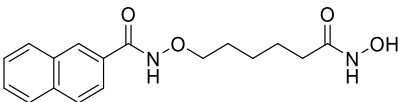
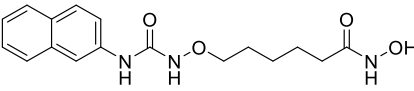
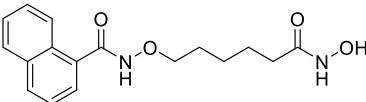
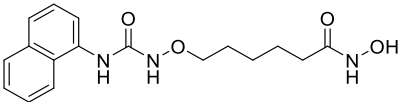
The pentanoic acid derivative **13** showed lower activity than the hexanoic analog **6r** in all assays. The reduction of potency in the HDAC assays could, in this case, be attributed to a less efficient interaction between the CU and the rim of the binding site of the targeted HDACs, however, further evaluation is required to elucidate this possibility.

In the design of the third set of compounds, the inclusion of the carboxylic acid was proposed to serve as evidence of the importance of the hydroxamate in the activity of the HDACi and also to verify if the cap-group and connecting unit could act as zinc-binding motif. The compound **18** was indeed not active in any of the performed assays in concentrations up to 100 μ M confirming the hypothesis.

The *ortho*-amino anilide **20** was less effective than the corresponding hydroxamate **6r** in the HDAC-assays of both cell lines but 2-fold more active in the A2780 MTT-assay. This class of HDACi is selective towards HDAC class I isoforms, suggesting that this class of HDACs plays a key role A2780 cell viability, which is in agreement with the results observed in several works involving ovarian carcinomas.¹⁴⁹

Alkoxyamides were previously shown to be more active than the respective alkoxyureas in the performed assays by Marek et al..¹⁵⁷ The comparison of **8e** containing 2-substituted naphthalene with the respective alkoxyurea KSK43¹⁵⁸ indeed showed an overall increase in activity (Table 5). However, **8f** was two times less active in A2780 HDAC assays than the alkoxyurea LMK163¹⁵⁷, showing equivalent potency in the MTT assays (Table 5).

Table 5: Comparison of the antiproliferative activity of alkoxyamides and ureas containing naphthalene rings as cap-groups.^{157,158}

Compound	A2780 (μM)		Cal27 (μM)	
	HDAC	MTT	HDAC	MTT
 8e	0.35 ^a	1.00 ^a	0.28 ^a	0.20 ^a
 KSK43	5.10 ^b	1.40 ^b	1.00 ^b	1.70 ^b
 8f	2.39 ^a	7.60 ^a	1.89 ^a	4.20 ^a
 LMK163	1.06 ^c	7.63 ^c	ND	ND

^a Values showed in Table 3 ^b Values described by Stenzel et al.¹⁵⁸ ^c Values described by Marek et al.¹⁵⁷
 ND = not determined. The standard deviations are <10% of the mean.

The reduction of activity in **8f** could be related to the presence of a substituent at 2 position of the benzenic ring, what was also observed in derivatives containing *ortho*-methyl benzoates as cap-groups.¹⁵⁷

Following the analysis of the cellular assays, the compounds **6r**, **8a**, **8c-e** and **20** were selected to be further evaluated regarding their biological activity. The first step was the determination of their potency against the enzymatic target in a cell-free assay system.

4.8. Evaluation of **6r**, **8a** and **8c** in Glioblastomas

Central nervous system neoplasms are classified according to their cell origin and behavior; the neoplasms originated from astrocytes are known as Astrocytomas and are responsible for 15% of all brain tumors. This kind of cancer is divided in type I, II, III and IV by the degree of

aggressiveness, type IV or Glioblastoma multiforme being the most aggressive type. This specific neoplasm is responsible for more than 50% of the Astrocytomas with an incidence of 2-3 cases per 100.000 persons per year¹⁶⁷, affecting especially elderly people.¹⁶⁸

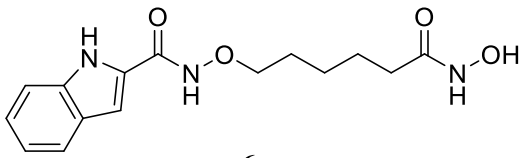
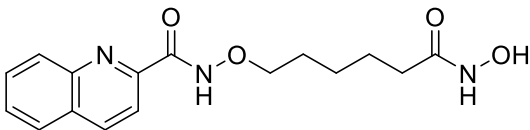
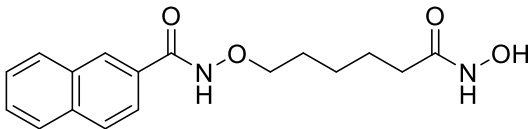
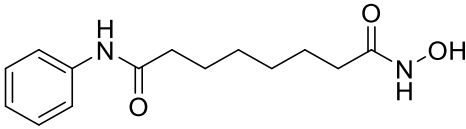
The first line of treatment of Glioblastomas (GBM) is surgery combined with radiation and the alkylating agent Temozolomide (TMZ). Despite the used combination therapy, the treatment of Glioblastomas is challenging, since the invasive nature of this malignancy restricts the effectiveness of complete eradication of the cancer cells by surgery. Also, the up-regulation of the DNA-repairing system have been already observed in these malignancies, the increase rate of DNA repair counterpoises the effects of the alkylating agent TMZ decreasing, even more, the success rate of the combination therapy.¹⁶⁹

The expression profile of HDAC in GBM is still being studied, but it has already been observed that in these cells HDAC1, 3 and HDAC6 are slightly increased when compared to non-neoplastic cells. Also, in more aggressive tumors higher levels of HDAC1 and 3 were found.¹⁷⁰

The introduction of HDACi in the combination therapy of GBM and single therapy have been demonstrated a valuable option. The clinical relevance of this class is increasing especially in combination therapies due to the radio and chemosensitizer properties of these inhibitors, allowing them to promote synergistic effect with both TMZ and radiotherapies. Among the different HDACi tested against GBM, Vorinostat has reached the most advanced stages, being present in several phase II studies in association with different antineoplastic agents.^{170,171}

To further investigate the effect of the HDACi against Glioblastomas, the hydroxamates **6r**, **8a** and **8c**, which showed the highest antiproliferative activity against the carcinoma cell lines previously tested in this work, were chosen to be tested against three different GBM cell lines. The assays were performed in collaboration with Dr. Marc Remke at the Universitätsklinikum of Düsseldorf and the results are shown in Table 6.

Table 6: Antiproliferative activities of **6r**, **8a**, **8c** and Vorinostat in Glioblastomas cells lines.

Compounds	IC ₅₀ (μ M) ^a		
	LN18	LN229	U251
 <p>6r</p>	0.73	2.50	2.43
 <p>8a</p>	0.50	2.13	2.07
 <p>8c</p>	0.58	1.88	1.88
 <p>Vorinostat</p>	1.69	6.42	3.46

^a Values are the mean of three independent experiments conducted in triplicate. The standard deviations are <10% of the mean.

The analysis of the results demonstrated that all the assayed compounds were at least 1.5-fold more active than Vorinostat in the three cell lines. The potency of the three inhibitors did not present significant difference among each other, a behavior also observed in the enzymatic assays and antiproliferative assays against the cell line Cal27.

Interestingly, the cell line LN18 was more sensitive to the presence of HDACi than LN229 and U251. The factors involved in the higher sensitivity of this cancer cell line to HDACi are still not elucidated and require further evaluation. However, in the recent work published by Patil et al.¹⁷², in which the authors evaluated the gene expression of six GBM cell lines including LN18, LN229, and U251, an overexpression of human telomerase reverse transcriptase (hTERT) was observed in LN229 and U251, but not in LN18.

The human telomerase reverse transcriptase is the catalytic subunit of Telomerase, which is essential for the senescence process and it is often overexpressed in cancer cells. Epigenetic mechanisms are deeply involved in the control of telomerase activity and the inhibition of HDACs results in the suppression of hTERT facilitating cell death.¹⁷³ Therefore cell lines where a overexpression of hTERT is likely less sensitive to the presence of HDACi, what is in accordance to the observed results.

4.9. Enzymatic assays

Initially, the assessment of HDAC enzymatic activity was performed by incubating the enzymes with radiolabeled histones and measuring the release of marked acetate. The dependence of acetate extraction and use of radioactive molecules have limited the application of this heterogeneous assay in large scale, what was later overcome by the advent of homogenous fluorogenic assays.¹⁷⁴

The HDAC assays are either performed using fluorogenic substrates or generating the fluorophores of the deacetylated lysine. Fluorogenic substrates such as MAL (Figure 24) and Cbz-Lys(ϵ -Ac)-AMC (ZMAL) (Figure 29A)¹⁷⁵ must have the fluorophore cleaved by proteases such as trypsin, while the reaction of the deacetylated lysine with fluorescamine results in a fluorogenic product that can be directly measured (Figure 29B).¹⁷⁶

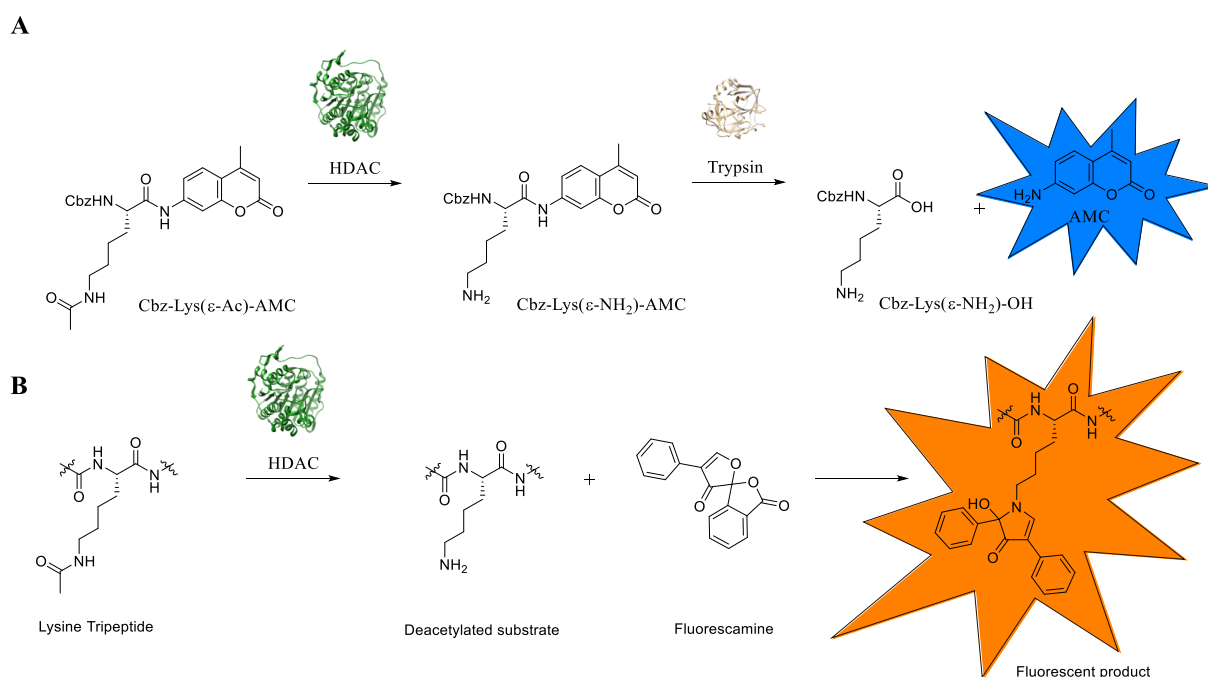
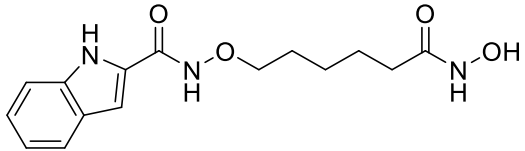
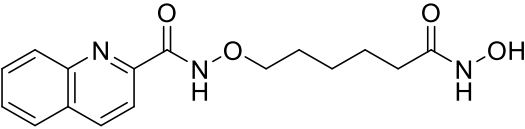
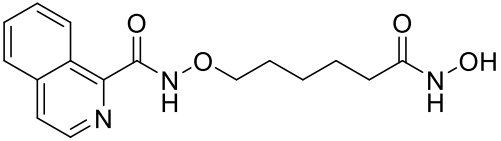
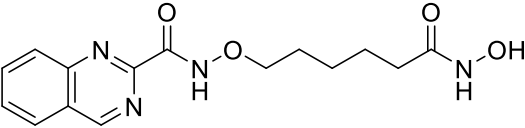
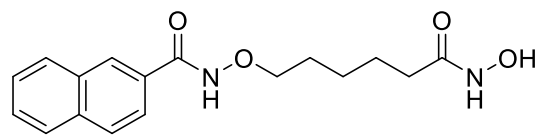
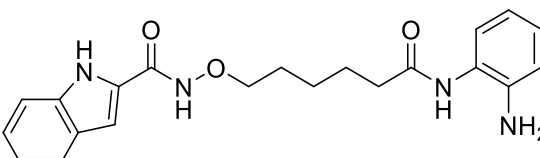
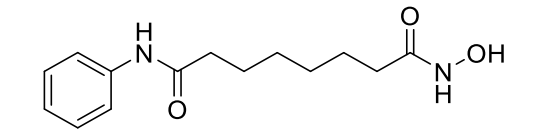


Figure 29: HDAC fluorogenic assays represented by the use of fluorogenic substrates (A) and label-free conditions (B)

The preliminary evaluation of enzymatic activity in cell-free system of **6r**, **8a**, **8c-e** and **20** was done by measuring the IC₅₀ of these compounds against HDAC1 and HDAC6 (Table 7). The assays were performed in collaboration with Dr. Marc Remke at the Universitätsklinikum of Heinrich Heine University in Düsseldorf. In these assays, the substrate ZMAL was chosen as the fluorogenic substrate due to the affinity of the tested enzyme towards this acetylated lysine analog.¹⁷⁷ The enzyme concentrations were 10 ng/ μL and 35 ng/ μL for HDAC1 and HDAC6 respectively. Trypsin was used for the cleavage of the fluorophore according to previously described procedures.¹⁵⁸

Table 7: Inhibition activities of **6r**, **8a**, **8c-e** and Vorinostat against HDAC1 and HDAC6.

Compounds	IC ₅₀ (μM) of HDAC isoforms		SI ^b
	HDAC1 ^a	HDAC6 ^a	
 <p>6r</p>	0.037	0.019	1.9
 <p>8a</p>	0.049	0.028	1.7
 <p>8c</p>	0.994	0.125	7.9
 <p>8d</p>	0.387	0.177	2.2

 <p style="text-align: center;">8e</p>	0.097	0.027	3.6
 <p style="text-align: center;">20</p>	0.689	>10	<0.06
 <p style="text-align: center;">Vorinostat</p>	0.080	0.101	1.2

^a Values are the mean of two independent experiments conducted in triplicate. ^b SI was calculated by dividing the IC₅₀ of HDAC1 by HDAC6. The standard deviations are <10% of the mean.

The analysis of Table 6 results showed that compounds **6r**, **8a**, and **8e** have potencies and isoform preference (SI 1.9, 1.7 and 3.6 respectively) comparable to Vorinostat (SI 1.2). Compound **8c** showed the highest preference towards HDAC6 among the assayed compounds with SI of 7.9 fold, a value similar to Ricolinostat (Figure 12) with SI of 12 fold.⁷⁹ However the potency of **8c** in both isoforms was lower than the other tested hydroxamates, suggesting that the isoquinoline ring has unfavorable interaction with the entrance of the binding side in HDAC1, being relatively well tolerated in HDAC6. The hydroxamate **8d** was 10 times less active in the enzymatic assay than **8a** and **8e**, which contain as cap-groups 2-substituted quinoline and naphthalene ring respectively. This shows that the presence of the second nitrogen of the quinazoline is unfavorable for the interaction of **8d** with both isoforms. Consistent with the isoform selectivity of *ortho*-amino anilides, the inhibitor **20** was not active against HDAC6 and 8-fold less active than the respective hydroxamate **6r**, what is explained by the time-dependent inhibition characteristic of this class (section 1.1.6).

4.10. Molecular docking

Binding modes of the synthesized compounds were evaluated in HDAC1 (PDB ID 4K BX) and HDAC6 (PDB ID HDAC6) assayed against HDAC1 and HDAC6 in docking studies of the HDACi in the respective crystals structures.

Metalloenzymes and many other biological targets like nucleic acids and aspartic-acid protease have special requirements to be applied in docking studies. Each of them presenting particular features to be accounted for in the dockings studies such as the metal coordination and interaction in metalloenzymes, the complex water network necessary for the interaction of small molecules with nucleic acids and the diaspertate protonation in aspartic acid protease.¹⁷⁸

The use of structure-based drug design (SBDD) in the design of HDACi inhibitors has been proved to be a promising approach to design novel and potent inhibitors.¹⁷⁸ Autodock3¹⁷⁹ in combination with DrugScore¹⁸⁰, for example, was successfully used to design novel HDACi containing alkoxyureas as connecting unit with improved isoform preference compared to their initial lead structure.¹⁵⁸ In this work, the molecular dockings aimed for a rationalization of the results obtained in the enzymatic assays rather than a tool for the design of new compounds. Therefore, a different approach from the already established docking protocol was used.

In the work performed by Ballante et al., the performance different software in docking studies involving different HDAC isoforms were evaluated. In this study, three different groups of co-crystallized ligands in HDACs were used; hydroxamic acids and thiols, the protonated forms of these hydroxamic acids and thiols and the available different ZBGs in their non-charged forms. Among the dockings software, Autodock4.2 (AD4.2) demonstrated high accuracy in predicting dockings poses with correct coordination of the ZBG, especially for hydroxamic acids and thiols in their anionic forms.¹⁸¹

Autodock4.2 uses a grid-based system to define the area for calculation of the interaction energy of the probes and the target and a semi-empiric force field to perform the energy calculations. The primary search algorithm of the program is the Lamarckian genetic algorithm, which combines traditional genetic algorithm concept with the hereditary exchange of information between populations.¹⁸²

Using the parameters described by Ballante et al.¹⁸¹ the redocking of TSA in the structure of HDAC6 CDII (PDB ID 5EDU)⁷⁹ was performed. In this validation study, 100 docking poses were generated and organized in clusters. The first docking pose of the highest populated cluster containing correct zinc coordination and lowest RMSD from the co-crystallized ligand was

chosen. Correct zinc pose was defined as distance lower than 3.5 Å from the hydroxylic oxygen of the hydroxamic acid and the zinc atom.⁸⁰

The chosen docking conformation in the redock of TSA in HDAC6 showed RMSD of 1.92 Å compared to the co-crystallized ligand, however different from the reference, the hydroxamate interacted with the zinc in a monodentate way. To test if the monodentate conformation depends on the protonation of the ligand, a second redock was performed with the protonated form of the hydroxamate. The bidentate interaction between TSA and the zinc ion was indeed observed in this condition, but a higher deviation from the reference was observed (RMSD 2.67 Å).

TSA was recently shown in the crystal structure of HDAC6 PDB ID 5WIG, to be able to alternate between mono and bidentate coordination. Both conformations of the hydroxamic acid moiety of TSA are superimposed in this crystal and interestingly, a similar behavior was observed when the two docked structures were superimposed (Figure 30), suggesting a correct prediction both forms by the software. Since hydroxamates mainly interact as bidentate ligands⁷⁹, the ligand protonation was kept in the further docking studies.

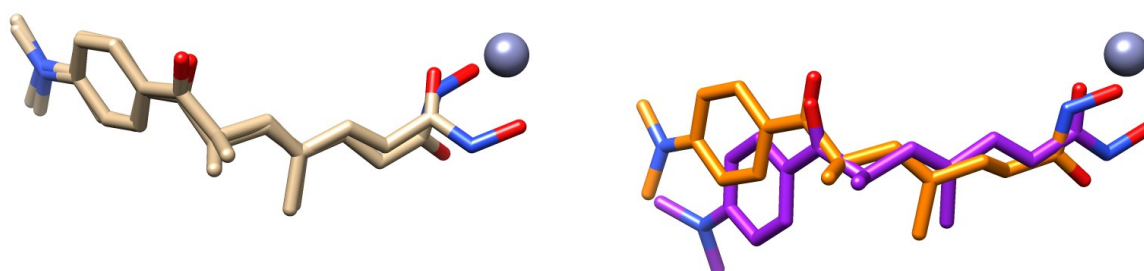


Figure 30: Structure of TSA in the HDAC6 crystal PDB ID 5IWG showing mono and bidentate zinc coordination (light brown) and superposition of the docked poses of the protonated (purple) and deprotonated (orange) forms of TSA.

In addition to the modification of the ligand protonation, protonation states of the two histidine residues His610 and His611, part of the catalytic His-Asp dyads (Figure 3), were analyzed. The redock of TSA in HDAC6 was performed using the given protonation state of the crystal structure, where both residues are in their protonated form (HID). In several works though, the deprotonated form of both histidine residues containing the hydrogen at the delta position of the imidazole ring (HD1) was successfully applied.^{43,183,184} Therefore, the role of the protonation of the side chain of these amino acids for the docking is still unclear.¹⁸³

To analyze the importance of the protonation of the histidine residues of the catalytic dyads, TSA was redocked in the HDAC6 crystal 5EDU containing both His610 and His611 in the HID forms and also only with His611 deprotonated (HD1).

The His611 in HDAC6 correspond to His143 in HDAC8, which was suggested by Gantt et al.¹⁷ as the dyad that acts as a basic and acidic catalyst. During the catalysis, specifically, this residue changes the protonation states, being deprotonated when the produced acetate interacts with the zinc in a bidentate way (Figure 3). Therefore, His611 was single evaluated with the proton assigned to the delta position of the imidazole ring (HD1).

In each docking study, according to the mentioned criteria for the selection, one docking pose was chosen. The RMSD values of the selected conformations and the TSA in the crystal 5EDU⁷⁷ were 2.35 Å when His610 and His611 were deprotonated and 2.40 Å for the single deprotonated His611. These RMSD values are comparable to initial obtained RMSD of 2.67 Å using the protonation found in the crystal. Based on these results, the further docking studies were conducted without alteration of the histidine protonation.

The compounds **6r**, **8a**, **8c-e** and **20** were docked in their protonated form in the structure of HDAC6 CDII with PDB ID 5EDU using Autodock4.2 and their docking poses were chosen according to the mentioned conditions.

The analysis of the docking poses showed that apart from **8d**, the alkoxyamide moiety of the docked inhibitors faced the Ser531, the residue responsible for the anchoring of peptide substrates located at the rim of the binding site (section 1.1.7.2). The positions of the alkoxyamide in the dockings suggest a direct interaction between the serine and CU of the inhibitors (Figure 31). In the binding pose of hydroxamate **8e**, instead of the alkoxyamide posing close to the Ser631, one of the nitrogen of the quinazoline ring is observed in this region, what could also lead to a favorable interaction with this part of the enzyme (Figure 31B).

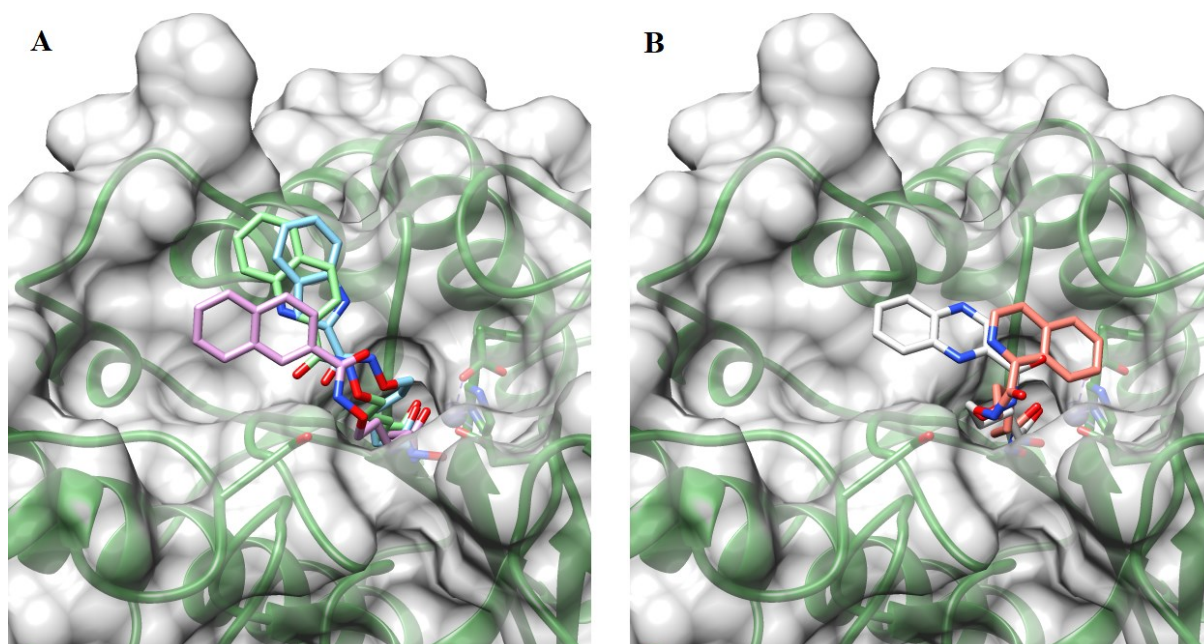


Figure 31: A) Docking of compounds **6r** (blue), **8a** (green) and **8e** (pink) in HDAC6 PDB 5EDU B) Docking of compounds **8c** (salmon) and **8d** (white) in HDAC6 PDB 5EDU.

The bicyclic cap-groups in compounds **6r**, **8a** and **8e** laid in the proximity of the hydrophobic region ranging from Asp460 to Pro484, a region that can accommodate the cap-groups of different HDACi (section 1.1.7.2). The quinazoline ring of **8d** in addition to the interaction with Ser531, occupied the entrance of the basin, a hydrophobic part of the recognition surface, which flanks the binding site of the enzyme (Figure 31B). The isoquinolinic cap-group of **8c** was positioned in the opposite side of the region occupied by the cap of the other inhibitors, positioning parallel to a small crevice in the shallow binding site of HDAC6. The *ortho*-amino anilide **20** did not present any docking pose with correct zinc binding group as expected since the ZBG size is incompatible with the catalytic site of HDAC6.

The docking of the selected compounds in HDAC1 were performed using the crystal structure PDB ID 4BKX¹⁸⁵ which is co-crystallized with an acetate molecule. The same docking conditions were applied as well as the parameters for selection of the docking poses.

Similarly, to the docking in HDAC1, the alkoxyamide group of the docked hydroxamic acids with exception of **8d** faced the amino acid residue responsible for the anchorage of the peptide substrates (in HDAC1 Asp99) indicating a formation of a hydrogen bond (Figure 32). In the same way, as observed in HDAC6, the connecting unit of **8d** stood distant from Asp99 suggesting no possible interaction between them (Figure 32B).

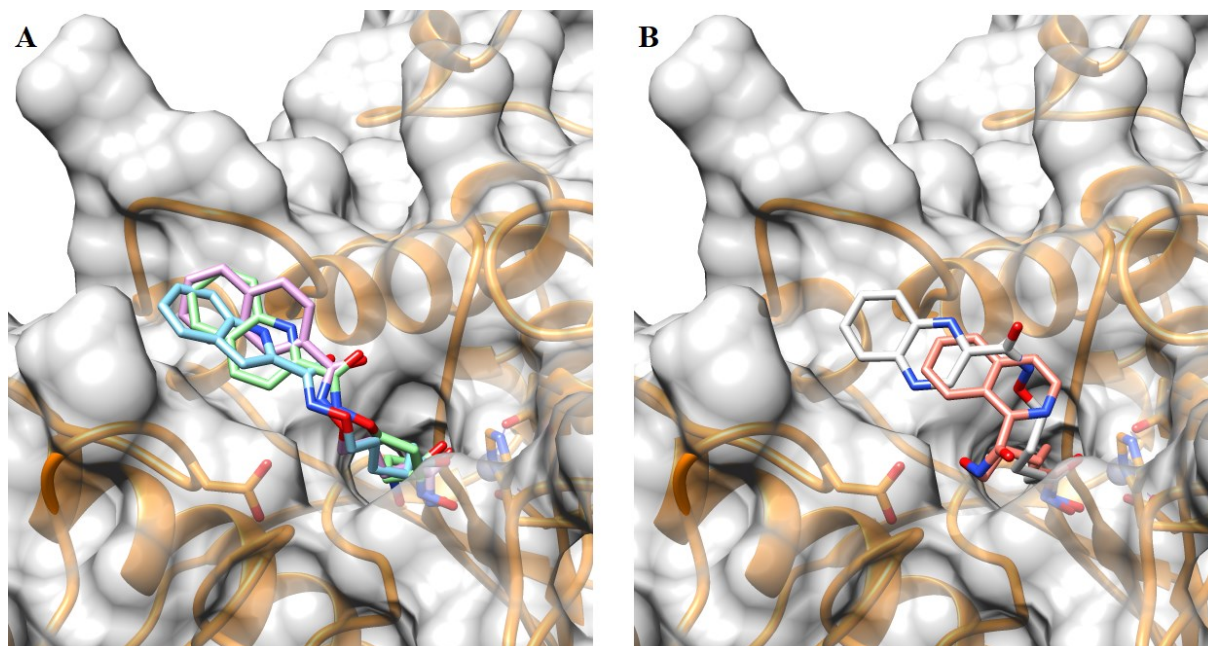


Figure 32: A) Docking of compounds **6r** (blue), **8a** (green) and **8e** (pink) in HDAC6 PDB 5EDU B) Docking of compounds **8c** (salmon) and **8d** (white) in HDAC1 PDB 4BKX.

In the binding conformation of **6r**, **8a**, **8d**, and **8e** in the structure of HDAC1, the cap-groups were situated in the hydrophobic cleft formed between Cys100-Pro101 and His28-Pro29 (Figure 32).

Different from HDAC6, in HDAC1 the isoquinoline ring of **8c** interact with the same region as the bicyclic cap of the other hydroxamates, however, due to the narrower entrance of HDAC1, only the half bicycle can interact with the hydrophobic cleft, leaving the other half of the heterocycle exposed to the solvent (Figure 32B). The smaller surface of interaction of **8c** cap-group with the entrance of HDAC1 is likely the cause of the decreased potency of this compound in the enzymatic assays performed using this enzyme and could explain the preference of this compound to HDAC6.

The binding mode of **20** in HDAC1 was considerably different from its hydroxamic homolog **6r**. In **20** the connecting unit formed a hydrogen bond with His173 instead of Asp99, while the indole ring posed parallel to the loop containing Leu271 and Cys273 in the opposite side of the cleft where the other cap groups were observed (Figure 33).

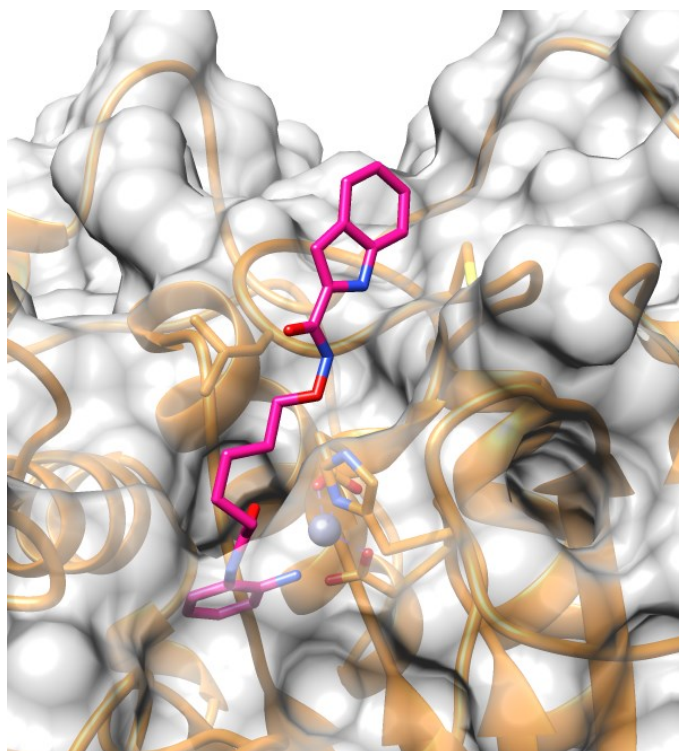


Figure 33: Docking of compound 20 (purple) in HDAC1 PDB 4KBX

The docking studies suggest that in general, the bicyclic cap of the HDACi interacts with hydrophobic regions of the enzyme substrate recognition surfaces. These results reinforce the hypothesis that the potency of the compounds containing hydrophobic bicyclic rings as cap-groups in the cellular assays would be a result of the strong interaction of the hydrophobic cap with the enzyme binding site and the consequent increased of cell permeability provided by these rings.

4.11. Evaluation of chemosensitizing effects of selected HDACi

As previously discussed in this work HDACi have been more successfully used in combination chemotherapies than as single agents, being also effective against drug-resistant cancers (section 1.1.9). Particularly, Marek et al. demonstrated that HDACi containing alkoxyamide as connecting unit were able to enhance the sensibility of four cancer cells lines, including A2780 and Cal27, to cisplatin.¹⁵⁷

Due to the fact that the most promising compounds synthesized in this work were more active against Cal27 (Table 3), this cell line was chosen for further studies. The evaluation of the chemosensitizing effects of **6r**, **8a**, and **8c-e** are currently being performed by MSc. Christian

Schrenk in the laboratory of Prof. Matthias U. Kassack at the Heinrich Heine Universität of Düsseldorf, however, some preliminary results are already available.

Initially, the activity of **6r**, **8a**, and **8c-e** against their biological targets were evaluated in hyperacetylation assays of tubulin and histone H3 in Cal27 sensitive and cisplatin-resistant cell lines (Figure 34).

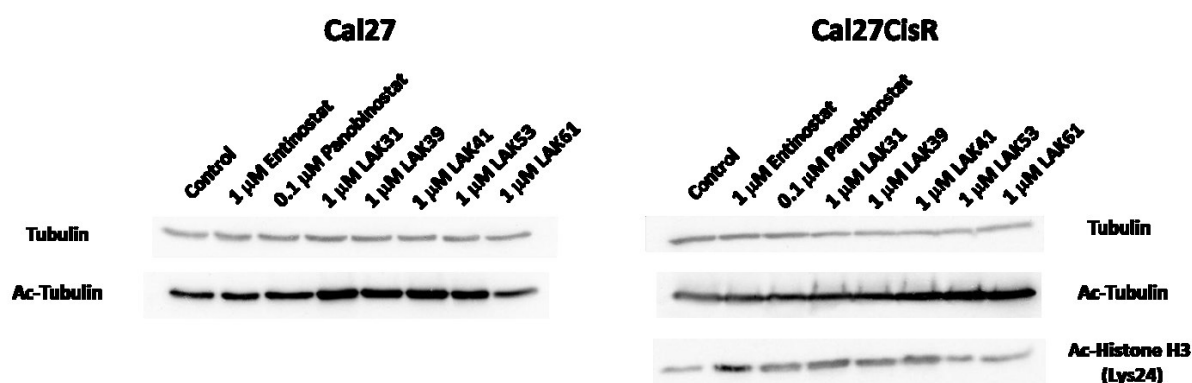


Figure 34: Induction of tubulin (Ac-tubulin) and histone H3 (Ac-Histone H3) acetylation by Panobinostat, Entinostat and the synthesized compounds **6r** (LAK31), **8a** (LAK41), **8c** (LAK53), **8d** (LAK61) and **8e** (LAK39). Western Blot Analysis was performed once.

The tumor cell lines Cal27 and the cisplatin-resistant clone Cal27CisR were treated with either 1 μM of Entinostat, **6r** (LAK31), **8a** (LAK41), **8c** (LAK53), **8d** (LAK61), **8e** (LAK39) or 0.1 μM Panobinostat. Protein extracts were prepared after 24 hours of incubation before they were analyzed by Western Blot immunostaining with antibodies against acetylated α -tubulin and acetylated Histone H3. α -Tubulin was used as protein loading control.

Entinostat, a class I selective HDACi, did not cause hyperacetylation of tubulin in both Cal27 cell lines but led to hyperacetylation of H3. This behavior can be explained by the major physiological role of class I HDACs in H3 deacetylation, while α -tubulin is a specific substrate of HDAC6 (section 1.1.6 and 1.1.7). Panobinostat, despite the high *in vitro* and *in vivo* activity, was not different from the control, what could be explained by the lower concentration of this inhibitor used in this preliminary assay.

The HDACi **6r**, **8a** and **8e** led to hyperacetylation of both H3 and α -tubulin, suggesting that these inhibitors can affect both classes I and IIb, a result that is in agreement with the enzymatic results presented in Table 6. Also, in agreement with the enzymatic assays, **8c**, the compound with the highest preference for HDAC6, promoted hyperacetylation mainly of α -tubulin.

The next step of the study was the evaluation of the combination of cisplatin with **6r**, **8a**, **8c** and **8e** (Table 7). IC₅₀ values were determined after treatment of Cal27 and Cal27CisR with

cisplatin alone or a combination of cisplatin with 0.3 μ M (Cal27)/0.5 μ M (Cal27CisR) **6r**, **8a**, **8e**, 2 μ M (Cal27)/3 μ M (Cal27CisR) **8c**, 3 μ M (Cal27)/4 μ M (Cal27CisR) **8d** respectively. Vorinostat was included as the control.

Table 8: Evaluation of cisplatin combination with **6r**, **8a**, **8c** and **8e** in Cal27 and the cisplatin-resistant clone Cal27CisR.

Compounds	Cell line			
	Cal27		Cal27CisR	
	IC ₅₀ (μ M) ^a	SF ^b	IC ₅₀ (μ M) ^a	SF ^b
Cisplatin	37.4	-	48.5	-
Cisplatin + 6r	5.01	7.5	ND	ND
Cisplatin + 8a	4.03	9.3	4	12
Cisplatin + 8c	2.03	18.4	5.2	9.3
Cisplatin + 8d	14.27	2.62	ND	ND
Cisplatin + 8e	10.1	3.7	10.1	4.8
Cisplatin + Vorinostat	2.08	18.0	6	8.1

^a Values are the mean of two independent experiments conducted in triplicate. ^b The shift factor (SF) was calculated by dividing the IC₅₀ of cisplatin alone and the IC₅₀ of the corresponding drug combinations. ND = not determined. The standard deviations are <10% of the mean.

The evaluated compounds were able to enhance the cisplatin potency in both sensitive and cisplatin-resistant cells. In these assays, compounds **8a** and **8c** demonstrated the largest increase in the sensibility to cisplatin in both cell lines, **8a** showing SF of 9.3 and 12 in the sensitive and resistant cell lines respectively and **8c** a SF of 18.4 against Cal27 and 9.3 in the Cal27CisR assay. To verify whether the increase in cisplatin potency in combination with the tested HDACi was additive or synergistic, synergy studies were performed using different combinations of cisplatin and HDACi (Table 9).

Table 9: Synergism studies between cisplatin and **6r**, **8a** and **8c** in Cal27.

		Cal27				
		6r (μM) ^a				
cisplatin		0.2	0.25	0.3	0.35	0.4
2		0.63	0.37	0.35	0.21	0.14
5		0.09	0.11	0.06	0.05	0.04
10		0.04	0.03	0.02	0.02	0.02

		Cal27				
		LAK41 (μM) ^a				
cisplatin		0.2	0.25	0.3	0.35	0.4
5		ND	0.03	0.03	0.03	0.02
10		0.01	0.01	0.02	0.02	0.01

		Cal27					
		LAK53 (μM) ^a					
cisplatin		0.5	0.75	1	1.25	1.5	2
5		ND	0.03	0.03	0.03	0.02	0.06
10		0.01	0.01	0.02	0.02	0.01	0.03

^a Values are the mean of three experiments. Standard deviation is < 10 % of the mean. ND = not determined.

The cancer cell line Cal27 was treated with different combinations of cisplatin and **6r**, **8a** or **8c**. CI (combination index) was calculated using the software Compusyn 1.0 based on the Chou-Talalay method.¹⁸⁶ CI > 1 indicates antagonism, CI = 1 indicates an additive effect and CI < 0.9 indicates synergism. All tested combinations showed combination indices lower than 0.7, demonstrating synergic effects.

Cisplatin alters the structure of DNA by cross-linking DNA strands. If not repaired by cellular repair-systems, DNA-platination leads to severe cellular responses predominantly leading to apoptosis-induced cell death.¹⁸⁷

Apoptosis, as mentioned before (section 4.1), is a programmed and regulated cell-death process, which is a natural process also essential in physiological processes. Apoptosis can occur through an intrinsic or extrinsic pathway. The first is a response to intra-cellular stimuli and the second is induced by external factors related to immune response. Both pathways are mediated

by a family of cysteine proteases called Caspases. Executioner caspases (caspase-3 and 7) are especially important in apoptotic cell death and their activation is considered as a hallmark of apoptosis.¹³⁸

To verify the effect of **6r**, **8a** or **8c** in apoptosis-induced cell death, compounds were tested in caspase activation assays using Cal27 cell line (Figure 35).

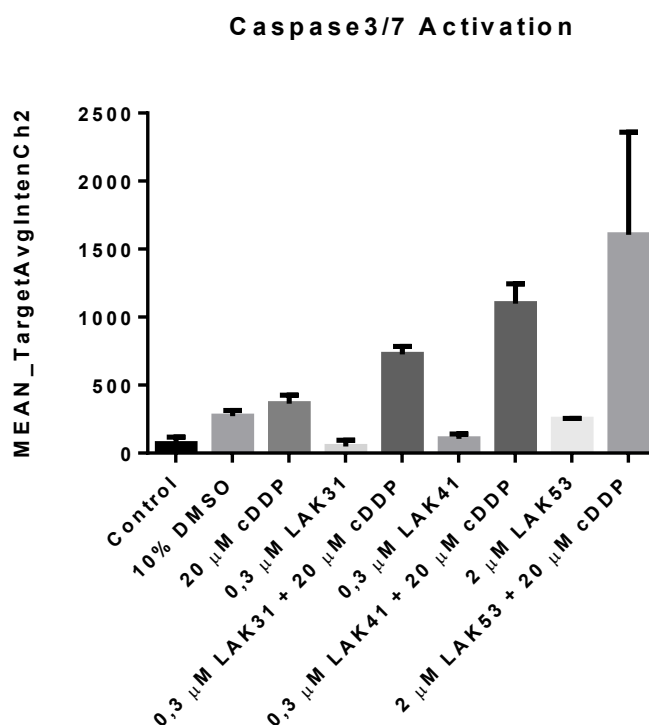


Figure 35: Induction of caspase3/7 activation by **6r**(LAK31), **8a**(LAK41) and **8c**(LAK53) alone or in combination with Cisplatin (cDDP).

The tumor cell line Cal27 was treated with cisplatin, **6r**, **8a**, **8c** alone or in combination. Drug-induced apoptosis was detected with CellEvent Caspase 3/7 Green Detection Reagent. Quantification was assessed via automated microscopy. Hoechst staining (blue) was used for nuclei (primary object) detection, while green fluorescence was used to detect Caspase 3/7 activation. Quantification of Caspase3/7 activation is depicted as the mean average intensity of the FITC channel (MEAN_TargetAvgIntenCh2). Untreated cells served as negative control. Values were derived from analyzing at least 200 cells per well. Mean from two wells is indicated.

The hydroxamates **6r**, **8a**, and **8c** assayed without cisplatin showed a low degree of caspase 3/7 induction, however, in combination with cisplatin, all three HDACi increased the pro-apoptotic effect of cisplatin. Compound **6r** and **8a** although tested in the same concentration in these

assays enhanced cisplatin activity differently. Compound **8a** led to a higher apoptosis induction, despite being 3-fold less potent than **6r** in the MTT-cytotoxicity assay against Cal27 (Table3).

4.12. Conclusion

An initial set of twelve HDACi (**6a-l**) previously assayed against malaria was evaluated for their antiproliferative and HDAC activities in cell-based assays against ovarian carcinoma (A2780) and oral squamous carcinoma (Cal27), two neoplasms with high prevalence and challenging treatment. Among this first set of inhibitors, the compounds containing bicyclic cap-groups **6g** and **6h** also **6k** and **6l** containing dimethyl amino in *para* and *meta* position of the phenyl ring (section 3.4 Table 1) showed activities similar to Vorinostat, the first approved HDACi, which has demonstrated clinical relevance in both tested carcinomas.

To further evaluate the effect of heterocycles as cap-groups, the second set of HDACi containing different heterocyclic rings (**6m-u** section 4.4 Table 2) was synthesized using the synthetic route used in the synthesis of the initial compounds. The second set of inhibitors was then evaluated against A2780 and Cal27 and the analysis of the results revealed a similar pattern observed in the assays performed with the first set. In both cases, the compounds containing bicyclic caps were overall more active than analogs bearing 5-membered heterocycles as cap-groups. The most potent compound of the two sets, the indole analog **6r**, was 2-fold more potent than Vorinostat in the HDAC-cell assays against both neoplastic cells and 10-fold more potent in the MTT-assays performed against Cal27, however, 2-fold less potent in the A2780 assays (section 4.4 Table 2).

Due to the promising results obtained with the indole analog **6r**, this inhibitor was chosen as the lead structure for the design of the third and final set of HDACi evaluated in this work. Focusing on the cap-region two types of modifications were performed, the variation on the position of the indole ring connected to the rest of the inhibitor (**6v-z** section 4.7 Table 3) and the inclusion of larger bicyclic groups (**8a-8f** section 4.7 Table 3). Furthermore, the linker of **6r** was shortened (**13**) and the hydroxamic ZBG group replaced by two classic ZBGs: a carboxylic acid (**18**) and ortho-amino anilide (**20**) (section 4.7 Table 4).

The synthesis of the analogs containing modification in the cap-region **6v-z**, **8a-8f** (section 4.3 Scheme 1) and the compound with the shorter linker **13** was achieved through the synthetic route used to obtain the previous analogs (section 4.6 Scheme 2). The initial synthesis of **20** was performed according to Marek et al.¹⁵⁷, since **18** was an intermediary product in this route (section 4.6 Scheme 3). Although, **18** and **20** were obtained, due to the low yields observed in

the initial synthesis **20**, the compound was resynthesized. The re-synthesis was conducted by adapting the synthetic route used to obtain the hydroxamates, which proved to be more efficient for the synthesis of this inhibitor (section 4.6 Scheme 4).

The analysis of the anticancer activity third set of synthesized HDACi in against A2780 and Cal27 showed that the modification of **6r** linker and the introduction of non-hydroxamic ZBG led to a general decrease in potency against both carcinomas (section 4.7 Table 3). Contrary to these modifications, compounds containing larger bicyclic cap **8a** and **8e** showed improvement of anticancer activity against both cells lines (section 4.7 Table 4). Another important observation was that **8c** and **8d**, containing isoquinoline and quinazoline rings respectively, were more active in the HDAC inhibition assays than the MTT-assays (section 4.7 Table 3).

The lead structure **6r** along with **8a**, and **8e**, the most potent synthesized inhibitors, were assayed against three cell lines of Glioblastomas, LN18, LN229, and U251. HDACi represents a promising therapeutic option in the treatment of these aggressive brain cancers with Vorinostat being currently evaluated in phase II clinical trials. In the cell availability assays conducted with **6r**, **8a**, **8e**, and Vorinostat against the Glioblastomas cells, all synthesized compounds were at least 1.5-fold more active than Vorinostat (section 4.8 Table 6), showing the potential of the synthesized inhibitors to be further studied against this type of neoplasm.

Based on the antiproliferative and HDAC-cell assays performed against A2780 and Cal27, the HDACi **6r**, **8a**, **8c-e** and **20** were chosen to be further evaluated. Currently, the selected inhibitors are being evaluated in enzymatic assays and for their chemosensitizing effects (section 4.11).

The preliminary evaluation of the compounds against class I (HDAC1) and class IIb (HDAC6) HDACs demonstrated that **6r**, **8a**, and **8e** have potencies and preference to isoforms comparable to Vorinostat, while **8c** was more active against HDAC6 than HDAC1 with a selectivity index of 7.9, a value close to Ricolinostat (SI: 12) (section 4.9 Table 7). In the docking studies of the inhibitors in the binding sites of the tested isoforms, the differences found in the enzymatic assays could indeed be also observed in the different interactions between the cap-groups and the surface of the binding sites.

HDACi have been demonstrated to be able to increase the sensibility of neoplastic cells to cisplatin, preliminary chemosensitizing assays using Cal27 cisplatin-sensitive and resistant clones revealed that compounds **8a** and **8e** were able to positively affect the potency of cisplatin in Cal27 sensitive (SF: 9.3 and 18.4) and cisplatin-resistant cells (SF: 12 and 9.3) (section 4.11 Table 8). An enhancement further demonstrated to occur due to synergistic effects (section 4.11 Table 9). Additionally, the evaluation of the combination of **6r**, **8a**, and **8c** with cisplatin

showed that in all cases, the combinations led to an increase of the apoptosis induction (section 4.11 Figure 35).

The anticancer activity of three sets of inhibitors designed and synthesized in this work, especially **8a**, demonstrated that the potency of the initial compounds could be improved and it confirmed the potential of HDACi containing bicyclic rings and alkoxyamides as CU as anticancer agents. Additionally, the preliminary results of chemosensitizing assays showed that **6r**, **8a**, and **8c** enhance cisplatin-induced apoptosis, making these inhibitors promising targets for further biologic evaluation and molecular modifications.

4.13. Experimental Part

4.13.1. General procedures for the synthesis of the designed compounds

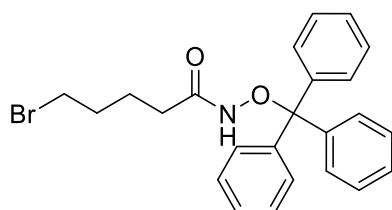
Chemicals and solvents were purchased from commercial suppliers (Sigma-Aldrich, Acros Organics, TCI, Fluorochem, Fluka, ABCR, Alfa Aesar, J&K, Carbolution and Merck) and used without further purification. The reactions were monitored by thin layer chromatography (TLC) using Merck precoated silica gel plates (with fluorescence indicator UV254), being visualized by irradiation with ultraviolet light (254 nm) or staining in potassium permanganate solution. Column chromatography was performed using Macherey-Nagel Silica 60 (0.040-0.063 mm) and Flash chromatography using prepacked silica cartridge with the solvent mixtures of hexane/ethyl acetate or dichloromethane/methanol according to the separation. Melting points (mp) analyses were performed using a Mettler FP 5 melting-point apparatus. Proton (¹H) and carbon (¹³C) NMR spectra were recorded on a Bruker Avance 300, 500 or 600 MHz using DMSO- d₆ as solvent. Chemical shifts are given in parts per million (ppm), relative to residual solvent peak for ¹H and ¹³C. High resolution mass spectra (HRMS) analysis was performed on a UHR-TOF maXis 4G, Bruker Daltonics, Bremen by electrospray ionization (ESI). Analytical HPLC analysis were carried out on a Varian Prostar system equipped with a Prostar 410 (autosampler), 210 (pumps) and 330 (UV-detector) using a Phenomenex Luna 5u C18 1.8 μm particle (250 mm × 4.6 mm) column, supported by Phenomenex Security Guard Cartridge Kit C18 (4.0 mm × 3.0 mm) or on in a AZURA P 6.1L (pumps) and Smartline 2600 VIS LWL (UV-detector) using a column type Vertex Plus Column (length 150 x 4 mm with precolumn). In both equipments the UV absorption was detected at 254 nm with a linear gradient of 10% B to 100% B in 30 min using HPLC-grade water +0.1% TFA (solvent A) and HPLC-grade acetonitrile +0.1% TFA (solvent B) for elution at a flow rate of 1 mL/min.

Starting materials and intermediates.

Protected hydroxamates **2**, **3** and **4**, also the esters **14**, **15** and **16** have been published earlier.^{154,157} The benzo[d]thiazole-2-carboxylic acid was prepared according to Shah et al.¹⁶¹ and the 1*H*-indole-4-carboxylic acid was synthesized by the base catalyzed hydrolysis of its respective methyl ester following the procedure described by Santillan et al.¹⁸⁸

Procedure for the synthesis of amide and alkoxyamides with ICBF (I)

The 5-bromopentanoic acid (1.1 eq) was dissolved in 100 mL tetrahydrofuran and the *N*-methylmorpholine (1.1 eq) was added. The solution was then cooled to -10°C and isobutyl chloroformate (1.1 eq) was added. After stirring for 5 min, *O*-(triphenylmethyl)hydroxylamine (1.0 eq) was added and the reaction mixture was left under stirring overnight. After the filtration, the solvent was removed. The crude product was dissolved in ethyl acetate and extracted two times with a saturated solution of NaHCO₃ and brine. The combined organic layers were dried over Na₂SO₄ and evaporated under reduced pressure. The crude product was purified by flash chromatography using a mixture of hexane/ethyl acetate (0-100% of ethyl acetate).



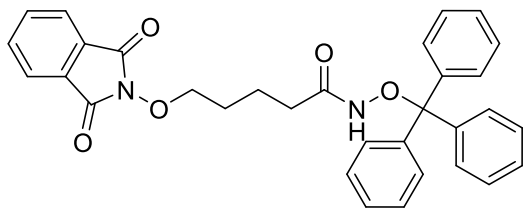
5-Bromo-*N*-(trityloxy)pentanamide (9): white solid, yield 56.0%, mp 144°C. ¹HNMR (600 MHz, DMSO-*d*₆) 1.32-1.35 (m, 2H), 1.46-1.49(m, 2H), 1.82(t, 2H, J = 7.1 Hz), 3.37 (t, 2H, J = 6.6 Hz), 7.28-7.34(m, 15H), 10.23 (s, 1H).

¹³CNMR (151 MHz, DMSO-*d*₆) 23.75, 31.35, 31.73, 35.10, 92.21, 127.88, 127.99, 129.09, 129.41, 142.89, 170.30.

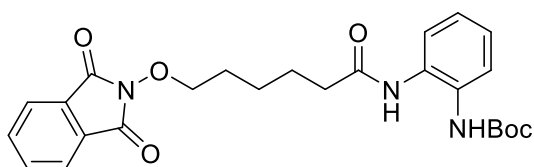
General procedure for the alkylation reactions with *N*-hydroxyphthalimide (II)

N-Hydroxyphthalimide (1.0 eq) was suspended in 100 mL acetonitrile, triethylamine (2.0 eq) was added, resulting in a red solution. To this solution, respective alkyl chloride (**10** and **22**) (1.1 eq) was added and the reaction was refluxed overnight. After cooling down to room temperature, the solvent was evaporated and ethyl acetate was added, followed by washing with a saturated solution of NaHCO₃. The organic phase was separated and dried under Na₂SO₄, the

solvent was evaporated and the crude product purified by flash chromatography using mixture of hexane/ethyl acetate (0-100% of ethyl acetate) as eluent.



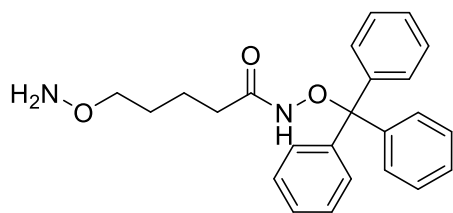
5-((1,3-Dioxoisindolin-2-yl)oxy)-N-(trityloxy)pentanamide (10): white solid, yield 77.5%, mp 173°C- ¹HNMR (600 MHz, DMSO-d₆) 1.42-1.44(m, 4H), 1.79(t, 2H, J = 6.8Hz), 4.03(t, 2H, J = 5.7Hz), 7.34-7.40(m, 15H), 7.91(s, 4H), 10.27 (s, 1H). ¹³CNMR (151 MHz, DMSO-d₆) 21.49, 27.40, 31.93, 77.74, 92.20, 123.67, 127.73, 127.99, 129.06, 129.42, 129.81, 135.22, 142.90, 163.71, 170.49.



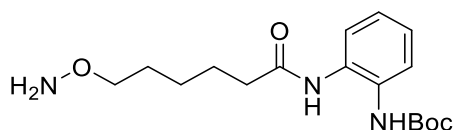
Tert-butyl (2-(6-((1,3-Dioxoisindolin-2-yl)oxy)hexanamido)phenyl)carbamate (22): colorless oil, yield 77.0%. ¹HNMR (600 MHz, DMSO-d₆): 1.47 (s, 9H), 1.49-1.53 (m, 2H), 1.65-1.75 (m, 4H), 2.39 (t, 2H, J = 7.3 Hz), 4.15 (t, 2H, J = 6.5 Hz), 7.06 (t, 1H, J = 8.3 Hz), 7.12 (t, 1H, J = 8.2 Hz), 7.41 (d, 1H, J = 7.7 Hz), 7.53 (d, 1H, J = 7.9 Hz), 8.32 (s, 1H), 9.47 (s, 1H). ¹³CNMR (151 MHz, DMSO-d₆): 25.18, 25.33, 27.96, 28.51, 36.29, 78.04, 79.80, 123.67, 124.11, 124.33, 125.33, 125.51, 129.05, 130.10, 131.56, 135.22, 153.32, 163.75, 172.17.

General procedure for the deprotection of *N*-hydroxyphthalimide (III)

The compounds **10** and **22** (1.0 eq) were suspended in 50 mL of methanol and hydrazine monohydrate (10.0 eq) was added. The reaction was left under stirring for 4h at room temperature, and then the solvent was evaporated; the crude materials were dissolved in 100 mL of dichloromethane and extracted with saturated solution of NaHCO₃. The organic phase was collected and dried under Na₂SO₄. The solvent was removed under reduced pressure and the crude product was purified by flash chromatography using mixtures of hexane/ethyl acetate (0-100% of ethyl acetate) as eluent.



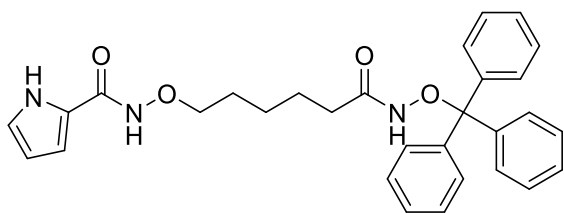
5-(Aminoxy)-N-(trityloxy)pentanamide (11): white solid, yield 64%, mp 121°C. ¹HNMR (600 MHz, DMSO-d₆): 1.19-1.24 (m, 4H), 1.78-1.80 (m, 2H), 3.36-3.38 (m, 2H), 5.81 (s, 2H), 7.31-7.34 (m, 15H), 10.18 (s, 1H). ¹³CNMR (151 MHz, DMSO-d₆): 27.93, 27.74, 32.22, 74.83, 92.17, 127.87, 127.97, 129.07, 129.42, 142.93, 170.69.



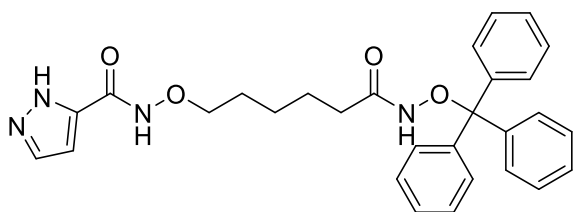
tert-Butyl (2-(6-(aminoxy)hexanamido)phenyl)carbamate (23): colorless oil, yield 81.0%. ¹HNMR (600 MHz, DMSO-d₆): 1.31-1.36 (m, 2H), 1.47 (s, 9H), 1.51-1.55 (m, 2H), 1.59-1.64 (m, 2H), 2.34 (t, 2H, J = 7.3 Hz), 3.52 (t, 2H, J = 6.6 Hz), 5.87 (s, 2H), 7.06-7.09 (m, 1H), 7.12-7.15 (m, 1H), 7.40 (d, 1H, J = 7.9 Hz), 7.53 (d, 1H, J = 8.1 Hz), 8.31 (s, 1H), 9.45 (s, 1H). ¹³CNMR (151 MHz, DMSO-d₆): 25.60, 25.66, 28.26, 36.41, 75.21, 79.81, 124.35, 125.29, 125.50, 130.13, 153.52, 172.22.

General procedure for the synthesis of amide and alkoxyamides with EDC/DMAP (IV)

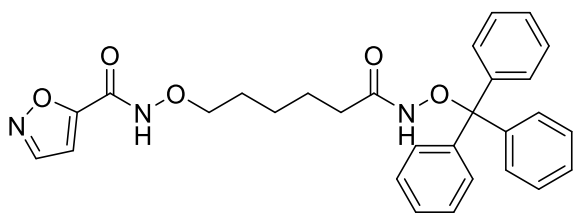
As described in Avelar et al.¹⁵⁴ the desired carboxylic acids (**5m-z** and **7a-f** 1.1 eq) were dissolved/suspended in DCM and left under stirring. The 1-ethyl-3-(3-dimethylaminopropyl) carbodiimide hydrochloride (EDCI) (1.1 eq) and 4-(dimethylamino)-pyridine (DMAP) (0.2 eq) were added and the reactions left under stirring at room temperature for 5-10 min. The respective amine/alkoxyamine (1.0 eq) were then added and the reactions were left under stirring overnight. The reactions were diluted with 50 mL of dichloromethane and extracted with 1 x 50 mL saturated solution of NaHCO₃, the organic phases were collected and dried under Na₂SO₄. After the evaporation of the solvent under reduced pressure, the crude products were purified by flash chromatography using mixtures of hexane/ethyl acetate (0-100% of ethyl acetate) as eluent.



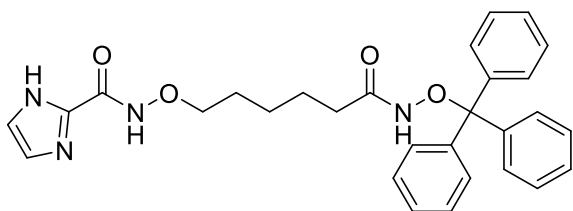
***N*-((6-Oxo-6-((trityloxy)amino)hexyl)oxy)-1*H*-pyrrole-2-carboxamide (5m)**: light yellow solid, yield 79%, mp 115°C, ¹HNMR (600 MHz, DMSO-*d*₆) 1.06-1.11 (m, 2H), 1.23-1.25 (m, 2H), 1.44 (t, 2H, *J* = 7.5 Hz), 3.74 (t, 2H, *J* = 6.7 Hz), 6.08 (d, 1H, *J* = 2.8 Hz), 6.68-6.69 (m, 1H), 6.90 (d, 1H, *J* = 2.3 Hz), 7.28-7.36 (m, 15H), 10.20 (s, 1H), 11.10 (s, 1H), 11.54 (s, 1H) ¹³CNMR (151 MHz, DMSO-*d*₆) 25.04, 25.22, 27.85, 32.37, 75.79, 92.20, 109.10, 122.40, 123.75, 127.97, 129.43, 142.94, 170.69. HRMS-ESI [*M*+*H*]: *m/z* calcd for C₃₀H₃₂N₃O₄: 498.2387, found: 498.2386.



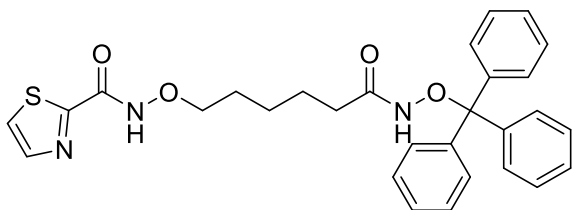
***N*-((6-Oxo-6-((trityloxy)amino)hexyl)oxy)-1*H*-pyrazole-5-carboxamide (5n)**: white solid, yield 69.4%, mp 104-105 °C, ¹HNMR (600 MHz, DMSO-*d*₆) 1.05-1.10 (m, 2H), 1.20-1.25 (m, 2H), 1.42-1.47 (m, 2H), 1.79 (t, 2H, *J* = 7.0 Hz), 3.74 (t, 2H, *J* = 6.6 Hz), 6.65(s, 1H), 7.30-7.35(m, 15H), 7.82(s, 1H), 10.20(s, 1H), 11.37(s, 1H), 13.27(s, 1H). ¹³CNMR (151 MHz, DMSO-*d*₆) 25.03, 25.19, 27.79, 32.37, 75.55, 92.19, 105.71, 127.87, 127.97, 129.43, 142.93, 170.69. HRMS-ESI [*M*+*H*]: *m/z* calcd for C₂₉H₃₁N₄O₄: 499.2340, found: 499.2338.



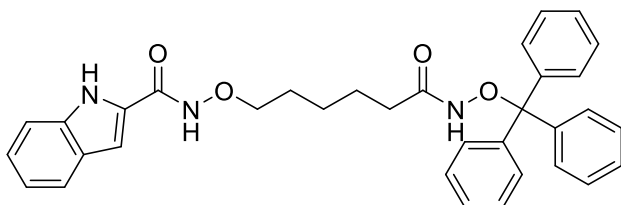
***N*-((6-Oxo-6-((trityloxy)amino)hexyl)oxy)isoxazole-5-carboxamide (5o)**: white solid, yield 70.0%, mp 184°C, ¹HNMR (500 MHz, DMSO-*d*₆) 1.07-1.10 (m, 2H), 1.22-1.26 (m, 2H), 1.45-1.48 (m, 2H), 1.79 (t, 2H, *J* = 7.4 Hz), 3.81 (t, 2H, *J* = 6.6 Hz), 7.05 (d, 1H, *J* = 1.9 Hz), 7.29-7.34 (m, 15H), 8.75 (d, 1H, *J* = 1.9 Hz), 10.16 (s, 1H), 12.17 (s, 1H). ¹³CNMR (125 MHz, DMSO-*d*₆) 24.83, 25.04, 27.61, 32.26, 75.96, 92.17, 106.56, 127.76, 127.86, 129.34, 142.85, 151.86, 153.71, 161.71, 170.59. HRMS-ESI [*M*+*H*]: *m/z* calcd. for C₂₉H₃₀N₃O₅: 500.2180, found: 500.2176.



***N*-((6-Oxo-6-((trityloxy)amino)hexyl)oxy)-1*H*-imidazole-2-carboxamide (5p):** white solid, yield 85.0%, mp 188 °C. ¹H NMR (600 MHz, DMSO-*d*₆) 1.05-1.08 (m, 2H), 1.21-1.24 (m, 2H), 1.43-1.46 (m, 2H), 1.79 (t, 2H, *J* = 7.2 Hz), 3.75 (t, 2H, *J* = 6.7 Hz), 7.28-7.34 (m, 17H), 10.20 (s, 1H), 11.73 (s, 1H), 13.05 (s, 1H). ¹³C NMR (151 MHz, DMSO-*d*₆) 25.02, 25.12, 27.73, 32.36, 75.70, 92.19, 127.87, 127.98, 129.42, 139.58, 142.93, 156.65, 170.71. HRMS-ESI [*M*+*H*]: *m/z* calcd for C₂₉H₃₁N₄O₄: 499.2340, found: 499.2340.

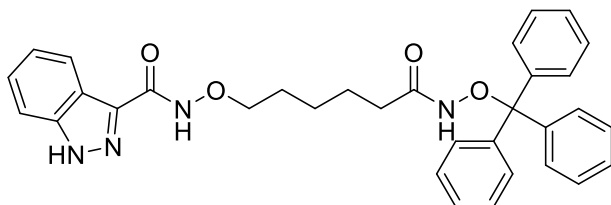


***N*-((6-Oxo-6-((trityloxy)amino)hexyl)oxy)thiazole-2-carboxamide (5q):** white solid, yield 89.3%, mp 73-75 °C. ¹H NMR (600 MHz, DMSO-*d*₆) 1.06-1.09 (m, 2H), 1.22-1.24 (m, 2H), 1.44-1.47 (m, 2H), 1.79 (t, 2H, *J* = 7.3 Hz), 3.79 (t, 2H, *J* = 6.6 Hz), 7.29-7.34 (m, 15H), 8.01 (d, 1H, *J* = 3.0 Hz), 8.07 (d, 1H, *J* = 3.1 Hz), 10.20 (s, 1H), 12.15 (s, 1H). ¹³C NMR (135 MHz, DMSO-*d*₆) 24.98, 25.11, 27.72, 32.34, 75.83, 92.19, 126.04, 127.86, 127.97, 129.43, 142.93, 144.45, 162.42, 170.67. HRMS-ESI [*M*+*H*]: *m/z* calcd for C₂₉H₃₀N₃O₄S: 516.1952, found: 516.1948.

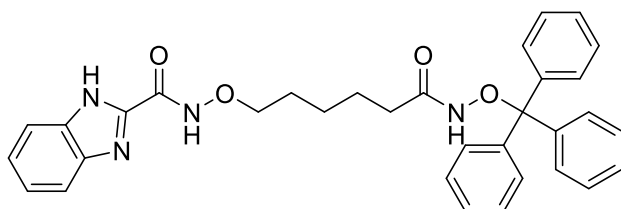


***N*-((6-Oxo-6-((trityloxy)amino)hexyl)oxy)-1*H*-indole-2-carboxamide (5r):** yellow solid, yield 64.2%, mp 102 °C. ¹H NMR (600 MHz, DMSO-*d*₆) 1.09-1.12 (m, 2H), 1.24-1.27 (m, 2H), 1.48-1.51 (m, 2H), 1.81 (t, 2H, *J* = 7.3 Hz), 3.81 (t, 2H, *J* = 6.6 Hz), 7.02 (s, 1H), 7.03 (t, *J* = 7.8 Hz, 1H), 7.18 (t, 1H, *J* = 8.0 Hz), 7.29-7.36 (m, 15H), 7.43 (d, 1H, *J* = 8.2 Hz), 7.61 (t, 1H, *J* = 8.0 Hz), 10.21 (s, 1H), 11.65 (s, 1H), 11.67 (s, 1H). ¹³C NMR (151 MHz, DMSO-*d*₆) 25.04,

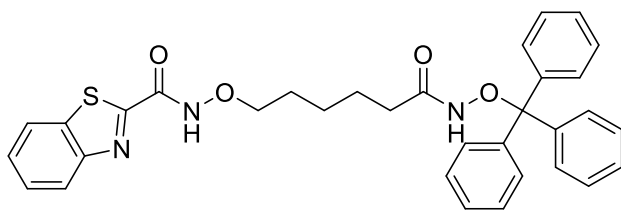
25.19, 27.84, 32.37, 75.89, 92.21, 112.75, 120.34, 122.02, 127.29, 127.98, 129.43, 136.94, 142.93, 160.00, 170.70. HRMS-ESI [M+H]: m/z calcd for C₃₄H₃₄N₃O₄: 548.2544, found: 548.2554.



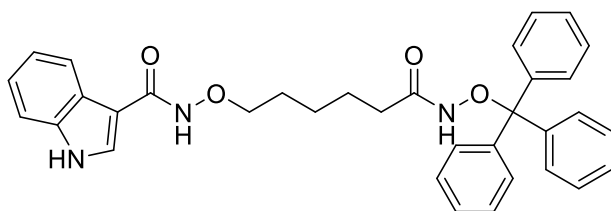
***N*-((6-Oxo-6-((trityloxy)amino)hexyl)oxy)-1*H*-indazole-3-carboxamide (5s):** white solid, yield 80.3%, mp 105°C. ¹HNMR (600MHz, DMSO-d₆) 1.09-1.12 (m, 2H), 1.23-1.27 (m, 2H), 1.47-1.51 (m, 2H), 1.81 (t, 2H, J = 7.0 Hz), 3.81 (t, 2H, J = 6.6 Hz, 2H), 7.24 (m, 1H), 7.29-7.36 (m, 15H), 7.41-7.44 (m 1H), 7.62 (d, 1H, J = 8.4 Hz), 8.12 (d, 1H, J = 8.2 Hz), 10.21 (s, 1H), 11.63 (s, 1H), 13.62 (s, 1H). ¹³CNMR (151 MHz, DMSO-d₆) 25.06, 25.23, 27.84, 32.39, 75.66, 92.20, 111.19, 121.70, 122.22, 122.56, 127.05, 127.86, 127.97, 129.44, 136.98, 141.21, 142.95, 160.59. HRMS-ESI [M+Na⁺]: m/z calcd for C₃₂H₃₆N₄NaO₄: 571.2316, found: 571.2310.



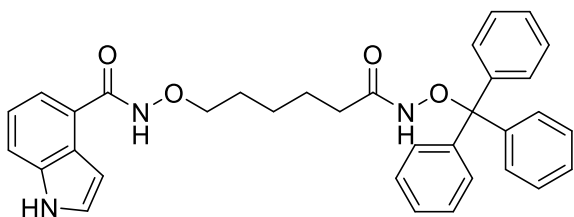
***N*-((6-oxo-6-((trityloxy)amino)hexyl)oxy)-1*H*-benzo[d]imidazole-2-carboxamide (5t):** white solid, yield 57.2%, mp 165-167°C. ¹HNMR (600 MHz, DMSO-d₆) 1.06-1.12 (m, 2H), 1.22-1.25 (m, 2H), 1.45-1.50 (m, 2H), 1.80 (t, 2H, J = 7.2 Hz), 3.81 (t, 2H, J = 6.7 Hz), 7.28-7.34 (m, 17H), 7.59-7.73 (m, 2H), 10.20(s, 1H), 12.26 (br, 1H), 13.32 (s, 1H). ¹³CNMR (151 MHz, DMSO-d₆) 25.02, 25.10, 27.73, 32.36, 75.8, 92.20, 127.87, 127.98, 129.43, 142.93, 144.49, 156.74, 170.70. HRMS-ESI [M+H]: m/z calcd for C₃₃H₃₃N₄O₄: 549.2496, found: 549.2499.



***N*-((6-Oxo-6-((trityloxy)amino)hexyl)oxy)benzo[d]thiazole-2-carboxamide (5u):** white solid, yield 91.0%, mp 72-75°C. ¹HNMR (600 MHz, DMSO-d₆) 1.07-1.12 (m, 2H), 1.22-1.26 (m, 2H), 1.46-1.51 (m, 2H), 1.80 (t, 2H, J = 7.1 Hz), 3.84 (t, 2H, J = 6.6 Hz), 7.28-7.35 (m, 15H), 7.58 (t, 1H, J = 7.5 Hz), 7.63 (t, 1H, J = 7.3 Hz), 8.13 (d, 1H, J = 8.1 Hz), 8.24 (d, 1H, J = 7.9 Hz), 10.20 (s, 1H), 12.50 (s, 1H). ¹³CNMR (151 MHz, DMSO-d₆) 24.98, 25.11, 27.71, 32.35, 75.91, 92.20, 123.45, 124.41, 127.41, 127.67, 127.87, 127.98, 129.43, 136.11, 142.93, 153.19, 157.27, 163.32, 170.69. HRMS-ESI [M+H]: m/z calcd for C₃₃H₃₂N₃O₄S:566.2108, found: 566.2110.

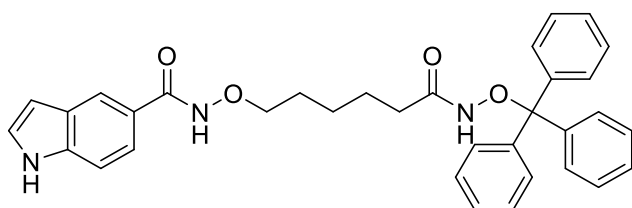


***N*-((6-Oxo-6-((trityloxy)amino)hexyl)oxy)-1*H*-indole-3-carboxamide (5v):** white solid, yield 91.7%, mp 104-106°C. ¹HNMR (600 MHz, DMSO-d₆) 1.08-1.13 (m, 2H), 1.23-1.26 (m, 2H), 1.46-1.51 (m, 2H), 1.80 (t, 2H, J = 6.9 Hz), 3.78 (t, 2H, J = 6.6 Hz), 7.10-7.13 (m, 1H), 7.15-7.18 (m, 1H), 7.28-7.36 (m, 15H), 7.43-7.45 (m, 1H), 7.90 (s, 1H), 8.07 (d, 1H, J = 7.9 Hz), 10.21 (s, 1H), 10.94 (s, 1H), 11.61 (s, 1H). ¹³CNMR (151 MHz, DMSO-D₆) 25.08, 25.29, 27.92, 32.41, 75.64, 92.20, 107.93, 112.36, 120.97, 121.27, 126.50, 127.87, 128.13, 129.43, 136.45, 142.93, 170.71. HRMS-ESI [M+H]: m/z calcd for C₃₄H₃₄N₃O₄: 548.2544, found: 548.2545.

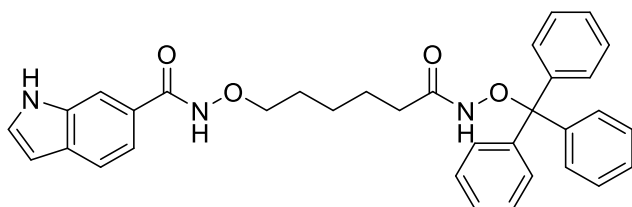


***N*-((6-Oxo-6-((trityloxy)amino)hexyl)oxy)-1*H*-indole-4-carboxamide (5w):** white solid, yield 87.9%, mp 178-180°C, ¹HNMR (600 MHz, DMSO-d₆) 1.10-1.13 (m, 2H), 1.20-1.25 (m,

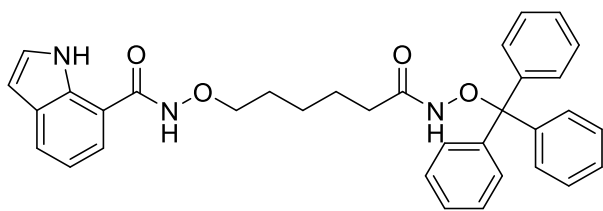
2H), 1.79 (t, 2H, J = 7.2 Hz), 3.80 (t, 2H, J = 6.6 Hz), 6.77-6.75 (m, 1H), 7.09 (t, 1H, J = 5.7 Hz), 7.28-7.36 (m, 16H), 7.43 (t, 1H, J = 7.4 Hz), 7.54 (d, 1H, J = 8.1 Hz), 10.21 (s, 1H), 11.30 (s, 2H). ¹³CNMR (151 MHz, DMSO-d₆) 25.09, 25.27, 27.91, 32.41, 75.41, 92.20, 101.97, 114.88, 118.83, 120.60, 124.72, 126.29, 127.07, 127.87, 129.44, 136.90, 142.94, 166.40, 170.70. HRMS-ESI [M+Na]: m/z calcd for C₃₄H₃₃N₃NaO₄: 570.2363, found: 570.2359.



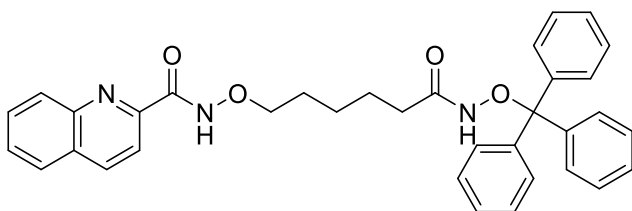
N-((6-Oxo-6-((trityloxy)amino)hexyl)oxy)-1H-indole-5-carboxamide (5x): White solid, yield 72.1%, White Solid, mp 86°C. ¹HNMR (600 MHz, DMSO-D₆) 1.08-1.13(m, 2H), 1.23-1.26(m, 2H), 1.46-1.51(m, 2H), 1.80(t, 2H, J = 7.3 Hz), 3.78 (t, 2H, J = 6.7 Hz), 6.52-6.54 (m, 1H), 7.29-7.36 (m, 16H), 7.42-7.44 (m, 2H), 7.51 (dd, 1H, J = 1.6 8.5 Hz), 8.02 (s, 1H), 10.21 (s, 1H), 11.35 (s, 1H), 11.39 (s, 1H). ¹³CNMR (151 MHz, DMSO-d₆) 25.06, 25.27, 27.89, 32.39, 75.40, 92.20, 102.56, 111.57, 120.25, 120.65, 123.72, 127.23, 127.44, 127.87, 127.98, 129.44, 137.97, 142.94, 166.11, 170.80. HRMS-ESI [M+H]: m/z calcd for C₃₄H₃₄N₃O₄: 548.2544, found: 548.2540.



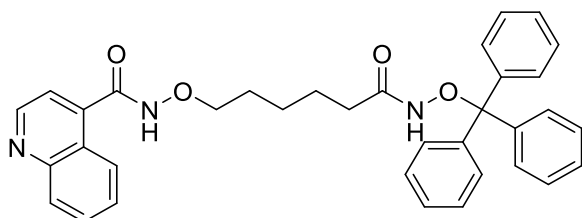
N-((6-Oxo-6-((trityloxy)amino)hexyl)oxy)-1H-indole-6-carboxamide (5y): white solid, yield 83.4%, mp 127 °C. ¹HNMR (600 MHz, DMSO-d₆) 1.09-1.12 (m, 2H), 1.24-1.26 (m, 2H), 1.47-1.50 (m, 2H), 1.80 (t, 2H, J = 7.4 Hz), 3.79 (t, 2H, J = 6.4 Hz), 6.49-6.50 (m 1H), 7.28-7.36 (m, 15H), 7.42 (dd, 1H, J = 1.5 8.3 Hz), 7.51 (t, 1H, J = 8.3 Hz), 7.57 (d, 1H, J = 8.3 Hz), 10.21 (s, 1H), 11.41 (s, 1H), 11.46 (s, 1H). ¹³CNMR (151 MHz, DMSO-d₆) 25.07, 25.27, 27.90, 32.39, 75.42, 92.20, 101.75, 111.51, 118.13, 120.07, 125.49, 127.87, 127.98, 130.49, 135.58, 142.94, 165.97. HRMS-ESI [M+Na]: m/z calcd for C₃₄H₃₃N₃NaO₄: 570.2363, found: 570.2362.



***N*-((6-Oxo-6-((trityloxy)amino)hexyl)oxy)-1*H*-indole-7-carboxamide (5z):** white solid, yield 72.1%, mp 86-87°C. ¹HNMR (600 MHz, DMSO-*d*₆) 1.11-1.17 (m, 2H), 1.24-1.28 (m, 2H), 1.49-1.52 (m, 2H), 1.81 (t, 2H, *J* = 7.2 Hz), 3.85 (t, 2H, *J* = 6.6 Hz), 6.50 (dd, 1H, *J* = 1.9 3.0 Hz), 7.03 (t, 1H, *J* = 7.6 Hz), 7.29-7.36 (m, 16H), 7.48 (d, 1H, *J* = 7.4 Hz), 7.74 (d, 1H, *J* = 7.8 Hz, 1H), 10.21 (s, 1H), 11.14 (s, 1H), 11.63 (s, 1H). ¹³CNMR (151 MHz, DMSO-*d*₆) 25.06, 25.31, 27.93, 32.37, 75.61, 92.21, 101.55, 115.40, 118.51, 119.98, 124.44, 127.23, 127.88, 127.98, 129.43, 129.63, 134.32, 142.93, 165.49, 170.70. HRMS-ESI [*M*+*H*]: *m/z* calcd for C₃₄H₃₄N₃O₄: 548.2544, found: 548.2540.

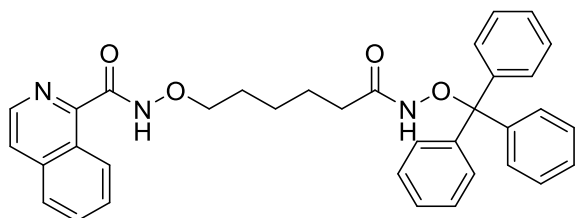


***N*-((6-Oxo-6-((trityloxy)amino)hexyl)oxy)quinoline-2-carboxamide (7a):** white solid, yield 91.5%, mp 79°C. ¹HNMR (600 MHz, DMSO-*d*₆) 1.10-1.15 (m, 2H), 1.23-1.27 (m, 2H), 1.48-1.51 (m, 2H), 1.81 (t, 2H, *J* = 7.2 Hz), 3.86 (t, 2H, *J* = 6.6 Hz), 7.29-7.35 (m, 15H), 7.72-7.74 (m, 1H), 7.86-7.89 (m, 1H), 8.07-8.09 (m, 2H), 8.12 (d, *J* = 8.60 Hz, 1H), 8.56 (d, *J* = 8.5 Hz, 1H), 10.21 (s, 1H), 12.00 (s, 1H). ¹³CNMR (151 MHz, DMSO-*d*₆) 25.02, 25.21, 27.82, 32.37, 75.64, 92.19, 119.24, 127.87, 127.98, 128.61, 129.26, 129.43, 131.02, 162.05, 170.70. HRMS-ESI [*M*+*H*]: *m/z* calcd for C₃₅H₃₄N₃O₄: 560.2544, found: 560.2542.

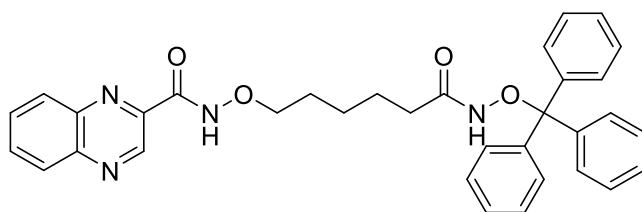


***N*-((6-Oxo-6-((trityloxy)amino)hexyl)oxy)quinoline-4-carboxamide (7b):** white solid, yield 62.6%, mp 110°C. ¹HNMR (600 MHz, DMSO-*d*₆) 1.12-1.15 (m, 2H), 1.25-1.29 (m, 2H), 1.52-1.54 (m, 2H), 1.82 (t, 2H, *J* = 7.2 Hz), 3.91 (t, 2H, *J* = 6.6 Hz), 7.29-7.36 (m, 15H), 7.56 (d, 1H, *J* = 4.2 Hz), 7.69-7.72 (m, 1H), 7.83-7.86 (m, 1H), 8.10-8.14 (m, 2H), 8.99 (d, 1H, *J* = 4.2 Hz),

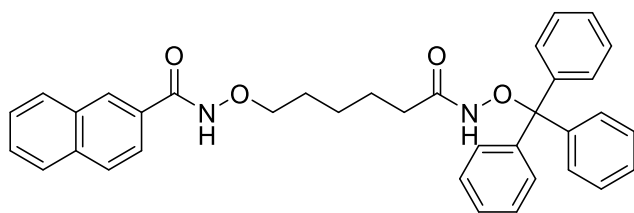
10.22 (s, 1H), 11.80 (s, 1H). ¹³CNMR (151 MHz, DMSO-d₆)25.03, 25.19, 27.83, 32.38, 75.87, 92.21, 120.06, 124.72, 125.51, 127.87, 127.98, 128.09, 129.44, 129.93, 130.46, 139.61, 142.94, 148.33, 150.68, 170.70. HRMS-ESI [M+H]: m/z calcd for C₃₅H₃₄N₃O₄: 560.2544, found: 560.2541.



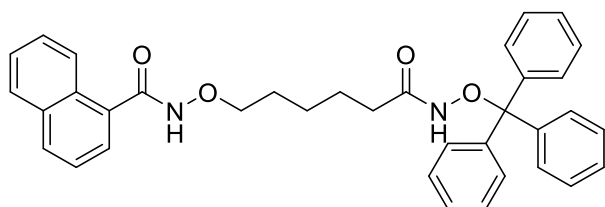
***N*-((6-Oxo-6-((trityloxy)amino)hexyl)oxy)isoquinoline-1-carboxamide (7c)**: white solid, yield 59.6%, mp 85°C. ¹HNMR (600 MHz, DMSO-d₆)1.12-1.15 (m, 2H), 1.27-1.28 (m, 2H), 1.50-1.54 (m, 2H), 1.81 (t, 2H, J = 7.1 Hz), 3.88 (t, 2H, J = 6.6 Hz), 7.31-7.35 (m, 15H), 7.73-7.76 (m, 1H), 7.83-7.86 (m, 1H), 8.02 (d, 1H, J = 5.6 Hz), 8.07 (d, 1H, J = 8.2 Hz), 8.53 (d, J = 5.6 Hz), 8.59 (d, J = 8.5 Hz, 1H), 10.21 (s, 1H), 11.83 (s, 1H). ¹³CNMR (151 MHz, DMSO-d₆) 25.05, 25.20, 27.83, 32.39, 75.67, 92.20, 123.58, 125.86, 127.66, 127.87, 127.98, 128.97, 129.44, 131.32, 136.71, 141.52, 142.94, 151.58, 163.72, 170.70. HRMS-ESI [M+H]: m/z calcd for C₃₅H₃₄N₃O₄: 560.2544, found: 560.2545.



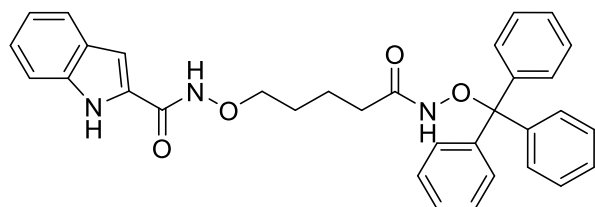
***N*-((6-Oxo-6-((trityloxy)amino)hexyl)oxy)quinoxaline-2-carboxamide (7d)**: white solid, yield 78.2%, mp 102°C. ¹HNMR (600 MHz, DMSO-d₆)1.11-1.114 (m, 2H), 1.25-1.28 (m, 2H), 1.50-1.52 (m, 2H), 1.81 (t, 2H, J = 6.5 Hz), 3.87 (t, 2H, J = 6.5 Hz), 7.31-7.35 (m, 15H), 7.97-8.01 (m, 2H), 8.18-8.20 (m, 2H), 9.41 (s, 1H), 10.21 (s, 1H), 12.08 (br, 1H). ¹³CNMR (151 MHz, DMSO-d₆) 25.01, 25.18, 27.81, 32.36, 75.76, 92.19, 127.86, 127.97, 129.43, 129.62, 129.88, 131.80, 132.41, 140.24, 142.94, 143.37, 144.08, 144.73, 170.69. HRMS-ESI [M+H]: m/z calcd for C₃₄H₃₃N₄O₄: 561.2496, found: 561.2496.



***N*-((6-Oxo-6-((trityloxy)amino)hexyl)oxy)-2-naphthamide (7e):** White solid, yield 74.5%, mp 95°C, ¹HNMR (500 MHz, DMSO-d₆) 1.09-1.15 (m, 2H), 1.22-1.29 (m, 2H), 1.48-1.52 (m, 2H), 1.81 (m, 2H), 3.83 (t, 2H, J = 6.5 Hz), 7.30-7.35 (m, 15H), 7.59-7.64 (m, 2H), 7.82 (dd, 1H, J = 1.6, 8.5 Hz), 7.98 (m, 3H), 8.36 (s, 1H), 10.18 (s, 1H), 11.72 (s, 1H). ¹³CNMR (125 MHz, DMSO-d₆) 24.93, 25.17, 27.78, 32.29, 75.52, 92.14, 124.18, 127.18, 127.78, 127.87, 128.01, 128.42, 129.16, 129.35, 130.22, 132.46, 134.60, 142.86. HRMS-ESI [M+H]: m/z calcd for C₃₄H₃₄N₃O₄: 548.2544, found: 548.2545.

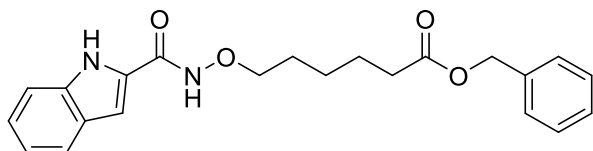


***N*-((6-Oxo-6-((trityloxy)amino)hexyl)oxy)-1-naphthamide (7f):** white solid 80.6%, White solid, mp 120°C, ¹HNMR (600 MHz, DMSO-d₆) 1.12-1.14 (m, 2H), 1.26-1.28 (m, 2H), 1.51-1.54 (m, 2H), 1.82 (t, 2H J = 7.5 Hz), 3.88 (t, J = 6.6 Hz, 2H), 7.29-7.36 (m, 15H), 7.54-7.60 (m, 4H), 7.99-8.01 (m, 4H), 8.05 (d, 1H, J = 8.0 Hz), 8.14 (d, 1H, J = 7.8 Hz), 10.22 (s, 1H), 11.56 (s, 1H). ¹³CNMR (151 MHz, DMSO-d₆) 25.05, 25.23, 27.86, 32.39, 75.63, 92.20, 125.39, 126.12, 126.86, 127.44, 127.44, 127.87, 127.98, 128.77, 129.44, 130.39, 130.76, 132.16, 133.58, 142.95, 165.90, 170.70. HRMS-ESI [M+H]: m/z calcd for C₃₆H₃₅N₂O₄: 559.2591, found: 559.2591.

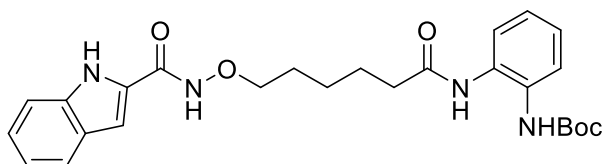


***N*-((5-Oxo-5-((trityloxy)amino)pentyl)oxy)-1H-indole-2-carboxamide (12):** white solid, yield 58.0%, mp 183-185°C. ¹HNMR (600 MHz, DMSO-d₆): 1.34-1.36 (m, 4H), 1.85-1.87 (m, 2H), 3.77-3.79 (m, 2H), 7.00 (s, 1H), 7.03 (t, 1H, J = 7.5 Hz), 7.18 (t, 1H, J = 8.0 Hz), 7.29-

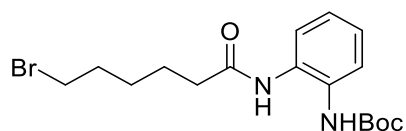
7.34 (m, 15H), 7.43 (d, 1H, J = 8.2 Hz), 7.60 (d, 1H, J = 8.0 Hz), 10.23 (s, 1H), 11.64 (s, 2H). ¹³CNMR (151 MHz, DMSO-d₆): 21.79, 27.37, 32.06, 75.66, 92.23, 112.76, 120.37, 122.02, 123.99, 127.38, 127.91, 128.01, 129.28, 129.40, 136.93, 142.87, 170.69. HRMS-ESI [M+H]: m/z calcd for C₃₃H₃₂N₃O₄:534.2387, found: 534.2385.



Benzyl 6-((1H-indole-2-carboxamido)oxy)hexanoate (17): white solid, yield 43.6 %, mp 119°C. ¹HNMR (600 MHz, DMSO-d₆): 1.39-1.44 (m, 2H), 1.59-1.66 (m, 4H), 2.38 (t, 2H, J = 7.4 Hz), 3.88 (t, 2H, 6.5 Hz), 5.10 (s, 2H), 7.01 (s, 1H), 7.03 (ddd, 1H, J = 1.0 6.9 8.0 Hz), 7.18 (ddd, 1H, J = 1.1 6.9 8.2 Hz), 7.32-7.39 (m, 5H), 7.42 (d, 1H, J = 8.2 Hz), 7.60 (d, 1H, J = 8.0 Hz), 11.66 (s, 2H). ¹³CNMR (151 MHz, DMSO-d₆): 24.72, 25.42, 27.83, 33.89, 65.80, 75.88, 112.75, 120.34, 122.02, 123.95, 127.39, 128.44, 128.90, 129.33, 136.75, 136.94, 173.22. HRMS-ESI [M+H]: m/z calcd for C₂₂H₂₅N₂O₄:381.1809, found: 381.1808.



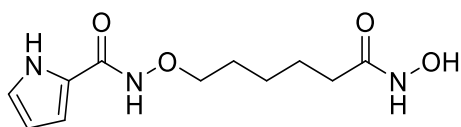
tert-Butyl (2-(6-((1H-indole-2-carboxamido)oxy)hexanamido)phenyl)carbamate (19): white solid, yield 25.5%/ 80.0%, mp 192°C. ¹HNMR (600 MHz, DMSO-d₆): 1.46 (s, 9H), 1.47-1.50 (m, 2H), 1.66-1.71 (m, 4H), 2.38 (t, 2H, J = 7.4 Hz), 3.93 (t, 2H, 6.5 Hz), 7.02-7.10 (m, 3H), 7.12-7.16 (m, 1H), 7.18 (ddd, 1H, J = 1.2 6.9 8.2 Hz), 7.42 (t, 2H, J = 7.4 Hz), 7.54 (d, 1H, J = 7.8 Hz), 7.61 (d, 1H, J = 7.9 Hz), 8.34 (s, 1H), 9.4 (s, 1H), 11.66 (s, 2H). ¹³CNMR (151 MHz, DMSO-d₆): 25.49, 27.98, 28.52, 36.38, 75.96, 79.83, 112.75, 120.33, 122.02, 123.95, 124.14, 124.36, 125.32, 125.52, 127.40, 129.34, 130.13, 131.55, 136.95, 153.54, 172.21. HRMS-ESI [M+H]: m/z calcd for C₂₆H₃₃N₄O₅:481.2445, found: 481.2444.



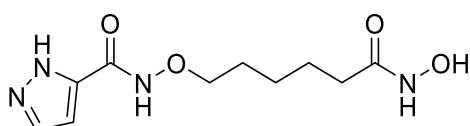
tert-Butyl (2-(6-bromohexanamido)phenyl)carbamate (21): Colorless oil, yield 54.0%. ¹HNMR (600 MHz, DMSO-d₆): 11.3-1.48 (m+s, 11H), 1.62-.165 (m, 2H), 1.73-1.87 (m, 2H), 2.35 (t, 2H, J = 7.3 Hz), 3.54 (t, 2H, J = 6.7 Hz), 7.06-7.09(m, 1H), 7.13 (t, 1H, J = 7.7 Hz), 7.41 (d, 1H, J = 7.3 Hz), 7.54 (d, 1H, J = 7.8 Hz), 8.32 (s, 1H), 9.45 (s, 1H). ¹³CNMR (151 MHz, DMSO-d₆): 24.76, 27.54, 32.46, 35.44, 36.20, 124.11, 124.32, 125.32, 125.32, 130.08, 131.56, 153.51, 172.08.

General procedure for deprotection of the Triphenylmethyl group (V)

Using the procedure described by Avelar et al. the removal of the trityl group from the protected hydroxamates **5m-z** and **7m-z** were performed by dissolving/suspending them in 30 mL of dichloromethane (1.0 eq) and adding triethylsilane (20.0 eq), followed by the addition of trifluoroacetic acid (20.0 eq). After 30 min under stirring the solvent was removed under reduced pressure and the crude product was purified by flash chromatography using mixtures of dichloromethane/ methanol as eluent (0-15% of methanol).

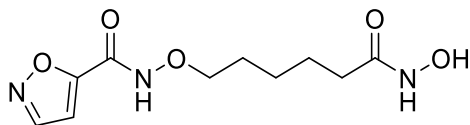


N-((6-(Hydroxyamino)-6-oxohexyl)oxy)-1H-pyrrole-2-carboxamide (6m): yellow solid, yield 53.6%, mp 165°-166°C, ¹HNMR (600 MHz, DMSO-d₆) 1.34-1.36 (m, 2H), 1.52-1.60 (m, 2H), 1.96 (t, J = 7.5 Hz, 2H), 3.82 (t, J = 6.5 Hz, 2H), 6.08 (s, 1H), 6.69 (s, 1H), 6.90 (s, 1H), 8.68 (s, 1H), 10.37 (s, 1H), 11.13 (s, 1H), 11.54 (s, 1H) ¹³CNMR (151 MHz, DMSO-d₆) 25.39, 25.55, 27.92, 32.66, 75.84, 109.11, 122.40, 123.40, 169.50. HRMS-ESI [M+H]: m/z calcd for C₁₁H₁₈N₃O₄: 256.1292, found: 256.1293. HPLC t_r: 8.54 min, purity 95.7%.

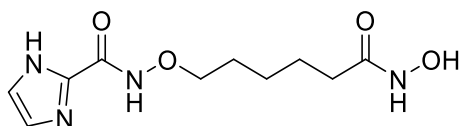


N-((6-(Hydroxyamino)-6-oxohexyl)oxy)-1H-pyrazole-5-carboxamide (6n): yellow solid, yield 82.3%, mp 80-81°C, ¹HNMR (600 MHz, DMSO-d₆) 1.33-1.37 (m, 2H), 1.50-1.59 (m, 4H), 1.95 (t, 2H, J = 7.35 Hz), 3.82 (m, 2H), 6.64 (s, 1H), 7.82 (s, 1H), 8.69 (s, 1H), 10.37 (s,

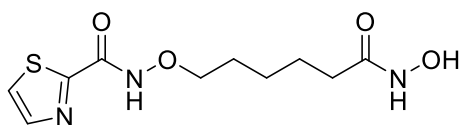
1H), 11.39 (s, 1H), 13.29 (s, 1H). ¹³CNMR (151 MHz, DMSO-d6) 25.38, 25.52, 27.86, 32.66, 75.59, 105.72, 130.21, 160.09, 169.53. HRMS-ESI [M+H]: m/z calcd for C₁₀H₁₇N₄O₄: 257.1244, found: 257.1242. HPLC retention time: 4.85 min, purity 96.5%.



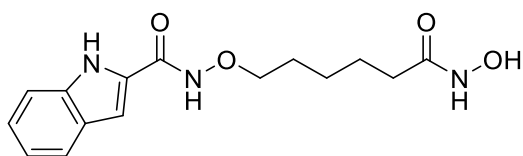
N-((6-(Hydroxyamino)-6-oxohexyl)oxy)isoxazole-5-carboxamide (6o): white solid, yield 69.4%, mp 130°-132°C, ¹HNMR (600 MHz, DMSO-d6) 1.33-1.37 (m, 2H), 1.52-1.61 (m, 4H), 1.95 (t, 2H, J = 7.4 Hz), 3.89 (t, 2H, J = 6.2 Hz), 7.06 (s, 1H), 8.68 (s, 1H), 8.78 (s, 1H), 10.36 (s, 1H), 12.23 (s, 1H). ¹³CNMR (151 MHz, DMSO-d6) 25.32, 25.43, 27.79, 32.63, 76.07, 106.73, 151.99, 153.76, 161.37, 169.47. HRMS-ESI [M+H]: m/z calcd for C₁₀H₁₆N₃O₅: 258.1084, found: 258.1086. HPLC retention time: 3.84 min, purity 98.5%.



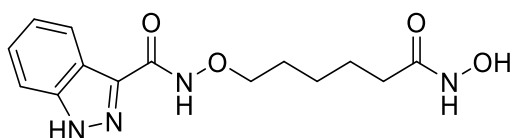
N-((6-(Hydroxyamino)-6-oxohexyl)oxy)-1H-imidazole-2-carboxamide (6p): white solid, yield 77.4%, mp 108-109°C. ¹HNMR (600 MHz, DMSO-d6) 1.32-1.37 (m, 2H), 1.50-1.60 (m, 4H), 1.95 (t, 2H, J = 7.3 Hz, 2H), 3.84 (t, 2H, J = 6.5 Hz), 7.20 (s, 2H), 10.36 (s, 1H), 11.76 (s, 1H). ¹³CNMR (151 MHz, DMSO-d6) 25.36, 25.46, 27.82, 32.66, 75.76, 107.41, 124.61, 139.39, 139.51, 169.51. HRMS-ESI [M+H]: m/z calcd for C₁₀H₁₇N₄O₄: 257.1244, found: 257.1243. HPLC retention time: 4.03 min, purity 97.5%.



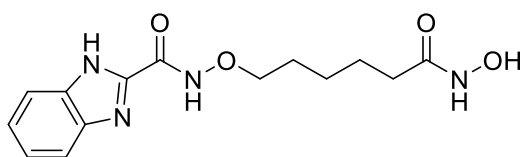
N-((6-(Hydroxyamino)-6-oxohexyl)oxy)thiazole-2-carboxamide (6q): yellow oil, yield 85.5%. ¹HNMR (600 MHz, DMSO-d6) 1.32-1.37 (m, 2H), 1.50-1.61 (m, 4H), 1.95 (t, 2H, J = 7.4 Hz), 2.87 (t, 2H, J = 6.5 Hz), 8.01 (d, 1H, J = 3.1 Hz), 8.07 (d, 1H, J = 3.1 Hz), 8.67 (s, 1H), 10.35 (s, 1H), 12.17 (s, 1H). ¹³CNMR (151 MHz, DMSO-d6) 25.34, 25.46, 27.80, 32.65, 75.90, 126.06, 144.46, 157.08, 162.40, 169.48. HRMS-ESI [M+H]: m/z calcd for C₁₀H₁₆N₃O₄S: 274.0856, found: 274.0856. HPLC retention time: 9.00 min, purity 95.3%.



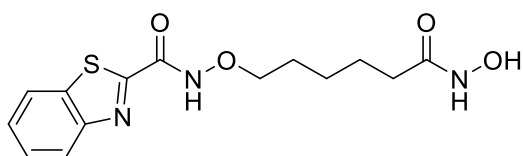
***N*-((6-(Hydroxyamino)-6-oxohexyl)oxy)-1*H*-indole-2-carboxamide (6r):** white solid, yield 62.1%, mp 137-138°C. ¹HNMR (600 MHz, DMSO-*d*₆) 1.37-1.41 (m, 2H), 1.55-1.65 (m, 4H), 1.98 (t, 2H, *J* = 7.3 Hz), 3.90 (t, 2H, *J* = 6.3 Hz), 7.02-7.06 (m, 2H), 7.18 (t, 1H, *J* = 7.6 Hz), 7.43 (d, 1H, 8.3 Hz), 7.61 (d, 1H, *J* = 8.0 Hz), 8.71 (s, 1H), 10.39 (s, 1H), 11.67 (s, 2H). ¹³CNMR (151 MHz, DMSO-*d*₆) 25.39, 25.55, 27.92, 32.67, 75.95, 112.75, 120.34, 122.03, 127.40, 129.35, 136.95, 160.06, 169.52. HRMS-ESI [*M*+*H*]: *m/z* calcd for C₁₅H₂₀N₃O₄: 306.1448, found: 306.1447. HPLC retention time: 11.90 min, purity 97.5%.



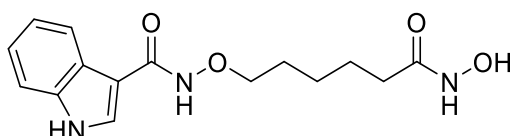
***N*-((6-(Hydroxyamino)-6-oxohexyl)oxy)-1*H*-indazole-3-carboxamide (6s):** white solid, yield 60.7%, mp 90°C. ¹HNMR (600MHz, DMSO-*d*₆) 1.35-1.41 (m 2H), 1.53-1.58 (m, 2H), 1.59-1.64 (m, 2H), 1.97 (t, 2H, *J* = 7.3 Hz), 3.89 (t, 2H, *J* = 6.5 Hz), 7.24 (t, 1H, *J* = 7.5 Hz), 7.41 (t, 1H, *J* = 7.4 Hz), 7.62 (d, 1H, *J* = 8.4 Hz), 8.68 (s, 1H), 10.37 (s, 1H), 11.65 (s, 1H), 13.63 (s, 1H). ¹³CNMR (151 MHz, DMSO-*d*₆) 25.42, 25.57, 27.93, 32.69, 75.73, 111.19, 121.68, 122.22, 122.57, 127.05, 136.96, 141.20, 160.61, 169.53. HRMS-ESI [*M*+*H*]: *m/z* calcd for C₁₄H₁₉N₄O₄: 307.1401, found: 307.1398. HPLC retention time: 8.55 min, purity 95.9%.



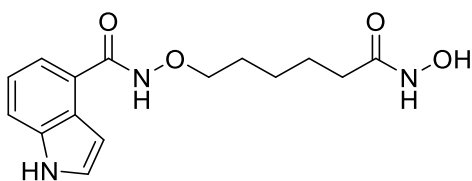
***N*-((6-(Hydroxyamino)-6-oxohexyl)oxy)-1*H*-benzo[*d*]imidazole-2-carboxamide (6t):** red solid, yield 83.6%, mp 118°C. ¹HNMR (600 MHz, DMSO-*d*₆) 1.35-1.40 (m, 2H), 1.52-1.57 (m, 2H), 1.59-1.64 (m, 2H), 1.96 (t, 2H, *J* = 7.4Hz), 3.90 (t, 2H, *J* = 6.5 Hz), 7.30-7.32 (m, 2H), 7.55 (s, 1H), 7.71 (s, 1H), 8.69 (s, 1H), 10.37 (s, 1H), 12.26 (s, 1H), 13.33 (s, 1H). ¹³CNMR (151 MHz, DMSO-*d*₆): 25.36, 25.47, 27.81, 32.67, 75.84, 112.94, 120.29, 123.11, 124.64, 134.61, 144.46, 156.75, 169.52. HRMS-ESI [*M*+*H*]: *m/z* calcd for C₁₄H₁₉N₄O₄: 307.1401, found 307.1401. HPLC retention time: 9.50 min, purity 97.6%.



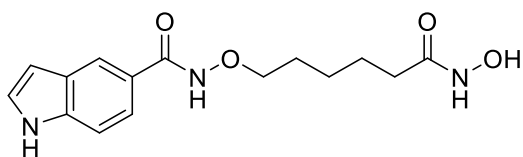
***N*-((6-(Hydroxyamino)-6-oxohexyl)oxy)benzo[d]thiazole-2-carboxamide (6u):** white solid, yield 90.5%, mp: 157-158°C. ¹HNMR (600 MHz, DMSO-*d*₆) 1.34-1.40 (m, 2H), 1.52-1.57 (m, 2H), 1.59-1.64 (m, 2H), 1.96 (t, 2H, *J* = 7.4 Hz), 3.92 (t, 2H, *J* = 6.4 Hz), 7.58-7.61 (m, 1H), 7.63-7.66 (m, 1H), 8.13 (d, 1H, *J* = 8.0 Hz), 8.24 (d, 1H, *J* = 7.9 Hz), 8.68 (s, 1H), 10.36 (s, 1H), 12.52 (s, 1H). ¹³CNMR (151 MHz, DMSO-*d*₆) 25.34, 25.46, 27.81, 32.66, 75.97, 123.44, 124.40, 127.40, 127.66, 136.10, 153.18, 157.28, 163.31, 169.50. HRMS-ESI [*M*+*H*]: *m/z* calcd for C₁₄H₁₈N₃O₄S: 324.1013, found: 324.1014. HPLC retention time: 12.85 min, purity 97.3%.



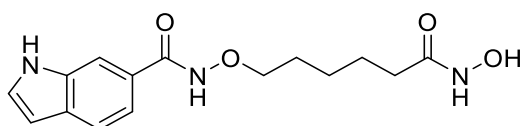
***N*-((6-(Hydroxyamino)-6-oxohexyl)oxy)-1*H*-indole-3-carboxamide (6v):** yellow solid, yield 63.8%, mp 120°C, ¹HNMR (600 MHz, DMSO-*d*₆) 1.36-1.40 (m, 2H), 1.53-1.64 (m, 4H), 1.97 (t, 2H, *J* = 7.3 Hz), 3.87 (t, 2H, *J* = 6.5 Hz), 7.10-7.13 (m, 1H), 7.15-7.18 (m, 1H), 7.44 (d, 1H, *J* = 8.0 Hz), 7.90 (d, 1H, *J* = 2.9 Hz), 8.06 (d, 1H, *J* = 7.8 Hz), 8.69 (s, 1H), 10.38 (s, 1H), 10.97 (s, 1H), 11.61 (s, 1H). ¹³CNMR (151 MHz, DMSO-*D*₆) 25.44, 25.62, 28.01, 32.69, 75.71, 107.91, 112.36, 122.52, 126.49, 128.15, 136.45, 169.55. HRMS-ESI [*M*+*H*]: *m/z* calcd for C₁₅H₂₀N₃O₄: 306.1448, found: 306.1447. HPLC retention time: 10.40 min, purity 99.1%.



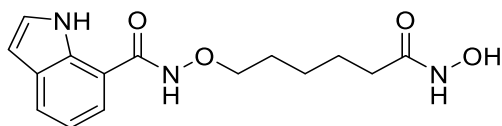
***N*-((6-(hydroxyamino)-6-oxohexyl)oxy)-1*H*-indole-4-carboxamide (6w):** white solid, yield 76.4%, mp 112°C, ¹HNMR (600 MHz, DMSO-*d*₆) 1.37-1.41 (m, 2H), 1.53-1.58 (m, 2H), 1.61-1.64 (m, 2H), 1.97 (t, 2H, *J* = 7.8 Hz), 3.90 (t, 2H, *J* = 6.3 Hz), 6.77 (s, 1H), 7.11 (t, 1H, *J* = 7.7 Hz), 7.30 (d, 1H, *J* = 7.3 Hz), 7.44 (t, 1H, *J* = 2.6 Hz), 7.55 (d, 1H, *J* = 7.6 Hz), 8.65 (br, 1H), 10.37 (s, 1H), 11.33 (s, 1H). ¹³CNMR (135 MHz, DMSO-*D*₆) 25.45, 25.61, 28.00, 32.70, 75.47, 101.97, 107.41, 114.89, 120.60, 124.69, 126.28, 127.08, 136.89, 166.42, 169.52. HRMS-ESI [*M*+*H*]: *m/z* calcd for C₁₅H₂₀N₃O₄: 306.1446, found: 306.1446. HPLC retention time: 7.57 min, purity 95.6%.



***N*-((6-(hydroxyamino)-6-oxohexyl)oxy)-1*H*-indole-5-carboxamide (6x)**: white solid, yield 50.8%, mp 97°C. ¹HNMR (600 MHz, DMSO-d₆) 1.35-1.40 (m, 2H), 1.54-1.64 (m, 4H), 1.97 (t, 2H, J = 7.5 Hz), 3.86 (t, 2H, J = 6.5 Hz), 6.53-6.54 (m, 1H), 7.42-7.44 (m, 2H), 7.51 (dd, 1H J = 1.6 8.5 Hz), 8.02 (s, 1H), 8.67 (br, 1H), 10.37 (s, 1H), 11.35 (s, 1H), 11.42 (s, 1H) ¹³CNMR (151 MHz, DMSO-d₆) 25.42, 25.60, 27.98, 32.69, 75.46, 102.56, 111.57, 120.25, 120.64, 123.70, 127.23, 127.44, 137.97, 166.13, 169.52. HRMS-ESI [M+H]: m/z calcd for C₁₅H₂₀N₃O₄:306.1448, found:306.1447. HPLC retention time: 9.52 min, purity 98.4%.

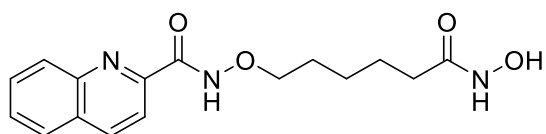


***N*-((6-(Hydroxyamino)-6-oxohexyl)oxy)-1*H*-indole-6-carboxamide (6y)**: yellow solid, yield 64.7%, mp 103-104°C. ¹HNMR (600 MHz, DMSO-d₆)1.35-1.40 (m, 2H), 1.52-1.64 (m, 4H), 1.97 (t, 2H, J = 7.4 Hz), 3.87 (t, 2H, J = 6.4 Hz), 6.49 (t, 1H, J = 2.3 Hz), 7.40 (dd, 1H, J = 1.5 8.3 Hz), 7.51(d, 1H, J = 8.2Hz), 7.86 (s, 1H), 8.68 (s, 1H), 10.37 (s, 1H), 11.42 (s, 1H), 11.49 (s, 1H). ¹³CNMR (151 MHz, DMSO-d₆) 25.43, 25.61, 27.99, 32.69, 75.48, 101.74, 111.51, 118.13, 120.08, 125.46, 128.57, 130.49, 135. 58, 169.52. HRMS-ESI [M+H]: m/z calcd for C₁₅H₂₀N₃O₄: 306.1448, found: 306.1444. HPLC retention time 9.23 min, purity 95.1%.

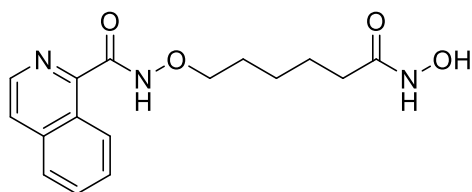


***N*-((6-(Hydroxyamino)-6-oxohexyl)oxy)-1*H*-indole-7-carboxamide (6z)**: yellow solid, yield 22.5%, mp142-143 °C. ¹HNMR (600 MHz, DMSO-d₆) 1.37-1.42 (m, 2H), 1.54-1.59 (m, 2H), 1.62-1.66 (m, 2H), 1.97 (t, 2H, J = 7.5 Hz), 3.93 (t, 2H, J = 6.4 Hz), 6.49-6.50 (m, 1H), 7.03 (t, 1H, J = 7.6 Hz), 7.35-7.37 (m ,1H), 7.48 (d, 1H, J = 7.4 Hz), 7.74 (d, 1H J = 7.8 Hz), 8.68 (s, 1H), 10.36 (s, 1H), 11.14 (s, 1H), 11.64 (s, 1H). ¹³CNMR (151 MHz, DMSO-d₆) 25.42, 25.65, 28.02, 32.68, 75.66, 101.55, 115.40, 118.51, 119.98, 124.44, 127.23, 129.63, 134.30, 165.49,

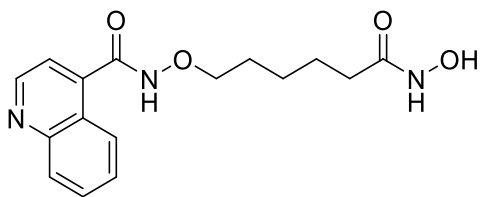
169.48. HRMS-ESI [M+H]: m/z calcd for C₁₅H₂₀N₃O₄: 306.1448, found: 306.1445. HPLC retention time: 12.2 min, purity 95.9%.



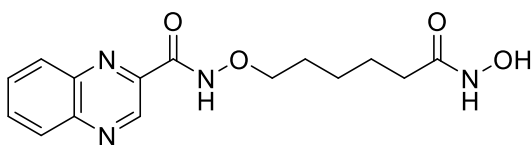
***N*-((6-(hydroxyamino)-6-oxohexyl)oxy)quinoline-2-carboxamide (8a)**: yellow solid, yield 88.2%, mp 67°C. ¹HNMR (600 MHz, DMSO-d₆) 1.37-1.42 (m, 2H), 1.54-1.59 (m, 2H), 1.61-1.66 (m, 2H), 1.97 (t, 2H, J = 7.3 Hz), 3.93 (t, 2H, J = 6.5 Hz), 7.72-7.74 (m, 1H), 7.86-7.89 (m, 1H), 8.08-8.09 (m, 2H), 8.12 (d, 1H, J = 8.5 Hz), 8.56 (d, 1H, J = 8.6 Hz), 8.68 (br, 1H), 10.37 (s, 1H), 12.03 (s, 1H). ¹³CNMR (151 MHz, DMSO-d₆) 25.38, 25.56, 27.91, 32.68, 75.70, 119.23, 128.60, 129.26, 131.01, 138.26, 146.49, 150.37, 162.06, 169.52. HRMS-ESI [M+H]: m/z calcd for C₁₆H₂₀N₃O₄: 318.1448, found: 318.1447. HPLC retention time: 12.06 min, purity 97.7%,



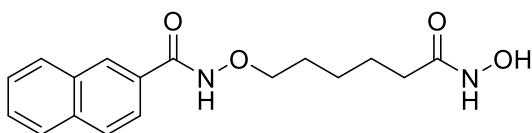
***N*-((6-(Hydroxyamino)-6-oxohexyl)oxy)isoquinoline-1-carboxamide (8b)**: white solid, yield 56.4%, mp 77 °C. ¹HNMR (600 MHz, DMSO-d₆) 1.38-1.43 (m, 2H), 1.54-1.59 (m, 2H), 1.63-1.68 (m, 2H), 1.98 (t, 2H, J = 7.4 Hz), 3.96 (t, 2H, J = 6.5 Hz), 7.75-7.77 (m, 1H), 7.83-7.86 (m, 1H), 8.02 (d, 1H, J = 5.6 Hz), 8.06 (d, 1H, J = 8.2 Hz), 8.53 (d, 1H, J = 5.6 Hz), 8.59 (d, 1H, J = 8.6 Hz), 10.36 (s, 1H), 11.86 (s, 1H). ¹³CNMR (151 MHz, DMSO-d₆) 25.41, 25.54, 32.69, 75.74, 123.59, 125.86, 126.36, 127.66, 128.99, 132.32, 136.71, 141.51, 151.56, 169.51. HRMS-ESI [M+H]: m/z calcd for C₁₆H₂₀N₃O₄: 306.1448, found: 306.1450. HPLC retention time: 8.75 min, purity 97.8%.



***N*-((6-(Hydroxyamino)-6-oxohexyl)oxy)quinoline-4-carboxamide (8c):** white solid, yield 83.2%, mp 86°C. ¹HNMR (600 MHz, DMSO-d₆) 1.38-1.42 (m, 2H), 1.54-1.59 (m, 2H), 1.64-1.69 (m, 2H), 1.98 (t, 2H, J = 7.3 Hz), 3.99 (t, 2H, J = 6.4 Hz), 7.57 (d, 1H, J = 4.0 Hz), 7.70 (t, J = 7.6 Hz), 7.83(t, J = 7.5Hz, 1H), 8.10(dd, J = 8.4Hz 15.6Hz, 2H), 8.69(br, 1H), 8.99(d, 1H, J = 4.2 Hz, 1H), 10.38 (s, 1H), 11.83 (s, 1H). ¹³CNMR (151 MHz, DMSO-d₆)25.40, 27.91, 32.68, 75.96, 120.06, 124.71, 125.52, 128.11, 129.91, 130.46, 139.64, 148.31, 150.67, 163.89, 169.49. HRMS-ESI [M+H]: m/z calcd for C₁₆H₂₀N₃O₄:318.1448, found: 318.1448. HPLC retention time: 5.77 min purity 95.5%.

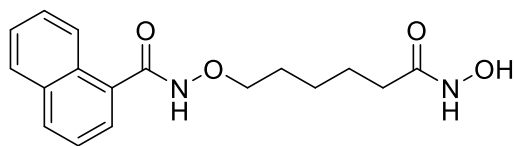


***N*-((6-(Hydroxyamino)-6-oxohexyl)oxy)quinoxaline-2-carboxamide (8d):** yellow solid, yield 85.5%, mp 117°C. ¹HNMR (600 MHz, DMSO-d₆)1.37-1.42(m, 2H), 1.54-1.59 (m ,2H), 1.62-1.66 (m, 2H), 1.97 (t, 2H, J = 7.3 Hz), 3.95 (t, 2H, J = 6.3 Hz), 7.98-8.00 (m ,2H), 8.18-8.20 (m, 2H), 8.68 (s, 1H), 9.41 (s, 1H), 10.37 (s, 1H), 12.27 (s, 1H). ¹³CNMR (151 MHz, DMSO-d₆) 25.36, 25.53, 27.88, 32.67, 75.85, 129.61, 129.88, 131.81, 132.44, 140.21, 143.39, 144.07, 144.70, 161.02, 169.50. HRMS-ESI [M+H]: m/z calcd for C₁₅H₁₉N₄O₄: 319.1401, found: 319.1399. HPLC retention time: 8.68 min, purity 97.5%.

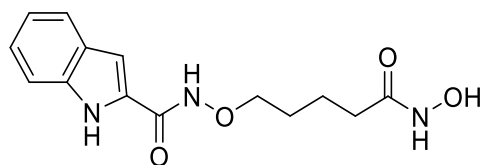


***N*-((6-(Hydroxyamino)-6-oxohexyl)oxy)-2-naphthamide (8e):** white solid, yield 83.0%, mp 109°C, ¹HNMR (600 MHz, DMSO-d₆).1.37-1.42 (m, 2H), 1.54-1.59 (m, 2H), 1.61 (m, 2H), 1.97 (t, 2H, J = 7.25 Hz), 3.91 (t, 2H, J = 6.5Hz), 7.59-7.65 (m, 2H), 7.82 (dd, 1H, J = 1.7 8.6 Hz), 7.98-8.04 (m, 3H), 8.36 (s, 1H), 8.68 (s, 1H), 10.37 (s, 1H), 11.78 (s, 1H). ¹³CNMR (151 MHz, DMSO-d₆): 25.40, 25.58, 27.95, 32.68, 75.66, 124.28, 127.30, 127.90, 128.14, 128.21,

128.54, 129.28, 130.25, 132.53, 134.69, 164.76, 169.50. HRMS-ESI [M+H]: m/z calcd for C₁₇H₂₁N₂O₄: 317.1496, found:317.1493. HPLC retention time: 12.78 min, purity 97.7%.



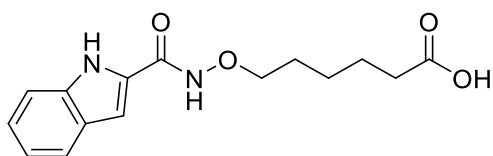
***N*-((6-(Hydroxyamino)-6-oxohexyl)oxy)-1-naphthamide (8f)**: white solid, yield 89.3%, mp 72-73°C. ¹HNMR (600 MHz, DMSO-d₆): 1.36-1.44 (m, 2H), 1.51-1.70 (m, 4H), 1.96 (t, 2H, J = 7.1 Hz), 3.95 (t, 2H, J = 6.5 Hz), 7.52 (m, 4H), 7.98-8.06 (m, 2H), 8.12-8.15 (m, 1H), 8.68 (s, 1H), 10.36 (s, 1H), 11.57 (s, 1H). ¹³CNMR (151 MHz, DMSO-d₆): 25.43, 25.57, 27.95, 32.70, 75.70, 125.40, 126.13, 126.86, 127.46, 128.77, 130.38, 130.76, 132.15, 133.57, 165.92, 169.50. HRMS-ESI [M+H]: m/z calcd for C₁₇H₂₁N₂O₄: 317.1496, found: 317.1498. HPLC: retention time: 11.98, purity 96.6%.



***N*-((5-(Hydroxyamino)-5-oxopentyl)oxy)-1H-indole-2-carboxamide (13)**: light yellow solid, yield 90%, mp 118°C. ¹HNMR (600 MHz, DMSO-d₆): 1.60-1.66 (m, 4H). 2.01 (t, 2H, J = 6.7 Hz), 3.90 (t, 2H, J = 5.7 Hz), 7.02 (s, 1H), 7.03 (t, 1H, J = 7.5 Hz), 7.18 (t, 1H, J = 7.6 Hz) 7.43 (d, 1H, J = 8.2 Hz), 7.61 (d, 1H, J = 8.0 Hz), 10.39 (s, 1H), 11.66 (s, 1H), 11.67 (s, 1H). ¹³CNMR (151 MHz, DMSO-d₆) 22.18, 27.67, 32.39, 75.75, 112.75, 120.24, 123.96, 127.39, 136.94, 169.44. HRMS-ESI [M+H]: m/z calcd for C₁₄H₁₈N₃O₄S:292.1292, found: 292.1294. HPLC retention time: 7.28 min, purity 95.5%.

General procedure for the catalytic hydrogenation of benzyl esters (VI)

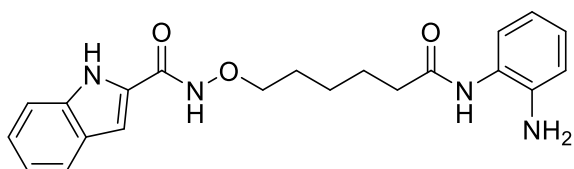
A solution of the benzyl ester (**17**) was dissolved in 20 mL of methanol and the Pd/C catalyst (15% w/w) was added and the reaction was left under stirring for 5 min at room temperature. The atmosphere was then changed to H₂ at atmospheric pressure. Upon completion (2h), the reaction was filtered through Celite and the methanol removed under reduced pressure. The crude residue was then purified by flash chromatography using mixtures of dichloromethane/methanol as eluent (0-15% of methanol).



6-((1*H*-Indole-2-carboxamido)oxy)hexanoic acid (18): White solid, yield 58.6%, mp 168-169°C. ¹HNMR (300 MHz, DMSO-*d*₆): 1.39-1.44 (m, 2H), 1.54-1.59 (m, 2H), 1.61-1.66 (m, 2H), 2.22 (t, 2H, *J* = 7.4 Hz), 3.90 (t, 2H, *J* = 6.5 Hz), 7.01 (s, 1H), 7.03 (t, 1H, *J* = 7.5 Hz), 7.18 (ddd, 1H, *J* = 1.2 6.9 8.2 Hz), 7.42 (d, 1H, *J* = 7.4 Hz), 7.60 (d, 1H, *J* = 7.9 Hz), 11.62 (s, 1H), 12.02 (br, 1H). ¹³CNMR (151 MHz, DMSO-*d*₆): 24.81, 25.54, 27.93, 34.19, 75.92, 112.74, 122.01, 123.92, 127.39, 129.37, 136.94, 175.00. HRMS-ESI [*M*+*H*]: *m/z* calcd for C₁₅H₁₉N₂O₄: 291.1339, found: 291.1341. HPLC retention time: 14.5 min 96.4%,

General procedure for the Boc deprotection (VII)

The protected amine (**19**) was dissolved in 20 mL of a solution of DCM/TFA 15% and left under stirring for 2h at room temperature. With the completion of the reaction, 20 mL of saturated aqueous solution of Na₂CO₃ was added. The aqueous phase was further extracted three times with DCM, the combined organic phases were dried with Mg₂SO₄ and evaporated. The resulting product was purified by flash chromatography using mixtures of hexane/ethyl acetate (0-100% of ethyl acetate) as eluent.



***N*-((6-((2-Aminophenyl)amino)-6-oxohexyl)oxy)-1*H*-indole-2-carboxamide (20):** White solid, yield 82%, mp 180-182°C. ¹HNMR (600 MHz, DMSO-*d*₆): 1.44-1.50 (m, 2H), 1.64-1.71 (m, 4H), 2.35 (t, 2H, *J* = 7.4 Hz), 3.93 (t, 2H, *J* = 6.5 Hz), 4.82 (s, 2H), 6.53-6.56 (m, 1H), 6.71 (dd, 1H, *J* = 1.5 7.5 Hz), 6.88-6.90 (m, 1H), 7.02 (s, 1H), 7.04 (ddd, 1H, *J* = 1.0 6.8 8.0 Hz), 7.16-7.21 (m, 2H), 7.43 (d, 1H, *J* = 8.3 Hz), 7.61 (d, 1H, *J* = 7.9 Hz), 9.11 (s, 1H), 11.66 (s, 2H). ¹³CNMR (151 MHz, DMSO-*d*₆): 25.57, 25.67, 28.00, 36.18, 75.99, 112.75, 116.35, 116.64, 120.32, 122.02, 124.03, 125.74, 126.15, 127.40, 129.37, 136.94, 142.34, 171.54. HRMS-ESI [*M*+*H*]: *m/z* calcd for C₂₁H₂₅N₄O₃: 381.1921, found: 381.1922. HPLC retention time: 8.50 min, purity 98.6%.

4.13.2. Computational details

Docking studies

The 2D structures of the ligands were drawn using the software ChemDraw 16.0¹⁸⁹, they were further used as input for Chem3D 16.0¹⁸⁹ for the generation of the 3D structures. The 3D structures were then minimized using MMP2 force fields and for the dockings using the standard procedure of AutoDock tools version 1.5.7 (ADT).¹⁸²

The structures of the proteins PDB ID 4KBX (HDAC1) and 5EDU (HDAC6) were downloaded from the Protein Data Base. Using the software UCSF Chimera¹⁹⁰, the structure of 4KBX was superimposed in 5EDU to maintain the same 3D coordinates. Also, all water molecules, buffer and noninteracting ions were removed from chain A of 5EDU and chain B of 4KBX. The clean structures were used as input for AutoDock tools for the alteration of protonation of His140 in HDAC1 and His611 in HDAC6 was performed and computation of the Gasteiger charges. After the calculation of the charges, the grid box with size 21 x 28 x 27 centered in the x, y and z coordinates 17.02, -44.55 and 101.80 with the spacing of 1.0 Å was created.

In AutoDock4.2, the Lamarckian genetic algorithm was used and the search parameters were set to 100 GA runs for each ligand with a population size of 150, maximum number of $2.5 \cdot 10^6$ energy evaluations, a maximum number of $2.7 \cdot 10^4$ generations, a mutation rate of 0.2 and a crossover rate of 0.8 and the default dockings parameters were used. Populations of 100 docking poses were generated for each run and organized in clusters.

5. Summary

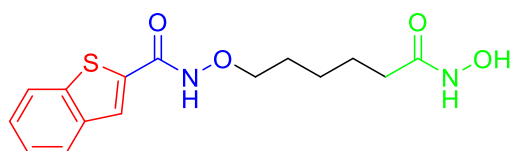
Modifications of gene expression without alteration of the genetic code, commonly known as epigenetics, are essential for several cellular processes. Their key players are studied as biological targets in a wide range of diseases. Among the epigenetic mechanism of gene regulation, the acetylation of histones is the major responsible for DNA accessibility. The enzymes performing histone deacetylation (HDACs) are validated targets in cancer therapy and so far, five inhibitors of this class of enzymes have been approved for the treatment of hematological malignancies. Eleven zinc-dependent HDAC isoforms are expressed in humans, organized according to their structures in three classes: class I (HDAC1-3 and 8); class II further divided in IIa (HDAC4, 5, 7 and 9) and IIb (HDAC6 and 10) and class IV (HDAC11). The pharmacophore of classical HDAC inhibitors can be divided into four parts: cap-group which interacts with the surface of the binding pocket, connecting unit (CU), linker and zinc-binding group (ZBG).

Initially, the focus of this work was to identify HDAC inhibitors to be used against Malaria, an infective disease caused by protozoa from genus *Plasmodium*, which represent a great burden on human health. *P. falciparum*, the most pathogenic species, can express three zinc-dependent HDACs (*Pf*HDAC1, 2 and 3). Due to the importance in multiple stages of the parasite, *Pf*HDAC1 was chosen as the target for the design of the first set of HDAC inhibitors. Based on the structure of *Pf*HDAC1, twelve alkoxyamide-based HDAC inhibitors were synthesized and assayed against *P. falciparum* strains 3D7 and Dd2 and human hepatocellular carcinoma cells HepG2 to evaluate the selectivity of the inhibitors towards host cells. The most potent compound of the series **6h** was able to inhibit the growth of *Pf*3D7 and *Pf*Dd2 in low nanomolar concentrations, showing 25-fold selectivity towards the parasite.

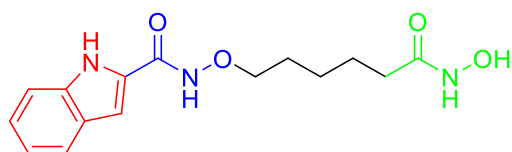
In the second part of the work, the first set of synthesized HDAC inhibitors was assayed against the ovarian carcinoma cell line A2780 and the oral squamous cell carcinoma cell line Cal27, in MTT-viability and HDAC cell-based assays. The results obtained in these studies revealed the potential of alkoxyamide derivatives containing bicyclic rings as cap-group in the treatment of these cancer types. To further evaluate the effect of different heterocycles on the anticancer activity, the second set of HDAC inhibitors was designed and synthesized. By analysis of the antineoplastic activity of the second set of inhibitors, the lead structure **6r** was chosen for further modifications. In the third and final set of inhibitors, modifications resulted in an increase of potency against the two carcinoma cells. In addition to the high potency of the synthesized HDAC inhibitors, compounds **6r**, **8a** and **8c** were shown to increase cisplatin sensibility in

cisplatin sensitive and cisplatin resistant Cal27 cells, increasing the cisplatin-induced apoptosis. Therefore, the synthesized HDAC inhibitors are promising structures for further anticancer studies and can be used as starting point for the design of novel inhibitors.

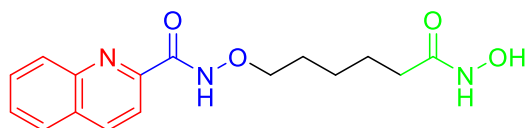
Cap-group CU Linker ZBG



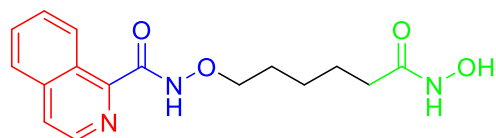
6h
Pf3D7: 0.07 μ M
PfDd2: 0.07 μ M
 SI: 25/25



6r
 Cal27: 0.21 μ M



8a
 Cal27: 0.70 μ M



8c
 Cal27: 1.90 μ M

Figure 36: Summary of the most promising compounds and their biological activity.

6. Zusammenfassung

Modifikationen der Gen-Expression ohne Veränderung des genetischen Codes, bekannt als Epigenetik, sind essentiell für viele zelluläre Prozesse. Deren Schlüsselenzyme werden als Angriffspunkte bei einer Vielzahl von Erkrankungen untersucht. Unter den epigenetischen Mechanismen der Gen-Regulation ist hauptsächlich die Acetylierung von Histonen für die Zugänglichkeit der DNA verantwortlich. Histon Deacetylasen (HDACs) sind bereits validierte Zielstrukturen in der Krebs-Therapie und bis heute wurden fünf Inhibitoren dieser Enzymklasse für die Behandlung von hämatologischen Krebsarten zugelassen. Der Mensch exprimiert elf Zink abhängige HDAC-Isoformen, die anhand ihrer Struktur in drei Klassen unterteilt werden: Klasse I (HDAC1-3 und 8); Klasse II, zusätzlich unterteilt in IIa (HDAC4, 5, 7 und 9) und IIb (HDAC6 und 10) und Klasse IV (HDAC11). Das Pharmakophor klassischer HDAC-Inhibitoren kann in vier Teile gegliedert werden, Cap-Gruppe, die mit der Oberfläche der Bindetasche interagiert, Connecting Unit (CU), Linker und Zink-bindende Gruppe (ZBG).

Zunächst lag der Fokus dieser Arbeit auf der Identifizierung von HDAC-Inhibitoren zur Behandlung der Malaria, einer Erkrankung, die von Protozoen des Genus *Plasmodium* verursacht wird und eine große gesundheitliche Belastung der Menschheit darstellt. Die am stärksten pathogene Spezies, *Plasmodium falciparum*, kann drei Zink-abhängige HDACs exprimieren (*Pf*HDAC1, 2 und 3). *Pf*HDAC1 wurde aufgrund seiner Wichtigkeit für alle Erreger-Stadien als Zielstruktur für die Entwicklung des ersten Sets von Verbindungen gewählt. Basierend auf der Struktur von *Pf*HDAC1 wurden HDAC-Inhibitoren mit Alkoxyamid-Struktur synthetisiert und gegen die *P. falciparum* Stämme 3D7 und Dd2, sowie humane Leberkarzinom-Zellen HepG2 evaluiert, um die Selektivität der HDAC-Inhibitoren gegenüber Wirtszellen zu untersuchen. Die aktivste Verbindung der Serie, **6h**, konnte das Wachstum im niedrigen nanomolaren Konzentrationsbereich hemmen und zeigte eine 25 fache Selektivität für den Parasiten gegenüber Wirtszellen.

Im zweiten Teil der Arbeit wurde das erste Set der HDAC-Inhibitoren hinsichtlich seiner Aktivität gegenüber der Ovarialkarzinom-Zelllinie A2780 und der Zungenkarzinom-Zelllinie Cal27 in MTT Zellviabilitäts und zellbasierten HDAC Assays getestet. Die Ergebnisse offenbarten das Potenzial von Alkoxyamid-basierten Derivaten mit bicyklischer Cap-Gruppe in der Behandlung dieser Krebs-Erkrankungen. Um den Effekt verschiedener weiterer heterozyklischer Cap-Gruppen auf die Zytotoxizität zu prüfen, wurde eine zweite Serie HDAC-Inhibitoren synthetisiert. Durch die Analyse der antineoplastischen Aktivität der zweiten Serie HDAC-Inhibitoren wurde Verbindung **6r** als Leitstruktur für weitere Modifikationen

ausgewählt. Die strukturellen Änderungen im dritten Set von HDAC-Inhibitoren resultierten in einer erhöhten zytotoxischen Aktivität der Verbindungen gegen beide Krebszelllinien. Zusätzlich zur hohen zytotoxischen Potenz konnten die Verbindungen **6r**, **8a** und **8c** die Cisplatin-Sensibilität von Cisplatin sensiblen und resistenten Cal27-Zellen erhöhen und die Cisplatin induzierte Apoptose verstärken. Daher sind die in dieser Arbeit synthetisierten HDAC Inhibitoren vielversprechende Strukturen für weitere zytotoxische Untersuchungen und Startpunkte für die Entwicklung neuer HDAC-Inhibitoren.

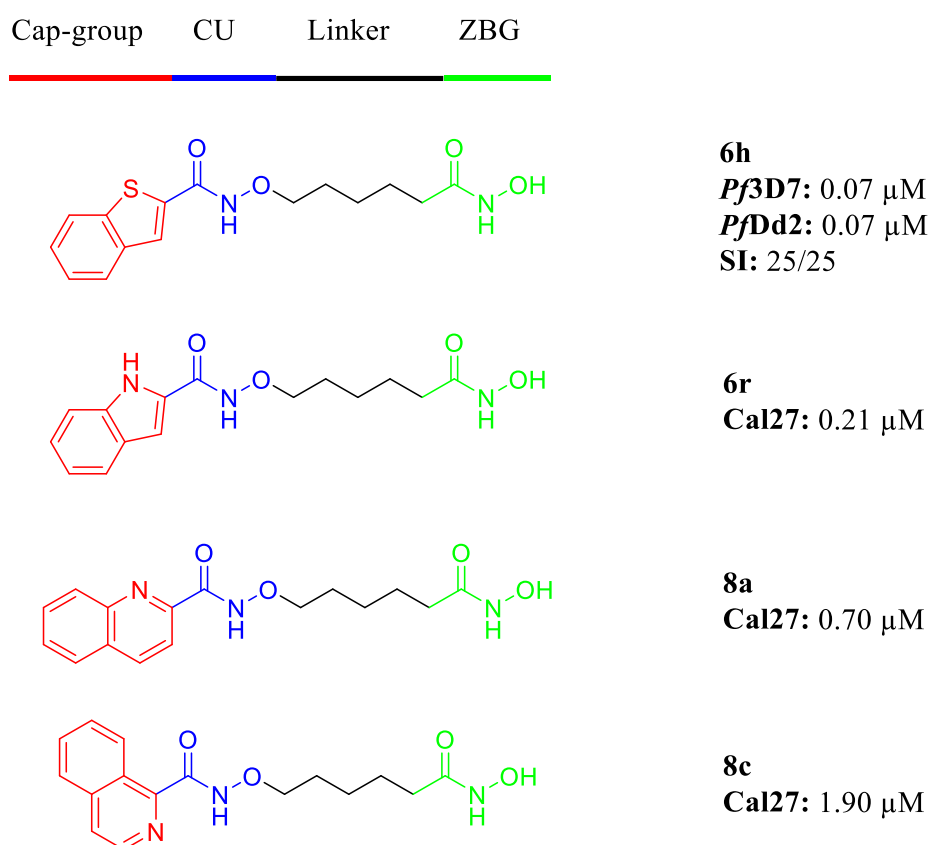


Abbildung 36: Zusammenfassung der vielversprechendsten Verbindungen und ihrer Aktivitäten.

7. References

- (1) Verdin, E.; Ott, M. 50 Years of Protein Acetylation: From Gene Regulation to Epigenetics, Metabolism and beyond. *Nat. Rev. Mol. Cell Biol.* **2015**, *16* (4), 258–264.
- (2) Pande, V. Understanding the Complexity of Epigenetic Target Space. *J. Med. Chem.* **2016**, *59* (4), 1299–1307.
- (3) Drazic, A.; Myklebust, L. M.; Ree, R.; Arnesen, T. The World of Protein Acetylation. *Biochim. Biophys. Acta - Proteins Proteomics* **2016**, *1864* (10), 1372–1401.
- (4) Filippakopoulos, P.; Knapp, S. Targeting Bromodomains: Epigenetic Readers of Lysine Acetylation. *Nat. Rev. Drug Discov.* **2014**, *13* (5), 337–356.
- (5) Halsall, J. A.; Turner, B. M. Histone Deacetylase Inhibitors for Cancer Therapy: An Evolutionarily Ancient Resistance Response May Explain Their Limited Success. *BioEssays* **2016**, *38* (11), 1102–1110.
- (6) Qiu, X.; Xiao, X.; Li, N.; Li, Y. Histone Deacetylases Inhibitors (HDACis) as Novel Therapeutic Application in Various Clinical Diseases. *Prog. Neuro-Psychopharmacology Biol. Psychiatry* **2017**, *72*, 60–72.
- (7) Heerboth, S.; Lapinska, K.; Snyder, N.; Leary, M.; Rollinson, S.; Sarkar, S. Use of Epigenetic Drugs in Disease: An Overview. *Genet. Epigenetics* **2014**, *1* (6), 9–19.
- (8) Leipe, D. D.; Landsman, D. Histone Deacetylases, Acetoin Utilization Proteins and Acetylpolyamine Amidohydrolases Are Members of an Ancient Protein Superfamily. *Nucleic Acids Res.* **1997**, *25* (18), 3693–3697.
- (9) Gregoret, I. V.; Lee, Y.; Goodson, H. V.; Dame, N.; Dame, N. Molecular Evolution of the Histone Deacetylase Family: Functional Implications of Phylogenetic Analysis. **2004**, 17–31.
- (10) Greiss, S.; Gartner, A. Sirtuin / Sir2 Phylogeny, Evolutionary Considerations and Structural Conservation. **2009**, 407–415.
- (11) López, J. E.; Sullivan, E. D.; Fierke, C. A. Metal-Dependent Deacetylases: Cancer and Epigenetic Regulators. *ACS Chem. Biol.* **2016**, *11* (3), 706–716.
- (12) Bradner, J. E.; West, N.; Grachan, M. L.; Greenberg, E. F.; Haggarty, S. J.; Warnow, T.; Mazitschek, R. Chemical Phylogenetics of Histone Deacetylases. *Nat. Chem. Biol.* **2010**, *6* (3), 238–243.
- (13) Finnin, M. S.; Donigian, J. R.; Cohen, A.; Richon, V. M.; Rifkind, R. A.; Marks, P. A.; Breslow, R.; Pavletich, N. P. Structures of a Histone Deacetylase Homologue Bound to the TSA and SAHA Inhibitors. *Nature* **1999**, *401* (6749), 188–193.
- (14) Somoza, J. R.; Skene, R. J.; Katz, B. A.; Mol, C.; Ho, J. D.; Jennings, A. J.; Luong, C.; Arvai, A.; Buggy, J. J.; Chi, E.; Tang, J.; Sang, B. C.; Verner, E.; Wynands, R.; Leahy, E. M.; Dougan, D. R.; Snell, G.; Navre, M.; Knuth, M. W.; Swanson, R. V.; McRee, D. E.; Tari, L. W. Structural Snapshots of Human HDAC8 Provide Insights into the Class I Histone Deacetylases. *Structure* **2004**, *12* (7), 1325–1334.
- (15) Wu, R.; Wang, S.; Zhou, N.; Cao, Z.; Zhang, Y. A Proton-Shuttle Reaction Mechanism for Histone Deacetylase 8 and the Catalytic Role of Metal Ions. *J Am Chem Soc* **2010**, *132* (27), 9471–9479.
- (16) Chen, K.; Zhang, X.; Wu, Y. D.; Wiest, O. Inhibition and Mechanism of HDAC8 Revisited. *J. Am. Chem. Soc.* **2014**, *136* (33), 11636–11643.
- (17) Gantt, S. M. L.; Decroos, C.; Lee, M. S.; Gullett, L. E.; Bowman, C. M.; Christianson, D. W. Crystal Structure of Human Histone Deacetylase 8 (HDAC8) Bound to the Inhibitor SAHA. *Structure* **2004**, *12* (7), 1335–1344.

- D. W.; Fierke, C. A. General Base-General Acid Catalysis in Human Histone Deacetylase 8. *Biochemistry* **2016**, *55* (5), 820–832.
- (18) Gantt, S. L.; Gattis, S. G.; Fierke, C. A. Catalytic Activity and Inhibition of Human Histone Deacetylase 8 Is Dependent on the Identity of the Active Site Metal Ion. *Biochemistry* **2006**, *45* (19), 6170–6178.
- (19) Dowling, D. P.; Gattis, S. G.; Fierke, C. A.; Christianson, D. W. Structures of Metal-Substituted Human Histone Deacetylase 8 Provide Mechanistic Inferences on Biological Function. *Biochemistry* **2010**, *49* (24), 5048–5056.
- (20) Watson, P. J.; Millard, C. J.; Riley, A. M.; Robertson, N. S.; Wright, L. C.; Godage, H. Y.; Cowley, S. M.; Jamieson, A. G.; Potter, B. V. L.; Schwabe, J. W. R. ARTICLE Insights into the Activation Mechanism of Class I HDAC Complexes by Inositol Phosphates. **2016**.
- (21) Sternson, S. M.; Wong, J. C.; Grozinger, C. M.; Schreiber, S. L. Synthesis of 7200 Small Molecules Based on a Substructural Analysis of the Histone Deacetylase Inhibitors Trichostatin and Trapoxin. *Org. Lett.* **2001**, *3* (26), 4239–4242.
- (22) Roche, J.; Bertrand, P. Inside HDACs with More Selective HDAC Inhibitors. *Eur. J. Med. Chem.* **2016**, *121*, 451–483.
- (23) Madsen, A. S.; Kristensen, H. M. E.; Lanz, G.; Olsen, C. A. The Effect of Various Zinc Binding Groups on Inhibition of Histone Deacetylases 1-11. *ChemMedChem* **2014**, *9* (3), 614–626.
- (24) Christianson, D. W. Structural Biology of Zinc. *Adv. Protein Chem.* **1991**, *42*, 281–355.
- (25) Laitaoja, M.; Valjakka, J.; Jänis, J. Zinc Coordination Spheres in Protein Structures. *Inorg. Chem.* **2013**, *52* (19), 10983–10991.
- (26) Chen, K.; Xu, L.; Wiest, O. Computational Exploration of Zinc Binding Groups for HDAC Inhibition. *J. Org. Chem.* **2013**, *78* (10), 5051–5055.
- (27) Suzuki, T.; Kouketsu, A.; Matsuura, A.; Kohara, A.; Ninomiya, S. I.; Kohda, K.; Miyata, N. Thiol-Based SAHA Analogues as Potent Histone Deacetylase Inhibitors. *Bioorganic Med. Chem. Lett.* **2004**, *14* (12), 3313–3317.
- (28) McClure, J. J.; Inks, E. S.; Zhang, C.; Peterson, Y. K.; Li, J.; Chundru, K.; Lee, B.; Buchanan, A.; Miao, S.; Chou, C. J. Comparison of the Deacylase and Deacetylase Activity of Zinc-Dependent HDACs. *ACS Chem. Biol.* **2017**, *12* (6), 1644–1655.
- (29) Knoepfler, P. S.; Eisenman, R. N. Sin Meets NuRD and Other Tails of Repression. *Cell* **1999**, *99* (5), 447–450.
- (30) Nakayama, J. I.; Hayakawa, T. Physiological Roles of Class I HDAC Complex and Histone Demethylase. *J. Biomed. Biotechnol.* **2011**, *2011*.
- (31) Kelly, R. D. W.; Cowley, S. M. The Physiological Roles of Histone Deacetylase (HDAC) 1 and 2: Complex Co-Stars with Multiple Leading Parts. *Biochem. Soc. Trans.* **2013**, *41* (3), 741–749.
- (32) Millard, C. J.; Varma, N.; Saleh, A.; Morris, K.; Watson, P. J.; Bottrill, A. R.; Fairall, L.; Smith, C. J.; Schwabe, J. W. R. The Structure of the Core NuRD Repression Complex Provides Insights into Its Interaction with Chromatin. *Elife* **2016**, *5* (APRIL2016), 1–21.
- (33) Guenther, M. G.; Barak, O.; Lazar, M. A. The SMRT and N-CoR Corepressors Are Activating Cofactors for Histone Deacetylase 3. *Mol. Cell. Biol.* **2001**, *21* (18), 6091–6101.
- (34) Bantscheff, M.; Hopf, C.; Savitski, M. M.; Dittmann, A.; Grandi, P.; Michon, A. M.; Schlegl, J.; Abraham, Y.; Becher, I.; Bergamini, G.; Boesche, M.; Delling, M.;

- Dümpelfeld, B.; Eberhard, D.; Huthmacher, C.; Mathieson, T.; Poeckel, D.; Reader, V.; Strunk, K.; Sweetman, G.; Kruse, U.; Neubauer, G.; Ramsden, N. G.; Drewes, G. Chemoproteomics Profiling of HDAC Inhibitors Reveals Selective Targeting of HDAC Complexes. *Nat. Biotechnol.* **2011**, *29* (3), 255–268.
- (35) Dose, A.; Sindlinger, J.; Bierlmeier, J.; Bakirbas, A.; Schulze-Osthoff, K.; Einsele-Scholz, S.; Hartl, M.; Essmann, F.; Finkemeier, I.; Schwarzer, D. Untersuchung Der Substratspezifität Und Zusammensetzung Endogener Histondeacetylase-Komplexe Durch Chemische Sonden. *Angew. Chemie* **2016**, *128* (3), 1208–1211.
- (36) Maolanon, A. R.; Madsen, A. S.; Olsen, C. A. Innovative Strategies for Selective Inhibition of Histone Deacetylases. *Cell Chem. Biol.* **2016**, *23* (7), 759–768.
- (37) Watson, P. J.; Fairall, L.; Santos, G. M.; Schwabe, J. W. R. Structure of HDAC3 Bound to Co-Repressor and Inositol Tetraphosphate. *Nature* **2012**, *481* (7381), 335–340.
- (38) Zhou, J.; Li, M.; Chen, N.; Wang, S.; Luo, H. Bin; Zhang, Y.; Wu, R. Computational Design of a Time-Dependent Histone Deacetylase 2 Selective Inhibitor. *ACS Chem. Biol.* **2015**, *10* (3), 687–692.
- (39) Ma, P.; Schultz, R. M. HDAC1 and HDAC2 in Mouse Oocytes and Preimplantation Embryos: Specificity versus Compensation. *Cell Death Differ.* **2016**, *23* (7), 1119–1127.
- (40) Dokmanovic, M.; Clarke, C.; Marks, P. A. Histone Deacetylase Inhibitors: Overview and Perspectives. *Mol. Cancer Res.* **2007**, *5* (10), 981–989.
- (41) Chakrabarti, A.; Oehme, I.; Witt, O.; Oliveira, G.; Sippl, W.; Romier, C.; Pierce, R. J.; Jung, M. HDAC8: A Multifaceted Target for Therapeutic Interventions. *Trends Pharmacol. Sci.* **2015**, *36* (7), 481–492.
- (42) Wang, D.; Wiest, O. G.; Helquist, P.; Norbert, L. Supporting Info: On the Function of the 14Å Long Internal Cavity of Histone Deacetylase Like Protein : Implication for the Design of Histone Deacetylase Inhibitors. *J. Med. Chem.* **2004**, 1–6.
- (43) Wambua, M. K.; Nalawansa, D. A.; Negmeldin, A. T.; Pflum, M. K. H. Mutagenesis Studies of the 14 Å Internal Cavity of Histone Deacetylase 1: Insights toward the Acetate-Escape Hypothesis and Selective Inhibitor Design. *J. Med. Chem.* **2014**, *57* (3), 642–650.
- (44) Micelli, C.; Rastelli, G. Histone Deacetylases: Structural Determinants of Inhibitor Selectivity. *Drug Discov. Today* **2015**, *20* (6), 718–735.
- (45) Decroos, C.; Bowman, C. M.; Moser, J. S.; Christianson, K. E.; Deardor, M. a; Christianson, D. W. Compromised Structure and Function of HDAC8 Mutants Identifi Fi Ed in Cornelia de Lange Syndrome Spectrum Disorders. **2015**.
- (46) Whitehead, L.; Dobler, M. R.; Radetich, B.; Zhu, Y.; Atadja, P. W.; Claiborne, T.; Grob, J. E.; McRiner, A.; Pancost, M. R.; Patnaik, A.; Shao, W.; Shultz, M.; Tichkule, R.; Tommasi, R. A.; Vash, B.; Wang, P.; Stams, T. Human HDAC Isoform Selectivity Achieved via Exploitation of the Acetate Release Channel with Structurally Unique Small Molecule Inhibitors. *Bioorganic Med. Chem.* **2011**, *19* (15), 4626–4634.
- (47) Chou, C. J.; Herman, D.; Gottesfeld, J. M. Pimelic Diphenylamide 106 Is a Slow, Tight-Binding Inhibitor of Class I Histone Deacetylases. *J. Biol. Chem.* **2008**, *283* (51), 35402–35409.
- (48) Methot, J. L.; Hoffman, D. M.; Witter, D. J.; Stanton, M. G.; Harrington, P.; Hamblett, C.; Siliphaivanh, P.; Wilson, K.; Hubbs, J.; Heidebrecht, R.; Kral, A. M.; Ozerova, N.; Fleming, J. C.; Wang, H.; Szewczak, A. A.; Middleton, R. E.; Hughes, B.; Cruz, J. C.; Haines, B. B.; Chenard, M.; Kenific, C. M.; Harsch, A.; Secrist, J. P.; Miller, T. A. Delayed and Prolonged Histone Hyperacetylation with a Selective HDAC1/HDAC2

- Inhibitor. *ACS Med. Chem. Lett.* **2014**, 5 (4), 340–345.
- (49) Suzuki, T.; Ando, T.; Tsuchiya, K.; Fukazawa, N.; Saito, A.; Mariko, Y.; Yamashita, T.; Nakanishi, O. Synthesis and Histone Deacetylase Inhibitory Activity of New Benzamide Derivatives. *J. Med. Chem.* **1999**, 42 (15), 3001–3003.
- (50) Moradei, O. M.; Mallais, T. C.; Frechette, S.; Paquin, I.; Tessier, P. E.; Leit, S. M.; Fournel, M.; Bonfils, C.; Trachy-Bourget, M. C.; Liu, J.; Yan, T. P.; Lu, A. H.; Rahil, J.; Wang, J.; Lefebvre, S.; Li, Z.; Vaisburg, A. F.; Besterman, J. M. Novel Aminophenyl Benzamide-Type Histone Deacetylase Inhibitors with Enhanced Potency and Selectivity. *J. Med. Chem.* **2007**, 50 (23), 5543–5546.
- (51) Methot, J. L.; Chakravarty, P. K.; Chenard, M.; Close, J.; Cruz, J. C.; Dahlberg, W. K.; Fleming, J.; Hamblett, C. L.; Hamill, J. E.; Harrington, P.; Harsch, A.; Heidebrecht, R.; Hughes, B.; Jung, J.; Kenific, C. M.; Kral, A. M.; Meinke, P. T.; Middleton, R. E.; Ozerova, N.; Sloman, D. L.; Stanton, M. G.; Szewczak, A. A.; Tyagarajan, S.; Witter, D. J.; Paul Secrist, J.; Miller, T. A. Exploration of the Internal Cavity of Histone Deacetylase (HDAC) with Selective HDAC1/HDAC2 Inhibitors (SHI-1:2). *Bioorganic Med. Chem. Lett.* **2008**, 18 (3), 973–978.
- (52) Kattar, S. D.; Surdi, L. M.; Zabierek, A.; Methot, J. L.; Middleton, R. E.; Hughes, B.; Szewczak, A. A.; Dahlberg, W. K.; Kral, A. M.; Ozerova, N.; Fleming, J. C.; Wang, H.; Secrist, P.; Harsch, A.; Hamill, J. E.; Cruz, J. C.; Kenific, C. M.; Chenard, M.; Miller, T. A.; Berk, S. C.; Tempest, P. Parallel Medicinal Chemistry Approaches to Selective HDAC1/HDAC2 Inhibitor (SHI-1:2) Optimization. *Bioorganic Med. Chem. Lett.* **2009**, 19 (4), 1168–1172.
- (53) Mai, A.; Perrone, A.; Nebbioso, A.; Rotili, D.; Valente, S.; Tardugno, M.; Massa, S.; De Bellis, F.; Altucci, L. Novel Uracil-Based 2-Aminoanilide and 2-Aminoanilide-like Derivatives: Histone Deacetylase Inhibition and in-Cell Activities. *Bioorganic Med. Chem. Lett.* **2008**, 18 (8), 2530–2535.
- (54) Marson, C. M.; Matthews, C. J.; Yiannaki, E.; Atkinson, S. J.; Soden, P. E.; Shukla, L.; Lamadema, N.; Thomas, N. S. B. Discovery of Potent, Isoform-Selective Inhibitors of Histone Deacetylase Containing Chiral Heterocyclic Capping Groups and a N-(2-Aminophenyl)benzamide Binding Unit. *J. Med. Chem.* **2013**, 56 (15), 6156–6174.
- (55) Zhang, Q. W.; Li, J. Q. Synthesis and Biological Evaluation of N-(Aminopyridine) Benzamide Analogues as Histone Deacetylase Inhibitors. *Bull. Korean Chem. Soc.* **2012**, 33 (2), 535–540.
- (56) Wagner, F. F.; Lundh, M.; Kaya, T.; Mccarren, P.; Zhang, Y.; Chattopadhyay, S.; Gale, J. P.; Galbo, T.; Fisher, S. L.; Meier, B. C.; Vetere, A.; Richardson, S.; Morgan, N. G.; Christensen, D. P.; Gilbert, T. J.; Hooker, J. M.; Walpita, D.; Mandrup-poulsen, T.; Wagner, B. K.; Holson, E. B. An Isochemogenic Set of Inhibitors To De Fi Ne the Therapeutic Potential of Histone Deacetylases in β - Cell Protection. **2016**.
- (57) Witter, D. J.; Harrington, P.; Wilson, K. J.; Chenard, M.; Fleming, J. C.; Haines, B.; Kral, A. M.; Secrist, J. P.; Miller, T. A. Optimization of Biaryl Selective HDAC1&2 Inhibitors (SHI-1:2). *Bioorganic Med. Chem. Lett.* **2008**, 18 (2), 726–731.
- (58) Wilson, K. J.; Witter, D. J.; Grimm, J. B.; Siliphaivanh, P.; Otte, K. M.; Kral, A. M.; Fleming, J. C.; Harsch, A.; Hamill, J. E.; Cruz, J. C.; Chenard, M.; Szewczak, A. A.; Middleton, R. E.; Hughes, B. L.; Dahlberg, W. K.; Secrist, J. P.; Miller, T. A. Phenylglycine and Phenylalanine Derivatives as Potent and Selective HDAC1 Inhibitors (SHI-1). *Bioorganic Med. Chem. Lett.* **2008**, 18 (6), 1859–1863.
- (59) Methot, J. L.; Hamblett, C. L.; Mampreian, D. M.; Jung, J.; Harsch, A.; Szewczak, A. A.; Dahlberg, W. K.; Middleton, R. E.; Hughes, B.; Fleming, J. C.; Wang, H.; Kral, A.

- M.; Ozerova, N.; Cruz, J. C.; Haines, B.; Chenard, M.; Kenific, C. M.; Secrist, J. P.; Miller, T. A. SAR Profiles of Spirocyclic Nicotinamide Derived Selective HDAC1/HDAC2 Inhibitors (SHI-1:2). *Bioorganic Med. Chem. Lett.* **2008**, *18* (23), 6104–6109.
- (60) Heidebrecht, R. W.; Chenard, M.; Close, J.; Dahlberg, W. K.; Fleming, J.; Grimm, J. B.; Hamill, J. E.; Harsch, A.; Haines, B. B.; Hughes, B.; Kral, A. M.; Middleton, R. E.; Mushti, C.; Ozerova, N.; Szewczak, A. A.; Wang, H.; Wilson, K.; Witter, D. J.; Secrist, J. P.; Miller, T. A. Exploring the Pharmacokinetic Properties of Phosphorus-Containing Selective HDAC 1 and 2 Inhibitors (SHI-1:2). *Bioorganic Med. Chem. Lett.* **2009**, *19* (7), 2053–2058.
- (61) Bressi, J. C.; Jennings, A. J.; Skene, R.; Wu, Y.; Melkus, R.; Jong, R. De; O’Connell, S.; Grimshaw, C. E.; Navre, M.; Gangloff, A. R. Exploration of the HDAC2 Foot Pocket: Synthesis and SAR of Substituted N-(2-Aminophenyl)benzamides. *Bioorganic Med. Chem. Lett.* **2010**, *20* (10), 3142–3145.
- (62) Wagner, F. F.; Weïwer, M.; Steinbacher, S.; Schomburg, A.; Reinemer, P.; Gale, J. P.; Campbell, A. J.; Fisher, S. L.; Zhao, W.-N.; Reis, S. A.; Hennig, K. M.; Thomas, M.; Müller, P.; Jefson, M. R.; Fass, D. M.; Haggarty, S. J.; Zhang, Y.-L.; Holson, E. B. Kinetic and Structural Insights into the Binding of Histone Deacetylase 1 and 2 (HDAC1, 2) Inhibitors. *Bioorg. Med. Chem.* **2016**, *24* (18), 4008–4015.
- (63) Tabackman, A. A.; Frankson, R.; Marsan, E. S.; Perry, K.; Cole, K. E. Structure of “linkerless” Hydroxamic Acid Inhibitor-HDAC8 Complex Confirms the Formation of an Isoform-Specific Subpocket. *J. Struct. Biol.* **2016**, *195* (3), 373–378.
- (64) Claudio, E. D. G. & Brancolini. Regulation of Class IIa HDAC Activities: It Is Not Only Matter of Subcellular Localization. *Epigenomics* **2016**, *8*, 251–269.
- (65) Yang, X.; Gre, S. Class II Histone Deacetylases : From Sequence to Function , Regulation , and Clinical Implication MINIREVIEW Class II Histone Deacetylases : From Sequence to Function , Regulation , and Clinical Implication. *Mol. Cell. Biol.* **2005**, *25* (8), 2873–2884.
- (66) Lahm, A.; Paolini, C.; Pallaoro, M.; Nardi, M. C.; Jones, P.; Neddermann, P.; Sambucini, S.; Bottomley, M. J.; Lo Surdo, P.; Carfi, A.; Koch, U.; De Francesco, R.; Steinkühler, C.; Gallinari, P. Unraveling the Hidden Catalytic Activity of Vertebrate Class IIa Histone Deacetylases. *Proc. Natl. Acad. Sci.* **2007**, *104* (44), 17335–17340.
- (67) Bottomley, M. J.; Lo Surdo, P. Lo; Di Giovine, P. Di; Cirillo, A.; Scarpelli, R.; Ferrigno, F.; Jones, P.; Neddermann, P.; De Francesco, R.; Steinkühler, C.; Gallinari, P.; Carfi, A. Structural and Functional Analysis of the Human HDAC4 Catalytic Domain Reveals a Regulatory Structural Zinc-Binding Domain. *J. Biol. Chem.* **2008**, *283* (39), 26694–26704.
- (68) Luckhurst, C. a; Aziz, O.; Matthews, K. L.; Yates, D.; Beconi, M.; Mcallister, G.; Breccia, P.; Stott, A. J.; Penrose, S. D.; Wall, M.; Lamers, M.; Leonard, P.; Richardson, C. M.; Jarvis, R.; Stones, L.; Hughes, S.; Wishart, G.; Haughan, A. F.; Mead, T.; Mcneil, H.; Vann, J.; Mangette, J.; Maillard, M.; Beaumont, V.; Munoz-sanjuan, I.; Dominguez, C. Design, Synthesis, and Biological Evaluation of Potent and Selective Class IIa Histone Deacetylase (HDAC) Inhibitors as a Potential Therapy for Huntington’s Disease. *J. Med. Chem.* **2013**, *56*, 9934–9954.
- (69) Luckhurst, C. A.; Breccia, P.; Stott, A. J.; Aziz, O.; Birch, H. L.; Bürli, R. W.; Hughes, S. J.; Jarvis, R. E.; Lamers, M.; Leonard, P. M.; Matthews, K. L.; McAllister, G.; Pollack, S.; Saville-Stones, E.; Wishart, G.; Yates, D.; Dominguez, C. Potent, Selective, and CNS-Penetrant Tetrasubstituted Cyclopropane Class IIa Histone Deacetylase (HDAC)

- Inhibitors. *ACS Med. Chem. Lett.* **2016**, 7 (1), 34–39.
- (70) Lobera, M.; Madauss, K. P.; Pohlhaus, D. T.; Wright, Q. G.; Trocha, M.; Schmidt, D. R.; Baloglu, E.; Trump, R. P.; Head, M. S.; Hofmann, G. A.; Murray-Thompson, M.; Schwartz, B.; Chakravorty, S.; Wu, Z.; Mander, P. K.; Kruidenier, L.; Reid, R. A.; Burkhart, W.; Turunen, B. J.; Rong, J. X.; Wagner, C.; Moyer, M. B.; Wells, C.; Hong, X.; Moore, J. T.; Williams, J. D.; Soler, D.; Ghosh, S.; Nolan, M. A. Selective Class IIa Histone Deacetylase Inhibition via a Nonchelating Zinc-Binding Group. *Nat. Chem. Biol.* **2013**, 9 (5), 319–325.
- (71) Sakamoto, K. M.; Aldana-Masangkay, G. I. The Role of HDAC6 in Cancer. *J. Biomed. Biotechnol.* **2011**, 2011.
- (72) Yang, P. HDAC6: Physiological Function and Its Selective Inhibitors for Cancer Treatment. *Drug Discov. Ther.* **2013**, 7 (6), 233–242.
- (73) Kalin, J. H.; Bergman, J. A. Development and Therapeutic Implications of Selective Histone Deacetylase 6 Inhibitors. *J. Med. Chem.* **2013**, 56 (16), 6297–6313.
- (74) Batchu, S. N.; Brijmohan, A. S.; Advani, A. The Therapeutic Hope for HDAC6 Inhibitors in Malignancy and Chronic Disease. *Clin. Sci.* **2016**, 130 (12), 987–1003.
- (75) Li, Y.; Shin, D.; Kwon, S. H. Histone Deacetylase 6 Plays a Role as a Distinct Regulator of Diverse Cellular Processes. *FEBS J.* **2013**, 280 (3), 775–793.
- (76) Seidel, C.; Schnekenburger, M.; Dicato, M.; Diederich, M. Histone Deacetylase 6 in Health and Disease. *Epigenomics* **2015**, 7 (1), 103–118.
- (77) Hai, Y.; Christianson, D. W. Histone Deacetylase 6 Structure and Molecular Basis of Catalysis and Inhibition. *Nat. Chem. Biol.* **2016**, 12 (9), 741–747.
- (78) Miyake, Y.; Keusch, J. J.; Wang, L.; Saito, M.; Hess, D.; Wang, X.; Melancon, B. J.; Helquist, P.; Gut, H.; Matthias, P. Structural Insights into HDAC6 Tubulin Deacetylation and Its Selective Inhibition. *Nat. Chem. Biol.* **2016**, 12 (9), 748–754.
- (79) Porter, N. J.; Mahendran, A.; Breslow, R.; Christianson, D. W. Unusual Zinc-Binding Mode of HDAC6-Selective Hydroxamate Inhibitors. *Proc. Natl. Acad. Sci.* **2017**, 1215 (37), 201718823.
- (80) Kawai, K.; Nagata, N. Metal-Ligand Interactions: An Analysis of Zinc Binding Groups Using the Protein Data Bank. *Eur. J. Med. Chem.* **2012**, 51, 271–276.
- (81) Guardiola, A. R.; Yao, T.-P. Molecular Cloning and Characterization of a Novel Histone Deacetylase HDAC10. *J. Biol. Chem.* **2002**, 277 (5), 3350–3356.
- (82) Hai, Y.; Shinsky, S. A.; Porter, N. J.; Christianson, D. W. Histone Deacetylase 10 Structure and Molecular Function as a Polyamine Deacetylase. *Nat. Commun.* **2017**, 8 (May), 1–9.
- (83) Oehme, I.; Linke, J.-P.; Bock, B. C.; Milde, T.; Lodrini, M.; Hartenstein, B.; Wiegand, I.; Eckert, C.; Roth, W.; Kool, M.; Kaden, S.; Grone, H.-J.; Schulte, J. H.; Lindner, S.; Hamacher-Brady, A.; Brady, N. R.; Deubzer, H. E.; Witt, O. Histone Deacetylase 10 Promotes Autophagy-Mediated Cell Survival. *Proc. Natl. Acad. Sci.* **2013**, 110 (28), E2592–E2601.
- (84) Shinsky, S. A.; Christianson, D. W. Polyamine Deacetylase Structure and Catalysis: Prokaryotic Acetylpolyamine Amidohydrolase and Eukaryotic HDAC10. *Biochemistry* **2018**, acs.biochem.8b00079.
- (85) Gao, L.; Cueto, M. A.; Asselbergs, F.; Atadja, P. Cloning and Functional Characterization of HDAC11, a Novel Member of the Human Histone Deacetylase Family. *J. Biol. Chem.* **2002**, 277 (28), 25748–25755.

- (86) Huang, J.; Wang, L.; Dahiya, S.; Beier, U. H.; Han, R.; Samanta, A.; Bergman, J.; Sotomayor, E. M.; Seto, E.; Kozikowski, A. P.; Hancock, W. W. Histone/protein Deacetylase 11 Targeting Promotes Foxp3⁺ Treg Function. *Sci. Rep.* **2017**, *7* (1), 1–11.
- (87) Kutil, Z.; Novakova, Z.; Meleshin, M.; Mikesova, J.; Schutkowski, M.; Barinka, C. HDAC11 Is a Fatty-Acid Deacylase. **2017**.
- (88) Mann, B. S.; Johnson, J. R.; Cohen, M. H.; Justice, R.; Pazdur, R. FDA Approval Summary: Vorinostat for Treatment of Advanced Primary Cutaneous T-Cell Lymphoma. *Oncologist* **2007**, *12* (10), 1247–1252.
- (89) Iyer, S. P.; Foss, F. F. Romidepsin for the Treatment of Peripheral T-Cell Lymphoma. *Oncologist* **2015**, *20* (9), 1084–1091.
- (90) Zhang, Y.; Xu, W.; Liu, H.; Li, J. Therapeutic Options in Peripheral T Cell Lymphoma. *J. Hematol. Oncol.* **2016**, *9* (1), 37.
- (91) Lee, H.-Z.; Kwitkowski, V. E.; Del Valle, P. L.; Ricci, M. S.; Saber, H.; Habtemariam, B. A.; Bullock, J.; Bloomquist, E.; Li Shen, Y.; Chen, X.-H.; Brown, J.; Mehrotra, N.; Dorff, S.; Charlab, R.; Kane, R. C.; Kaminskas, E.; Justice, R.; Farrell, A. T.; Pazdur, R. FDA Approval: Belinostat for the Treatment of Patients with Relapsed or Refractory Peripheral T-Cell Lymphoma. *Clin. Cancer Res.* **2015**, *21* (12), 2666–2670.
- (92) Lu, X.; Ning, Z.; Li, Z.; Cao, H.; Wang, X. Development of Chidamide for Peripheral T-Cell Lymphoma, the First Orphan Drug Approved in China. *Intractable Rare Dis. Res.* **2016**, *5* (3), 185–191.
- (93) Moreau, P.; Attal, M.; Facon, T. Frontline Therapy of Multiple Myeloma. **2015**, *125* (20), 3076–3085.
- (94) Raedler, B. L. A.; Writer, M. Farydak (Panobinostat): First HDAC Inhibitor Approved for Patients with Relapsed Multiple Myeloma. *Am. Heal. Drug Benefits* **2016**, *9* (March), 84–89.
- (95) Garnock-Jones, K. P. Cobimetinib: First Global Approval. *Drugs* **2015**, *75* (15), 1823–1830.
- (96) Eckschlager, T.; Plch, J.; Stiborova, M.; Hrabeta, J. Histone Deacetylase Inhibitors as Anticancer Drugs. *Int. J. Mol. Sci.* **2017**, *18* (7), 1–25.
- (97) de Lera, A. R.; Ganesan, A. Epigenetic Polypharmacology: From Combination Therapy to Multitargeted Drugs. *Clin. Epigenetics* **2016**, *8* (1), 1–21.
- (98) Mazzone, R.; Zwergel, C.; Mai, A.; Valente, S. Epi-Drugs in Combination with Immunotherapy: A New Avenue to Improve Anticancer Efficacy. *Clin. Epigenetics* **2017**, *9* (1), 1–15.
- (99) Ganesan, A. Multitarget Drugs: An Epigenetic Epiphany. *ChemMedChem* **2016**, 1227–1241.
- (100) Deeks, S. G. HIV: Shock and Kill. *Nature* **2012**, *487* (7408), 439–440.
- (101) Cole, J.; Morris, P.; Dickman, M. J.; Dockrell, D. H. The Therapeutic Potential of Epigenetic Manipulation during Infectious Diseases. *Pharmacol. Ther.* **2016**, *167*, 85–99.
- (102) Hailu, G. S.; Robaa, D.; Forgione, M.; Sippl, W.; Rotili, D.; Mai, A. Lysine Deacetylase Inhibitors in Parasites: Past, Present, and Future Perspectives. *J. Med. Chem.* **2017**, *60* (12), 4780–4804.
- (103) Scholte, L. L. S.; Mourão, M. M.; Pais, F. S. M.; Melesina, J.; Robaa, D.; Volpini, A. C.; Sippl, W.; Pierce, R. J.; Oliveira, G.; Nahum, L. A. Evolutionary Relationships among Protein Lysine Deacetylases of Parasites Causing Neglected Diseases. *Infect. Genet. Evol.* **2017**, *53*, 175–188.

- (104) Fraczek, J.; Vanhaecke, T.; Rogiers, V. Toxicological and Metabolic Considerations for Histone Deacetylase Inhibitors. *Expert Opin. Drug Metab. Toxicol.* **2013**, *9* (4), 441–457.
- (105) Shultz, M. D.; Cao, X.; Chen, C. H.; Cho, Y. S.; Davis, N. R.; Eckman, J.; Fan, J.; Fekete, A.; Firestone, B.; Flynn, J.; Green, J.; Growney, J. D.; Holmqvist, M.; Hsu, M.; Jansson, D.; Jiang, L.; Kwon, P.; Liu, G.; Lombardo, F.; Lu, Q.; Majumdar, D.; Meta, C.; Perez, L.; Pu, M.; Ramsey, T.; Remiszewski, S.; Skolnik, S.; Traebert, M.; Urban, L.; Uttamsingh, V.; Wang, P.; Whitebread, S.; Whitehead, L.; Yan-Neale, Y.; Yao, Y. M.; Zhou, L.; Atadja, P. Optimization of the in Vitro Cardiac Safety of Hydroxamate-Based Histone Deacetylase Inhibitors. *J. Med. Chem.* **2011**, *54* (13), 4752–4772.
- (106) Lee, M. S.; Isobe, M. Metabolic Activation of the Potent Mutagen, 2-Naphthohydroxamic Acid, in Salmonella Typhimurium TA98. *Cancer Res.* **1990**, *50* (14), 4300–4307.
- (107) Shen, S.; Kozikowski, A. P. Why Hydroxamates May Not Be the Best Histone Deacetylase Inhibitors - What Some May Have Forgotten or Would Rather Forget? *ChemMedChem* **2016**, *11* (1), 15–21.
- (108) Cohen, S. M. A Bioinorganic Approach to Fragment-Based Drug Discovery Targeting Metalloenzymes. *Acc. Chem. Res.* **2017**, *50* (8), 2007–2016.
- (109) Hermant, P.; Bosc, D.; Piveteau, C.; Gealageas, R.; Lam, B.; Ronco, C.; Roignant, M.; Tolojanahary, H.; Jean, L.; Renard, P. Y.; Lemdani, M.; Bourotte, M.; Herledan, A.; Bedart, C.; Biela, A.; Leroux, F.; Deprez, B.; Deprez-Poulain, R. Controlling Plasma Stability of Hydroxamic Acids: A MedChem Toolbox. *J. Med. Chem.* **2017**, *60* (21), 9067–9089.
- (110) WHO. *World Malaria Report 2017*; 2017.
- (111) Cowman, A. F.; Healer, J.; Marapana, D.; Marsh, K. Malaria: Biology and Disease. *Cell* **2016**, *167* (3), 610–624.
- (112) Wells, T. N. C.; Van Huijsduijnen, R. H.; Van Voorhis, W. C. Malaria Medicines: A Glass Half Full? *Nat. Rev. Drug Discov.* **2015**, *14* (6), 424–442.
- (113) Medicines for Malaria Venture | Developing antimalarials to save lives <https://www.mmv.org/> (accessed Feb 10, 2018).
- (114) Okombo, J.; Chibale, K. Recent Updates in the Discovery and Development of Novel Antimalarial Drug Candidates. *Medchemcomm* **2018**, *9*, 437–453.
- (115) Flannery, E. L.; Chatterjee, A. K.; Winzeler, E. A. Antimalarial Drug Discovery - Approaches and Progress towards New Medicines. *Nat. Rev. Microbiol.* **2013**, *12* (1), 70–70.
- (116) Phillips, M. A.; Burrows, J. N.; Manyando, C.; Van Huijsduijnen, R. H.; Van Voorhis, W. C.; Wells, T. N. C. Malaria. *Nat. Rev. Dis. Prim.* **2017**, *3*.
- (117) Jiménez-díaz, M. B.; Ebert, D.; Salinas, Y.; Pradhan, A.; Lehane, A. M.; Loughlin, K. G. O.; Shackelford, D. M.; Almeida, M. J. De; Carrillo, A. K.; Clark, J. A.; Dennis, A. S. M.; Diep, J.; Deng, X.; Duffy, S.; Endsley, A. N.; Fedewa, G.; Armand, W.; Gómez, M. G.; Holbrook, G.; Kim, C. C.; Liu, J.; Lee, M. C. S.; Matheny, A.; Martínez, M. S.; Miller, G.; Rodríguez-alejandro, A.; Sanz, L.; Sigal, M.; Spillman, N. J.; Stein, P. D.; Wang, Z.; Zhu, F.; Waterson, D.; Knapp, S.; Shelat, A.; Avery, V. M.; Fidock, D. A.; Charman, S. A.; Mirsalis, J. C.; Ma, H.; Ferrer, S.; Kirk, K.; Angulo-barturen, I.; Dennis, E.; Derisi, J. L.; Floyd, D. M.; Guy, R. K.; Jiménez-díaz, M. B.; Ebert, D.; Salinas, Y.; Pradhan, A.; Lehane, A. M. Correction for Jiménez-Díaz et Al., (+)-SJ733, a Clinical Candidate for Malaria That Acts through ATP4 to Induce Rapid Host-Mediated Clearance of *Plasmodium* : Fig. 5. *Proc. Natl. Acad. Sci.* **2015**, *112* (42), E5764–E5764.

- (118) Brücher, K.; Illarionov, B.; Held, J.; Tschan, S.; Kunfermann, A.; Pein, M. K.; Bacher, A.; Gräwert, T.; Maes, L.; Mordmüller, B.; Fischer, M.; Kurz, T. α -Substituted β -Oxa Isosteres of Fosmidomycin: Synthesis and Biological Evaluation. *J. Med. Chem.* **2012**, *55* (14), 6566–6575.
- (119) Duffy, S.; Avery, V. M. Identification of Inhibitors of Plasmodium Falciparum Gametocyte Development. **2013**, 1–15.
- (120) Plouffe, D. M.; Wree, M.; Du, A. Y.; Meister, S.; Li, F.; Patra, K.; Lubar, A.; Okitsu, S. L.; Flannery, E. L.; Kato, N.; Tanaseichuk, O.; Comer, E.; Zhou, B.; Kuhen, K.; Zhou, Y.; Leroy, D.; Schreiber, S. L.; Scherer, C. A.; Vinetz, J.; Winzeler, E. A. High-Throughput Assay and Discovery of Small Molecules That Interrupt Malaria Transmission. *Cell Host Microbe* **2016**, *19* (1), 114–126.
- (121) Phillips, M. A.; Lotharius, J.; Marsh, K.; White, J.; Dayan, A.; White, K. L.; Njoroge, J. W.; El Mazouni, F.; Lao, Y.; Kokkonda, S.; Tomchick, D. R.; Deng, X.; Laird, T.; Bhatia, S. N.; March, S.; Ng, C. L.; Fidock, D. A.; Wittlin, S.; Lafuente-Monasterio, M.; Benito, F. J. G.; Alonso, L. M. S.; Martinez, M. S.; Jimenez-Diaz, M. B.; Bazaga, S. F.; Angulo-Barturen, I.; Haselden, J. N.; Louttit, J.; Cui, Y.; Sridhar, A.; Zeeman, A. M.; Kocken, C.; Sauerwein, R.; Dechering, K.; Avery, V. M.; Duffy, S.; Delves, M.; Sinden, R.; Ruecker, A.; Wickham, K. S.; Rochford, R.; Gahagen, J.; Iyer, L.; Riccio, E.; Mirsalis, J.; Bathhurst, I.; Rueckle, T.; Ding, X.; Campo, B.; Leroy, D.; Rogers, M. J.; Rathod, P. K.; Burrows, J. N.; Charman, S. A. A Long-Duration Dihydroorotate Dehydrogenase Inhibitor (DSM265) for Prevention and Treatment of Malaria. *Sci. Transl. Med.* **2015**, *7* (296).
- (122) Kuhen, K. L.; Chatterjee, A. K.; Rottmann, M.; Gagaring, K.; Borboa, R.; Buenviaje, J.; Chen, Z.; Francek, C.; Wu, T.; Nagle, A.; Barnes, S. W.; Plouffe, D.; Lee, M. C. S.; Fidock, D. A.; Graumans, W.; Van De Vegte-Bolmer, M.; Van Gemert, G. J.; Wirjanata, G.; Sebayang, B.; Marfurt, J.; Russell, B.; Suwanarusk, R.; Price, R. N.; Nosten, F.; Tungtaeng, A.; Gettayacamin, M.; Sattabongkot, J.; Taylor, J.; Walker, J. R.; Tully, D.; Patra, K. P.; Flannery, E. L.; Vinetz, J. M.; Renia, L.; Sauerwein, R. W.; Winzeler, E. A.; Glynn, R. J.; Diagana, T. T. KAF156 Is an Antimalarial Clinical Candidate with Potential for Use in Prophylaxis, Treatment, and Prevention of Disease Transmission. *Antimicrob. Agents Chemother.* **2014**, *58* (9), 5060–5067.
- (123) Paquet, T.; Le Manach, C.; Cabrera, D. G.; Younis, Y.; Henrich, P. P.; Abraham, T. S.; Lee, M. C. S.; Basak, R.; Ghidelli-Disse, S.; Lafuente-Monasterio, M. J.; Bantscheff, M.; Ruecker, A.; Blagborough, A. M.; Zakutansky, S. E.; Zeeman, A. M.; White, K. L.; Shackelford, D. M.; Mannila, J.; Morizzi, J.; Scheurer, C.; Angulo-Barturen, I.; Santosmartínez, M.; Ferrer, S.; Sanz, L. M.; Gamo, F. J.; Reader, J.; Botha, M.; Dechering, K. J.; Sauerwein, R. W.; Tungtaeng, A.; Vanachayangkul, P.; Lim, C. S.; Burrows, J.; Witty, M. J.; Marsh, K. C.; Bodenreider, C.; Rochford, R.; Solapure, S. M.; Jiménez-Díaz, M. B.; Wittlin, S.; Charman, S. A.; Donini, C.; Campo, B.; Birkholtz, L. M.; Khanson, K.; Drewes, G.; Kocken, C. M.; Delves, M. J.; Leroy, D.; Fidock, D. A.; Waterson, D.; Street, L. J.; Chibale, K. Antimalarial Efficacy of MMV390048, an Inhibitor of Plasmodium Phosphatidylinositol 4-Kinase. *Sci. Transl. Med.* **2017**, *9* (387).
- (124) Delves, M.; Plouffe, D.; Scheurer, C.; Meister, S.; Wittlin, S.; Winzeler, E. A.; Sinden, R. E.; Leroy, D. The Activities of Current Antimalarial Drugs on the Life Cycle Stages of Plasmodium: A Comparative Study with Human and Rodent Parasites. *PLoS Med.* **2012**, *9* (2).
- (125) Spillman, N. J.; Kirk, K. The Malaria Parasite Cation ATPase PfATP4 and Its Role in the Mechanism of Action of a New Arsenal of Antimalarial Drugs. *Int. J. Parasitol. Drugs Drug Resist.* **2015**, *5* (3), 149–162.

- (126) Magistrado, P. A.; Corey, V. C.; Lukens, A. K.; Lamonte, G.; Sasaki, E.; Meister, S.; Wree, M.; Winzeler, E.; Wirth, D. F. Plasmodium Falciparum Cyclic Amine Resistance Locus (PfCARL), a Resistance Mechanism for Two Distinct Compound Classes. *ACS Infect. Dis.* **2016**, *2* (11), 816–826.
- (127) Okombo, J.; Chibale, K. Insights into Integrated Lead Generation and Target Identification in Malaria and Tuberculosis Drug Discovery. *Acc. Chem. Res.* **2017**, *50* (7), 1606–1616.
- (128) Masini, T.; Kroezen, B. S.; Hirsch, A. K. H. Druggability of the Enzymes of the Non-Mevalonate-Pathway. *Drug Discov. Today* **2013**, *18* (23–24), 1256–1262.
- (129) Chua, M. J.; Arnold, M. S. J.; Xu, W.; Lancelot, J.; Lamotte, S.; Späth, G. F.; Prina, E.; Pierce, R. J.; Fairlie, D. P.; Skinner-Adams, T. S.; Andrews, K. T. Effect of Clinically Approved HDAC Inhibitors on Plasmodium, Leishmania and Schistosoma Parasite Growth. *Int. J. Parasitol. Drugs Drug Resist.* **2017**, *7* (1), 42–50.
- (130) Andrews, K.; Tran, T.; Wheatley, N.; Fairlie, D. Targeting Histone Deacetylase Inhibitors for Anti-Malarial Therapy. *Curr. Top. Med. Chem.* **2009**, *9* (3), 292–308.
- (131) Melesina, J.; Robaa, D.; Pierce, R. J.; Romier, C.; Sippl, W. Homology Modeling of Parasite Histone Deacetylases to Guide the Structure-Based Design of Selective Inhibitors. *J. Mol. Graph. Model.* **2015**, *62*, 342–361.
- (132) Engel, J. A.; Jones, A. J.; Avery, V. M.; Sumanadasa, S. D. M.; Ng, S. S.; Fairlie, D. P.; Adams, T. S.; Andrews, K. T. Profiling the Anti-Protozoal Activity of Anti-Cancer HDAC Inhibitors against Plasmodium and Trypanosoma Parasites. *Int. J. Parasitol. Drugs Drug Resist.* **2015**, *5* (3), 117–126.
- (133) Vreese, R. De; Kock, C. de; Smith, P. J.; Chibale, K.; D’hooghe, M. Exploration of Thiaheterocyclic H HDAC6 Inhibitors as Potential Antiplasmodial Agents. *Future Med. Chem.* **2017**, *9* (4), 357–364.
- (134) Hansen, F. K.; Sumanadasa, S. D. M.; Stenzel, K.; Duffy, S.; Meister, S.; Marek, L.; Schmetter, R.; Kuna, K.; Hamacher, A.; Mordmüller, B.; Kassack, M. U.; Winzeler, E. A.; Avery, V. M.; Andrews, K. T.; Kurz, T. Discovery of HDAC Inhibitors with Potent Activity against Multiple Malaria Parasite Life Cycle Stages Dedicated to Prof. Dr. Alan R. Katritzky, in Memoriam. *Eur. J. Med. Chem.* **2014**, *82*, 204–213.
- (135) Sun, W.; Tanaka, T. Q.; Magle, C. T.; Huang, W.; Southall, N.; Huang, R.; Dehdashti, S. J.; McKew, J. C.; Williamson, K. C.; Zheng, W. Chemical Signatures and New Drug Targets for Gametocytocidal Drug Development. *Sci. Rep.* **2015**, *4*, 1–11.
- (136) Hanahan, D.; Weinberg, R. A. The Hallmarks of Cancer. *Cell* **2000**, *100* (1), 57–70.
- (137) Hanahan, D.; Weinberg, R. A. Hallmarks of Cancer: The next Generation. *Cell* **2011**, *144* (5), 646–674.
- (138) Fernald, K.; Kurokawa, M. Evading Apoptosis in Cancer. *Trends Cell Biol.* **2013**, *23* (12), 620–633.
- (139) Dawson, M. A. The Cancer Epigenome: Concepts, Challenges, and Therapeutic Opportunities. *Science* (80-.). **2017**, No. 355, 1147–1152.
- (140) Pfister, S. X.; Ashworth, A. Marked for Death: Targeting Epigenetic Changes in Cancer. *Nat. Rev. Drug Discov.* **2017**, *16* (4), 241–263.
- (141) Ceccacci, E.; Minucci, S. Inhibition of Histone Deacetylases in Cancer Therapy: Lessons from Leukaemia. *Br. J. Cancer* **2016**, *114* (6), 605–611.
- (142) Newbold, A.; Falkenberg, K. J.; Prince, H. M.; Johnstone, R. W. How Do Tumor Cells Respond to HDAC Inhibition? *FEBS J.* **2016**, *283* (22), 4032–4046.

- (143) Lorente, J.; Velandia, C.; Leal, J. A.; Garcia-Mayea, Y.; Lyakhovich, A.; Kondoh, H.; Lleonart, M. E. The Interplay between Autophagy and Tumorigenesis: Exploiting Autophagy as a Means of Anticancer Therapy. *Biol. Rev.* **2017**.
- (144) Rao, R. S.; Patil, S.; Ghosh, S.; Kumari, K. Current Aspects and Future Strategies in Oral Cancer Research: A Review. *J. Med. Radiol. Pathol. Surg.* **2015**, *1* (January), 8–13.
- (145) Tasoulas, J.; Giaginis, C.; Patsouris, E.; Manolis, E.; Theocharis, S. Histone Deacetylase Inhibitors in Oral Squamous Cell Carcinoma Treatment. *Expert Opin. Investig. Drugs* **2015**, *24* (1), 69–78.
- (146) Goncalves, P. H.; Heilbrun, L. K.; Barrett, M. T.; Kummar, S.; Hansen, A. R.; Siu, L. L.; Piekarz, R. L.; Sukari, A. W.; Chao, J.; Jo Pilat, M.; Smith, D. W.; Casetta, L.; Boerner, S. A.; Chen, A.; Lenkiewicz, E.; Malasi, S.; LoRusso, P. M. A Phase 2 Study of Vorinostat in Locally Advanced, Recurrent, or Metastatic Adenoid Cystic Carcinoma. *Oncotarget* **2017**, *8* (20), 32918–32929.
- (147) Christian, J.; Thomas, H. Ovarian Cancer Chemotherapy. *Cancer Treatment Reviews*. 2001, pp 99–109.
- (148) Raja, F. A.; Chopra, N.; Ledermann, J. A. Optimal First-Line Treatment in Ovarian Cancer. *Ann. Oncol.* **2012**, *23* (SUPPL. 10).
- (149) Pchejetski, D.; Alfraidi, A.; Sacco, K.; Alshaker, H.; Muhammad, A.; Monzon, L. Histone Deacetylases as New Therapy Targets for Platinum-Resistant Epithelial Ovarian Cancer. *J. Cancer Res. Clin. Oncol.* **2016**, *142* (8), 1659–1671.
- (150) Yano, M.; Yasuda, M.; Sakaki, M.; Nagata, K.; Fujino, T.; Arai, E.; Hasebe, T.; Miyazawa, M.; Miyazawa, M.; Ogane, N.; Hasegawa, K.; Narahara, H. Association of Histone Deacetylase Expression with Histology and Prognosis of Ovarian Cancer. *Oncol. Lett.* **2018**, *15* (3), 3524–3531.
- (151) Smith, H. J.; Straughn, J. M.; Buchsbaum, D. J.; Arend, R. C. Epigenetic Therapy for the Treatment of Epithelial Ovarian Cancer: A Clinical Review. *Gynecol. Oncol. Reports* **2017**, *20*, 81–86.
- (152) Tomao, F.; Marchetti, C.; Romito, A.; Di Pinto, A.; Di Donato, V.; Capri, O.; Palaia, I.; Monti, M.; Muzii, L.; Benedetti Panici, P. Overcoming Platinum Resistance in Ovarian Cancer Treatment: From Clinical Practice to Emerging Chemical Therapies. *Expert Opin. Pharmacother.* **2017**, *18* (14), 1443–1455.
- (153) Matsuo, K.; Lin, Y. G.; Roman, L. D.; Sood, A. K. Overcoming Platinum Resistance in Ovarian Carcinoma. *Expert Opin. Investig. Drugs* **2010**, *19* (11), 1339–1354.
- (154) Alves Avelar, L. A.; Held, J.; Engel, J. A.; Sureechatchaiyan, P.; Hansen, F. K.; Hamacher, A.; Kassack, M. U.; Mordmüller, B.; Andrews, K. T.; Kurz, T. Design and Synthesis of Novel Anti-Plasmodial Histone Deacetylase Inhibitors Containing an Alkoxyamide Connecting Unit. *Arch. Pharm. (Weinheim)*. **2017**, *350* (3–4), 1–11.
- (155) Ong, L. C.; Song, I. C.; Jin, Y.; Kee, I. H. C.; Siew, E.; Yu, S.; Thng, C. H.; Huynh, H.; Chow, P. K. H. Effective Inhibition of Xenografts of Hepatocellular Carcinoma (hepg2) by Rapamycin and Bevacizumab in an Intrahepatic Model. *Mol. Imaging Biol.* **2009**, *11* (5), 334–342.
- (156) Llovet, J. M.; Villanueva, A.; Lachenmayer, A.; Finn, R. S. Advances in Targeted Therapies for Hepatocellular Carcinoma in the Genomic Era. *Nat. Rev. Clin. Oncol.* **2015**, *12* (7), 408–424.
- (157) Marek, L.; Hamacher, A.; Hansen, F. K.; Kuna, K.; Gohlke, H.; Kassack, M. U.; Kurz, T. Histone Deacetylase (HDAC) Inhibitors with a Novel Connecting Unit Linker Region Reveal a Selectivity Profile for HDAC4 and HDAC5 with Improved Activity against

- Chemoresistant Cancer Cells. *J. Med. Chem.* **2013**, *56* (2), 427–436.
- (158) Stenzel, K.; Hamacher, A.; Hansen, F. K.; Gertzen, C. G. W.; Senger, J.; Marquardt, V.; Marek, L.; Marek, M.; Romier, C.; Remke, M.; Jung, M.; Gohlke, H.; Kassack, M. U.; Kurz, T. Alkoxyurea-Based Histone Deacetylase Inhibitors Increase Cisplatin Potency in Chemoresistant Cancer Cell Lines. *J. Med. Chem.* **2017**, *60* (13), 5334–5348.
- (159) Mueller, H.; Matthias U., K.; Wiese, M. Comparison of the Usefulness of the MTT, ATP, and Calcein Assays to Predict the Potency of Cytotoxic Agents in Various Human Cancer Cell Lines. *J. Biomol. Screen.* **2004**, *9*, 506–515.
- (160) Olsen, J. V.; Ong, S.-E.; Mann, M. Trypsin Cleaves Exclusively C-Terminal to Arginine and Lysine Residues. *Mol. Cell. Proteomics* **2004**, *3* (6), 608–614.
- (161) Shah, P.; Dhameliya, T. M.; Bansal, R.; Nautiyal, M.; Kommi, D. N.; Jadhavar, P. S.; Sridevi, J. P.; Yogeewari, P.; Sriram, D.; Chakraborti, A. K. N-Arylalkylbenzo[d]thiazole-2-Carboxamides as Anti-Mycobacterial Agents: Design, New Methods of Synthesis and Biological Evaluation. *Med. Chem. Commun.* **2014**, *5* (10), 1489–1495.
- (162) Schneider, P.; Schneider, G. Privileged Structures Revisited. *Angew. Chemie - Int. Ed.* **2017**, *56* (27), 7971–7974.
- (163) Lipinski, C. A. Lead- and Drug-like Compounds: The Rule-of-Five Revolution. *Drug Discov. Today Technol.* **2004**, *1* (4), 337–341.
- (164) Atadja, P.; Perez, L. Discovery and Development of Farydak (NVP-LBH589, Panobinostat) as an Anticancer Drug. In *Successful Drug Discovery*; Wiley-VCH Verlag GmbH & Co. KGaA, 2016; pp 59–88.
- (165) Remiszewski, S. W.; Sambucetti, L. C.; Bair, K. W.; Bontempo, J.; Cesarz, D.; Chandramouli, N.; Chen, R.; Cheung, M.; Cornell-Kennon, S.; Dean, K.; Diamantidis, G.; France, D.; Green, M. A.; Howell, K. L.; Kashi, R.; Kwon, P.; Lassota, P.; Martin, M. S.; Mou, Y.; Perez, L. B.; Sharma, S.; Smith, T.; Sorensen, E.; Taplin, F.; Trogani, N.; Versace, R.; Walker, H.; Weltchek-Engler, S.; Wood, A.; Wu, A.; Atadja, P. N-Hydroxy-3-Phenyl-2-Propenamides as Novel Inhibitors of Human Histone Deacetylase with in Vivo Antitumor Activity: Discovery of (2E)-N-Hydroxy-3-[4-[[[(2-hydroxyethyl)[2-(1H-Indol-3-Yl)ethyl] Amino]methyl]-Phenyl]-2-Propenamide (NVP-LAQ824). In *Journal of Medicinal Chemistry*; 2003; Vol. 46, pp 4609–4624.
- (166) Dai, Y.; Guo, Y.; Guo, J.; Pease, L. J.; Li, J.; Marcotte, P. A.; Glaser, K. B.; Tapang, P.; Albert, D. H.; Richardson, P. L.; Davidsen, S. K.; Michaelides, M. R. Indole Amide Hydroxamic Acids as Potent Inhibitors of Histone Deacetylases. *Bioorganic Med. Chem. Lett.* **2003**, *13* (11), 1897–1901.
- (167) De Robles, P.; Fiest, K. M.; Frolkis, A. D.; Pringsheim, T.; Atta, C.; St. Germaine-Smith, C.; Day, L.; Lam, D.; Jette, N. The Worldwide Incidence and Prevalence of Primary Brain Tumors: A Systematic Review and Meta-Analysis. *Neuro. Oncol.* **2015**, *17* (6), 776–783.
- (168) Reni, M.; Mazza, E.; Zanon, S.; Gatta, G.; Vecht, C. J. Central Nervous System Gliomas. *Crit. Rev. Oncol. Hematol.* **2017**, *113*, 213–234.
- (169) Paolillo, M.; Boselli, C.; Schinelli, S. Glioblastoma under Siege: An Overview of Current Therapeutic Strategies. *Brain Sci.* **2018**, *8* (1).
- (170) Lee, D. H.; Ryu, H.-W.; Won, H.-R.; Kwon, S. H. Advances in Epigenetic Glioblastoma Therapy. *Oncotarget* **2017**, *8* (11), 18577–18589.
- (171) Lee, P.; Murphy, B.; Miller, R.; Menon, V.; Banik, N.; Giglio, P.; Lindhorst, S.; Varma, A.; Vandergrift, W.; Patel, S.; Das, A. Mechanisms and Clinical Significance of Histone

- Deacetylase Inhibitors:epigenetic Glioblastoma Therapy. *Anticancer Res* **2015**, *35* (2), 615–625.
- (172) Patil, V.; Pal, J.; Somasundaram, K. Elucidating the Cancer-Specific Genetic Alteration Spectrum of Glioblastoma Derived Cell Lines from Whole Exome and RNA Sequencing. *Oncotarget* **2015**, *6* (41).
- (173) Sui, X.; Kong, N.; Wang, Z.; Pan, H. Epigenetic Regulation of the Human Telomerase Reverse Transcriptase Gene: A Potential Therapeutic Target for the Treatment of Leukemia (Review). *Oncol. Lett.* **2013**, *6* (2), 317–322.
- (174) Hauser, A.-T.; Jung, M. M.; Jung, M. M.; Mira, J. Assays for Histone Deacetylases. *Curr. Top. Med. Chem.* **2009**, *9* (3), 227–234.
- (175) Heltweg, B.; Dequiedt, F.; Verdin, E.; Jung, M. Nonisotopic Substrate for Assaying Both Human Zinc and NAD⁺-Dependent Histone Deacetylases. *Anal. Biochem.* **2003**, *319* (1), 42–48.
- (176) Toro, T. B.; Watt, T. J. KDAC8 Substrate Specificity Quantified by a Biologically Relevant, Label-Free Deacetylation Assay. *Protein Sci.* **2015**, *24* (12), 2020–2032.
- (177) Heltweg, B.; Trapp, J.; Jung, M. In Vitro Assays for the Determination of Histone Deacetylase Activity. *Methods* **2005**, *36* (4), 332–337.
- (178) Moitessier, N.; Pottel, J.; Therrien, E.; Englebienne, P.; Liu, Z.; Tomberg, A.; Corbeil, C. R. Medicinal Chemistry Projects Requiring Imaginative Structure-Based Drug Design Methods. *Acc. Chem. Res.* **2016**, *49* (9), 1646–1657.
- (179) Morris, G. M.; Goodsell, D. S.; Halliday, R. S.; Huey, R.; Hart, W. E.; Belew, R. K.; Olson, A. J. Automated Docking Using a Lamarckian Genetic Algorithm and an Empirical Binding Free Energy Function. *J. Comput. Chem.* **1998**, *19* (14), 1639–1662.
- (180) Gohlke, H.; Klebe, G. Statistical Potentials and Scoring Functions Applied to Protein-Ligand Binding. *Curr. Opin. Struct. Biol.* **2001**, *11* (2), 231–235.
- (181) Ballante, F.; Marshall, G. R. An Automated Strategy for Binding-Pose Selection and Docking Assessment in Structure-Based Drug Design. *J. Chem. Inf. Model.* **2016**, *56* (1), 54–72.
- (182) Morris G Huey R Lindstrom W Sanner M Belew R et. al. AutoDock4 and AutoDockTools4: Automated Docking with Selective Receptor Flexibility. *J. Comput. Chem.* **2009**, *28* (1), 2785–2791.
- (183) Kalyaanamoorthy, S.; Chen, Y. P. P. Quantum Polarized Ligand Docking Investigation to Understand the Significance of Protonation States in Histone Deacetylase Inhibitors. *J. Mol. Graph. Model.* **2013**, *44*, 44–53.
- (184) Olson, D. E.; Udeshi, N. D.; Wolfson, N. A.; Pitcairn, C. A.; Sullivan, E. D.; Jaffe, J. D.; Svinkina, T.; Natoli, T.; Lu, X.; Paulk, J.; McCarren, P.; Wagner, F. F.; Barker, D.; Howe, E.; Lazzaro, F.; Gale, J. P.; Zhang, Y. L.; Subramanian, A.; Fierke, C. A.; Carr, S. A.; Holson, E. B. An Unbiased Approach to Identify Endogenous Substrates Of “histone” deacetylase 8. *ACS Chem. Biol.* **2014**, *9* (10), 2210–2216.
- (185) Millard, C. J.; Watson, P. J.; Celardo, I.; Gordiyenko, Y.; Cowley, S. M.; Robinson, C. V.; Fairall, L.; Schwabe, J. W. R. Class I HDACs Share a Common Mechanism of Regulation by Inositol Phosphates. *Mol. Cell* **2013**, *51* (1), 57–67.
- (186) Chou, T.-C. Theoretical Basis, Experimental Design, and Computerized Simulation of Synergism and Antagonism in Drug Combination Studies.
- (187) Basu, A.; Krishnamurthy, S. Cellular Responses to Cisplatin-Induced DNA Damage. *J. Nucleic Acids* **2010**, *2010*, 1–16.

- (188) Santillan, A.; McClure, K. J.; Allison, B. D.; Lord, B.; Boggs, J. D.; Morton, K. L.; Everson, A. M.; Nepomuceno, D.; Letavic, M. A.; Lee-Dutra, A.; Lovenberg, T. W.; Carruthers, N. I.; Grice, C. A. Indole- and Benzothiophene-Based Histamine H₃antagonists. *Bioorganic Med. Chem. Lett.* **2010**, *20* (21), 6226–6230.
- (189) CambridgeSoft. ChemOffice2016. Perkin Elmer 2016.
- (190) Pettersen, E. F.; Goddard, T. D.; Huang, C. C.; Couch, G. S.; Greenblatt, D. M.; Meng, E. C.; Ferrin, T. E. UCSF Chimera - A Visualization System for Exploratory Research and Analysis. *J. Comput. Chem.* **2004**, *25* (13), 1605–1612.